



UNIVERSIDADE ESTADUAL DE CAMPINAS
INSTITUTO DE GEOCIÊNCIAS

GUSTAVO HENRIQUE COELHO DE MELO

***“TEMPORAL EVOLUTION AND SOURCE OF FLUIDS OF THE SALOBO AND
IGARAPÉ BAHIA IOCG DEPOSITS, CARAJÁS PROVINCE”***

**“EVOLUÇÃO TEMPORAL E FONTE DE FLUIDOS DOS DEPÓSITOS IOCG
SALOBO E IGARAPÉ BAHIA, PROVÍNCIA CARAJÁS”**

CAMPINAS
2018

GUSTAVO HENRIQUE COELHO DE MELO

***TEMPORAL EVOLUTION AND SOURCE OF FLUIDS OF THE SALOBO AND
IGARAPÉ BAHIA IOCG DEPOSITS, CARAJÁS PROVINCE”***

**“EVOLUÇÃO TEMPORAL E FONTE DE FLUIDOS DOS DEPÓSITOS IOCG
SALOBO E IGARAPÉ BAHIA, PROVÍNCIA CARAJÁS”**

TESE DEFESA APRESENTADO AO INSTITUTO DE GEOCIÊNCIAS DA
UNICAMP PARA OBTENÇÃO DO TÍTULO DE DOUTOR EM CIÊNCIAS
NA ÁREA DE GEOLOGIA E RECURSOS NATURAIS .

*THESIS PRESENTED TO THE INSTITUTE OF GEOSCIENCES OF THE
UNIVERSITY OF CAMPINAS TO OBTAIN THE DEGREE OF DOCTOR OF
SCIENCE IN GEOSCIENCES IN THE AREA OF GEOLOGY AND NATURAL
RESOURCES*

ORIENTADORA: PROF. DRA. LENA VIRGÍNIA SOARES MONTEIRO

COORIENTADOR: PROF. DR. ROBERTO PEREZ XAVIER

ESTE EXEMPLAR CORRESPONDE À VERSÃO FINAL
DA TESE DEFENDIDA PELO ALUNO GUSTAVO HENRIQUE
COELHO DE MELO, ORIENTADO PELA PROFA. DRA. LENA
VIRGÍNIA SOARES MONTEIRO.

CAMPINAS

2018

Agência(s) de fomento e nº(s) de processo(s): CNPq, 481969/2013-6; FAPESP,

2016/13162-7

ORCID: <http://orcid.org/0000-0002-0703-3513>

Ficha catalográfica
Universidade Estadual de Campinas
Biblioteca do Instituto de Geociências
Marta dos Santos - CRB 8/5892

M491e	Melo, Gustavo Henrique Coelho de, 1989- Evolução temporal e fonte de fluidos dos depósitos IOCG Salobo e Igarapé Bahia, Província Carajás / Gustavo Henrique Coelho de Melo. – Campinas, SP : [s.n.], 2018. Orientador: Lena Virgínia Soares Monteiro. Coorientador: Roberto Perez Xavier. Tese (doutorado) – Universidade Estadual de Campinas, Instituto de Geociências. 1. Depósitos de óxido de Fe-Cu-Au. 2. Minérios de Cobre. 3. Depósitos Hidrotermais. 4. Isótopos Estáveis. I. Monteiro, Lena Virgínia Soares, 1970-. II. Xavier, Roberto Perez, 1958-. III. Universidade Estadual de Campinas. Instituto de Geociências. IV. Título.
-------	---

Informações para Biblioteca Digital

Título em outro idioma: Temporal evolution and sources of fluids of the Salobo and Igarapé Bahia IOCG deposits, Carajás Province

Palavras-chave em inglês:

Iron oxide-copper-gold deposits

Copper ores

Hydrothermal deposits

Stable isotopes

Área de concentração: Geologia e Recursos Naturais

Titulação: Doutor em Ciências

Banca examinadora:

Lena Virginia Soares Monteiro

Raimundo Netuno Nobre Villas

Claudinei Gouveia de Oliveira

Rafael Rodrigues de Assis

Maria José Maluf de Mesquita

Data de defesa: 23-03-2018

Programa de Pós-Graduação: Geociências



UNIVERSIDADE ESTADUAL DE CAMPINAS
INSTITUTO DE GEOCIÊNCIAS

AUTOR: Gustavo Henrique Coelho De Melo

***TEMPORAL EVOLUTION AND SOURCE OF FLUIDS OF THE SALOBO AND
IGARAPÉ BAHIA IOCG DEPOSITS, CARAJÁS PROVINCE”***

**EVOLUÇÃO TEMPORAL E FONTE DE FLUIDOS DOS DEPÓSITOS IOCG
SALOBO E IGARAPÉ BAHIA, PROVÍNCIA CARAJÁS**

ORIENTADORA: Prof. Dra. Lena Virgínia Soares Monteiro

COORIENTADOR: Prof. Dr. Roberto Perez Xavier

Aprovado em: 23 / 03 / 2018

EXAMINADORES:

Prof. Dra. Lena Virgínia Soares Monteiro - Presidente

Profa. Dra. Maria José Maluf Mesquita

Prof. Dr. Claudinei Gouveia de Oliveira

Prof. Dr. Raimundo Netuno Nobre Villas

Prof. Dr. Rafael Rodrigues de Assis

A Ata de Defesa assinada pelos membros da Comissão Examinadora, consta no processo de vida acadêmica do aluno.

Campinas, 23 de março de 2018

SÚMULA CURRICULAR

Gustavo Henrique Coelho de Melo

Geólogo (2011), Mestre (2014) e Doutor (2018) pela Universidade Estadual de Campinas – UNICAMP. Tem experiência na área de Geociências, com ênfase em Evolução Crustal e Metalogênese, Geoquímica Isotópica, Inclusões Fluidas, Petrografia e Geologia de Campo. Atuou como monitor de diversas disciplinas da graduação em Geologia pela UNICAMP, incluindo Petrologia e Petrografia Metamórfica, Prospecção, Geologia Econômica, Geologia de Campo e Mineralogia.

Finalizou o mestrado no ano de 2014 na área de Geociências pela Universidade Estadual de Campinas com ênfase em estudos petrográficos de rochas hospedeiras e minério, além de estudos geocronológicos no depósito de óxido de ferro-Cu-Au Salobo, Província Carajás, Pará.

Atuou como professor visitante na Universidade Federal do Oeste do Pará (UFOPA) lecionando as disciplinas de “Geologia Estrutural” e “Geologia Econômica e Prospecção”. É recém aprovado em 1º lugar do concurso público referente ao preenchimento da vaga de Prospecção do curso de Engenharia Geológica da Universidade Federal de Ouro Preto (UFOP).

Atualmente está finalizando o doutorado na área de Geociências pela Universidade Estadual de Campinas. O trabalho de doutorado é baseado em estudos petrográficos de rochas hospedeiras e minério, geocronologia U-Pb em zircão e monazita e geoquímica isotópica (O, H, C, S e B) nos depósitos Salobo e Igarapé Bahia, na Província Carajás.

*Dedico este doutorado à minha mãe,
meu pai, minhas irmãs e à toda minha família,
que durante todos os momentos estiveram ao
meu lado. Obrigado!*

AGRADECIMENTOS

Eu gostaria de começar dizendo que certa vez um amigo me disse que “há pessoas que fazem universidade e pessoas que VIVEM a universidade”. Sinceramente, eu acho que eu fui o segundo tipo de pessoa. Foram 11 anos VIVENDO a UNICAMP, o que faz desse agradecimento uma difícil missão.

Aos verdadeiros Doutores da minha vida: minha mãe e meu pai. Mãe, você foi, sem dúvidas, toda minha inspiração de vida e de força que eu penso para minha vida. Não tenho dúvidas que você é a melhor mãe que alguém poderia desejar. Aquela que me apoiou sempre! Pai, obrigado por cada momento que, com uma palavra, gesto e/ou abraço que você fez com que eu me sentisse mais seguro para continuar nessa jornada.

À minha maravilhosa orientadora; a melhor geóloga e uma das melhores pessoas que eu tive o privilégio de conhecer e espero levar por toda essa vida. Lena, eu agradeço até hoje a oportunidade que eu tive de trabalhar com você desde minha primeira IC. Tenho certeza que cresci muito (em vários aspectos) com todos os seus ensinamentos. Muito, mas MUITO obrigado mesmo! Ao meu Co-orientador e amigo Roberto Xavier. Robertinho, obrigado por tudo que você me proporcionou ao longo desses anos. Espero levar essa amizade sempre! À minha Co-orientadora (informal e de coração) e amiga Carolina Moreto: obrigado por toda ajuda ao longo desses anos de convivência.

À CAPES por minha bolsa de doutorado. Ao CNPq (Projetos 481969/2013-6 e 457689/2014-5) e à FAPESP (Projeto 2016/13162-7). Ao INCT/Geociam por todo apoio de campo. À *Society of Economic Geologist* por meu prêmio que possibilitou o pagamento de minhas análises.

À VALE por possibilitar eu fazer esse doutorado. Em especial aos geólogos Fernando Mattos, Sergio Hunh, Benevides Aires e Samuel Nunes por toda ajuda e conhecimento que me passaram.

Às minhas irmãs Talita e Tainá. Espero que eu tenho um pouquinho de cada uma de vocês na minha vida.

À toda minha família Coelho e Melo. Gostaria de agradecer aos meus avôs maternos e paternos. Aos meus tios: Tia Sandra, Tio João, Tia Sônia e Tia Silvia. Aos meus primos, que gostaria de expressar minha gratidão em especial (mas em nome de todos) ao Jé: obrigado por entender o quanto isso foi importante para mim...e acho que ao longo do tempo todos entenderam!

Àqueles que possivelmente mais contribuíram para o meu crescimento como geólogo: meus professores. Ticiano (orientador de vida), Wagner (Lobinho), Vinicius (Micuim), Jeff, MJ, Bernardino, Elson, Emilson, Alvaro, Diego, Batezeli, Celso Dal Ré, Chico e Wanilson. Gostaria de algum dia poder alcançar um pouquinho da sabedoria de vocês.

À Secretaria de Pós Graduação do IG em geral. Sem vocês, nós, da pós, não somos nada. Muito obrigado Val, Gorete, Cris, Valdir e Aninha. Levarei vocês para sempre em meu coração.

Aos técnicos do IG que fazem com que tudo aconteça. Erica, Margareth, Dailto, Lucia e muitos outros. Muito obrigado.

Dizem que é possível conhecer uma pessoa pelos amigos que ela tem. Acho que esse doutorado também é uma parte de cada um dos meus amigos que falarei agora. À melhor das melhores amigas que uma pessoa pode ter: Marília, obrigado simplesmente por você ser e fazer parte da minha vida! Aos meus irmãos e irmã de coração: Mel, Modelo, Jesus e Aline. Aos meus amigos que espero levar para a vida Tio, Adriano, Paulo, Bob, Bill, Edinei, Isa, Gi, Figuinha, Dock, Anderson y Juanita, Dani, Carolzinha, Jaque, Ju, Celina, Eli e Alê. A todos os 07 que fizeram meus anos de graduação mais felizes. Aos 08, em especial Robs, Rafa, Mindinho, Marçola, Gui, Julia, Mika e Pedrinha!

À Nádia: “Importemo-nos apenas com o lugar onde estamos, há beleza bastante em estar aqui e não noutra parte qualquer”. Obrigado por cada momento, Na!

Se há pessoas que de fato participaram e tem parte nessa tese foram os meus amigos da eterna sala 11. Primeiramente aos mais velhos né: Rafael Assis, Mani, Paula, Marco e Maurício. Aos que me proporcionaram momentos de muita alegria e aprendizados nesses últimos anos: Zé (obrigado por tudo cara...por cada momento que a gente fingiu não se gostar ou não se importar com o outro, mas no fundo se importava), Danilo (pelos ensinamentos com Cirão, Karnal, Cortella...) e Raphinha (meu filho!). Poli, Bia e Pati: obrigado por cada palavra, abraço, zuação, ou qualquer coisa... vocês são e serão SEMPRE especiais em minha vida! Que a sala 11 prospere sempre....

A todos meus amigos de pós-graduação que com um simples cafezinho me deram a força para continuar nesse caminho...e apenas espero que cada um de vocês sigam e realizem seus sonhos. Em especial à Marcelinha (em muito especial), JP (meu lindo Ceará!), Dan (avante Sumaré!), Brunão, Bilica, Tais Magaldi, João Motta, Ton, Luciano, Sapo, Keyla, Bel, Raisa, Paola, Alcione, Saeid, Emanuel, Taynah, Igor, Johan, Veronica, Ananda e Rafa.

Aos funcionários da UNICAMP que fazem nosso cotidiano ser mais especial. Gostaria aqui de agradecer a todos eles em nome de Ednalva, Guerreiro e Lúcia. Conviver com vocês me fez crescer como ser humano.

Aos meus eternos amigos do Karatê que levarei para sempre em minha vida. Em especial ao meu sempre Sensei Ernesto Tarô Nishibara, por todo o ensinamento de vida que me transmitiu. Oss!

Agradeço, por fim, à toda sociedade brasileira. Que cada dia mais a universidade PÚBLICA E DE QUALIDADE seja mais acessível à pobres, negros, indígenas, LBGT's, aos alunos de escola pública e todas as minorias em geral. A universidade é de todos e para todos!

“What we do in life, echoes in eternity”

Maximus Decimus Meridius

RESUMO

Os depósitos Salobo e Igarapé Bahia representam importantes depósitos de óxido de ferro–cobre–ouro (IOCG) da Província Carajás. O depósito Salobo é hospedado por gnaisses do Complexo Xingu, granitoides da Suíte Igarapé Gelado e por unidades metasedimentares. Alteração hidrotermal formou rochas miloníticas ricas em grunerita–almandina–faialita–magnetita–(turmalina) e (grunerita–almandina)–magnetita–biotita. O depósito Igarapé Bahia é hospedado por rochas metavulcanossedimentares do Grupo Igarapé Bahia e metassedimentares da Formação Águas Claras. Xenólitos embasamento ocorrem no depósito e forneceram idades de 2935 ± 36 Ma (MSWD = 0,85), sugerindo uma crosta ensiálica prévia a instalação da bacia. Idades U–Pb de zircão detritítico das metagrauvacas do Grupo Igarapé Bahia (2,82 – 2,88 Ga e 2,94 – 2,99 Ga) e da Formação Águas Claras (2,81 – 2,89 Ga e 2,91 – 3,03 Ga) apontam para predominância de fontes do embasamento mesoarqueano. Nódulos e *layers* de calcopirita em metarritmitos da unidade superior representam uma mineralização singenética coeva à deposição do Grupo Igarapé Bahia no Neoarqueano. A composição isotópica de enxofre dessa geração de calcopirita (+0,29 e +1,56‰) e os seus elevados conteúdos de Ni, Co e Bi apontam para enxofre e metais lixiviados das rochas metavulcânicas da unidade inferior. Extensas zonas de alteração hidrotermal com rochas ricas em (turmalina)–carbonato–magnetita e (turmalina)–carbonato–clorita envelopam a mineralização IOCG. Geocronologia U–Pb em monazita forneceu idade 2559 ± 34 Ma no corpo Alemão. A assinatura geoquímica de minério com elevados valores de ΣETR e conteúdos significativos de U, Mo, Sn, W, Y, Nb e Sr são característicos da mineralização IOCG. No depósito Salobo, fluidos em equilíbrio com grunerita ($\delta^{18}\text{O}_{\text{H}_2\text{O}} = +6,66$ a $+7,96\text{\textperthousand}$, $\delta\text{D}_{\text{H}_2\text{O}} = -10,65$ a $-1,33\text{\textperthousand}$), granada ($\delta^{18}\text{O}_{\text{H}_2\text{O}} = +6,88$ a $+7,77\text{\textperthousand}$) e turmalina ($\delta^{18}\text{O}_{\text{H}_2\text{O}} = +4,11$ a $+6,41\text{\textperthousand}$, $\delta\text{D}_{\text{H}_2\text{O}} = -15,40$ a $+5,12\text{\textperthousand}$), a 429 ± 45 °C, e fluidos em equilíbrio com biotita ($\delta^{18}\text{O}_{\text{H}_2\text{O}} = +7,16$ a $7,96\text{\textperthousand}$, $\delta\text{D}_{\text{H}_2\text{O}} = -36,96$ a $-21,93\text{\textperthousand}$) e quartzo ($\delta^{18}\text{O}_{\text{H}_2\text{O}} = +6,88 \pm 0,35\text{\textperthousand}$), a 520 ± 45 °C, apresentam composição semelhante à da água magmática. No depósito Igarapé Bahia, fluidos associados com a formação de turmalina ($\delta^{18}\text{O}_{\text{H}_2\text{O}} = +5,54$ a $6,24\text{\textperthousand}$, $\delta\text{D}_{\text{H}_2\text{O}} = -46,98$ a $-32,70\text{\textperthousand}$) e calcita ($\delta^{18}\text{O}_{\text{H}_2\text{O}} = +1,68$ a $+3,10\text{\textperthousand}$; $\delta^{13}\text{C}_{\text{CO}_2} = -9,04$ a $-4,65\text{\textperthousand}$, 398 ± 85 °C) também evidenciam fontes magmáticas. A participação de fontes externas no Igarapé Bahia é marcada pela clorita ($\delta^{18}\text{O}_{\text{H}_2\text{O}} = +2,13$ e $+3,41\text{\textperthousand}$). Isótopos de enxofre apontam para fontes magmáticas no depósito Salobo ($-0,37$ e $+1,63\text{\textperthousand}$) e externa para o Igarapé Bahia ($+1,36$ e $+5,35\text{\textperthousand}$). Isótopos de boro em turmalina nos depósitos Salobo ($+3,4$ a $+17,0\text{\textperthousand}$), Igarapé Bahia ($+3,4$ a $+14,6\text{\textperthousand}$), Furnas ($+13,1$ a $+17,2\text{\textperthousand}$), Grotta Funda ($+8,2$ a $+13,6\text{\textperthousand}$) e GT-46

(+5,4 a +6,4‰) sugerem a participação de fontes híbridas, que incluem salmoras derivadas de fluidos hidrotermais submarinhos e/ou evaporação da água do mar associada com boro proveniente de salmoras magmáticas. A sobreposição de episódios de mineralização de Cu–Au reflete os diversos eventos tectônicos e magmáticos do Domínio Carajás.

Palavras-chave: Depósitos de óxido de Fe-Cu-Au, Minérios de Cobre, Depósitos Hidrotermais, Isótopos Estáveis

ABSTRACT

The Salobo and Igarapé Bahia deposits represent important iron oxide-copper-gold (IOCG) deposits at Carajás Province. The Salobo deposit is hosted by gneiss from the Xingu Complex, granites from the Igarapé Gelado suite and by metasedimentary units. Hydrothermal alteration formed grunerite–almandine–fayalite–magnetite–(tourmaline) and (grunerite–almandine)–magnetite–biotite mylonitic rocks. The Igarapé Bahia deposit is hosted by metavolcanosedimentary rocks from the Igarapé Bahia Group and metasedimentary sequences from the Águas Claras Formation. Basement xenoliths occur within the deposit with ages of $2,935 \pm 36$ Ma (MSWD = 0.85), evidencing the presence of an ensialic crust prior to rifting. U-Pb ages in detrital zircon of the metagraywackes of the Igarapé Bahia Group (2.82 – 2.88 Ga e 2.94 – 2.99 Ga) and of the Águas Claras Formation (2.81 – 2.89 Ga and 2.91 – 3.03 Ga) point to mesoarchean basement sources. Chalcopyrite nodules and layers within metarhytmites of the upper sequence represent a syngenetic mineralization coeval with deposition of the Igarapé Bahia Group in the Neoarchean. Sulfur isotopes in this chalcopyrite generation (+0.29 and +1.56‰) and elevated contents of Ni, Co and Bi suggest that sulfur and metals were leached from the metavolcanic rocks of the lower sequence. Zones of hydrothermal alteration with (tourmaline)–carbonate–magnetite and (tourmaline)–carbonate–chlorite envelop the IOCG mineralization. U-Pb geochronology in monazite yielded ages of $2,559 \pm 34$ Ma in the Alemão orebody. Ore geochemistry signature at IOCG mineralization exhibit elevated ΣETR values and expressive contents of U, Mo, Sn, W, Y, Nb and Sr. In the Salobo deposit, fluids associated with grunerite ($\delta^{18}\text{O}_{\text{H}_2\text{O}} = +6.66$ to $+7.96\text{\textperthousand}$, $\delta\text{D}_{\text{H}_2\text{O}} = -10.65$ to $-1.33\text{\textperthousand}$), garnet ($\delta^{18}\text{O}_{\text{H}_2\text{O}} = +6.88$ to $+7.77\text{\textperthousand}$) and tourmaline ($\delta^{18}\text{O}_{\text{H}_2\text{O}} = +4.11$ to $+6.41\text{\textperthousand}$, $\delta\text{D}_{\text{H}_2\text{O}} = -15.40$ to $+5.12\text{\textperthousand}$), at 429 ± 45 °C, and fluids in equilibrium with biotite ($\delta^{18}\text{O}_{\text{H}_2\text{O}} = +7.16$ to $7.96\text{\textperthousand}$, $\delta\text{D}_{\text{H}_2\text{O}} = -36.96$ to $-21.93\text{\textperthousand}$) and quartz ($\delta^{18}\text{O}_{\text{H}_2\text{O}} = +6.88 \pm 0.35\text{\textperthousand}$), at 520 ± 45 °C, fall into the magmatic water field. In the Igarapé Bahia deposit, fluids in equilibrium with tourmaline ($\delta^{18}\text{O}_{\text{H}_2\text{O}} = +5.54$ to $6.24\text{\textperthousand}$, $\delta\text{D}_{\text{H}_2\text{O}} = -46.98$ to $-32.70\text{\textperthousand}$) and calcite ($\delta^{18}\text{O}_{\text{H}_2\text{O}} = +1.68$ to $+3.10\text{\textperthousand}$; $\delta^{13}\text{C}_{\text{CO}_2} = -9.04$ to $-4.65\text{\textperthousand}$, 398 ± 85 °C) also point to magmatic sources. External sources in the Igarapé Bahia deposit is constrained by chlorite ($\delta^{18}\text{O}_{\text{H}_2\text{O}} = +2.13$ e $+3.41\text{\textperthousand}$). Sulfur isotopes point to magmatic sources at Salobo (-0.37 and $+1.63\text{\textperthousand}$) and external sources for Igarapé Bahia ($+1.36$ and $+5.35\text{\textperthousand}$). Boron isotopes in tourmaline at Salobo ($+3.4$ to $+17.0\text{\textperthousand}$), Igarapé Bahia ($+3.4$ to $+14.6\text{\textperthousand}$), Furnas ($+13.1$ to $+17.2\text{\textperthousand}$), Grotá Funda ($+8.2$ to $+13.6\text{\textperthousand}$) and GT-46 ($+5.4$ to $+6.4\text{\textperthousand}$) evidence the

participation of exhalative fluids and/or evaporated seawater brines associated with magmatic brines. These results suggest that seawater and magmatic boron sources took part in the mineral system during distinct Neoarchean tectono-magmatic events separated in time.

Keywords: Iron oxide-copper-gold, Copper ores, Hydrothermal deposits, Stable isotopes

ÍNDICE DE FIGURAS

- Fig. 1. Mapa das províncias e domínios tectônicos do Cráton Amazônico no Estado do Pará (modificado de Vasquez et al. 2008).....27
- Fig. 2. Mapa geológico do Domínio Carajás com a localização dos principais depósitos minerais da região. As caixas em vermelho mostram a localização dos depósitos Salobo e Igarapé Bahia (modificado de Vasquez et al. 2008).....28
- Fig. 3. Compilação de dados geoquímicos dos principais granitos da Província Carajás. Diagramas de discriminação tectônica a), b) e c) de Frost et al. (2001); d) diagrama de discriminação de granitos (>68 % de SiO₂) de Sylvester (1989); e) diagrama de Eby (1992) com discriminação de granitos do tipo A; f) e g) Diagramas de diferenciação de granitos do tipo A de Whalen (1987); h) e i) Diagramas de Pearce et al. (1984) de discriminação de ambiente tectônico. Dados obtidos de Lindenmayer (1990), Barbosa (2004), Dall'Agnol et al. (2005), Barros et al. (2009), Feio (2012).....31
- Fig. 4. Imagem SRTM com a localização dos principais depósitos IOCG e dos dados geocronológicos da Tabela 2 no Domínio Carajás. Veja tabela 2 para informações das amostras datadas (extraído de Melo et al. 2016).....38
- Fig. 5. Dados relativos à composição isotópica de oxigênio ($\delta^{18}\text{O}_{\text{H}_2\text{O}}$) dos fluidos em equilíbrio com minerais hidrotermais de depósitos IOCG da Província Carajás, obtidos de: 1 - Dreher et al. 2008, 2 - Monteiro et al. 2008, 3 - Torresi et al. 2011, 4 - Silva et al. 2015, 5 - Pestilho 2011. Campos da água do mar e água magmática são extraídos de Taylor (1997). Distribuição de valores de $\delta^{18}\text{O}$ para água meteórica, rochas sedimentares, rochas metamórficas, rochas graníticas e rochas basálticas obtidos de Hoefs (2007).....44
- Fig. 6. Dados de $\delta^{34}\text{S}$ em sulfetos dos depósitos IOCG de Província Carajás. Dados de $\delta^{18}\text{O}$ obtidos de: 1- Réquia e Fontboté (2001), 2 - Dreher et al. (2008), 3 - Galarza et al. (2008), 4 - Villas et al. (2001), 5 - Fleck e Lindenmayer (2003), 6 - Monteiro et al. (2008), 7 - Ribeiro et al. (2009), 8 - Torresi et al. (2011), 9 - Pestilho (2011), 10 - Silva et al. (2010). Campo do enxofre magmático e evaporitos/sulfatos arqueanos obtidos de Ohmoto e Goldhaber (1997) e Eldridge et al. (1991), respectivamente. Distribuição de valores de $\delta^{34}\text{S}$ rochas sedimentares, rochas metamórficas, rochas graníticas e rochas basálticas obtidos de Hoefs (2007).....46
- Fig. 7. Mapa e perfil geológico do depósito Salobo com a disposição das rochas hospedeiras distais e rochas hidrotermalizadas na porção central do depósito marcadas pela forte deformação dúctil da Zona de Cisalhamento do Cinzento de direção WNW-ESE (modificado de VALE).....48
- Fig. 8. a) Mapa geológico do depósito Igarapé Bahia com as principais unidades geológicas e a projeção dos corpos de minério. Perfil geológico do corpo a) Furo 30, b) Acampamento Sul, c) Acampamento Norte e d) Alemão (modificado de VALE).....50

ÍNDICE DE TABELAS

Tabela. 1. Eventos tectono-termais que afetaram o nordeste da Província Carajás (Tavares 2015).....34

Tabela. 2. Dados geocronológicos para as principais unidades regionais, alteração hidrotermal e mineralização dos depósitos IOCG do Domínio Carajás.....40

SUMÁRIO

1.	INTRODUÇÃO.....	19
2.	OBJETIVOS.....	21
3.	MATERIAIS E MÉTODOS.....	22
4.	CONTEXTO GEOLÓGICO REGIONAL DA PROVÍNCIA CARAJÁS	26
4.1	Arcabouço Litoestratigráfico	26
4.2	Evolução Geotectônica do Domínio Carajás	32
5.	DEPÓSITOS IOCG NO DOMÍNIO CARAJÁS	35
5.1	Características gerais dos depósitos IOCG	35
5.2	Geocronologia dos depósitos IOCG de Carajás	37
5.3	Geoquímica isotópica na caracterização dos depósitos IOCG de Carajás	42
6.	GEOLOGIA DOS DEPÓSITOS SALOBO E IGARAPÉ BAHIA	47
6.1	Geologia do depósito Salobo	47
6.2	Geologia do depósito Igarapé Bahia.....	48
7.	SÍNTESE DOS ARTIGOS.....	51
7.1	Artigo I – “The evolution of the Cu-Au Igarapé Bahia deposit: early syngenetic sulfides overprinted by IOCG mineralization, Carajás Province (Brazil)”	51
7.2	Artigo II – “Tracing fluid sources for the giant Salobo and Alemão-Igarapé Bahia IOCG deposits: implications for the genesis of the IOCG deposits in the Carajás Mineral Province”	53
7.3	Artigo III – “Boron isotopes in tourmaline of the IOCG deposits in the northern sector of the Carajás Domain, Carajás Province (Brazil)”	54
8.	CONCLUSÕES	56
	REFERÊNCIAS	59
	Anexo I – “The evolution of the Cu-Au Igarapé Bahia deposit: early syngenetic sulfides overprinted by IOCG mineralization, Carajás Province (Brazil)”	70
	Appendix.....	129

Anexo II – “Tracing fluid sources for Salobo and Igarapé Bahia IOCG deposits, Carajás Province: implications for the genesis of the IOCG deposits” 136

Anexo III – “Boron isotopes in tourmaline of the IOCG deposits in the northern sector of the Carajás Domain, Carajás Province (Brazil)” 182

1. INTRODUÇÃO

Os depósitos de óxido de ferro–cobre–ouro (ou IOCG) de classe mundial Salobo e Igarapé Bahia destacam-se como os mais importantes depósitos de cobre–ouro da Província Carajás, concentrando-se exclusivamente no Domínio Carajás, na parte norte da província. O depósito Salobo possui reservas estimadas em 1112 Mt, com 0,69% Cu e 0,43 g/t Au (VALE 2012) e situa-se ao longo da Zona de Cisalhamento Cinzento de direção WNW–ESE, próximo ao limite norte entre a Província Carajás e o Domínio Bacajá da Província Transamazonas (2,26 – 1,90 Ga, Vasquez *et al.* 2008). Por outro lado, o depósito Igarapé Bahia possui reservas com 219 Mt e 1,4% Cu e 0,86 g/t Au (Tallarico *et al.* 2005) e ocorre em uma janela tectônica na Formação Águas Claras, hospedado na sequência de rochas supracrustais do Supergrupo Itacaiúnas, próximo à Falha Carajás.

Embora o contexto geológico (e.g. rochas hospedeiras, controle estrutural, paragenêse mineral) desses depósitos já tenha sido caracterizado em estudos prévios (Lindenmayer 1990, 2003; Réquia *et al.* 2003; Tallarico *et al.* 2005; Dreher *et al.* 2008; Melo *et al.* 2016), alguns pontos chave para a compreensão da evolução desses depósitos ainda devem ser desvendados. Esses incluem principalmente: (i) as idades e processos responsáveis pela formação das rochas hospedeiras; (ii) a correlação das idades de mineralização com possíveis eventos tectono-magnéticos na Província Carajás; (iii) o ambiente tectônico de formação desses depósitos e (iv) a(s) principal(is) fonte(s) de fluido(s) mineralizante(s). Adicionalmente, a geologia e evolução do sistema hidrotermal do corpo Alemão no depósito Igarapé Bahia é pouco conhecida, o que pode trazer novas e importantes informações a respeito desse depósito.

Estudos recentes mostram que os depósitos IOCG do Cinturão Sul do Cobre, localizados na porção sul do Domínio Carajás, que incluem os depósitos de classe mundial de Sossego e Alvo 118, além de alvos satélites menores (e.g. Bacaba, Bacuri, Visconde), foram formados por múltiplos eventos hidrotermais que se sobrepunderam durante o Neoarqueano (ca. 2,71 a 2,68 Ga; corpos Sequeirinho e Pista da Mina Sossego, e depósitos Bacaba e Bacuri) e o Paleoproterozoico (ca. 1,90 a 1,88 Ga; corpos Sossego e Curral da Mina Sossego e depósito Alvo 118; Moreto *et al.* 2015a,b).

Nos depósitos Salobo e Igarapé Bahia, localizados na porção norte do Domínio Carajás, idades precisas (2576 ± 8 Ma, Re–Os em molibdenita, Réquia *et al.* 2003; 2575 ± 12 Ma, U–Pb em monazita, Tallarico *et al.* 2005) apontam para a instalação de um

sistema magmático-hidrotermal em ca. 2,57 Ga, que seria responsável pela formação desses depósitos em um evento metalogenético distinto daqueles caracterizados nos depósitos IOCG do Cinturão Sul do Cobre. Esse sistema tem sido atribuído à cristalização de corpos graníticos de ca. 2,57 Ga (e.g. granito *Old Salobo*, Réquia *et al.* 2003, Tallarico *et al.* 2005). Por outro lado, as idades de ca. 2,57 Ga também têm sido interpretadas como relativas a um evento tectono-termal relacionado à reativação da Zona de Cisalhamento do Cinzento (e.g. Machado *et al.* 1991; Barbosa 2004), o que explicaria seu registro mais evidente na porção norte da província (Melo *et al.* 2016).

O conjunto de dados geocronológicos para os depósitos cupro-auríferos da Província Carajás evidenciam a importância de distintos episódios metalogenéticos no Cinturão Sul do Cobre e na porção norte do Domínio Carajás. Esses dados levantam a questão se todos depósitos IOCG de Carajás evoluíram de forma similar. Estudos de inclusões fluidas, isótopos estáveis, isótopos de boro e cloro, além de razões Cl/Br, permitiram a caracterização da natureza híbrida dos sistemas IOCG de Carajás, nos quais a mistura de fluidos de diferentes origens (magmática, mantélica, bacinal, derivada da dissolução de evaporitos, metamórfica, e meteórica) pode ter representado um mecanismo de importância fundamental para a precipitação dos metais (Villas *et al.* 2006; Chiaradia *et al.* 2006; Dreher *et al.*, 2008, Monteiro *et al.*, 2008a; Xavier *et al.* 2008; 2009, Torresi *et al.* 2011; Pestilho 2011). Contudo, a participação de cada uma dessas fontes de fluidos e metais na formação dos depósitos IOCG e a relação desses com os diferentes pulsos hidrotermais ainda precisam ser melhor compreendidas.

Essa tese de doutorado traz uma análise da geologia dos depósitos Salobo e Igarapé Bahia, aliados a estudos geocronológicos (U–Pb em zircão e monazita), estudos de geoquímica isotópica (O, H, S, C e B) e geoquímica de elementos-traço em calcopirita. Esses estudos visam delimitar diferentes eventos metalogenéticos e caracterizar a participação de distintas fontes de fluidos nos depósitos Salobo e Igarapé Bahia, assim como suas relações com a evolução tectono-magmática da Província Carajás.

Os resultados dessa Tese de Doutorado poderão trazer uma nova perspectiva no entendimento da dinâmica e evolução dos complexos sistemas IOCG em Carajás e no mundo, possibilitando o refinamento de modelos genéticos existentes.

2. OBJETIVOS

O estudo tem como objetivo principal a caracterização e comparação dos sistemas metalogenéticos responsáveis pela formação dos depósitos Salobo e Igarapé Bahia da Província Mineral de Carajás. Os objetivos específicos incluem:

- i. Caracterização de rochas hospedeiras e de associação paragenética detalhada das diferentes zonas de alteração hidrotermal e mineralização nos depósitos Salobo e Igarapé Bahia, incluindo o corpo Alemão;
- ii. Delimitação do intervalo de idades de formação das mineralizações de óxido de ferro-cobre-ouro e de estágios de alteração hidrotermal e suas relações com processos ou eventos geológicos regionais da Província Carajás;
- iii. Identificação da natureza das fontes de fluidos em cada evento hidrotermal caracterizado, assim como a história de interação fluido-rocha a partir de estudos de geologia isotópica.
- iv. Estabelecimento de modelos evolutivos para os depósitos Salobo e Igarapé Bahia, incluindo ambiente tectônico de formação, e comparação com os sistemas bem caracterizados no Domínio Carajás.

3. MATERIAIS E MÉTODOS

Revisão Bibliográfica

A revisão bibliográfica foi realizada durante todo o desenvolvimento das pesquisas, com ênfase nos depósitos de óxido de Fe–Cu–Au da Província Carajás, especialmente no depósito Salobo e Igarapé-Bahia, e de outras províncias mundiais, assim como na evolução de sistemas hidrotermais. Adicionalmente, uma criteriosa revisão foi realizada na aplicação de diferentes sistemáticas geocronológicas e geoquímica isotópica em diversos sistemas visando à reconstituição da história de interação fluido-rocha em depósitos minerais.

Trabalho de Campo

O trabalho de campo foi realizado no mês de julho de 2014 na Mina Igarapé Bahia e visou à descrição detalhada e sistemática de testemunhos de sondagem enfatizando-se a caracterização dos litotipos hospedeiros, a identificação de estilos e geometria das zonas de alteração hidrotermal, a identificação de tipos de minério e seus modos de ocorrência, as relações texturais entre os minerais de minério e de ganga e a influência de estruturas regionais no depósito, além de coleta sistemática de amostras. As amostras do depósito Salobo foram coletadas em etapas prévias no ano de 2012, durante a realização da etapa de campo de mestrado do doutorando.

Estudos petrográficos em luz transmitida e refletida

Estudos petrográficos em luz transmitida e refletida foram desenvolvidos no Instituto de Geociências da UNICAMP em lâminas delgadas-polidas confeccionadas a partir de amostras de testemunhos de sondagem e de minério. Esses estudos visaram à caracterização dos litotipos hospedeiros das mineralizações, da evolução paragenética, das relações texturais entre os minerais de minério e de ganga, assim como as relações entre paragêneses e microestruturas. Também foi realizada caracterização detalhada de fases minerais passíveis de datação, incluindo seu modo de ocorrência, associação paragenética, relação temporal com hidrotermalismo e mineralização e padrões de zoneamento.

Microscopia Eletrônica de Varredura

Análises com uso de microscópio eletrônico de varredura (MEV) acoplado a EDS (*Energy Dispersive X-Ray Spectrometer*) foram realizadas no Laboratório de Quantificação Mineral, no Instituto de Geociências da UNICAMP. Essas análises visaram a identificação de fases minerais não reconhecidas com o uso do microscópio óptico, possíveis inclusões minerais, zoneamentos compostionais em minerais de minério e outras fases hidrotermais. Ênfase foi dada também em imagens de elétrons retroespalhados de minerais passíveis de datação no intuito de identificar fraturas ou mesmo inclusões minerais.

Preparação de amostras e separação mineral

A separação de zircão foi realizada nos laboratórios de Preparação de Amostras e de Concentração de Minerais do Instituto de Geociências da UNICAMP. Os grãos de zircão foram concentrados a partir de métodos gravimétricos e magnéticos convencionais, seguindo as etapas de britagem em britador de mandíbulas, moagem em moinho vibratório, bateamento manual, separação magnética com imã, separação magnética através do separador isodinâmico Frantz e separação manual dos grãos em lupa binocular. Os grãos selecionados na etapa de separação manual em lupa binocular foram colados em uma lâmina e montados com resina epóxi em um *mount* de 1 polegada e polidos com pasta diamantada.

Grãos de monazita e turmalina foram localizados e selecionados diretamente em seções delgadas-polidas ao microscópio óptico. As seções delgadas-polidas com cristais de monazita foram enviadas para análise pelo método U-Pb SHRIMP II *in situ* no *John de Laeter Centre* da *Curtin University*, Austrália. As seções delgadas-polidas com cristais de turmalina foram enviadas para a *Faculty of Earth Resources* da *China University of Geosciences*, China, onde foram realizadas análises *in situ* de isótopos de boro e elementos-traço em turmalina por MC-LA-ICP-MS.

Anfibólio, biotita, clorita, granada, quartzo, turmalina, calcita, magnetita, calcopirita e bornita foram extraídos de amostras de testemunho de sondagem e minério com o auxílio de uma microretífica. Esses minerais foram posteriormente analisados com a ajuda de uma lupa binocular para a retirada de possíveis impurezas presentes, e com o auxílio de um almofariz de ágata esses minerais foram pulverizados.

Difratometria de Raios-X

Análises por Difratometria de Raios-X foram realizadas no Laboratório de Quantificação Mineral do Instituto de Geociências da Universidade Estadual de Campinas com uso de um Difratômetro Bruker D2 Phaser de bancada. Anfibólio, biotita, clorita, granada, quartzo, turmalina, calcita e magnetita, pulverizados foram analisados visando a caracterização de possíveis impurezas nessas amostras para posterior envio para análises de isótopos de oxigênio e hidrogênio.

Geocronologia U–Pb em zircão e monazita

Análises geocronológicas pelo método U–Pb em zircão foram realizadas nos principais litotipos hospedeiros do depósito Igarapé Bahia. As análises foram obtidas por LA–SF–ICP–MS (*Laser Ablation Sector Field Inductively Coupled Plasma Mass Spectrometry*) no Laboratório de Geologia Isotópica do Instituto de Geociências da Universidade Estadual de Campinas. A aquisição desses dados visou a obtenção de idades de cristalização no caso de rochas ígneas, proveniência de zircão detritico para rochas metassedimentares e possíveis evidências de eventos metamórficos ou hidrotermais registrados nesses grãos.

Análises *in situ* de grãos de monazita em seções delgadas-polidas foram realizadas por SHRIMP II no *John de Laeter Centre* da *Curtin University*, Austrália. A amostra analisada compreendia monazita hidrotermal pertencente ao principal estágio mineralizante no corpo Alemão do depósito Igarapé Bahia. Devido à falta de grãos grossos de monazita, apenas um *spot* em um grão de monazita foi realizado.

Elementos traço em calcopirita

As amostras de concentrados de calcopirita foram dissolvidas utilizando uma mistura de ácidos nítrico, clorídrico e fluorídrico em forno de microondas. Todas as soluções foram preparadas com água ultra-pura (18,2 MΩ.cm), obtida por sistema Milli-Q. O ácido nítrico (HNO₃) foi purificado por sub-ebulição. Os frascos utilizados para as diluições foram previamente limpos com HNO₃ 5% e enxaguados com água ultra-pura. O limite de detecção (LD) foi determinado como sendo a média (x) mais 3 desvios-padrão (s) de dez medidas do branco (LD= x +3s). As medições foram realizadas em ICP-MS XseriesII (Thermo) equipado com CCT (Collision Cell Technology). A calibração do instrumento foi efetuada com soluções multielementares preparadas gravimetricamente a partir de soluções-padrão monoelementares de 100 mg/L

(AccuStandards). O controle de qualidade foi efetuado pela análise do material de referência: WMS-1 (sulphide ore powder)

Isótopos Estáveis: O, H, S, C e B

Análises de isótopos de oxigênio em biotita, carbonato, clorita, granada, grunerita, magnetita, quartzo e turmalina, e hidrogênio em biotita, clorita, grunerita e turmalina foram analisados na *Queen's Facilities for Isotope Research* (QFIR) da *Queen's University*, Canada. Análises complementares de oxigênio e carbono em carbonato foram obtidas também no Centro de Pesquisas Geocronológicas (CPGeo) da Universidade de São Paulo e de oxigênio em granada no Núcleo de Estudos de Granitos - Laboratório de Isótopos Estáveis (NEG-LABISE) da Universidade Federal de Pernambuco. As análises isotópicas de oxigênio e hidrogênio são reportadas em relação ao padrão *Vienna Standard Mean Ocean Water* (VSMOW) e de carbono em relação ao padrão internacional, *Pee Dee Belemnite* (PDB).

Análises de isótopos de enxofre foram realizadas em calcopirita e bornita das zonas mineralizadas dos depósitos Salobo e Igarapé Bahia. As medições foram realizadas no Laboratório de Geocronologia da Universidade de Brasília. Os valores de $\delta^{34}\text{S}$ têm precisão de 0,01‰ e foram reportados em relação ao padrão CDT (*Canion Diablo Troilite*).

Análises de isótopos de boro foram obtidas em cristais de turmalina dos depósitos Salobo e Igarapé Bahia. Essas análises foram conduzidas na *China University of Geosciences*, Wuhan, China, a partir de MC-LA-ICP-MS que possibilitam análises isotópicas *in situ* nas seções delgada-polidas.

As análises de isótopos estáveis visaram à caracterização da(s) fonte(s) de fluido(s), enxofre e boro, além da comparação da evolução do sistema hidrotermal nos dois depósitos estudados.

4. CONTEXTO GEOLÓGICO REGIONAL DA PROVÍNCIA CARAJÁS

4.1 Arcabouço Litoestratigráfico

A Província Carajás compreende um núcleo crustal arqueano inserido na porção sudeste do Cráton Amazônico (Tassinari & Macambira 1999) e representa uma das províncias minerais mais importantes do mundo, hospedando importantes depósitos de Fe (e.g. depósito Serra Norte, Minas N4 e N5), Mn (e.g. Mina do Azul), Fe–Cu–Au (e.g. Salobo, Igarapé Bahia e Sossego), Cu–Au (e.g. Breves, Santa Lúcia), Au (e.g. Serra Pelada) e Ni–EGP (e.g. Luanga). Essa província é dividida em dois blocos tectônicos: o Domínio Rio Maria, ao sul, e o Domínio Carajás, ao norte (Fig. 1, Santos 2003, Vasquez *et al.* 2008). Adicionalmente, estudos recentes dividiram o Domínio Carajás em Bacia Carajás, a norte, e Domínio Canaã dos Carajás, a sul; enquanto que o Domínio Rio Maria foi dividido em Domínio Sapucaia na sua porção norte e Domínio Rio Maria na parte sul (Dall’Agnol *et al.* 2013).

O Domínio Rio Maria constitui um típico terreno granito-*greenstone* arqueano no Cráton Amazônico (Vasquez *et al.* 2008). As sequências *greenstone belts* são representadas pelos grupos Babaçu, Lagoa Seca, Serra do Inajá, Gradaús, Sapucaia e Tucumã (Vasquez *et al.* 2008), pertencentes ao Supergrupo Andorinhas (DOCEGEO 1988). Diversos granitoides e gnaisses da série TTG (e.g. Tonalito Arco Verde e Tonalito Caracol; Rolando e Macambira 2003, Leite *et al.* 2004, Macambira e Lancelot 2006) e sanukitoides (e.g. Granodiorito Rio Maria, Oliveira *et al.* 2009) ocorrem por todo o Domínio Rio Maria, com idades entre 3,05 – 2,92 Ga e 2,88 – 2,82 Ga (Vasquez *et al.* 2008). Complexos máficos-ultramáficos mesoarqueanos, representados pelos corpos Serra Azul e Guará-Pará, intrudem o Grupo Gradaús. Granitos anorogênicos de 1,88 Ga também são reconhecidos por todo o Domínio Rio Maria (e.g. granitos Jamon e Musa; Machado *et al.* 1991, Dallagnol *et al.* 1999).

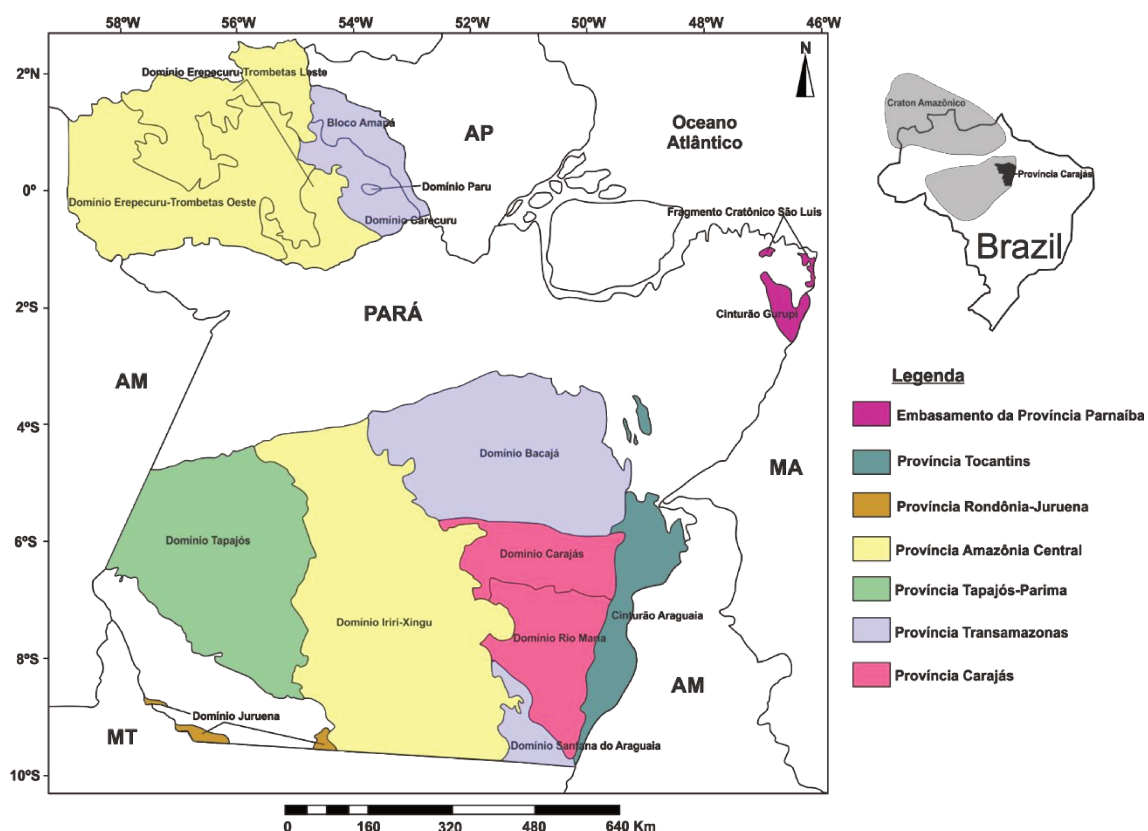


Fig. 1. Mapa das províncias e domínios tectônicos do Cráton Amazônico no Estado do Pará (modificado de Vasquez *et al.* 2008).

O Domínio Carajás, no qual se concentram os principais depósitos minerais da província, compreende tanto o embasamento mesoarqueano quanto sequências supracrustais neoarqueanas (Fig. 2, Machado *et al.* 1991).

O embasamento arqueano tem sido atribuído ao Complexo Xingu, composto por gnaisses tonalíticos a trondjemíticos e migmatitos ($3066 \pm 6,6$ Ma, Delinardo da Silva 2014) e ao Ortogranulito Chicrim-Cateté (ou Complexo Pium; 3002 ± 14 Ma, Pidgeon *et al.* 2000). Dados geocronológicos sugerem que o processo de migmatização do Complexo Xingu (2859 ± 2 Ma e 2860 ± 2 Ma, U-Pb em zircão, Machado *et al.* 1991) e granulitização (2859 ± 9 Ma, U-Pb SHRIMP zircão; Pidgeon *et al.* 2000) podem ter sido contemporâneos. Estudos recentes discriminam unidades geológicas composicionalmente distintas, anteriormente atribuídas ao Complexo Xingu no Domínio Canaã dos Carajás, que incluem: 1) ca. $3,0\text{--}2,99$ Ga: Tonalito Bacaba e Granito Sequeirinho (Moreto *et al.* 2011, 2015); (2) $2,96\text{--}2,93$ Ga: Granito Canaã dos Carajás (Feio *et al.* 2013); (3) $2,87\text{--}2,83$ Ga: Trondjemito Rio Verde, Tonalito Campina Verde e os granitos Bom Jesus, Cruzadão e Serra Dourada (Moreto *et al.* 2011, Feio *et al.* 2013).

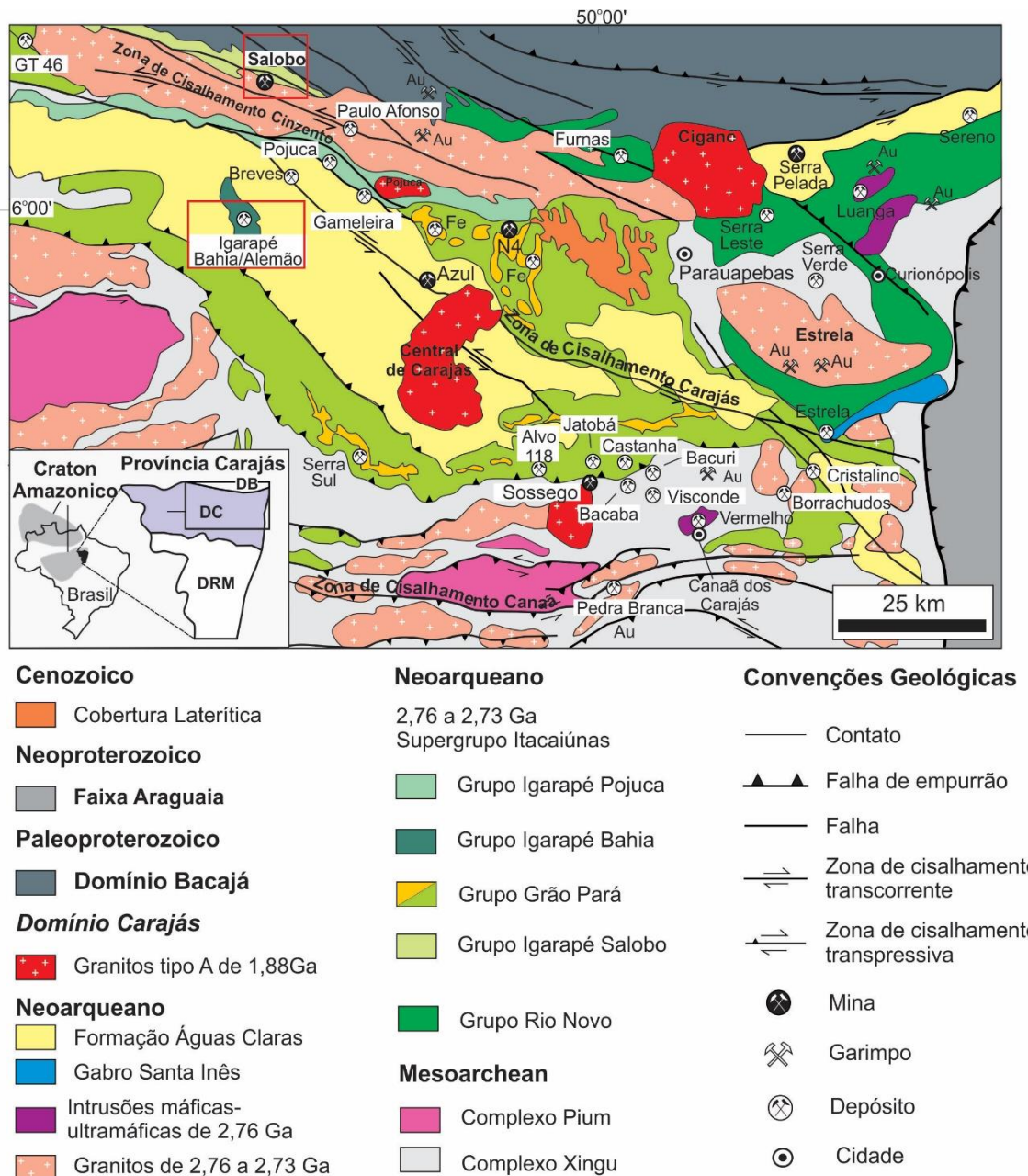


Fig. 2. Mapa geológico do Domínio Carajás com a localização dos principais depósitos minerais da região. As caixas em vermelho mostram a localização dos depósitos Salobo e Igarapé Bahia (modificado de Vasquez *et al.* 2008).

As rochas do embasamento são sobrepostas pelas rochas supracrustais do Grupo Rio Novo (Hirata *et al.* 1982) e do Supergrupo Itacaiúnas (Wirth *et al.* 1986, DOCEGEO 1988, Machado *et al.* 1991). O Grupo Rio Novo compreende anfíbolitos, xistos, metagrauvacas, rochas metavulcânicas tholeíticas e gabros (Hirata *et al.* 1982). O Supergrupo Itacaiúnas foi dividido por DOCEGEO (1988) em unidades aproximadamente cronocorrelatas, designadas de grupos Igarapé Salobo, Igarapé Pojuca, Grão Pará e Igarapé Bahia.

O Grupo Igarapé Salobo, considerado hospedeiro do depósito de óxido de ferro–Cu–Au de Salobo, inclui paragnaisse, anfibolitos, quartzitos, meta-arcósios e formações ferríferas (DOCEGEO 1988). No entanto, anfibolitos, meta-arcósios e formações ferríferas bandadas têm sido reinterpretados como resultantes de intenso hidrotermalismo sobre rochas do embasamento e granitoides da suíte Igarapé Gelado que gerou rochas ricas em grunerita, almandina, turmalina, magnetita e biotita (Lindenamyer 2003, Melo *et al.* 2016), enquanto que o quartzito representa parte da sequência supracrustal do Grupo Igarapé Salobo, ao menos na área da Mina do Salobo (Melo *et al.* 2016).

O Grupo Igarapé Pojuca hospeda o depósito de óxido de ferro–Cu–Au Gameleira e contém rochas metavulcânicas básicas, xistos e rochas com cordierita–antofilita. Essas últimas foram interpretadas como resultantes do metamorfismo de produtos de alteração hidrotermal vulcano-exalativa, possivelmente associada à mineralização de Cu–(Zn–Au–Ag) do depósito de Pojuca, também hospedado nesse grupo (Winter 1994). O Grupo Grão Pará é constituído por metabasaltos, rochas metavulcânicas félsicas e jaspilitos que hospedam os importantes depósitos de ferro em Carajás (DOCEGEO 1988).

O Grupo Igarapé Bahia é dividido em unidade inferior e unidade superior. A unidade inferior é constituída principalmente por rochas metavulcânicas, metapiroclásticas e formações ferríferas bandadas (DOCEGEO 1988). Dados U–Pb em zircão das rochas metavulcânicas apontam para idade de vulcanismo da unidade inferior em 2748 ± 34 Ma (Tallarico *et al.* 2005). A unidade superior compreende rochas metassedimentares interpretadas como resultado de diversos fluxos turbidíticos (DOCEGEO 1988, Dreher *et al.* 2005). Essas rochas foram metamorfisadas em condições de fácies xisto verde inferior, incluindo as rochas que hospedam o depósito de óxido de ferro–Cu–Au Igarapé Bahia/Alemão (DOCEGEO 1988).

A Formação Águas Claras é a unidade que se sobrepõe, aparentemente em discordância angular, às sequências metavulcanossedimentares do Supergrupo Itacaiúnas. É composta por rochas siliciclásticas, representadas em sua base por metapelitos, metaconglomerados e meta-arenitos formados em ambiente marinho a costeiro, enquanto que a sequência de topo compreende meta-arenitos e metaconglomerados depositados em ambiente fluvial a marinho raso (Nogueira *et al.* 1995). Idades Pb–Pb em pirita diagenética apontam para idade de deposição da Formação Águas Claras em 2,06 Ga (Mougeot *et al.* 1996). Por outro lado, idades de

2708 ± 37 Ma de diques máficos intrusivos na sequência, além da população de zircão detritico com idades calculadas de 2645 ± 12 Ma e 2681 ± 5 Ma podem apontar para uma idade de deposição mais antiga (Mougeot *et al.* 1996b, Dias *et al.* 1996, Trendall *et al.* 1998).

Complexos máficos-ultramáficos acamadados representadas pelo Complexo Luanga (ca. 2,76 Ga, Machado *et al.* 1991) e pela Suíte Intrusiva Cateté (Macambira & Vale 1997) interceptam as rochas do embasamento mesoarqueano e da Bacia Carajás, além de hospedarem ocorrências de níquel, crômio e planitóides (Ferreira Filho *et al.* 2007). Corpos intrusivos representados pelo Gabro Santa Inês e pelo Diopsídio Norito Pium também são reconhecidos no Domínio Carajás (Ricci 2006).

O magmatismo granítico no Domínio Carajás é representado por três eventos que ocorreram durante o Neoarqueano (i.e. 2,76–2,73 Ga) e o Paleoproterozoico (i.e. 1,88 Ga). Os granitos de ca. 2,76 a 2,73 Ga são representados pelo corpos Estrela, Igarapé Gelado e *stock* Geladinho na porção norte e pelas suítes Planalto e Plaquê e granitos Serra do Rabo e Cristalino na porção sul do domínio (Huhn *et al.* 1999a, 1999b, Avelar *et al.* 1999, Sardinha *et al.* 2006, Barros *et al.* 2009). Esses granitos são semelhantes aos do tipo A, alcalinos a metaluminosos, considerados como sintectônicos em relação ao desenvolvimento de zonas de cisalhamento transcorrentes (Fig. 3). Granitos de afinidade cálcio-alcalina também são reconhecidos (e.g. Plaquê e Igarapé Gelado; Hunh *et al.* 1999a, Barbosa 2004). Esses corpos graníticos exibem forte deformação com estiramento preferencial na direção NNW-ESE. Alguns desses corpos exibem bandamentos compostionais (e.g. Igarapé Gelado e Estrela, Barbosa 2004, Barros *et al.* 2009, 2009, Melo *et al.* 2016), interpretados como indício de bandamento magmático primário (Barros *et al.* 2009). Foliações anastomosadas com mergulhos subverticais são atribuídas ao desenvolvimento de zonas de cisalhamento sobre estes corpos (Huhn *et al.* 1999a, Barros *et al.* 2009, Sardinha *et al.* 2006). Valores de $\epsilon_{\text{Nd}}(t)$ de $-0,38$ e $-2,06$ e idades modelo T_{DM} 2,97 e 3,19 Ga indicam fontes crustais mesoarqueanas para esses corpos (Barros *et al.* 2004).

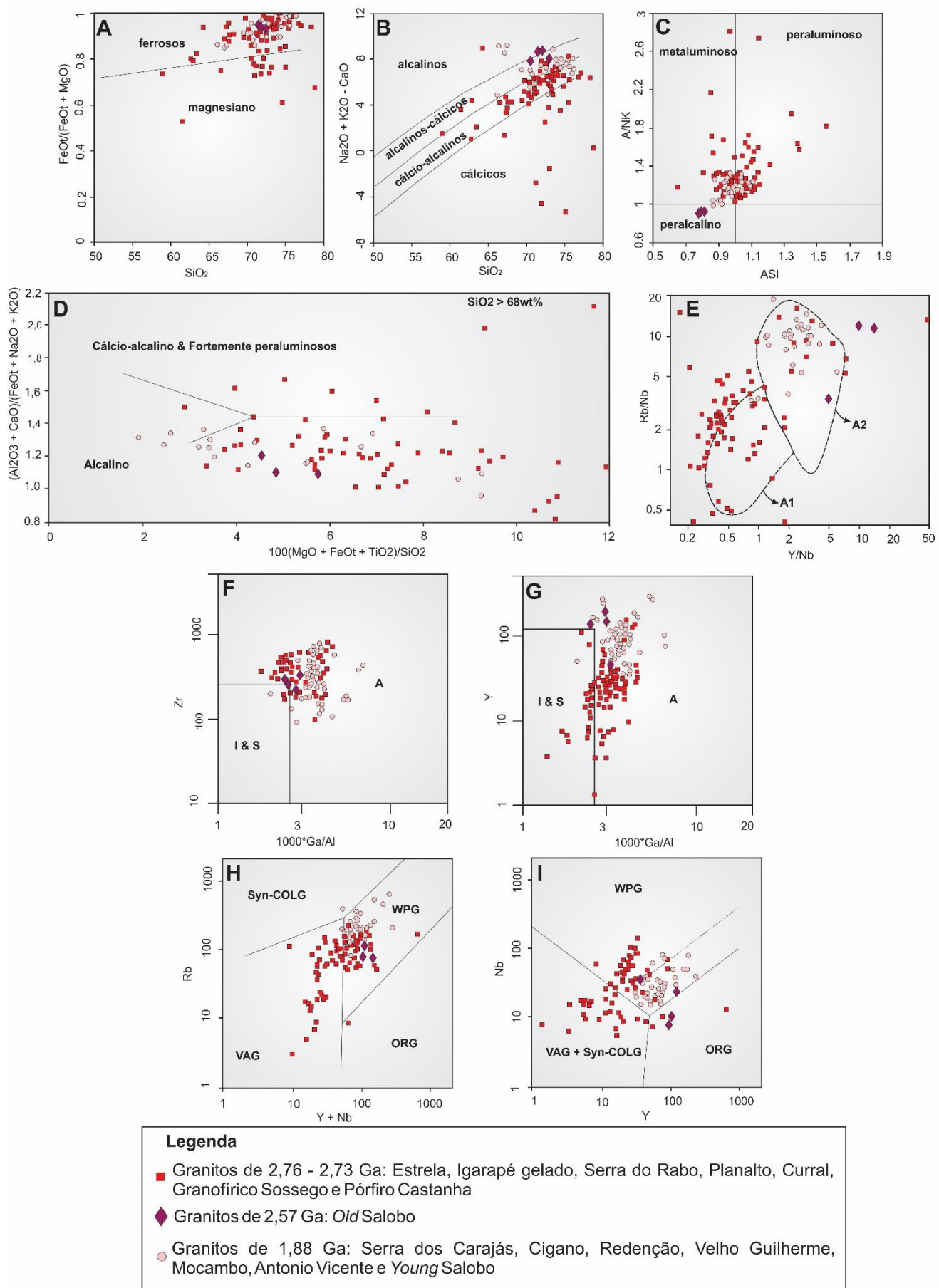


Fig. 3. Compilação de dados geoquímicos dos principais granitos da Província Carajás. Diagramas de discriminação tectônica a), b) e c) de Frost et al. (2001); d) diagrama de discriminação de granitos (>68 % de SiO₂) de Sylvester (1989); e) diagrama de Eby (1992) com discriminação de granitos do tipo A; f) e g) Diagramas de diferenciação de granitos do tipo A de Whalen (1987); h) e i) Diagramas de Pearce et al. (1984) de discriminação de ambiente tectônico. Dados obtidos de Lindenmayer (1990), Barbosa (2004), Dall'Agnol et al. (2005), Barros et al. (2009), Feio (2012).

O magmatismo granítico de 2,57 Ga é mais restrito ou ainda pouco caracterizado no Domínio Carajás e ocorre preferencialmente em sua porção norte. Compreende magmatismo granítico de caráter peralcalino a metaluminoso, ferroso, semelhante aos granitos do tipo A. Esse magmatismo é representado por dois pequenos corpos graníticos deformados que ocorrem ao longo da Zona de Cisalhamento do Cinzento, denominados de granitos *Old Salobo* e *Itacaiúnas* (Machado et al. 1991; Souza et al. 1996), embora novos corpos graníticos com essa idade tenham sido recentemente descritos no depósito GT-46 (Toledo 2017).

Os granitos anorogênicos de 1,88 Ga são agrupados na Suíte Intrusiva Serra dos Carajás, que inclui os granitos Central de Carajás, *Young Salobo*, *Cigano*, *Pojuca* e *Breves* (Machado et al. 1991, Lindenmayer & Teixeira 1999, Tallarico 2003). Correspondem a granitos do tipo A, de natureza intra-placa e caráter metaluminoso a levemente peraluminoso (Dall'Agnol 2005). Dados de Sm-Nd obtidos por Dall'Agnol (2005) mostram idades T_{DM} entre 3,35 a 2,61 Ga e valores de ϵ Nd(t) de -9,7 e -7,9, apontando para fontes crustais meso a neoarqueanas.

4.2 Evolução Geotectônica do Domínio Carajás

O ambiente tectônico para a formação das sequências supracrustais do Grupo Rio Novo e Supergrupo Itacaiúnas ainda permanece motivo de muito debate, embora diversos estudos já tenham sido realizados nesse âmbito (Wirth et al. 1986, Gibbs et al. 1986, DOCEGEO 1988, Meirelles & Dardenne 1991, Teixeira 1994, Lindenmayer et al. 2005, Lobato et al. 2005).

Assinatura geoquímica tholeítica dos basaltos do Grupo Grão Pará e a presença de magmatismo bimodal no Supergrupo Itacaiúnas parecem constituir fortes evidências de que as sequências supracrustais se formaram em um ambiente de rifte continental (Wirth et al. 1986, Gibbs et al. 1986, DOCEGEO 1988, Olszewski et al. 1989). Uma nova abordagem geoquímica para os basaltos da Formação Parauapebas, Grupo Grão Pará, mostram que essas rochas são resultados de um processo de rifteamento de uma

crosta continental mais antiga (Martins *et al.* 2017). Neste caso, o processo de rifteamento teria ocorrido em um regime extensional desenvolvido em ambiente pós orogênico na passagem do Meso para o Neoarqueano (Martins *et al.* 2017).

Por outro lado, afinidade cálcio-alcalina também foi caracterizada em basaltos do Grupo Grão Pará e em rochas intrusivas por alguns autores (Meirelles & Dardenne 1991, Teixeira 1994, Lindenmayer *et al.* 2005, Lobato *et al.* 2005), sugerindo que essas rochas teriam se formado em ambiente de arco magmático. Alternativamente, Zucchetti (2007) considerou que os metabasaltos do Grupo Grão Pará possuem características geoquímicas de arco continental, porém extravasados sobre crosta continental em ambiente de retroarco.

A Província Carajás apresenta principalmente estruturas com direção NW-SE e E-W. A formação dessas estruturas parece estar relacionada a um encurtamento com vetor de convergência de NNE para SSW que produziu foliação WNW-ESE, dobramento e falhamentos reversos e transcorrentes (Pinheiro *et al.* 2013).

De acordo com Araújo *et al.* (1988) essas estruturas desenvolveram-se a partir de um regime de transtruturação dextral permitindo a formação de uma bacia do tipo *pull-apart* e criando os sistemas transcorrentes de Carajás e Cinzento. Essa bacia foi posteriormente invertida por transpressão sinistral em uma estrutura em flor positiva (Araújo *et al.* 1988).

Alternativamente, Pinheiro & Holdsworth (1997) e Holdsworth & Pinheiro (2000) sugerem que as rochas supracrustais do Supergrupo Itacaiúnas se depositaram sobre o embasamento mesoarqueano deformado por transpressão sinistral. Um segundo evento de transpressão sinistral ocorreu durante a deposição dessas rochas e foi responsável pela inversão da bacia, que deve ter durado de 2,7 a 2,6 Ga (Domingos 2009). Essa transpressão foi acompanhada por metamorfismo em condições compatíveis com xisto verde média a alta (Domingos 2010). Transtruturação dextral foi responsável pela formação dos sistemas transcorrentes de Carajás e do Cinzento (Pinheiro & Holdsworth 1997, Holdsworth & Pinheiro 2000).

Estudos recentes propõem a divisão do Domínio Carajás em três domínios estruturais, representados pelas zonas de cisalhamento transcorrentes de: (i) Carajás; (ii) Cinzento; e (iii) Canaã, com idades de ca. 2,7–2,5 Ga. Os sistemas Carajás e Cinzento correspondem a grandes zonas de transcorrência de direção NW-SE com intensa deformação ao longo desses segmentos (Pinheiro *et al.* 2013). A sul de tais sistemas, encontra-se a Zona de Cisalhamento Canaã, caracterizada por transpressão sinistral de

direção E-W (Pinheiro *et al.* 2013). A presença dessas zonas de cisalhamento parece ter grande importância na formação do formato sigmoidal da Bacia Carajás (Pinheiro *et al.* 2013).

A relação das estruturas regionais principais e eventos tectono-termais na Província Carajás tem sido discutida de acordo com uma complexa evolução proposta por Tavares (2015). Essa evolução pode ser sumarizada na tabela 1.

Tabela. 1. Eventos tectono-termais que afetaram a porção nordeste da Província Carajás (Tavares 2015).

Idade	Regime Tectônico	Descrição
0,22 – 0,10 Ga	Extensão (?)	Reflexos da abertura do oceano Atlântico equatorial
0,55 – 0,50 Ga (?)	Compressão	Reflexo do Cinturão Araguaia
0,75 Ga (?)	Extensão	Reflexo da abertura do <i>rift</i> Araguaia
1,93 – 1,85 Ga	Extensão	Colapso orogenético e magmatismo pós-tectônico
2,01 – 1,93 Ga	Compressão	Colisão Carajás-Oeste Africano (Evento Sereno)
2,10 – 2,05 Ga	Compressão	Colisão Carajás-Bacajá (Orógeno Transamazônico)
2,61 – 2,52 Ga	Extensão	Fragmentação do paleocontinente Carajás
2,68 – 2,63 Ga (?)	Compressão	Inversão da Bacia Carajás (reativação do Cinturão Itacaiúnas)
2,76 – 2,68 Ga	Extensão	Abertura e evolução do <i>rift</i> Carajás
2,87 – 2,83 Ga	Compressão	Colisão Rio Maria-Carajás (Cinturão Itacaiúnas)

5. DEPÓSITOS IOCG NO DOMÍNIO CARAJÁS

5.1 Características gerais dos depósitos IOCG

O Domínio Carajás, na porção norte da Província Carajás, contém uma grande concentração de depósitos de óxido de ferro-cobre-ouro (*iron oxide–copper–gold deposits* ou IOCG; Hitzman *et al.* 1992) de classe mundial e possui grande importância global juntamente com depósitos de outros distritos IOCG mundiais, tais como os dos Andes Central (Chile e Peru; e.g. depósitos Candelária, Manto Verde e Raul Condestable; Sillitoe 2003, Marschik *et al.* 2003, Haller *et al.* 2006, Rieger *et al.* 2012), do Cráton Gawler (Austrália; e.g. depósitos Olympic Dam e Prominent Hill; Haynes *et al.* 2005, Skirrow 2003, Skirrow *et al.* 2007) e do distrito de Cloncurry (Austrália; e.g. depósitos Ernest Henry e Starra; Mark *et al.* 2005, Duncan *et al.* 2009).

A Província Carajás hospeda uma grande quantidade de depósitos IOCG de classe mundial, que incluem Salobo (1112 Mt @ 0,69 wt% Cu, 0,43 g/t Au, 55 g/t Ag; VALE 2012), Cristalino (500 Mt @ 1,0 wt% Cu; 0,3 g/t Au, Huhn *et al.* 1999), Sossego (355 Mt @ 1,1 % Cu e 0,28 g/t Au; Lancaster Oliveira *et al.* 2000), Igarapé Bahia/Alemão (219 Mt @ 1,4 wt% Cu, 0,86 g/t Au; Tallarico *et al.* 2005) e Alvo 118 (70 Mt @ 1,0 wt% Cu, 0,3 g/t Au, Rigon 2000). No entanto, há ainda uma grande variedade de outros depósitos em avaliação, com grande importância para o conhecimento geológico da região, que incluem os depósitos Igarapé Cinzento/GT46, Furnas, Paulo Alfonso e Grotá Funda no norte, e Castanha, Bacaba, Bacuri, Jatobá, Visconde, Borrachudos e Pantera no sul.

Diferentes modelos de depósitos minerais já foram propostos para os depósitos cupríferos, ricos em óxidos de ferro, de Carajás. A gênese dos depósitos de Salobo e Igarapé Bahia foi inicialmente atribuída a modelos singenéticos ou híbridos que incluem estágios de mineralização vulcano-exalativa (Lindenmayer, 1990; Vieira *et al.* 1998, Almada & Villas, 1999, Dreher 2004, Dreher *et al.* 2008). Huhn & Nascimento (1997) foram os primeiros a indicar que esses depósitos poderiam fazer parte da classe de depósitos IOCG, definida por Hitzman *et al.* (1992), tendo como depósito-tipo o gigante Olympic Dam, na Austrália. Esse modelo foi adotado em estudos posteriores (Réquia *et al.* 2003, Tallarico *et al.* 2005, Monteiro *et al.* 2008a, 2008b, Xavier *et al.* 2012, Monteiro *et al.* 2014, Silva *et al.* 2015, Moreto *et al.* 2015a,b).

Apesar das singularidades de cada depósito, os depósitos de óxido de ferro-cobre-ouro de Carajás apresentam algumas similaridades que incluem: (i) associação espacial e temporal com o desenvolvimento de zonas de cisalhamento; (ii) associação com brechas hidrotermais; (ii) alteração potássica (<450°C) com biotita e feldspato potássico espacialmente associada às zonas mineralizadas; (iii) formação de magnetita seguida por precipitação de sulfetos, (vi) cloritização, alteração cárnea tardia (clorita-epidoto-calcita) ou hidrolítica (sericita-hematita) desenvolvidas a menores temperaturas (< 350 °C) e condições rúpteis, coevas com a precipitação do minério nas porções mais rasas do(s) sistema hidrotermal(is), (vii) coexistência de fluidos com elevadas e baixas temperaturas de homogeneização (100 a 570 °C) e salinidades baixas a muito elevadas (0 a 69% eq. peso NaCl), indicando a mistura de fluidos de origens diversas que possibilitaram o transporte e precipitação dos metais (Monteiro *et al.* 2008, Xavier *et al.* 2012, Monteiro *et al.* 2014).

Os depósitos IOCG de Carajás situam-se preferencialmente ao longo ou próximo a grandes estruturas regionais de direção WNW-ESE (Xavier *et al.* 2012). Os depósitos da porção norte situam-se preferencialmente nas Zonas de Cisalhamento do Cinzento e de Carajás (Xavier *et al.* 2012), enquanto que os depósitos do Cinturão Sul do Cobre localizam-se ao longo da Zona de Cisalhamento Canaã dos Carajás (Pinheiro *et al.* 2013).

Os depósitos da porção norte, que incluem principalmente Salobo, Igarapé Bahia, Igarapé Cinzento/GT46 e Furnas, parecem mostrar algumas diferenças em relação aos depósitos localizados no Cinturão Sul do Cobre. O depósito de Salobo apresenta associação hidrotermal de mais alta temperatura, incluindo faialita e granada (Lindenmayer 2003, Melo *et al.* 2016). Associações minerais com *end-members* ricos em ferro, como almandina e grunerita, além da grande presença de turmalina próxima às zonas mineralizadas, são características comuns desses depósitos (Lindenmayer 2003, Tallarico *et al.* 2005, Silva *et al.* 2005, Xavier *et al.* 2008, Melo *et al.* 2016).

No Cinturão Sul do Cobre, os depósitos de classe mundial, Sossego, Cristalino e Alvo 118, e vários outros em avaliação (Bacaba, Bacuri, Castanha, Jatobá, Visconde, GT 34) apresentam extensas zonas de alteração alcalina (sódica e potássica), a presença de zonas com escapolita (e.g. Bacaba, Bacuri, Castanha, Jatobá e Borrachudos) e o reconhecimento de feições tardias rúpteis nesses depósitos (Monteiro *et al.* 2008a; 2008b, Augusto *et al.* 2008, Craveiro 2011, Pestilho 2011, Torresi *et al.* 2012, Melo *et al.* 2014).

Os modelos genéticos para os depósitos IOCG de Carajás os vinculam a sistemas (i) não-magmáticos, (ii) magmático-hidrotermais e/ou (iii) híbridos que envolvem fluidos magmáticos e não magmáticos (Xavier *et al.* 2012). O modelo não-magmático foi especificamente proposto para os depósitos Salobo e Igarapé Bahia, nos quais processos vulcano-exalativos teriam sido responsáveis pela mineralização cuprífera singenética (Lindenmayer, 1990, Almada & Villas, 1999, Dreher, 2004, Dreher *et al.*, 2008). O modelo magmático-hidrotermal tem sido relacionado por alguns autores a um dos três eventos de granitogênese reconhecidos no Domínio Carajás em: (i) ca. 2,76 a 2,73 Ga (Galarza *et al.* 2003), (ii) ca. 2,57 Ga (Réquia *et al.* 2003, Tallarico *et al.* 2005, Grainger *et al.* 2008), e (iii) ca. 1,88 Ga (Pimentel *et al.* 2003, Silva *et al.* 2005). O evento de ca. 2,57 Ga seria responsável pelo estabelecimento de sistemas magmáticos-hidrotermais regionais (Tallarico *et al.* 2005, Tavaza & Oliveira 2000, Réquia *et al.* 2003, Grainger *et al.* 2008), possibilitando a geração e circulação de fluidos em grande escala, ainda que a ocorrência desses corpos seja espacialmente restrita. Alternativamente, sistemas híbridos com participação com fluidos externamente derivados e componentes magmáticos têm sido proposto para os depósitos IOCG de Carajás (Monteiro *et al.* 2008a).

5.2 Geocronologia dos depósitos IOCG de Carajás

Estudos geocronológicos relacionados à caracterização do *timing* das mineralizações IOCG (e.g. Réquia *et al.* 2003, Tallarico *et al.* 2005, Silva *et al.* 2005, Moreto *et al.* 2015a,b) mostram uma complexa evolução desses depósitos (Fig. 4, Tab. 2).

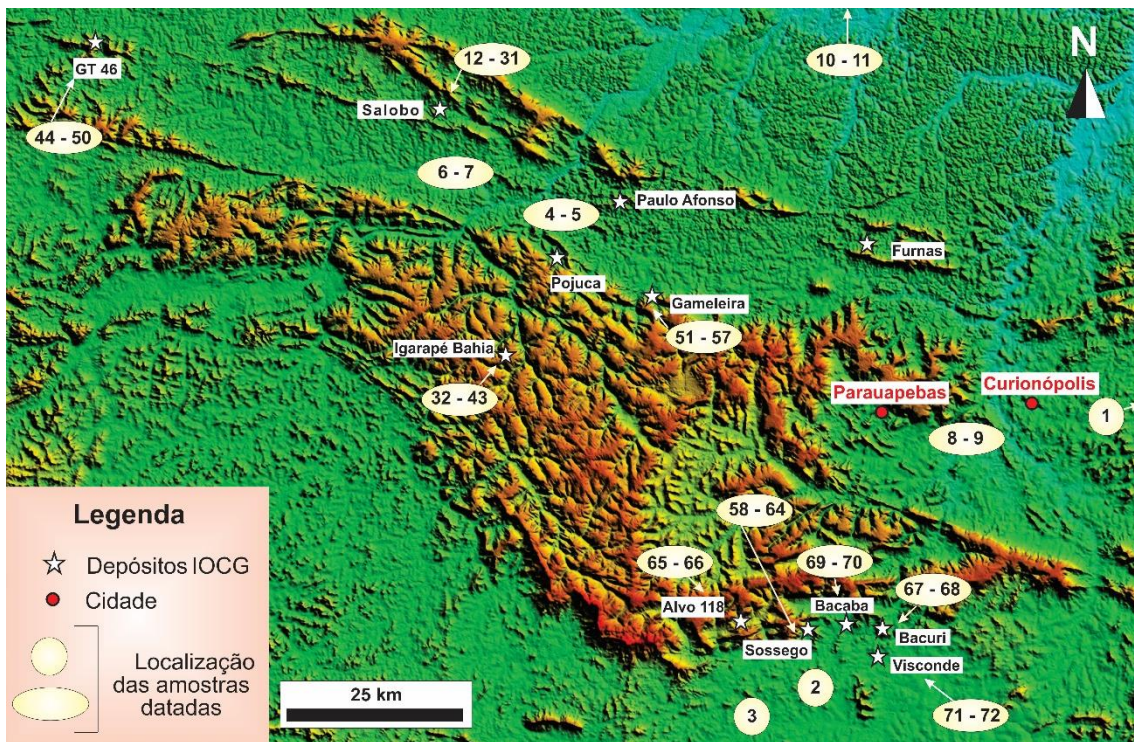


Fig. 4. Imagem SRTM com a localização dos principais depósitos IOCG e dos dados geocronológicos da Tabela 2 no Domínio Carajás. Veja tabela 2 para informações das amostras datadas (extraído de Melo et al. 2016).

Na porção norte do Domínio Carajás, dados geocronológicos disponíveis para os depósitos Salobo (2576 ± 8 Ma e 2562 ± 8 Ma, Re–Os em molibdenita, Réquia *et al.* 2003) e Igarapé Bahia (2575 ± 12 Ma; U–Pb em monazita, Tallarico *et al.* 2005) apontam para formação sincrônica desses em um evento metalogenético em ca. 2,57 Ga. Essas idades são próximas à da cristalização do granito Old Salobo (2573 ± 2 Ma, $2547 \pm 5,3$ Ma; U–Pb zircão; Machado *et al.* 1991, Melo *et al.* 2016), sugerindo que intrusões dessa idade teriam importante papel no estabelecimento de extensos sistemas magmático-hidrotermais responsáveis pela gênese dos depósitos IOCG de Carajás (Tallarico *et al.* 2005, Grainger *et al.* 2008, Groves *et al.* 2010).

No entanto, idades relativas à Zona de Cisalhamento do Cinzento (2555 ± 4 Ma, Machado *et al.* 1991) e idades mais jovens em monazita hidrotermal (2452 ± 14 Ma; Melo *et al.* 2016) sugerem que ao menos a formação do depósito Salobo está ligada a sucessivas reativações da Zona de Cisalhamento do Cinzento possivelmente associadas com pulsos hidrotermais.

O depósito Gameleira, também localizado na porção norte do Domínio Carajás, exibe diversas idades interpretadas como de mineralização (2614 ± 14 Ma, Re–Os em molibdenita; Marshick *et al.* 2005, 2419 ± 12 Ma, 2217 ± 19 Ma e 2180 ± 84 Ma, Pb–Pb calcopirita, Galarza & Macambira, 2002; 1734 ± 8 Ma, Ar–Ar em biotita, Pimentel *et al.* 2003), dependendo do método utilizado. De forma análoga, o depósito de Igarapé Cinzento/GT46, localizado no mesmo *trend* do depósito Salobo, mostra tanto idades neoarqueanas (2711 ± 9 Ma e 2554 ± 8 Ma, Re–Os em molibdenita, Silva *et al.* 2005) como paleoproterozoicas (1809 ± 6 Ma e 1845 ± 5 Ma, Ar–Ar em biotita, Silva *et al.* 2005) para fases minerais hidrotermais e de minério.

Nos depósitos IOCG localizados no Cinturão Sul do Cobre, idades Re–Os em molibdenita e U–Pb em monazita evidenciaram que tais depósitos foram formados em múltiplos eventos hidrotermais durante o Neoarqueano (2,71 a 2,68 Ga; Corpos Sequeirinho e Pista no depósito Sossego e depósitos Bacaba e Bacuri) e Paleoproterozoico (1,88 Ga; Corpo Sossego no depósito Sossego e depósito Alvo 118; Tallarico 2003, Moreto *et al.* 2015a,b).

Tabela. 2. Dados geocronológicos das principais unidades regionais, alteração hidrotermal e mineralização dos depósitos IOCG do Domínio Carajás.

Amostra	Rocha/Mineral	Idade (Ma)	Método	Referência
UNIDADES				
1	Migmatito Complexo Xingu	2859 ±2	U–Pb em zircão	Machado <i>et al.</i> 1991
2	Migmatito Complexo Xingu	3066 ± 6,6	U–Pb em zircão	Delinardo da Silva 2014
3	Granulitos Máficos Complexo Pium	3002 ±14	U–Pb em zircão	Pidgeon <i>et al.</i> 2000
4	Suíte Igarapé Gelado	2731 ±3 2508 ±14 2588 ±5	Pb–Pb em zircão	Barbosa 2004
5	Suíte Igarapé Gelado	2533 ±7 2576 ±4 2574 ±8	Pb–Pb em zircão	Barbosa 2004
6	Granito Itacaiúnas	2560 ±37	Pb–Pb em zircão	Souza <i>et al.</i> 1996
7	Granito Itacaiúnas	2480 ±40	Rb–Sr em rocha total	Montavão <i>et al.</i> 1984
8	Granito Estrela	2763 ±4,4	Pb–Pb em zircão	Barros <i>et al.</i> 2009
9	Granito Estrela	2527 ±34	Rb–Sr em rocha total	Barros & Barbey 1998
10	Gnaisses Tonalíticos	2503 ±10	U–Pb em zircão Pb–Pb	Santos 2003
11	Gnaisses Tonalíticos	2440 ±7	evaporção em zircão	Vasquez <i>et al.</i> 2005
DEPÓSITOS IOCG				
SALOBO				
12	Rochas ricas em magnetita	2551 ±2	U–Pb em monazita	Machado <i>et al.</i> 1991
13	Rochas ricas em anfibólio	2581 ±5	U–Pb em titanita	Machado <i>et al.</i> 1991
14	Rochas ricas em anfibólio	2497 ±5	U–Pb em titanita	Machado <i>et al.</i> 1991
15	Rochas ricas em anfibólio	2555 +4/-3	U–Pb em zircão	Machado <i>et al.</i> 1991
16	Granito Old Salobo	2573 ±2	U–Pb em zircão	Machado <i>et al.</i> 1991
17	Veio granítico	2758	U–Pb em zircão	Machado <i>et al.</i> 1991
18	Anfibolito foliado	2761 ±3	U–Pb em zircão	Machado <i>et al.</i> 1991
19	Rochas com alteração pós-mineralização	2950 ±25	U–Pb em zircão	Melo <i>et al.</i> 2016
20	Gnaisse Cascata	2763 ±4,4	U–Pb em zircão	Melo <i>et al.</i> 2016
21	Gnaisse Cascata	2701 ±30	U–Pb em zircão	Melo <i>et al.</i> 2016
22	Granito Old Salobo	2547 ±5,3	U–Pb em zircão	Melo <i>et al.</i> 2016
23	Minério Salobo	2535 ±8,4	U–Pb em zircão	Melo <i>et al.</i> 2016
24	Minério Salobo	2452 ±14	U–Pb em monazita	Melo <i>et al.</i> 2016
25	Magnetita	2112 ±12	Pb–Pb em magnetita	Tassinari <i>et al.</i> 2003
26	Calcopirita	2427 ±130	Pb–Pb em calcopirita	Tassinari <i>et al.</i> 2003
27	Molibdenita	2562 ±8	Re–Os em molidbenita	Réquia <i>et al.</i> 2003
28	Molibdenita	2576 ±8	Re–Os molidbenita	Réquia <i>et al.</i> 2003
29	Bornita-calcopirita	2579 ±71	Pb–Pb em bornita	Réquia <i>et al.</i> 2003
30	Turmalina	2587 ±150	Pb–Pb em	Tassinari <i>et al.</i> 2003

31	Calcocita	2705 ± 42	turmalina Pb–Pb em calcocita	Tassinari <i>et al.</i> 2003
IGARAPÉ BAHIA				
32	rocha metavulcânica máfica	2748 ± 34	U–Pb em zircão	Tallarico <i>et al.</i> 2005
33	Rocha metavulcânica máfica	2758 ± 75	Sm–Nd em rocha total	Galarza <i>et al.</i> 2003
34	Rocha metavulcânica máfica	2776 ± 12	Pb–Pb em rocha total	Galarza <i>et al.</i> 2003
35	Rocha metavulcânica máfica	2745 ± 1	Pb–Pb em zircão	Galarza <i>et al.</i> 2008
36	Calcopirita	2385 ± 122	Pb–Pb	Galarza <i>et al.</i> 2008
37	Calcopirita	2417 ± 120	Pb–Pb	Galarza <i>et al.</i> 2008
38	Monazita da brecha mineralizada	2575 ± 12	U–Pb (*)	Tallarico <i>et al.</i> 2005
39	Ouro	2744 ± 12	Pb–Pb	Galarza <i>et al.</i> 2008
40	Calcopirita (rocha metapioclástica)	2754 ± 36	Pb–Pb	Galarza <i>et al.</i> 2008
41	Calcopirita (rocha Metavulcânica máfica)	2756 ± 24	Pb–Pb	Galarza <i>et al.</i> 2008
42	Calcopirita (brecha hidrotermal)	2772 ± 46	Pb–Pb	Galarza <i>et al.</i> 2008
43	Calcopirita (rocha intrusiva máfica)	2777 ± 22	Pb–Pb	Galarza <i>et al.</i> 2008
GT 46 – IGARAPÉ CINZENTO				
44	Brecha mineralizada	1752 ± 77	Sm–Nd em rocha total	Silva <i>et al.</i> 2005
45	Biotita (alteração potássica)	1810 ± 15	Ar–Ar	Silva <i>et al.</i> 2005
46	Biotita (alteração potássica)	1858 ± 7	Ar–Ar	Silva <i>et al.</i> 2005
47	Molibdenita de pegmatito	2554 ± 8	Re–Os	Silva <i>et al.</i> 2005
48	Molibdenita de granito pegmatítico	2557 ± 8	Re–Os	Silva <i>et al.</i> 2005
49	Molibdenita de granito	2600 ± 8	Re–Os	Silva <i>et al.</i> 2005
50	Molibdenita de anfibolito	2711 ± 9	Re–Os	Silva <i>et al.</i> 2005
GAMELEIRA				
51	Veios com biotita de sulfetos	1700 ± 31	Sm–Nd em rocha total	Pimentel <i>et al.</i> 2003
52	Alteração potássica com biotita	1734 ± 8	Ar–Ar em biotita	Lindenmayer <i>et al.</i> , 2001; Pimentel <i>et al.</i> 2003
53	Veio de quartzo-grunerita-ouro	1837 ± 30	Sm–Nd em rocha total	Lindenmayer <i>et al.</i> 2001
54	Granada-biotita xisto	1958 ± 230	Sm–Nd em rocha total	Pimentel <i>et al.</i> 2003
55	Concentrados de calcopirita	$2180 \pm 84, 2217 \pm 19$	Pb–Pb em calcopirita	Galarza and Macambira 2002
56	Calcopirita de veios de quartzo	2419 ± 12	Pb–Pb em calcopirita	Galarza and Macambira 2002
57	Molibdenita	2614 ± 14	Re–Os em molibdenita	Marschik <i>et al.</i> 2005
SOSSEGO				
58	Corpo Sequeirinho: brecha	$3076 \pm 5,3$	U–Pb em zircão	Moreto <i>et al.</i> 2015a
59	Corpo Sequeirinho: brecha	$2712 \pm 4,7$	U–Pb em monazita	Moreto <i>et al.</i> 2015a
60	Corpo Sequeirinho: metavulcânica Pista	2685 ± 11	Re–Os em molibdenita	Moreto <i>et al.</i> 2015a
61	Corpo Sossego: Metavulcânica Pista com alteração Na	2710 ± 11	Re–Os em molibdenita	Moreto <i>et al.</i> 2015a
62	Corpo Sossego: brecha	$1879 \pm 4,1$	U–Pb em	Moreto <i>et al.</i> 2015a

63	Corpo Sossego: brecha	$1904 \pm 5,2$	monazita U–Pb em monazita	Moreto <i>et al.</i> 2015a
64	Corpo Sossego: brecha	$1890 \pm 8,5$	U–Pb em monazita	Moreto <i>et al.</i> 2015a
ALVO 118				
65	Brecha mineralizada	1868 ± 7	U–Pb em xenotima	Tallarico, 2003
66	Brecha mineralizada	1869 ± 7	U–Pb em xenotima	Tallarico, 2003
BACURI				
67	Alteração clorítica	$2703 \pm 6,2$	U–Pb em monazita	Moreto <i>et al.</i> 2015b
68	Molibdenita em veio cortando o Granito Serra Dourada	2758 ± 11	Re–Os em molibdenita	Moreto <i>et al.</i> 2015b
BACABA				
69	Granito Serra Dourada com alteração Na-Ca	2720 ± 15	U–Pb em monazita	Moreto <i>et al.</i> 2015b
70	Monazita da brecha mineralizada	$2060 \pm 9,6$	U–Pb em monazita	Moreto <i>et al.</i> 2015b
VISCONDE				
71	Minério Visconde	2729 ± 150	Pb–Pb em calcopirita	Silva <i>et al.</i> 2015
72	Minério Visconde	2736 ± 100	Pb–Pb em calcopirita	Silva <i>et al.</i> 2015

Esses dados evidenciam a complexidade da formação desses depósitos em relação aos diferentes eventos tectono-magmáticos registrados na Província Carajás. Adicionalmente, os eventos metalogenéticos IOCG de Carajás parecem estar distribuídos também no espaço. Idades de ca. 2,57 Ga são escassas no Cinturão Sul do Cobre, uma vez que apenas datações Pb–Pb em calcopirita do depósito Sossego registraram tais idades (2574 ± 130 Ma, 2530 ± 25 Ma, Neves 2006). Por outro lado, as idades de ca. 2,7 Ga parecem ser restritas ou ainda pouco caracterizadas na parte norte do Domínio Carajás.

5.3 Geoquímica isotópica na caracterização dos depósitos IOCG de Carajás

A caracterização da natureza dos fluidos mineralizantes em depósitos IOCG tem sido motivo de diversos estudos. Os principais modelos genéticos propostos envolvem fluidos de fontes (i) magmáticas (Pollard 2000, Tornos *et al.* 2012) e (ii) não-magmáticas, incluindo fluidos metamórficos, bacinais ou mesmo derivados de sequências evaporíticas (Jong and Williams 1995, Barton & Johnson 1996, Xavier *et al.* 2008).

A Província Carajás apresenta uma complexa história tectono-magmática especialmente durante o Meso e Neoarqueano. Contudo, a porção norte dessa província,

na qual se localizam os depósitos Salobo e Igarapé-Bahia, parece ter também influência de um evento tectônico paleoproterozoico em ca. 2,05 Ga, bem caracterizado no Domínio Bacajá ao norte da província (Teixeira *et al.* 1989, Vasquez *et al.* 2008, Tavares 2015). Por fim, magmatismo anorogênico em ca. 1,88 Ga é amplamente reconhecido na província. Essa complexa evolução se reflete na formação dos depósitos IOCG de Carajás, especialmente no que diz respeito à natureza e circulação dos fluidos mineralizantes.

Estudos de isótopos estáveis apontam para intensa interação fluido-rocha durante a formação dos depósitos IOCG de Carajás (Fig. 5). No depósito Igarapé Bahia, por exemplo, valores de $\delta^{13}\text{C}$ entre $-6,7$ e $-13,4\text{\textperthousand}$ indicam que o carbono pode ter origem magmática, enquanto que os dados de $\delta^{18}\text{O}_{\text{H}_2\text{O}}$ ($+5$ a $+16,5\text{\textperthousand}$) em equilíbrio com magnetita, quartzo e siderita sugerem que esses fluidos eram oriundos de fontes magmáticas e/ou interagiram com rochas, principalmente sedimentares, ricas em ^{18}O (Dreher *et al.* 2008). As assinaturas isotópicas dos fluidos em equilíbrio com actinolita no depósito Sossego ($+6,9\text{\textperthousand}$), calcita no Alvo 118 ($-1,0$ e $+7,5\text{\textperthousand}$) e actinolita e magnetita no depósito Visconde ($+4,2$ e $+9,4\text{\textperthousand}$) apontam para a participação de fluidos magmáticos e/ou formacionais/metamórficos (Monteiro *et al.* 2008a, Torresi *et al.* 2011, Silva *et al.* 2015). Os três depósitos mostraram ainda valores de $\delta^{18}\text{O}_{\text{H}_2\text{O}}$ menores durante a mineralização e os estágios de alteração hidrotermal de mais baixa temperatura, o que indica que fluidos meteóricos tiveram importância durante a precipitação do minério (Monteiro *et al.* 2008a, Torresi *et al.* 2011, Silva *et al.* 2015).

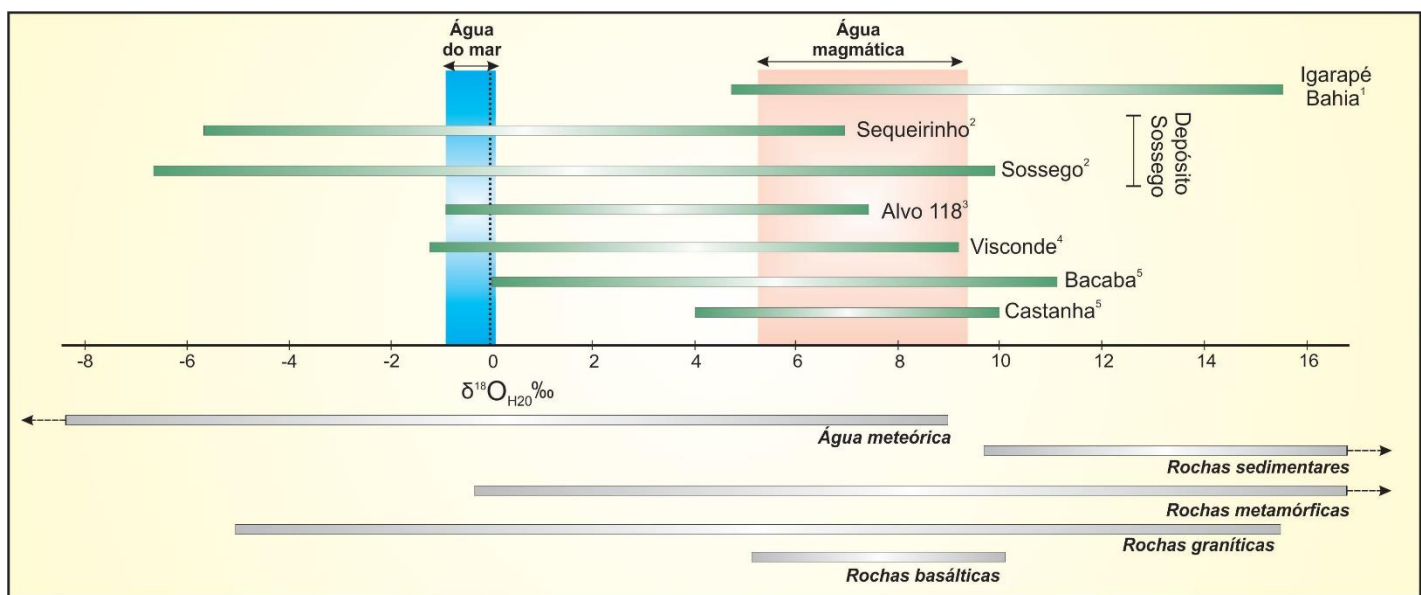


Fig. 5. Dados relativos à composição isotópica de oxigênio ($\delta^{18}\text{O}_{\text{H}_2\text{O}}$) dos fluidos em equilíbrio com minerais hidrotermais de depósitos IOCG da Província Carajás, obtidos de: 1- Dreher *et al.* 2008, 2 – Monteiro *et al.* 2008, 3 – Torresi *et al.* 2011, 4 – Silva *et al.* 2015, 5 – Pestillo 2011. Campos da água do mar e água magmática são extraídos de Taylor (1997). Distribuição de valores de $\delta^{18}\text{O}$ para água meteórica, rochas sedimentares, rochas metamórficas, rochas graníticas e rochas basálticas obtidos de Hoefs (2007).

Os valores de $\delta^{34}\text{S}$ em sulfetos variam entre os depósitos da porção norte do Domínio Carajás (Fig. 6). O depósito Salobo mostra valores ($\delta^{34}\text{S}_{\text{cpy}} = +0,2$ a $+1,6\text{\textperthousand}$, Réquia & Fontboté 2001) compatíveis com os do enxofre derivado de fonte magmática. O depósito Igarapé Bahia, por outro lado, apresenta maior variação dos valores de $\delta^{34}\text{S}$ ($-2,1\text{\textperthousand}$ a $5,6\text{\textperthousand}$, Villas *et al.* 2001, Galarza *et al.* 2008, Dreher *et al.* 2008), que são próximos ao do enxofre magmático, mas incluem valores mais elevados que poderiam ser adquiridos através da redução de sulfato da água do mar. Estudos recentes de múltiplos isótopos de enxofre ($\Delta^{33}\text{S}_{\text{V-CDT}}$ e $\Delta^{36}\text{S}_{\text{V-CDT}}$) evidenciam que tanto os depósitos IOCG neoarqueanos quanto os paleoproterozoicos mostram presença de MIF (*mass independent fractionation*) dos isótopos de enxofre (Santiago 2016). Assinaturas negativas e positivas de $\Delta^{33}\text{S}_{\text{V-CDT}}$ e $\Delta^{36}\text{S}_{\text{V-CDT}}$ sugerem que espécies oxidadas (sulfato) e reduzidas de enxofre estavam presentes durante a formação dos sulfetos nesses depósitos (Santiago 2016). Esses dados revelam uma mistura de sulfato da água do mar, caracterizado pelo efeito MIF, e de enxofre de origem magmática nesses depósitos (Santiago 2016).

Os depósitos do Cinturão Sul do Cobre mostram uma clara distinção entre a assinatura isotópica de enxofre dos depósitos neoarquenos e os paleoproterozoicos. No depósito Sossego, o corpo Pista-Sequeirinho exibe valores de $\delta^{34}\text{S}$ próximos a +2,2‰, enquanto que o corpo Sossego-Currall tem valores de $\delta^{34}\text{S}$ de até +7,6‰ (Monteiro et al. 2008a). Esses valores mostram uma participação maior de fluidos externamente derivados como fonte do enxofre para o corpo paleoproterozoico Sossego-Currall (Monteiro et al. 2008a). Por outro lado, os depósitos menores próximos ao depósito Sossego, que incluem Castanha (+0,1 a +3‰), Bacuri (-0,8 a +1,1‰), Visconde (-1,2 a +3,4‰) e Jatobá (+0,9 a +1,8‰) (Pestilho 2011; Silva *et al.* 2015) mostram uma menor variação nos valores de $\delta^{34}\text{S}$, o que sugere que boa parte do enxofre seja de fonte magmática. A exceção é o depósito Bacaba que exibe uma variação maior nos valores de $\delta^{34}\text{S}$ (+1,3 a +5,4‰, Pestilho 2011), o que pode sugerir fontes externas para o enxofre nesse depósito.

Isótopos de boro nos Salobo e Igarapé Bahia sugerem que o boro e as altas salinidades dos fluidos mineralizantes sejam resultantes de evaporitos marinhos (Xavier *et al.* 2008). Por outro lado, isótopos de cloro combinados com razões Cl/Br e Na/Cl realizados nos depósitos Salobo, Igarapé Bahia, Sossego, Gameleira e Alvo 188 indicam que esses depósitos tiveram grande contribuição de fluidos residuais da evaporação da água do mar (*bittern fluids*) que se misturaram com salmoras magmáticas (Chiaradia *et al.* 2006, Xavier *et al.* 2009).

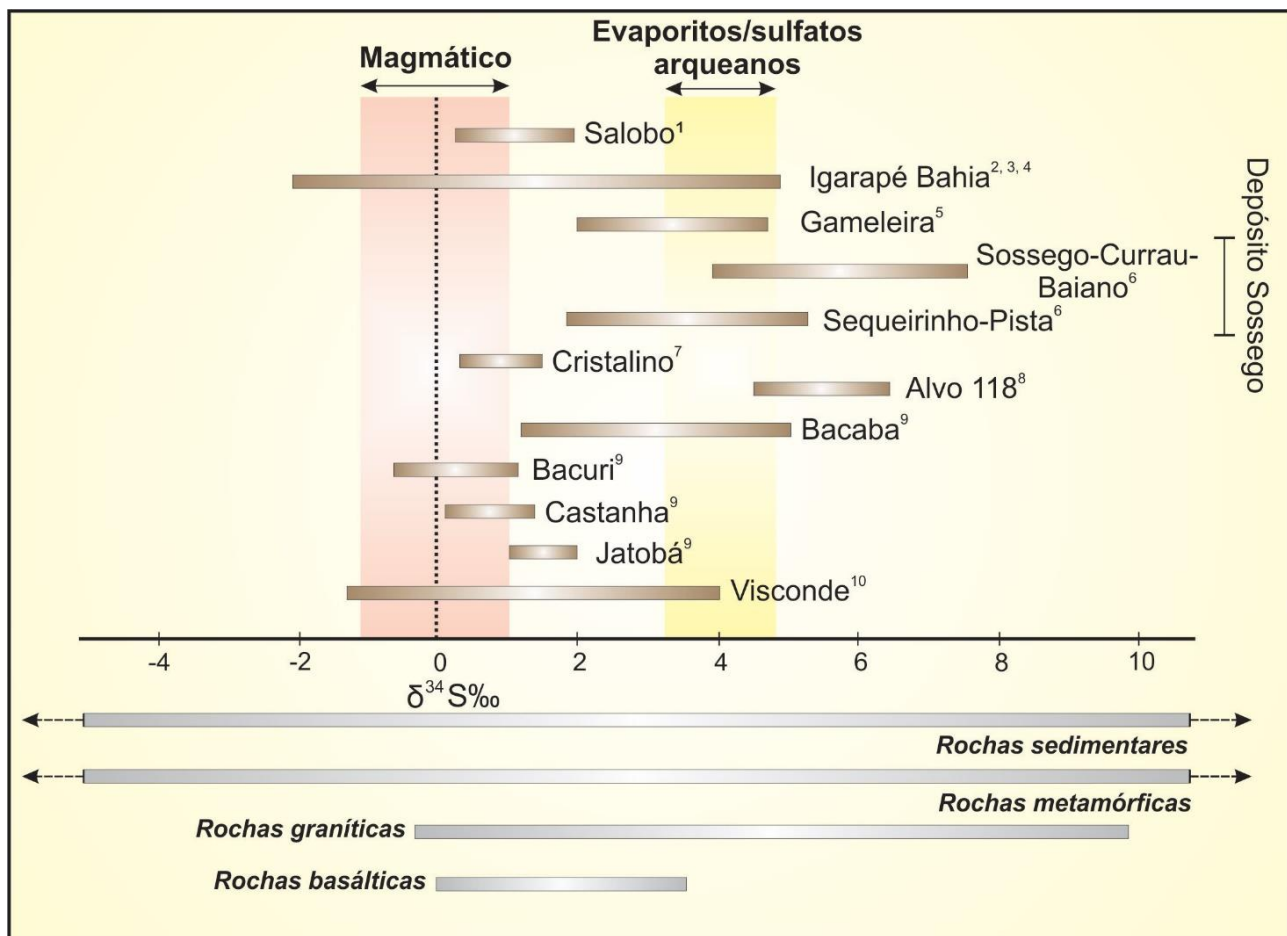


Fig. 6. Dados de $\delta^{34}\text{S}$ em sulfetos dos depósitos IOCG da Província Carajás. Dados de $\delta^{18}\text{O}$ obtidos de: 1- Réquia e Fontboté (2001), 2 – Dreher et al. (2008), 3 – Galarza et al. (2008), 4 - Villas et al. (2001), 5 – Fleck e Lindenmayer (2003), 6 – Monteiro et al. (2008), 7 – Ribeiro et al. (2009), 8 – Torresi et al. (2011), 9 – Pestilho (2011), 10 – Silva et al. (2010). Campo do enxofre magmático e evaporitos/sulfatos arqueanos obtidos de Ohmoto e Goldhaber (1997) e Eldridge et al. (1991), respectivamente. Distribuição de valores de $\delta^{34}\text{S}$ rochas sedimentares, rochas metamórficas, rochas graníticas e rochas basálticas obtidos de Hoefs (2007).

6. GEOLOGIA DOS DEPÓSITOS SALOBO E IGARAPÉ BAHIA

6.1 Geologia do depósito Salobo

O depósito Salobo é hospedado por gnaisses do embasamento mesoarqueano pertencentes ao Complexo Xingu com idades de 2950 ± 25 Ma e $2857 \pm 6,7$ Ma interpretadas, respectivamente, como de cristalização e metamorfismo/deformação de tais rochas, gnaisses da suíte Igarapé Gelado com idade de $2763 \pm 4,4$ Ma (Fig. 7, Melo *et al.* 2016) e unidades supracrustais do Grupo Igarapé Salobo, que inclui quartzo milonito com idades de proveniência de 3,1 – 3,0 Ga, 2,96 Ga, 2,86 Ga e 2,74 Ga. Os litotipos hospedeiros foram intensamente deformados na Zona de Cisalhamento do Cinzento (2555 ± 4 Ma, Machado *et al.* 1991), apresentando foliação milonítica subvertical, de direção NW–SE.

O sistema hidrotermal evoluiu a partir de estágios iniciais e distais de alteração sódica-cálcica (hastingsita e actinolita), seguido por um estágio de enriquecimento em ferro (grunerita–almandina–faialita–magnetita) e formação de turmalina (Melo *et al.* 2016). Alteração potássica com biotita subsequente foi acompanhada pela formação de magnetita e parece ser coeva a precipitação do minério. Paragênese mineral de mais baixa temperatura inclui stilpnometano, grenalita e clorita e ocorreu concomitante à precipitação do minério. Grandes quantidades de fluorita e grafita também são comuns nas zonas hidrotermalizadas do depósito Salobo (Réquia *et al.* 2003). O minério é constituído por bornita, calcocita, calcopirita e ouro, além de variáveis proporções de molibdenita, cobaltita, safflorita, nicollita, siegenita, covellita (Réquia *et al.* 2003, Lindenmayer 2003, Melo *et al.* 2016).

Rochas graníticas representadas pelos granitos *Old* Salobo e *Young* Salobo intrudem as rochas hospedeiras do depósito. O Granito *Old* Salobo ($2547 \pm 5,3$ Ma, U–Pb em zircão, Melo *et al.* 2016) é um granito alcalino, com augita como máfico principal, metaluminoso, mesozonal e sin-tectônico (Lindenmayer 2003). O granito *Young* Salobo (1.880 ± 80 Ma, Rb–Sr em rocha total, Cordani 1981) é alcalino, metaluminoso e anorogênico (Lindenmayer 1990) e não exibe feições de alteração hidrotermal e deformação.

Fluidos ricos em CO_2 –(CH_4) foram reconhecidos no depósito Salobo e atribuídos à desidratação de rochas metamórficas em fácies anfibolito, interpretados como os fluidos de mais alta temperatura (Réquia 1995). Fluidos ricos em H_2O – NaCl –

(CaCl_2) teriam sido posteriormente introduzidos no sistema com temperaturas de 485 °C e salinidades que variam entre 30,6 to 58,4 % eq. NaCl (Réquia 1995).

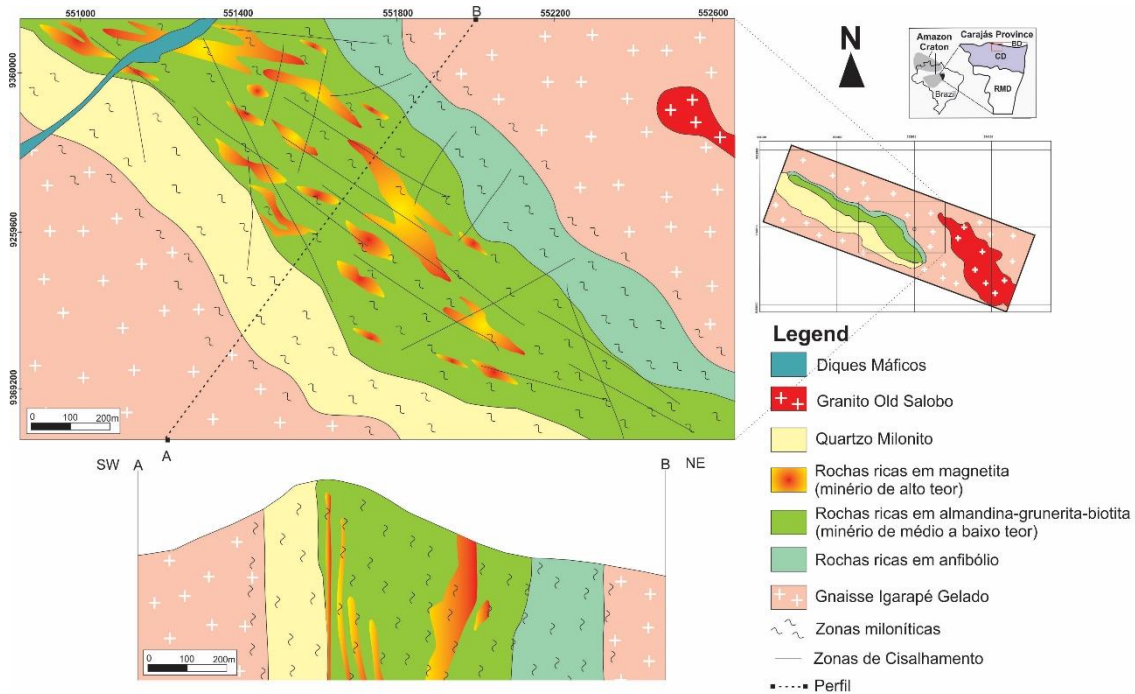


Fig. 7. Mapa e perfil geológico do depósito Salobo com a disposição das rochas hospedeiras distais e rochas hidrotermalizadas na porção central do depósito marcadas pela forte deformação dúctil da Zona de Cisalhamento do Cinzento de direção WNW–ESE (modificado de VALE).

Idades Re–Os em molibdenita das zonas mineralizadas sugerem que a idade de mineralização no depósito Salobo é de 2576 ± 8 Ma, associada a colocação do granito *Old Salobo* (Réquia *et al.* 2003), embora a relação espacial das zonas mineralizadas com o corpo do granito *Old Salobo* não seja tão clara (Melo *et al.* 2016). No entanto, idades isocrônicas Pb–Pb em calcocita (2705 ± 42 Ma) e magnetita (2112 ± 12 Ma) obtidas por Tassinari *et al.* (2003), embora imprecisas, podem revelar uma história metalogenética mais complexa para esse depósito com eventos hidrotermais mais antigos.

6.2 Geologia do depósito Igarapé Bahia

O depósito Igarapé Bahia é hospedado pelas rochas do Grupo Igarapé Bahia, pertencentes ao Supergrupo Itacaiúnas, que ocorrem em uma janela erosional dentro da Formação Águas Claras e apresentam foliação na direção NW e mergulhos subverticais (Fig. 8). O Grupo Igarapé Bahia é dividido em unidade inferior e unidade superior.

A unidade inferior é constituída por rochas metavulcânicas basálticas, andesíticas e dacíticas (Sachs 1983, Ferreira Filho 1985), afaníticas, amigdaloidais e microporfiríticas (Tallarico *et al.* 1998), intercaladas a metatufo de cristais e formações ferríferas, constituídas predominantemente por *chert* e magnetita. Na unidade superior predominam rochas metapiroclásticas, metatufo de *lapilli*, metatufo de cristais, metatufo laminados, formações ferríferas bandadas, metarenitos, metarritmitos e brechas com fragmentos de rochas metavulcânicas (Tallarico *et al.* 2000).

A parte superior do depósito apresenta capa laterítica com grandes quantidades de ouro supérigeno, que foi explotado pela VALE até 2003 (Tallarico 2003). Abaixo dessa capa, os corpos de minério primário de cobre-ouro apresentam reservas estimadas em 219 Mt @ 1,4% Cu e 0,86 g/t Au (Tallarico *et al.* 2005). A mineralização de cobre-ouro está contida em brechas hidrotermais no contato com rochas metavulcânicas maficas e metassedimentares. As brechas contém grunerita, feldspato potássico, stilpnomelano, biotita, muscovita e fluorita, que resultantes de metassomatismo rico em Fe-(K) (Tallarico *et al.* 2005; Dreher *et al.* 2008). Intensa cloritização, carbonatação, magnetitização e sulfetação, além de silicificação e turmalinização subordinadas, também representam alterações hidrotermais caracterizadas nas rochas hospedeiras das mineralizações (Almada & Villas 1999; Tallarico *et al.* 1998a; Galarza & Macambira 2002).

A mineralização é representada principalmente por calcopirita, calcocita, digenita e covellita e, subordinadamente, por bornita, pirita, molibdenita, cobaltita, fluorita, hessita e uraninita. Algumas gerações de veios tardios preenchidos por calcita-quartzo-calcopirita e quartzo-calcopirita interceptam diversos litotipos do Grupo Igarapé Bahia (Ferreira Filho 1985).

Estudos de inclusões fluidas em quartzo mostraram que fluidos salinos (5 a 45% NaCl + CaCl₂) juntamente com fluidos ricos em CO₂-(CH₄) e fluidos aquo-carbônicos de baixa salinidade (6% eq. NaCl) participaram do sistema hidrotermal no depósito Igarapé Bahia (Dreher *et al.* 2008).

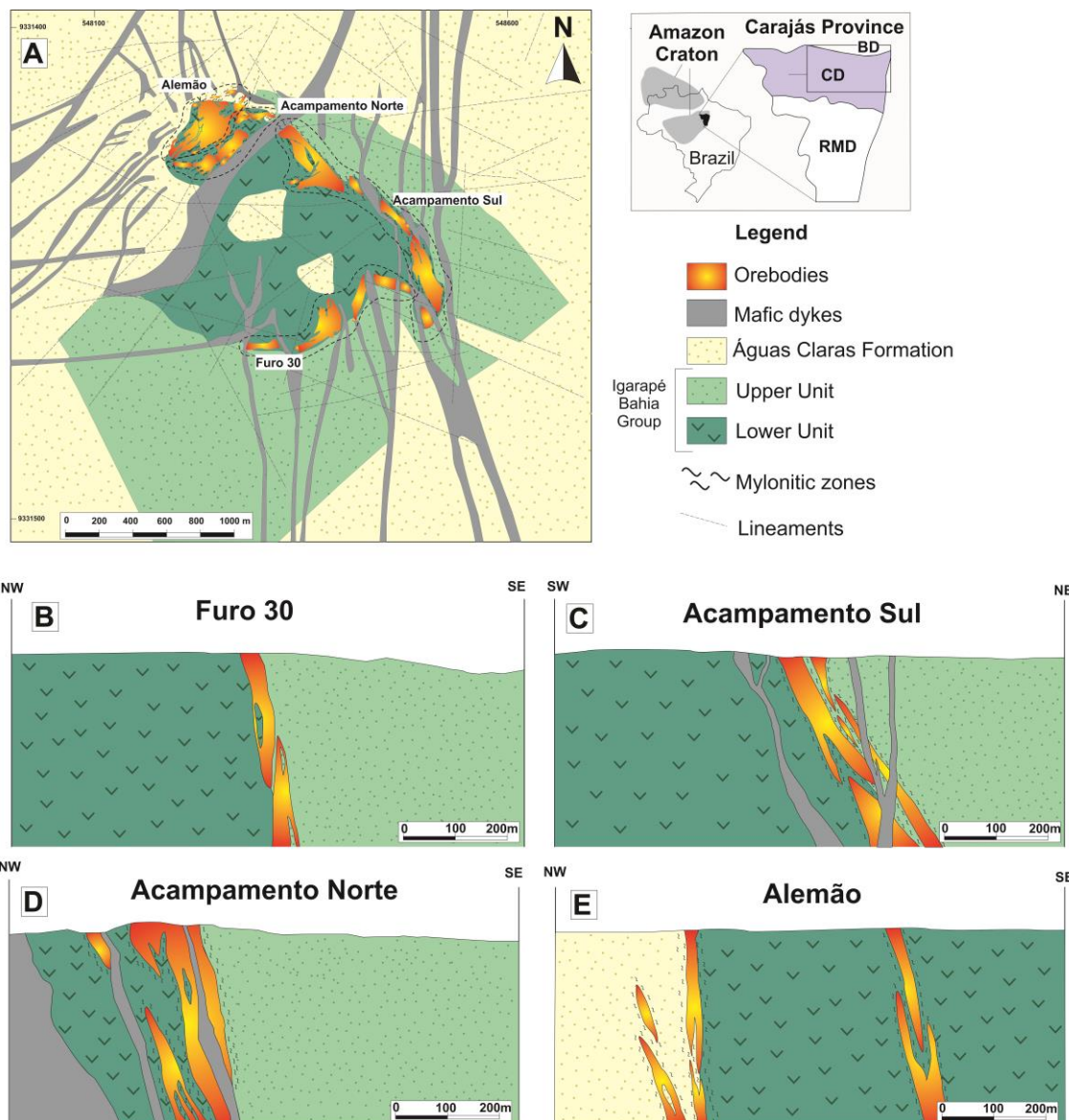


Fig. 8. a) Mapa geológico do depósito Igarapé Bahia com as principais unidades geológicas e a projeção dos corpos de minério. Perfil geológico do corpo a) Furo 30, b) Acampamento Sul, c) Acampamento Norte e d) Alemão (modificado de VALE).

Idades U-Pb em monazita hidrotermal da principal zona de minério do depósito Igarapé Bahia apontam para idade de mineralização em 2575 ± 12 Ma (Tallarico *et al.* 2005), similar à do evento metalogenético caracterizado no depósito Salobo (Réquia *et al.* 2003). Idades Pb-Pb em ouro (2744 ± 12 Ma; Galarza *et al.* 2008) e em calcopirita (2772 ± 46 Ma, 2754 ± 36 Ma, 2756 ± 24 Ma, 2777 ± 22 Ma; Galarza *et al.* 2008) foram interpretadas como indicativas de um evento mineralizante mais antigo no depósito Igarapé Bahia.

7. SÍNTESE DOS ARTIGOS

Serão apresentados nessa tese de doutorado três artigos científicos que serão submetidos aos periódicos *Ore Geology Reviews* (Artigo I), *Economic Geology* (Artigo II) e *Chemical Geology* (Artigo III).

7.1 Artigo I – “The evolution of the Cu-Au Igarapé Bahia deposit: early syngenetic sulfides overprinted by IOCG mineralization, Carajás Province (Brazil)”

O depósito Igarapé Bahia é hospedado pelo Grupo Igarapé Bahia e pela Formação Águas Claras. As rochas do Grupo Igarapé Bahia incluem rochas metavulcânicas ácidas e básicas e rochas metagabroicas da unidade inferior, além de metarritmitos, rochas epiclásticas e formação ferrífera bandada da unidade superior. Rocha granítica fina, que ocorre como xenólito na unidade inferior, forneceu idade U-Pb LA-ICP-MS de intercepto superior em 2935 ± 36 Ma (MSWD = 0,85), sugerindo uma crosta ensiálica prévia a instalação da bacia, possivelmente devido ao rifteamento. A sequência de rochas metavulcanoclásticas da unidade superior mostraram populações de zircão detritico com concentração de idades U-Pb em ca. 2,82 – 2,88 Ga e ca. 2,94 – 2,99 Ga, indicativas de embasamento como a principal fonte de zircão. Essas rochas mostraram uma idade máxima de deposição em 2784 ± 27 Ma. Rochas epiclásticas representam o principal litotipo da Formação Águas Claras no depósitos Igarapé Bahia. A geocronologia da Formação Águas Claras também mostrou concentração na população de zircão em 2,81 – 2,89 Ga e 2,91 – 3,03 Ga, apontando semelhante proveniência a partir de rochas mesoarqueanas do embasamento. Idade máxima de deposição é dada em 2763 ± 32 Ma e 2774 ± 19 Ma.

Um estágio inicial de mineralização cuprífera, singenética e *stratabound*, foi reconhecida na sequência dos metarritmitos da unidade superior e caracteriza-se pela ocorrência da calcopirita em nódulos e *layers* concordantes ao acamamento, sem halos de alteração hidrotermal expressivos e sem óxidos de ferro. Em conjunto, dados de $\delta^{34}\text{S}_{\text{cpy}}$ nos nódulos e *layers* de calcopirita (+0,29 a +1,56‰) e elevados conteúdos de Ni, Co e Bi, apontam para fontes de enxofre e metais derivadas da rochas metavulcânicas da unidade inferior para esse estilo de mineralização.

As rochas hospedeiras, que incluem as rochas da Formação Águas Claras, e a mineralização singenética são cortadas pela mineralização de óxido de ferro-cobre-ouro

(IOCG). A mineralização IOCG é envelopada por grandes zonas de alteração hidrotermal nos quatro corpos de minério do depósito. A evolução paragenética desse sistema hidrotermal inclui um estágio inicial e restrito de (i) alteração sódico-cálcica com actinolita e escapolita seguido por alteração (ii) potássica com biotita. Formação de (iii) turmalina e carbonato, associado à precipitação de magnetita ocorreu pré a sin precipitação da calcopirita. A formação de (iv) clorita foi tardia e amplamente distribuída no depósito. Deformação dúctil e forte pressão de fluidos foram coevos à alteração hidrotermal e formaram rochas miloníticas e brechas hidrotermais.

Os corpos de minério incluem principalmente milonitos e brechas hidrotermais com foliação subvertical com grandes conteúdos de calcopirita e magnetita, embora lentes maciças também possam ocorrer. A calcopirita exibe valores de $\delta^{34}\text{S}$ entre +1,36 e +5,35‰, indicando fonte magmática, além de possível contribuição de fontes externas de enxofre e mecanismo de redução termoquímica de sulfato da água do mar. Elevados valores de ΣREE e conteúdos significativos de U, Mo, Sn, W, Y, Nb e Sr são típicos da calcopirita associada a essas zonas ricas em magnetita.

Datação U–Pb em monazita hidrotermal do corpo Alemão forneceu idade $^{207}\text{Pb}/^{206}\text{Pb}$ de 2559 ± 34 Ma. Essa idade é similar à obtida por Tallarico *et al.* (2005) (U–Pb em monazita, 2575 ± 12 Ma) para o corpo Acampamento Sul, mostrando que não há diferenças nas idades dos corpos de minério do depósito Igarapé Bahia. Essas idades divergem das idades já reconhecidas no Cinturão Sul do Domínio Carajás (Moreto *et al.* 2015a, b), mostrando que um importante evento metalogenético pode estar restrito à porção norte do Domínio Carajás.

Um ponto ainda a ser mais investigado é o significado metalogenético e a idade dos veios tardios de quartzo–carbonato–calcopirita que cortam toda a sequência mineralizada. Esses veios representam uma mineralização tardia com valores de $\delta^{34}\text{S}$ entre -0,3 e +4‰, muito próximo aos valores obtidos para calcopirita associada com o sistema IOCG. Se esses veios podem representar uma remobilização dos sulfetos mais antigos durante um evento metalogenético rúptil no Paleoproterozoico é algo ainda incerto.

O depósito Igarapé Bahia registra sobreposição de eventos de mineralização cuprífera (i.e. nódulos e *layers* de calcopirita; IOCG e veios tardios com carbonato–quartzo–calcopirita). A existência de uma mineralização singenética pode ser importante na compreensão das mineralizações epigenéticas do tipo IOCG em Carajás.

7.2 Artigo II – “Tracing fluid sources for the giant Salobo and Alemão-Igarapé Bahia IOCG deposits: implications for the genesis of the IOCG deposits in the Carajás Mineral Province”

Esse artigo baseia-se na comparação das assinaturas isotópicas de $\delta^{18}\text{O}$ e δD de fases minerais hidrotermais representativas dos diferentes estágios de alteração hidrotermal dos depósitos Salobo e Igarapé Bahia, visando caracterizar as principais fontes de fluidos dos dois depósitos. Adicionalmente, análises de isótopos de enxofre foram realizadas nos sulfetos do depósito Salobo para determinar as principais fontes de enxofre e comparar com os resultados já obtidos para o depósito Igarapé Bahia (Dreher *et al.* 2008, Galarza *et al.* 2008, Melo *et al.* in prep.).

Os estudos de isótopos estáveis possibilitaram estimar temperaturas relativas à evolução do sistema hidrotermal responsável pela formação dos depósitos Salobo e Igarapé Bahia. Os principais estágios de alteração hidrotermal no depósito Salobo, representados por enriquecimento em ferro e alteração potássica com biotita, formaram-se, respectivamente, a $429 \pm 45^\circ\text{C}$ e $512 \pm 45^\circ\text{C}$. Estágios tardios com formação de clorita, posteriores à precipitação do minério, mostram temperaturas de 347°C . O depósito Igarapé Bahia, por sua vez, exibe temperaturas menores ($398 \pm 85^\circ\text{C}$) nos estágios que precederam a mineralização cuprífera, durante a precipitação de magnetita. O estágio principal de alteração no depósito Igarapé Bahia, representado pela formação de clorita, mostra temperaturas também inferiores de $255 \pm 15^\circ\text{C}$.

No depósito Salobo, os fluidos hidrotermais associados com o estágio de enriquecimento em ferro (grunerita–almandina–turmalina), a $429 \pm 45^\circ\text{C}$, e alteração potássica (biotita–quartzo), a $540 \pm 45^\circ\text{C}$, apresentam composições isotópicas calculadas ($\delta^{18}\text{O}_{\text{H}_2\text{O}} = +5,3$ a $+7,96\text{\textperthousand}$; $\delta\text{D}_{\text{H}_2\text{O}} = -36,93$ a $+5,12\text{\textperthousand}$) compatíveis com a de fluidos derivados de água magmática primária. Calcopirita e bornita das zonas mineralizadas de alto teor mostram valores de $\delta^{34}\text{Sc}_{\text{py}}$ de $-0,37$ a $+1,63\text{\textperthousand}$, evidenciando fontes também magmáticas para o enxofre do Salobo.

No depósito Igarapé Bahia, a composição isotópica dos fluidos em equilíbrio com turmalina ($\delta^{18}\text{O}_{\text{H}_2\text{O}} = +5,54$ a $+6,24\text{\textperthousand}$; $\delta\text{D}_{\text{H}_2\text{O}} = -46,98$ e $-32,70\text{\textperthousand}$), a $398 \pm 85^\circ\text{C}$, são restritos ao campo da água magmática primária, enquanto que fluidos associados à calcita ($\delta^{18}\text{O}_{\text{H}_2\text{O}} = +1,68$ a $+3,10\text{\textperthousand}$) e aos estágios finais de formação de clorita ($\delta^{18}\text{O}_{\text{H}_2\text{O}} = +2,13$ to $+3,41\text{\textperthousand}$, $\delta\text{D}_{\text{H}_2\text{O}} = -57,69$ e $-21,67\text{\textperthousand}$), sugerem a participação de fluidos formacionais (i.e. água meteórica evoluída). Os valores calculados de $\delta^{13}\text{C}_{\text{CO}_2}$ para

fluidos em equilíbrio com calcita variaram de $-9,04$ a $-4,65\text{\textperthousand}$, evidenciando uma fonte magmática para o carbono. Os valores encontrados em magnetita ($\delta^{18}\text{O}_{\text{H}_2\text{O}} = +11,71\text{\textperthousand}$) podem sugerir uma intensa interação fluido-rocha.

Os resultados de $\delta^{18}\text{O}$ e δD no depósito Salobo e $\delta^{18}\text{O}$, δD e $\delta^{13}\text{C}$ nos estágios iniciais do depósito Igarapé Bahia apontam para fontes magmáticas. A exsolução de fluidos magmáticos durante a cristalização de magmas graníticos em ca. 2,57 Ga (i.e. Granito Old Salobo e Granito Itacaiúnas) pode representar o mecanismo de geração de fluidos mineralizantes hipersalinos e quentes. O fluido magmático possivelmente se exsolveu dos magmas em profundidade, se canalizou em zonas de cisalhamento profundas e ascendeu até níveis crustais mais rasos. Os valores de $\delta^{34}\text{S}_{\text{cpy}}$ no depósito Salobo também corroboram para fontes magmáticas para o enxofre.

O depósito Igarapé Bahia, no entanto, mostra uma forte contribuição de fluidos externamente derivados, evidenciado pelos menores valores de $\delta^{18}\text{O}_{\text{H}_2\text{O}}$. A natureza das rochas hospedeiras do depósito Igarapé Bahia e a circulação de fluidos formacionais promovendo intensa interação fluido-rocha poderia explicar a variação das composições isotópicas de $\delta^{18}\text{O}$ e δD . Esse estudo mostra que, apesar das fontes magmáticas comuns, esses depósitos representam porções distintas de um amplo sistema mineral, no qual processos locais de interação fluido-rocha foram responsáveis pela diversidade em seus atributos geológicos.

7.3 Artigo III – “Boron isotopes in tourmaline of the IOCG deposits in the northern sector of the Carajás Domain, Carajás Province (Brazil)”

O terceiro artigo oriundo dessa tese faz uma análise sistemática da aplicação de isótopos de boro em turmalina de diferentes depósitos IOCG localizados na porção norte do Domínio Carajás, visando à caracterização das fontes de boro e possíveis fontes de fluidos mineralizantes.

Os depósitos IOCG analisados nesses estudos incluíram os depósitos Salobo, GT-46, Furnas, Grotá Funda e Igarapé Bahia. Os depósitos Salobo, GT-46 e Furnas localizam-se ao longo na Zona de Cisalhamento do Cinzento de direção WNW-ESE, onde rochas do embasamento, granitoides neoarqueanos deformados e resquícios de sequências supracrustais são preservadas. Por outro lado, os depósitos Grotá Funda e Igarapé Bahia são hospedados nas sequências metavulkanossedimentares do Supergrupo

Itacaiúnas, ductilmente deformadas pela Zona de Cisalhamento Carajás, também de direção WNW–ESE.

Nos depósitos Salobo e Igarapé Bahia foram reconhecidos tanto altos valores de $\delta^{11}\text{B}$ nos núcleos de cristais de turmalina (Salobo: +14,9 a +17,0‰; Igarapé Bahia: +11,0‰ a +14,6‰), quanto valores baixos nas suas bordas (Salobo: +3,4 a +8,2‰; Igarapé Bahia: +3,4 to +9,8‰). Valores relativamente elevados de $\delta^{11}\text{B}$ também foram reconhecidos no depósito Furnas e variam de +13,1 a +17,2‰. No depósito Grotá Funda valores intermediários de $\delta^{11}\text{B}$ (+8,2 a +13,6‰). Por outro lado, o depósito GT–46 parece registrar os valores mais baixos de $\delta^{11}\text{B}$ em turmalina desses depósitos (+5,4 a +6,4‰).

Os valores mais elevados de $\delta^{11}\text{B}$ sugerem a participação de salmouras derivadas de fluidos hidrotermais submarinhos vinculados à atividade exalativa e/ou da evaporação da água do mar. A circulação desses fluidos deve ter ocorrido de forma sincrônica à deposição das sequências metavulcanosedimentares do Supergrupo Itacaiúnas entre 2,76 e 2,73 Ga.

Por outro lado, os baixos valores de $\delta^{11}\text{B}$, especialmente registrados no depósito GT–46 e nas bordas dos cristais de turmalina do Salobo e Igarapé Bahia, sugerem participação de boro proveniente de salmouras magmáticas exsolvidas a partir da cristalização de granitos cristalizados em ca. 2,57 Ga.

Os resultados obtidos nesse estudo reportam os maiores valores de $\delta^{11}\text{B}$ para depósitos IOCG no mundo, mostrando que diferentes fontes de fluidos e demais componentes para o sistema mineral (boro e metais) podem ser responsáveis pela gênese desses depósitos.

8. CONCLUSÕES

Os resultados obtidos nessa Tese de Doutorado evidenciam uma complexa evolução metalogenética nos depósitos Salobo e Igarapé Bahia. Essa complexidade é reflexo da longa história evolutiva do Domínio Carajás, responsável por originar os diferentes atributos geológicos desses depósitos.

O depósito Salobo é hospedado por gnaisses do Complexo Xingu com idade de 2950 ± 25 Ma e $2857 \pm 6,7$ Ma, granitoides deformados da Suíte Igarapé Gelado cristalizados em $2763 \pm 4,4$ Ma e, subordinadamente, unidades metavulcanossedimentares do Supergrupo Itacaiúnas. As rochas do embasamento mesoarqueano (e.g. Complexo Xingu) também foram reconhecidas como xenólitos datados em 2935 ± 36 Ma ($\text{MSWD} = 0,85$) inseridos nas rochas metavulcânicas no depósito Igarapé Bahia, evidenciando a presença de crosta siálica prévia à deposição do Supergrupo Itacaiúnas. O depósito Igarapé Bahia, no entanto, é principalmente hospedado por sequências supracrustais do Grupo Igarapé Bahia (Supergrupo Itacaiúnas) e da Formação Águas Claras. Essas rochas hospedeiras incluem metavulcânicas básicas e ácidas da unidade inferior sobrepostas por metarritmitos e rochas epiclásticas da unidade superior. Essas sequências metassedimentares apresentam idade máxima de deposição em 2784 ± 27 Ma. As rochas epiclásticas da Formação Águas Claras, que também hospedam o depósito Igarapé Bahia, especialmente o corpo Alemão, exibem idade máxima de deposição em 2763 ± 32 Ma e 2774 ± 19 Ma. Rochas mesoarqueanas representam a principal fonte de zircão para unidade superior do Grupo Igarapé Bahia e para a Formação Águas Claras, embora fontes neoarquenas também estejam presentes.

No depósito Igarapé Bahia, nódulos e *layers* de calcopirita, encontrados concordantes às estruturas primárias dos metarritmitos da unidade superior, representam um estágio inicial de mineralização cuprífera, singenética e *stratabound*, desenvolvido entre ca. 2,76 e 2,73 Ga. Os dados isotópicos de enxofre ($\delta^{34}\text{S} = +0,29$ a $+1,56\text{\textperthousand}$) e elementos traço (i.e. elevados conteúdos de Ni, Co e Bi) nessa geração de calcopirita mostram que suas fontes de metais e enxofre foram provenientes principalmente das rochas metavulcânicas. Nesse período, a circulação de fluidos exalativos vinculados a sistemas hidrotermais em assoalho oceânico pode ter sido responsável tanto pela precipitação dos nódulos e *layers* de calcopirita no depósito Igarapé Bahia quanto para a formação de outras mineralizações singenéticas. A presença desses sistemas

hidrotermais submarinhos, possivelmente com associação de salmoras derivadas da evaporação da água do mar, possibilitaram a cristalização de cristais de turmalina enriquecidos em ^{11}B ($\delta^{11}\text{B} = +8,2$ a $+17,2\text{\textperthousand}$) nos depósitos Salobo, Igarapé Bahia, Furnas e Grotá Funda. A redução termoquímica do sulfato da água do mar em ca. 2,76 – 2,73 Ga pode ter gerado sulfetos que se precipitaram na sequência sedimentar e foram posteriormente remobilizados.

Análise geocronológica U–Pb *in situ* em monazita forneceu idade $^{207}\text{Pb}/^{206}\text{Pb}$ de 2559 ± 34 Ma no corpo Alemão, de forma similar às idades de mineralização previamente obtidas nos depósitos Igarapé Bahia e Salobo, que registam um importante evento metalogenético em 2,57 Ga. Diferenças nas assembleias hidrotermais de Salobo (hastingsita–actinolita, grunerita–almandina–faialita–magnetita–(turmalina) e (grunerita–almandina)–magnetita–biotita) e Igarapé Bahia (turmalina)–carbonato–magnetita, (turmalina)–carbonato–clorita e (turmalina)–(biotita)–clorita) parecem refletir diferentes histórias de interação fluido-rocha.

Dados de isótopos estáveis nesses minerais hidrotermais do depósito Salobo ($\delta^{18}\text{O}_{\text{H}_2\text{O}} = +5,3$ a $+7,96\text{\textperthousand}$; $\delta\text{D}_{\text{H}_2\text{O}} = -36,93$ a $+5,12\text{\textperthousand}$) e nos estágios iniciais do depósito Igarapé Bahia ($\delta^{18}\text{O}_{\text{H}_2\text{O}} = +5,54$ a $+6,24\text{\textperthousand}$; $\delta\text{D}_{\text{H}_2\text{O}} = -46,98$ a $-32,70\text{\textperthousand}$) apontam principalmente para fontes de fluidos magmáticos. Assinatura geoquímica de elementos traço em calcopirita da mineralização IOCG no depósito Igarapé Bahia, com elevados conteúdos de ΣETR e valores significativos de U, Mo, Sn, W, Y, Nb e Sr, podem também ser associados com corpos graníticos, especialmente do tipo A. Esse mesmo magmatismo parece ser a principal fonte de enxofre no depósito Salobo ($\delta^{34}\text{S}_{\text{Cpy}} = -0,37$ e $+1,63\text{\textperthousand}$).

No depósito Igarapé Bahia, em contraste, valores de $\delta^{34}\text{S}$ entre $+1,36$ e $+5,35\text{\textperthousand}$ indicam, contribuição adicional de enxofre oriundo da lixiviação dos sulfetos previamente precipitados nas sequências sedimentares. Bordas de turmalina nos depósitos Salobo e Igarapé Bahia ($\delta^{11}\text{B} = +3,4$ a $+9,8\text{\textperthousand}$) e cristais de turmalina espacialmente associados à corpos pegmatíticos no depósito GT-46 ($\delta^{11}\text{B} = +5,4$ a $+6,4\text{\textperthousand}$) também apontam para fonte magmática do boro, embora no caso de Salobo e Igarapé Bahia os núcleos registrem uma história mais antiga ao evento IOCG associada aos valores mais altos de $\delta^{11}\text{B}$. Em conjunto, esses dados mostram que fluidos hidrotermais parecem ter se exsolvido a partir da cristalização de granitos em ca. 2,5 Ga, durante um importante evento tectônico. A presença de fluidos externamente derivados, tais como águas formacionais (i.e. água meteórica evoluída), é bem

registrada a partir da assinatura dos fluidos hidrotermais em equilíbrio com calcita ($\delta^{18}\text{O}_{\text{H}_2\text{O}} = +1,68$ a $+3,10\text{\textperthousand}$) e clorita ($\delta^{18}\text{O}_{\text{H}_2\text{O}} = +2,13$ a $+3,41\text{\textperthousand}$) no depósito Igarapé Bahia.

Veios tardios de quartzo–carbonato–calcopirita, amplamente reconhecidos no depósito Igarapé Bahia, cortam toda a sequência de rochas e a mineralização IOCG, e são possivelmente associados a um evento metalogenético paleoproterozoico.

Assim, a metalogênese do cobre em Carajás registra, no mínimo, quatro eventos mineralizantes de Cu e Cu–Au. Esses eventos podem ser temporalmente divididos em: i) ca. 2,76 – 2,73 Ga (evento exalativo associado a sistemas hidrotermais de fundo oceânico); ii) ca. 2,71 – 2,68 Ga (evento IOCG, reconhecido principalmente no setor sul do Domínio Carajás); ca. 2,5 Ga (evento IOCG, reconhecido principalmente no setor norte do Domínio Carajás); e iv) ca. 1,88 Ga (possível remobilização).

A sobreposição desses eventos singenéticos e epigenéticos está intimamente ligada aos eventos tectônicos e magmáticos do Domínio Carajás. A existência de sistemas exalativos, a presença de sucessivos eventos de magmatismo granítico e a ativação/reactivação de grandes descontinuidades crustais foi registrada nesses depósitos, o que evidencia a complexidade da evolução metalogenética da Província Carajás.

REFERÊNCIAS

- Almada M.C.O., Villas R.N. 1999. O depósito Bahia: um possível exemplo de depósito vulcanogenênico tipo Besshi arqueano em Carajás. Revista Brasileira de Geociências **29**: 579-592.
- Araújo O.J.B., Maia, R.G.N. 1991. Serra dos Carajás: folha SB.22-Z-A. Estado do Pará. Escala 1:250.000. Texto explicativo. DNPM/CPRM. 164 p. il.
- Araújo O.J.B., Maia R.G.N., Jorge-João, X.S. Costa, J.B.S., 1988. A megaestruturação da folha Serra dos Carajás. In: Congr. Latino Am. Geol., **7**: 324–333.
- Augusto R.A., Monteiro L.V.S., Xavier R.P., Souza Filho C.R. 2008. Zonas de alteração hidrotermal e paragênese do minério de cobre do Alvo Bacaba, Província Mineral de Carajás (PA). Revista Brasileira de Geociencias **38**: 263–277
- Avelar V.G., Lafon J.M., Correia F.C.Jr., Macambira B.E.M. 1999. O magmatismo arqueano da região de Tucumã, Província Mineral de Carajás, Amazônia Oriental, Brasil: novos dados geocronológicos. Revista Brasileira de Geociências **29**: 453–460.
- Barbosa J.P.O. 2004. Geologia Estrutural, Geoquímica, Petrografia e Geocronologia de granitóides da região do Igarapé Gelado, norte da Província Mineral de Carajás. Dissertação de Mestrado, UFFPA, 96p.
- Barros C.E.M., Sardinha A.S., Barbosa J.P.O., Macambira M.J.B. 2009. Structure, Petrology, Geochemistry and zircon U/Pb and Pb/Pb geochronology of the synkinematic Archean (2.7 Ga) A-type granites from the Carajás Metallogenic Province, northern Brazil, Canadian Mineralogist **47**:1423-1440
- Barros C.E.M., Macambira M.J.B., Barbey P., Scheller T. 2004. Dados isotópicos Pb-Pb em zircão (evaporação) e Sm-Nd do Complexo granítico Estrela, Província Mineral de Carajás, Brasil: implicações petrológicas e tectônicas. Revista Brasileira de Geociências **34**:531–538.
- Barros C.E.M., Barbey P., 1998. A importância da granitogênese tardí-arqueana (2,5 Ga) na evolução tectono-metamórfica da Província Mineral de Carajás – o complexo granítico estrela e sua auréola de contato. Revista Brasileira de Geociências **28(4)**:513–522.
- Barton M.D., Johnson D.A. 1996. Evaporitic-source model for igneous-related Fe oxide-(REE-Cu–Au–U) mineralization. Geology **24**:259–262
- Craveiro G.S. 2011. Geologia, fluidos hidrotermais e origem do depósito cupro-aurífero Visconde, Província Mineral de Carajás. Dissertação de Mestrado, UFFPA.

- Dall'Agnol R., Rämö O.T., Magalhães M.S., Macambira M.J.B. 1999. Petrology of the anorogenic, oxidised Jamon and Musa granites, Amazonian craton: implications for the genesis of Proterozoic A-type granites. *Lithos* **46**: 431–462.
- Dall'agnol R., Oliveira M.A., Almeida J.A.C., Althoff F.J., Leite A.A.S., Oliveira D.C., Barros C.E.M. 2006. General Aspects of the Granitogenesis of the Carajás Metallogenic Province, in Dall'Agnol, R., Rosa-Costa, L.T., Klein, E.L., eds, Archaean and paleoproterozoic granitoids of the Carajás Metallogenic Province, Eastern Amazonian Craton, 1st ed.: Belém, PRONEX-UFPB/SBG-NO.
- Dall'agnol, R, Oliveira, D.C. de., Lamarão, C.N. 2013. Magmatismo granitoide arqueano e evolução geológica do Subdomínio de Transição da Província Carajás, sudeste do Cráton Amazônico, Brasil. *Boletim do Museu Paraense Emílio Goeldi. Ciências Naturais*, **8**: 251-256.
- Dardenne M.A., Ferreira Filho C.F., Meirelles M.R. 1988. The role of shoshonitic and calc-alkaline suites in the tectonic evolution of the Carajás district, Brazil. *Journal of South American Earth Sciences*, **1**: 363-372.
- Delinardo da Silva MA 2014. Metatexitos e diatexitos do Complexo Xingu na região de Canaã dos Carajás: Implicações para a evolução mesoarqueana do Domínio Carajás, PA. Dissertação de Mestrado, Instituto de Geociências, Universidade Estadual de Campinas, Campinas.
- Dias, G.S., Macambira, M.B., Dall'Ágnol, R., Soares, A.D.V. Barros, C.E.M., 1996. Datações de zircões de sill de metagabro: comprovação de idade arqueana da Formação Águas Claras, Carajás, Pará. In: Simp. Geol. Amaz., 5, SBG, Belém, pp. 376-378.
- DOCEGEO 1988. Revisão litoestratigráfica da Província Mineral de Carajás - Litoestratigrafia e principais depósitos minerais. In: 35º Congresso Brasileiro de Geologia. Belém, Anais.
- Domingos, F.H.G. 2010. The Structural Setting of the Canaã dos Carajás Region and Sossego-Sequeirinho Deposits, Carajás – Brazil. PhD Thesis, University of Durham.
- Dreher A.M., 2004. O depósito primário de Cu-Au de Igarapé Bahia, Carajás: Rochas fragmentárias, fluidos mineralizantes e modelo metalogenético. Tese de Doutorado, UNICAMP, 221p.
- Dreher A.M., Xavier R.P., Taylor B.E., Martini S. 2008. New geologic, fluid inclusion and stable isotope studies on the controversial Igarapé Bahia Cu-Au deposit, Carajás province, Brazil. *Mineralium Deposita* **43**:161–184.

- Dreher A.M., Xavier R.P., Taylor B.E., Martini S. 2005. Fragmental rocks of the Igarapé Bahia Cu-Au deposit, Carajás Mineral Province, Brazil. *Revista Brasileira de Geociências*. **35**(3):359–368.
- Duncan R.J., Stein H.J., Evans K., Hitzman M.W., Nelson E.P., Kirwin D.J. 2011. A New Geochronological Framework for Mineralization and Alteration in the Selwyn-Mount Dore Corridor, Eastern Fold Belt, Mount Isa Inlier, Australia: Genetic Implications for Iron Oxide Copper-Gold Deposits. *Economic Geology* **106**:169–192.
- Eby G.N. 1992. Chemical subdivision of the A-type granitoids: petrogenetic and tectonic implications. *Geology* **20**:641–644.
- Eldridge C.S., Compston W., Williams I.S., Harris J.W., Bristow J.W. 1991. Isotope evidence for the involvement of recycled sediments in diamond formation. *Nature*, **353**:649–653
- Feio G.R.L., Dall’Agnol R., Dantas E.L., Macambira M.J.B., Gomes A.S., Sardinha D.C., Oliveira D.C., Santos R.D., Santos P.A. 2012. Geochemistry, geochronology, and origin of the Neoarchean Planalto Granite suite, Carajás, Amazonian craton: A-type or hydrated charnockitic granites? *Lithos*. Online. <http://dx.doi.org/10.1016/j.lithos.2012.02.020>
- Feio G.R.L., Dall’Agnol R, Dantas E.L., Macambira M.J.B., Santos J.O.S., Althoff F.J., Soares J.E.B. 2013. Archean granitoid magmatism in the Canaã dos Carajás area: implications for crustal evolution of the Carajás province, Amazonian craton, Brazil. *Precambrian Research* **227**: 157-185.
- Ferreira Filho, C.F., Cançado, F., Correa, C., Macambira, E.M.B., Junqueira-Brod, T.C., Siepierski, L. 2007. Mineralizações estratiformes de PGE-Ni associadas a complexos acamadados em Carajás: os exemplos de Luanga e Serra da Onça. In: Rosa-Costa, L. T., Klein, E.L., Viglio, E.P. (Ed.). Contribuições à geologia da Amazônia. Belém: SBG-Núcleo Norte, **5**: 1-14.
- Ferreira Filho C.F. 1985. Geologia e mineralizações sulfetadas do Prospecto Bahia, Província Mineral de Carajás. Dissertação de Mestrado, Universidade de Brasília, Brasília.
- Fletcher I.R., McNaughton N.J., William J.D., Rasmussen B. 2010. Matrix effects and calibration limitations in ion probe U-Pb and Th-Pb dating of monazite. *Chemical Geology*, **270**, 31-44.
- Frost B.R., Barnes C.G., Collins W.J., Arculus R.J., Ellis D.H., Frost C.D. 2001. A geochemical classification for granitic rocks. *Journal of Petrology* **42**:2033–2048.
- Galarza M.A., Macambira M.J.B., Villas R.N. 2008. Dating and isotopic characteristics (Pb and S) of the Fe oxide–Cu–Au–U–REE Igarapé Bahia ore deposit, Carajás mineral province, Pará state, Brazil. *Journal of South American Earth Sciences* **25**:377-397.

- Galarza M.A., Macambira M.J.B. 2002. Geocronologia e evolução crustal da área do depósito de Cu-Au Gameleira, Província Mineral de Carajás (Pará), Brasil. Revista do Instituto de Geociências da USP, **2**:143-159.
- Gibbs A.K., Wirth K.R., Hirata W.K., Olszewski Jr., W.J. 1986. Age and composition of the Grão Pará Group volcanics, Serra dos Carajás. Revista Brasileira de Geociências, **16**: 201–211.
- Grainger C.J., Groves D.I., Tallarico F.H.B., Fletcher I.R. 2008. Metallogenesis of the Carajás Mineral Province, Southern Amazon Craton, Brazil: Varying styles of Archean through Paleoproterozoic to Neoproterozoic base- and precious-metal mineralisation. Ore Geology Reviews **33**:451-489.
- Groves D.I., Bierlein, F.P., Meinert, L.D., Hitzman, M.W. 2010. Iron oxide copper-gold (IOCG) deposits through Earth history: implications for origin, lithospheric setting, and distinction from other epigenetic iron oxide deposits. Economic Geology **105**: 641–654
- Haller A., Fontboté, L., 2009. The Raúl-Condestable Iron Oxide Copper-Gold Deposit, Central Coast of Peru: Ore and Related Hydrothermal Alteration, Sulfur Isotopes, and Thermodynamic Constraints. Economic Geology **104**:365-384.
- Hirata W.K., Rigon J.C., Kadekaru K., Cordeiro A.A.C., Meireles E.A. 1982. Geologia Regional da Província Mineral de Carajás. In: 1º Simpósio de Geologia da Amazônia, Belém. (Anais)
- Hitzman M.W. 2000. Iron oxide–Cu–Au deposits: what, where, when, and why. In: Porter TM (ed) Hydrothermal iron oxide copper-gold and related deposits: a global perspective Austral Miner Fund, Adelaide, p 9–25.
- Hoefs J. 2007. Stable Isotope Geochemistry: 7th edition. Springer-Verlag Berlin Heidelberg, pp. 402.
- Huhn S.R.B., Souza, C.I.J., Albuquerque, M.C., Leal, E.D., Brustolin, V., 1999a. Descoberta do depósito Cu(Au) Cristalino: Geologia e mineralização associada região da Serra do Rabo - Carajás - PA, in VI Simp. Geol. Amaz., Proceedings, SBG, Belém, pp. 140-143.
- Huhn S.R.B., Nascimento J.A.S. 1997. São os depósitos cupríferos de Carajás do tipo Cu-Au-U-ETR? In: Costa M.L., Angélica R.S. (eds), Contribuições a geologia da Amazônia, SBG, Belém, p. 143-160.
- Leite A.A.S., Dallagnol R., Macambira M.J.B., Althoff F.J. 2004. Geologia e geocronologia dos granitóides arqueanos da Região de Xinguara-PA e suas implicações na evolução do Terreno Granito- Greenstone de Rio Maria, Cráton Amazônico. Revista Brasileira de Geociências, **34**: 447-458.

- Lancaster J.O., Fanton, J., Almeida, A.J., Leveille, R.A. Vieira, S., 2000. Discovery and geology of the Sossego copper-gold deposit, Carajás District, Pará State, Brazil. *Inter. Geol. Congr.*, 31, Abstracts, RJ, [CD-ROM].
- Lindenmayer Z.G. 1990. Salobo sequence, Carajás, Brasil: Geology, Geochemistry and Metamorphism. PhD thesis, University of Ontario, Canada, 407p.
- Lindenmayer Z.G., 2003. Depósito de Cu-Au do Salobo, Serra dos Carajás: Uma revisão, in Ronchi, L.H., Althoff, F.J., (eds.), Caracterização e modelamento de depósitos minerais, Ed. Unisinos, pp. 69-98.
- Lindenmayer Z.G., Fleck A., Gomes C.H., Santos A.B.S., Caron R., Paula F. de C., Laux J.H., Pimentel M.M., Sardinha A.S. 2005. Caracterização geológica do Alvo Estrela (Cu-Au), Serra dos Carajás, Pará. In: O.J. Marini, B.W. Ramos, E.T. Queiroz. (Orgs.), Caracterização de Depósitos Minerais de Distritos Mineiros da Amazônia. Brasília. DNPM-CT-Mineral-FINEP-ADIMB, p. 137-205.
- Lobato L.M., Rosière C.A., Silva R.C.F., Zucchetti M., Baars F.J., Sedane J.C.S., Javier Rios F., Pimentel M., Mendes G.E., Monteiro A.M. 2005. A mineralização hidrotermal de ferro da Província Mineral de Carajás – controle estrutural e contexto na evolução metalogenética da província. In: Marini, O.J., Queiroz, E.T., Ramos, B.W. (Eds.). Caracterização de Depósitos Minerais em Distritos Mineiros da Amazônia, DNPM-CT-Mineral-FINEP-ADIMB, pp. 25-92.
- Macambira E.M.B., Vale, A.G. 1997. Programa Levantamentos Geológicos Básicos do Brasil. São Felix do Xingu. Folha SB.22-Y-B. Estado do Pará. DNPM/CPRM. Brasília, 384p.
- Macambira M.J.B.; Lancelot J.R. 1996. Time constraints for the formation of the Archean Rio Maria crust, southeastern Amazonian Craton, Brazil. *International Geology Review*, **38**:1134-1142
- Machado N., Lindenmayer D.H., Krough T.E., Lindenmayer Z.G. 1991. U-Pb geochronology of Archean magmatism and basement reactivation in the Carajás Area, Amazon Shield, Brazil. *Precambrian Research* **49**: 1–26.
- Mark G., Wilde A., Oliver N.H.S., Williams P.J., Ryan C.G. 2005. *Journal of Geochemical Exploration* **85**:31–46.
- Marschik, R., Chiaradia, M., and Fontboté, L., 2003a, Implications of Pb isotope signatures of rocks and iron oxide Cu-Au ores in the Candelaria-Punta del Cobre district, Chile: *Mineralium Deposita*, **35**: 900–912.

- Martins P.L.G., Toledo, C.L.B., Silva, A.M., Chemale Jr., F., Santos, J.O.S., Assis, L.M. 2018. Neoarchean magmatism in the southeastern Amazonian Craton, Brazil: Petrography, geochemistry and tectonic significance of basalts from the Carajás Basin. *Precambrian Research* **302**: 340-357.
- Meirelles, M.R., Dardenne, M.A., 1991 - Vulcanismo basáltico de afinidade shoshonítica em ambiente de arco arqueano, Grupo Grão Pará, Serra dos Carajás, Pa. *Revista Brasileira de Geociências* **21**: 41-50.
- Melo, G.H.C., Monteiro, L.V.S., Xavier, R.P., Moreto, C.P.N., Santiago, E.B.S., Dufrane, S.A., Aires, B., Santos, A.F.F. 2016. Temporal evolution of the giant Salobo IOCG deposit, Carajás Province (Brazil): constraints from paragenesis of hydrothermal alteration and U-Pb geochronology. *Mineralium Deposita*, **52**:709-732.
- Mougeot R., Respaut J.P., Briqueu L., Ledru P., Milesi J.P., Macambira M.J.B., Huhn S.B. 1996. Geochronological constrains for the age of the Águas Claras Formation (Carajás Province, Pará, Brazil). In: 39º Congresso Brasileiro de Geologia. Salvador, Anais.
- Montalvão R.G.M., Tassinari C.C.G., Bezerra P.E.L., Prado P.A. 1984. Geocronologia dos granitóides e gnaisses das regiões de Rio Maria, Fazenda Mata Geral e Rio Itacaiúnas, sul do Pará (Distrito Carajás - Cumaru). In: 33th Congresso Brasileiro de Geologia, Rio de Janeiro. (Proceedings).
- Monteiro L.V.S., Xavier, R.P., Souza Filho, C.R., Moreto, C.P.N. 2014. Metalogenia da Província Carajás. In: -Metalogenia das Províncias Tectônicas Brasileira.. Serviço geológico do Brasil- CPRM. 1 ed, 50p (in Portuguese).
- Monteiro L.V.S., Xavier R.P., Carvalho E.R., Hitzman M.W., Johnson C.A., Souza Filho C.R., Torresi I. 2008a. Spatial and temporal zoning of hydrothermal alteration and mineralization in the Sossego iron oxide–copper–gold deposit, Carajás Mineral Province, Brazil: paragenesis and stable isotope constraints. *Miner. Depos.*, **43**:129–159.
- Monteiro L.V.S., Xavier R.P., Hitzman M.W., Juliani C., Souza Filho C.R., Carvalho E.R. 2008b. Mineral chemistry of ore and hydrothermal alteration at the Sossego iron oxide–copper–gold deposit, Carajás Mineral Province, Brazil. *Ore Geol. Rev.*, **34**:317-336.
- Moreto C.P.N., Monteiro L.V.S., Xavier R.P., Amaral W.S., Santos T.J.S., Juliani C., Souza Filho C.R. 2011a. Mesoarchean (3.0 and 2.86 Ga) host rocks of the iron oxide-Cu-Au Bacaba deposit, Carajás Mineral Province: U-Pb geochronology and metallogenetic implications. *Mineralium Deposita* **46**: 789-811.

- Moreto C.P.N., Monteiro L.V.S., Xavier R.P., Creaser R.A., Dufrane S.A., Tassinari C.C.G., Sato K., Kemp A.I.S., Amaral W.S. 2015b. Neoarchean and Paleoproterozoic Iron Oxide-Copper-Gold events at the Sossego deposit, Carajás Province, Brazil, Re-Os and U-Pb geochronological evidence. *Economic Geology*, **110**: 809–835.
- Neves M.P. 2006. Estudos isotópicos (Pb-Pb, Sm-Nd, C e O) do depósito Cu-Au do Sossego, Província Mineral de Carajás. Dissertação de Mestrado, UFPA.
- Nogueira A.C.R., Truckenbrodt W., Pinheiro R.V.L. 1995. Formação Águas Claras, Pré-Cambriano da Serra dos Carajás: redescrição e redefinição litoestratigráfica. *Boletim Museu Paraense Emilio Goeldi*, **7**: 177-277.
- Ohmoto H., Goldhaber M.B. 1997. Sulfur and carbon isotopes. In: Barnes HL (eds), *Geochemistry of hydrothermal ore deposits*, Wiley, New York, pp. 517–611.
- Olszewski W.J., Wirth, K.R., Gibbs, A.K., Gaudette, H.E. 1989. The age, origin, and tectonics of the Grão Pará Group and associated rocks, Serra dos Carajás, Brazil: Archean continental volcanism and rifting. *Precambrian Research* **42**:229–254.
- Oliveira M.A., Dall'agnol R., Althoff F.J., Leite A.S.S., 2009. Mesoarchean sanukitoid rocks of the Rio Maria Granite-Greenstone Terrane, Amazonian craton, Brazil. *Journal of South American Earth Sciences*, **27(2-3)**: 146-160.
- Oreskes N., Einaudi, M.T., 1990. Origin of rare earth element-enriched hematite breccias at the Olympic Dam Cu-U-Ag deposit, Roxby Downs, South Australia. *Economic Geology*, **85**: 1 – 28.
- Pidgeon R.T., Macambira M.J.B., Lafon J.M. 2000. Th–U–Pb isotopic systems and internal structures of complex zircons from an enderbite from the Pium Complex, Carajás Province, Brazil: evidence for the ages of granulite facies metamorphism and the protolith of the enderbite. *Chemical Geology*, **166**:159–171.
- Pimentel M.M., Lindenmayer Z.G., Laux J.H., Armstrong R., Araújo J.C. 2003. Geochronology and Nd geochemistry of the Gameleira Cu-Au deposit, Serra dos Carajás, Brazil: 1.8–1.7 Ga hydrothermal alteration and mineralization. *J. South Am. Earth Sci.*, **15**: 803-813.
- Pinheiro R.V.L 2013. Carajás, Brazil – A short tectonic review. In: 13º Simpósio de Geologia da Amazônia. Belém, Anais.
- Pinheiro R.V.L., Holdsworth R.E. 1997. Reactivation of Archean strike-slip fault systems, Amazon region, Brazil. *Journal of the Geological Society*, **154**: 99–103.
- Pearce J. 1996. Sources and settings of granitic rocks. *Episodes* **19**:120–125.
- Pollard J.P. 2006. An intrusion-related origin for Cu-Au mineralization in iron oxide-copper-gold (IOCG) provinces. *Mineralium Deposita*, **41**:179.

- Ricci P.S.F. Rocks of the Pium-Area, Carajás Block, Brazil – a deep-seated high-T gabbroic pluton (charnockitoidlike) with xenoliths of enderbitic gneisses dated at 3002 Ma – the basement problem revisited. In: 9º Simpósio de Geologia da Amazônia, 2006, Belém, Anais.
- Riger A.A., Marschik R., Diaz M. 2012. The evolution of the hydrothermal IOCG system in the Mantoverde district, northern Chile: new evidence from microthermometry and stable isotope geochemistry. *Mineralium Deposita* **47**:359–369.
- Rigon J.C., Munaro, P., Santos, L.A., Nascimento, J.A.S., Barreira, C.F., 2000. Alvo 118 copper-gold deposit: geology and mineralization, Serra dos Carajás, Pará, Brazil. In: Inter. Geol. Congr, 31, Rio de Janeiro, SBG-IUGS, [CD-ROM].
- Réquia K.C.M. 1995. O papel do metamorfismo e fases fluidas na gênese da mineralização de cobre de Salobo, Província Mineral de Carajás, Pará. Dissertação de Mestrado, UNICAMP.
- Réquia K., Stein H., Fontboté L., Chiaradia M. 2003. Re–Os and Pb–Pb geochronology of the Archean Salobo iron oxide copper–gold deposit, Carajás Mineral Province, northern Brazil. *Mineralium Deposita*, **38**:727–738.
- Rolando A.P., Macambira M.J.B. 2003. Archean crust formation in Inajá range area, SSE of Amazonian craton, Brazil, based on zircon ages and Nd isotopes. In: 4º South American symposium on isotope geology. Salvador, p. 268-270.
- Sachs L.L.B., 1993. O magmatismo associado ao depósito mineral cupro-aurífero do Igarapé Bahia, Carajás, PA, Brasil. Universidade Estadual de Campinas, Dissertação de Mestrado, 142p.
- Santiago E.S.B. 2016. Elementosn traço (*in situ* LA-ICP-MS) e isótopos estáveis ($\Delta^{33}\text{S}$, $\Delta^{34}\text{S}$, $\delta^{56}\text{Fe}$ e $\delta^{18}\text{O}$) em magnetita e sulfetos: origem e evolução de sistemas de Cu-Au Neoarqueanos e Paleoproterozoicos da Província Mineral de Carajás, Brasil, pp 199.
- Santos J.O.S. 2003. Geotectônica do Escudo das Guianas e Brasil-Central. In: Bizzi LA,(ed) Geologia, tectônica e recursos minerais do Brasil: texto, mapas e SIG. Brasília, CPRM, pp 169-226.
- Sardinha A.S., Barros C.E. de M., Krymsky M. 2006. Geology, geochemistry and U–Pb geochronology of the Archean (2.74Ga) Serra do Rabo granite stocks, Carajás Metallogenetic Province, northern Brazil. *Journal of South American Earth Sciences* **20**: 327–339.
- Sillitoe R.H. 2003. Iron oxide copper-gold deposits: an Andean view. *Mineralium Deposita* **38**:787–812.

- Skirrow R.G., Bastrakov E.N., Barovich K., Fraser G.L., Creaser R.A., Fanning C.M., Raymond O.L., Davidson G.J. 2007. Timing of Iron Oxide Cu-Au-(U) Hydrothermal Activity and Nd Isotope Constraints on Metal Sources in the Gawler Craton, South Australia. *Economic Geology* **102**:1441–1470.
- Silva M.G., Teixeira J.B.G., Pimentel M.M., Vasconcelos P.M., Ariel A. e Rocha W.J.S.F. 2005. Geologia e mineralizações de Fe-Cu-Au do Alvo GT46 (Igarapé Cinzento, Carajás). In: Marini, O.J., Queiroz, E.T., Ramos, B.W. (eds.), Caracterização de Depósitos Minerais em Distritos Mineiros da Amazônia, DNPM-CT-Mineral-FINEP-ADIMB, p. 94-151.
- Souza S.R.B., Macambira M.J.B., Sheller T. 1996. Novos dados geocronológicos para os granitos deformados do Rio Itacaiúnas (Serra dos Carajás, PA), implicações estratigráficas. In: Simp. Geol. Amaz., 5, Belém, Anais, 380–383.
- Sylvester P.J. 1989. Post-collisional alcaline granites. *The journal of Geology* **97**:261–280.
- Taylor H.P. Jr 1997. Oxygen and hydrogen isotope relationships in hydrothermal mineral deposits. In: Barnes H.L. (eds.) *Geochemistry of hydrothermal ore deposits*. Wiley, New York, pp. 229–302.
- Tallarico F.H.B. 2003. O cinturão cupro-aurífero de Carajás, Brasil. Tese de Doutorado, UNICAMP, 229p.
- Tallarico F.H.B., Figueiredo B.R., Groves D.I., Kositcin N., McNaughton N.J., Fletcher I.R., Rego J.L. 2005. Geology and SHRIMP U-Pb geochronology of the Igarapé Bahia deposit, Carajás copper-gold belt, Brazil: an Archean (2.57 Ga) example of iron-oxide Cu-Au-(U-REE) mineralization. *Economic Geology* **100**: 7-28.
- Tallarico F.H.B., Oliveira C.G., Figueiredo B.R. 2000. The Igarapé Bahia Cu-Au mineralization, Carajás Province. *Revista Brasileira de Geociências*, **30**(2):230-233.
- Tallarico F.H.B.; Rego, J.L.; Oliveira, C.G. 1998. A mineralização de Au-Cu de Igarapé Bahia – Carajás: um depósito da classe óxido de Fe (Cu-U-Au-ETR). In: Cong. Bras. Geol., 40, Belo Horizonte, *Anais*, p. 116.
- Tassinari C.C.G., Mellito, M.K., Babinski, M., 2003. Age and origin of the Cu (Au-Mo-Ag) Salobo 3A ore deposit, Carajás Mineral Province, Amazonian Craton, northern Brazil, *Episodes* **26**: 2-9.
- Tassinari C.C.G., Macambira M.J.B. 1999. Geochronological Provinces of the Amazonian Craton. *Episodes*, **22**:174-182.
- Tavares F., 2015, Evolução Geotectônica do nordeste da Província Carajás. Unpublished PhD Thesis, Rio de Janeiro, University of Rio de Janeiro. pp. 130.

- Teixeira J.B.G. 1994. Geochemistry, petrology, and tectonic setting of archean basaltic and dioritic rocks from the N4 Iron deposit, Serra dos Carajás, Pará, Brazil. 1994. 161 f. Thesis (Doctor of Philosophy). Department of Geosciences, Penn State University.
- Teixeira W., Tassinari, C.C.G., Cordani, U.G., Kawashita, K. 1989. A review of the geochronological of the Amazonian Craton: tectonic implications. *Precambrian Research* **42**: 213-227.
- Torresi I, Bortholoto D.F.A., Xavier R.P., Monteiro L.V.S. 2012. Hydrothermal alteration, fluid inclusions and stable isotope systematics of the Alvo 118 iron oxide–copper–gold deposit, Carajás Mineral Province (Brazil): implications for ore genesis. *Miner Deposita*, 47: 299-323.
- Trendall A.F., Basei M.A.S., De Laeter J.R., Nelson D.R. 1998. SHRIMP U-Pb constraints on the age of the Carajás formation, Grão Pará Group, Amazon Craton. *Journal of South American Earth Sciences* **11**:265-277.
- Toledo P.I.F., 2017. Geologia do depósito IOCG Igarapé Cinzento/GT-46, Província Carajás. Dissertação de Mestrado, Campinas, Universidade Estadual de Campinas, p. 115.
- VALE 2002. Nova Fase da mina de Igarapé Bahia. VALE information Market, press releases. <http://www.vale.com/brasil/PT/investors/information-market/press-releases/Paginas/nova-fase-da-mina-de-igarape-bahia.aspx>. Acessado em 4 de novembro de 2016.
- Vasquez, M.L., Sousa, C.S., Carvalho, J.M.A. (Orgs) 2008b. Mapa Geológico e de Recursos Minerais do Estado do Pará, escala 1:1.000.000. Programa Geologia do Brasil (PGB), Integração, Atualização e Difusão de Dados da Geologia do Brasil, Mapas Geológicos Estaduais. CPRM – Serviço Geológico do Brasil, Superintendência Regional de Belém.
- Villas R.N., Santos, M.D. 2001. Gold deposits of the Carajás Mineral Province: deposit types and metallogenesis. *Mineralium Deposita* **36**: 300-331.
- Whalen J.B., Currie K.L., Chappell B.W. 1987. A-type granites: geochemical characteristics, discrimination and petrogenesis. *Contributions to mineralogy and petrology* **95**:407–418.
- Winter, C. J. 1994. Geology and Base Metal Mineralization associated with Archean Iron Formation in the Pojuca Corpo Quatro Deposit, Carajás, Brazil. Tese de Doutorado, University of Southampton.
- Wirth K.R., Gibbs A.K., Olszewski W.J. 1986. U-Pb ages of zircons from the Grão Pará Group and Serra dos Carajás Granite, Pará, Brazil. *Revista Brasileira de Geociências* **16**: 195-200.

- Xavier R.P., Monteiro L.V.S., Moreto C.P.N., Pestilho A.L.S., Melo G.H.C., da Silva M.A.D., Aires B., Ribeiro C, Freitas e Silva F.H. 2012. The iron oxide copper-gold systems of the Carajás Mineral Province. In: Hedenquist J., Harris M., Camus F. (eds) SEG special publication 16, Geology and genesis of major copper deposits and districts of the world: a tribute to Richard H. Sillitoe. Society of Economic Geologists, Inc, Littleton, pp 433–454
- Xavier R.P., Wiedenbeck M., Trumbull R.B., Dreher A.M., Monteiro L.V.S., Rhede D., Araújo C.E.G., Torresi I. 2008. Tourmaline B-isotopes fingerprint marine evaporites as the source of high-salinity ore fluids in iron oxide-copper-gold deposits, Carajás Mineral Province (Brazil). *Geology* **36**: 743-746.

**Anexo I – “The evolution of the Cu-Au
Igarapé Bahia deposit: early syngenetic
sulfides overprinted by IOCG
mineralization, Carajás Province (Brazil)”**

**The evolution of the Cu-Au Igarapé Bahia deposit: early
syngenetic sulfides overprinted by IOCG mineralization,
Carajás Province (Brazil)**

GUSTAVO H. C. DE MELO¹; LENA V. S. MONTEIRO²; ROBERTO P. XAVIER¹,
CAROLINA P. N. MORETO¹, RAUL M. ARQUAZ¹, MARCO A. D. SILVA¹

*¹Institute of Geosciences, University of Campinas (UNICAMP), R. João Pandiá
Calógeras, 51, 13083-870 Campinas (SP), Brazil*

*²Institute of Geosciences, University of São Paulo (USP), Rua do Lago, 562, 05508-080
São Paulo (SP), Brazil*

Abstract

The Cu–Au Igarapé Bahia deposit, located in the Carajás Domain, northern part of the Carajás Province in the Amazon Craton, comprises one of the most important deposits in the province. The deposit is hosted by the metavolcanosedimentary Igarapé Bahia Group and the metasedimentary Águas Claras Formation. The Igarapé Bahia Group encompasses metavolcanic rocks and metagabbros (lower unit) and metasedimentary rocks (metarhytmites, epiclastic rocks and banded iron formation) of the upper unit. Epiclastic rocks are predominant in the Águas Claras Formation. Basement xenoliths within the lower unit yielded an U–Pb zircon age of $2,935 \pm 36$ Ma, suggesting that a sialic crust was present prior to basin installation likely due to rifting. U–Pb dating of detrital zircon yielded maximum deposition age at $2,784 \pm 27$ Ma for the upper unit, and $2,763 \pm 32$ Ma and $2,774 \pm 19$ Ma for the Águas Claras Formation. Chalcopyrite nodules and layers are found within metarhytmites, concordant to primary structures, but without hydrothermal alteration halos and iron oxide. This chalcopyrite generation seems to have precipitated synchronously to the deposition of the Igarapé Bahia Group. Chalcopyrite nodules and layers shows $\delta^{34}\text{S}_{\text{VCDT}}$ values ranging from +0.29 to +1.56‰, and has considerable contents of Ni, Co and Bi. These data indicate that most of its sulfur and metals were derived from the metavolcanic rocks of the lower unit. Host rocks and chalcopyrite nodules and layers were overprinted by the IOCG mineralization. The latter formed extensive halos of hydrothermal alteration accompanied by ductile deformation and hydrothermal brecciation. These processes resulted in (tourmaline)-carbonate-magnetite, (tourmaline)-carbonate-chlorite and (tourmaline)-(biotite)-chlorite mylonites and breccias. Chalcopyrite from magnetite-rich zones (i.e. IOCG mineralization) displays $\delta^{34}\text{S}_{\text{VCDT}}$ values from +1.36 to +5.35‰. In addition to magmatic sulfur, seawater-derived sulfate may have been incorporated in sulfides via thermochemical sulfate-reduction reactions. High ΣREE values associated with large contents of U, Mo, Sn, W, Y, Nb and Sr are characteristic of chalcopyrite from magnetite-rich zones. The timing of the IOCG mineralization was constrained at $2,559 \pm 34$ Ma in the Alemão orebody. These data suggest that an important IOCG metallogenetic event in ca. 2.5 Ga overprinted an older syngenetic exhalative copper mineralization.

Keywords: IOCG, Igarapé Bahia, Carajás Province

1. Introduction

The Igarapé Bahia deposit is located in the Carajás Domain of the Carajás Province, one of the most important mineral provinces in Brazil. The deposit has estimated reserves of 219 Mt @ 1.4% Cu and 0.86 g/t Au (Tallarico et al. 2005). Mine operation started in 1990, producing 3,119 ounces of supergene gold until its closure in 2002. During this period, Igarapé Bahia was the largest gold mine in Brazil. It is currently under evaluation to become a copper mine (VALE 2002). Discovered in 1996, the Alemão orebody has been reported as the main segment of the Igarapé Bahia deposit, although its geology is still poorly described.

The deposit lies in an erosional window with a circular shape within the metasedimentary rocks of the Águas Claras Formation, close to the regional scale Carajás Shear Zone. It is mainly hosted by metavolcanosedimentary rocks of the Neoarchean Igarapé Bahia Group, Itacaiúnas Supergroup (Lindenmayer 1998, Tallarico et al. 2005, Dreher et al. 2005, 2008).

The Igarapé Bahia deposit consists of four separate orebodies, which include Alemão, Acampamento Norte, Acampamento Sul and Furo 30. Within these orebodies, features of syngenetic and epigenetic copper mineralization are observed. Extensive halos of hydrothermal alteration, ductile deformation with tilting of the host rocks, and sulfides associated with large contents of magnetite could be assigned to the epigenetic IOCG mineralization. Nevertheless, chalcopyrite nodules and layers parallel to primary sedimentary structures and with no association with iron oxides are also recognized in the Igarapé Bahia deposit. These could be evidence of the earliest manifestations of hydrothermal copper mineralization in the Carajás Domain, synchronous with the deposition of the Neoarchean Itacaiúnas Supergroup.

A syngenetic exhalative origin for the copper–gold mineralization at Igarapé Bahia deposit was proposed by Almada and Villas (1999), Galarza et al. (2008) and Dreher et al. (2005, 2008), similar to that of volcanic-hosted massive sulfide deposits (VHMS). According to this model, the timing of the copper-gold mineralization and associated brecciation was coeval with the formation of the metavolcanosedimentary sequence of the Igarapé Bahia Group (Almada and Villas 1999, Galarza et al. 2008, Dreher *et al.* 2005, 2008). In contrast, the structural control of the orebodies, style of mineralization (i.e. steeply dipping mylonitic ore lenses and hydrothermal breccias), intense K–Fe alteration and its high magnetite content have led other authors to define

this deposit as epigenetic and linked to an iron oxide–copper–gold (IOCG)-type hydrothermal system (Tallarico *et al.* 2005).

The IOCG mineralization at Igarapé Bahia deposit has already been dated at $2,575 \pm 12$ Ma (U–Pb in monazite, Tallarico *et al.* 2005) and correlated with the emplacement of ca. 2.57 Ga granites (e.g. Old Salobo granite; Réquia *et al.* 2003, Tallarico *et al.* 2005). Recent studies on IOCG deposits in the southern part of the Carajás Domain (Southern Copper Belt, Moreto *et al.* 2015a, b) distinguish other two major IOCG metallogenetic events: (i) 2.71 – 2.68 Ga (e.g. Sequeirinho orebody at Sossego deposit, Bacaba and Bacuri deposits) and (ii) ca. 1.88 Ga (e.g. Sossego orebody at Sossego deposit and Alvo 188 deposit), contrasting with that of the IOCG deposits located in the northern sector (i.e. Salobo and Igarapé Bahia deposits).

All these attributes reveal a more complex metallogenetic evolution of the Igarapé Bahia deposit. This evolution might include episodes of an early syngenetic copper mineralization, which was overprinted by a later epigenetic IOCG system. Additionally, the geometry of the deposit with four different orebodies raises the question of whether they have formed in a single hydrothermal event or are the result of multiple and distinct events, analogous to what has been described in the IOCG deposits of the Southern Copper Belt (i.e. Sossego deposit, Moreto *et al.* 2015a, b).

This paper focus on the nature and U–Pb ages of the host rocks and their implications to tectonic environment and evolution of the hydrothermal system responsible for different styles of copper mineralization in the four orebodies. It also brings new sulfur isotope data and trace elements geochemistry of early/syngenetic and IOCG chalcopyrite, leading to a new overview of the metallogeny at the Igarapé Bahia deposit. The unique geology of the Igarapé Bahia deposit, consisting of IOCG style mineralization overprinting an ancient syngenetic copper mineralization, opens new frontiers for the metallogenesis of the Carajás Domain.

2. Geological Setting

The Carajás Province represents a well-preserved Archean nucleus within the Amazon Craton, northern Brazil (Tassinari *et al.* 1999, Santos 2003). This province comprises two tectonic domains: the southern Rio Maria and the northern Carajás domains (Fig. 1A, B; Santos 2003, Vasquez *et al.* 2008).

In the Carajás Domain, basement rocks include mainly Mesoarchean orthogneisses and migmatites from the Xingu Complex with ages at $2,859 \pm 2$ Ma, interpreted as related to the last migmatization event (Machado *et al.* 1991). The Chicrim-Cateté Orthogranulite (Vasquez *et al.* 2008) was recently individualized from the Pium Complex and shows ages of $3,002 \pm 14$ Ma and $2,859 \pm 9$ Ma (Pidgeon *et al.* 2000), representing crystallization and metamorphism, respectively. Other undeformed granitoids also comprise basement rocks (e.g. ca 3.0 Ga Bacaba Tonalite and Sequeirinho Granite; ca. 2.96 Ga Canaã dos Carajás Granite; Moreto *et al.* 2011, Feio *et al.* 2013, Moreto *et al.*, 2015a).

Metavolcanosedimentary sequences of the Rio Novo Group and Itacaiúnas Supergroup overlie the basement rocks. The Rio Novo Group includes amphibolite, schist, metagraywacke, metavolcanic rocks and gabbro (Hirata *et al.* 1982). The Itacaiúnas Supergroup was divided into Igarapé Salobo, Igarapé Pojuca, Grão Pará and Igarapé Bahia groups. These consist mainly of metavolcanic, metavolcaniclastic and metasedimentary rocks (DOCEGEO 1988). Recent studies divided the Itacaiúnas Supergroup into lower (i.e. metavolcanic rocks), intermediate (i.e. banded iron formation) and upper sequences (i.e. metasedimentary units) (Tavares 2015).

The Igarapé Bahia Group was divided into the lower metavolcanic unit and the upper metasedimentary unit (DOCEGEO 1988, Dreher *et al.* 2008). The lower unit encompasses primarily metavolcanic and metapyroclastic rocks, and banded iron formation (DOCEGEO 1988). U-Pb zircon data constrain the age of the volcanic rocks of the lower unit at $2,748 \pm 34$ Ma (Tallarico *et al.* 2005). The upper unit comprises metasedimentary rocks interpreted to have formed during successive turbiditic flows (DOCEGEO 1998, Dreher *et al.* 2005). These rocks underwent low greenschist metamorphism and ductile deformation (DOCEGEO 1988).

The tectonic setting of both Rio Novo Group and Itacaiúnas Supergroup is debatable. Some authors proposed a continental rift tectonic setting for the formation of these sequences (Gibbs *et al.* 1986, Wirth *et al.* 1986, DOCEGEO 1988, Tallarico 2003). This idea was endorsed by Martins *et al.* (2017), who considered that mafic volcanic

rocks were produced due to rifting of an older continental crust. In contrast, an arc-related setting has also been proposed based on the high-potassium calc-alkaline affinity of the basalts from the Itacaiúnas Supergroup (Dardenne et al. 1988, Teixeira 1994, Lindenmayer 2005).

The Águas Claras Formation (Nogueira et al. 1995) covers part of the metavolcanosedimentary sequence of the Rio Novo Group and Itacaiúnas Supergroup. Basal metapelites, metaarenites and metaconglomerates were formed in marine to coastal depositional environments, whereas upper metaarenites and metaconglomerates were deposited in fluvial setting (Nogueira et al. 1995). Dating of intrusive mafic dykes in the Águas Claras Formation constrains the minimum age of its deposition at 2,708 ±37 Ma (U–Pb in zircon, Mugeot et al. 1996), although Pb–Pb ages in diagenetic pyrite from the Águas Claras Formation yielded ages of ca. 2.06 Ga (Mugeot et al. 1996), suggesting that the Águas Claras deposition could be younger.

Neoarchean mafic-ultramafic layered igneous intrusions also occur in the Carajás Domain (e.g. 2.76 Ga Luanga Complex; Machado et al. 1991). Important episodes of granite formation are broadly recognized in the province at (i) 2.76 – 2.73 Ga: A-type syn-tectonic granites, (e.g. Planalto, Estrela, Igarapé Gelado; Barros et al. 2004, 2009; Feio et al. 2013); (ii) ca. 2.57 Ga: peralkaline to metaluminous A-type granite magmatism, represented by the Old Salobo and Itacaiúnas granites; and (iii) ca. 1.88 Ga: A-type anorogenic granites (e.g. Central de Carajás, Cigano, Pojuca, and Breves, Machado et al. 1991; Lindenmayer and Teixeira 1999; Tallarico 2003).

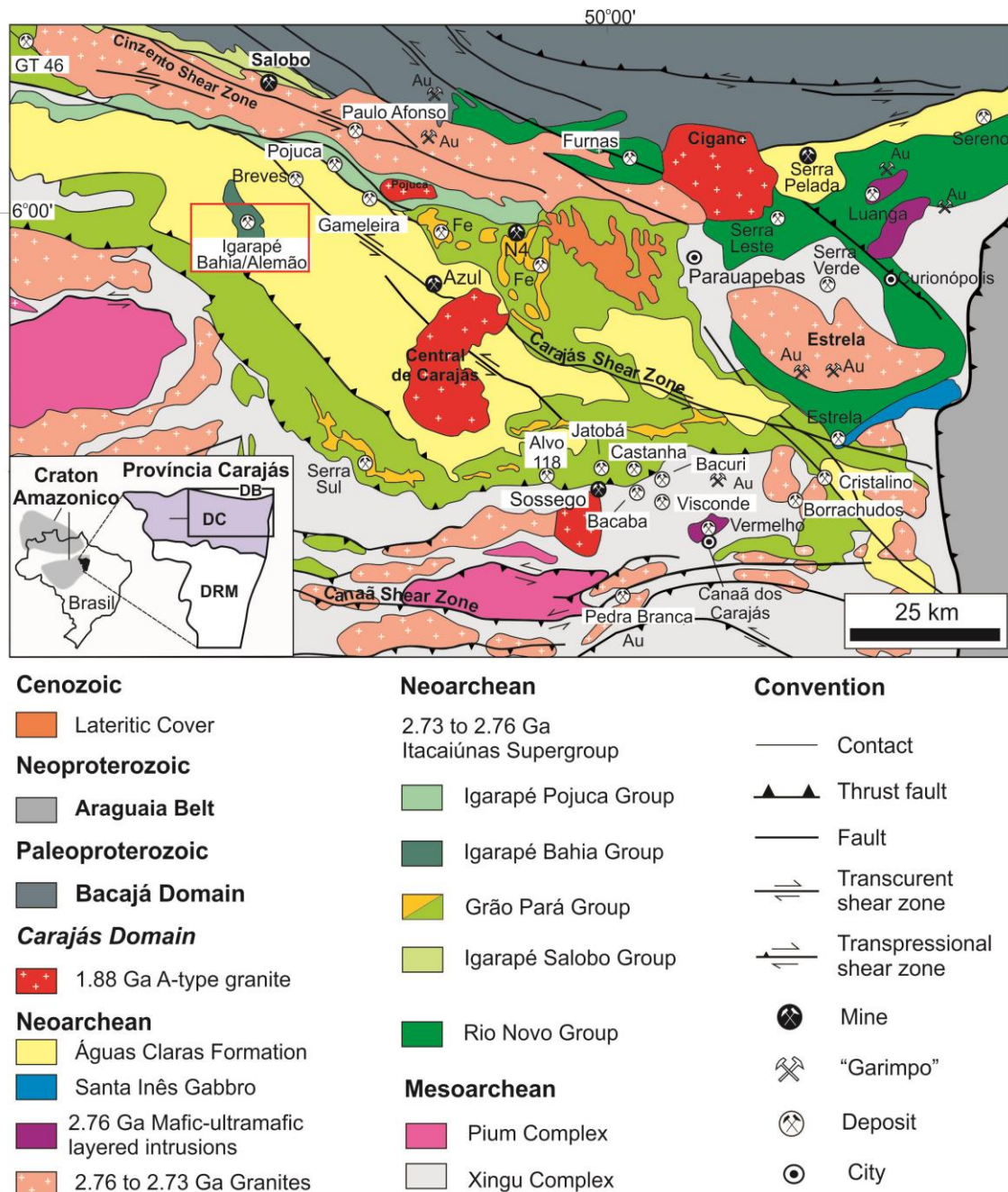


Fig. 1. Geological map of the Carajás Domain with the location of the main ore deposits. BD = Bacajá Domain, CD = Carajás Domain, RMD = Rio Maria Domain. Modified from Vasquez et al. (2008).

The structural framework of the Carajás Domain comprises mainly NW–SE and E–W trend structures. According to Araújo et al. (1988), the province evolved from a dextral transtension regime allowing the formation of a pull-apart basin. This basin was later inverted by a sinistral transpression, developing the Carajás and Cinzento strike-slip systems (Araújo et al. 1988). Alternatively, Pinheiro and Holdsworth (1997) suggested that these systems formed during a regional dextral transtension. Stronger

deformation is widely recognized in the E–W Canaã Shear Zone at southern of the Carajás Domain (Pinheiro et al. 2013). This set of strike-slip shear zones might have been responsible for the sigmoidal “S-shape” of the Carajás Basin (Pinheiro et al. 2013).

3. Previous Studies on the Igarapé Bahia deposit

Previous works have recognized massive, amygdaloidal and vesicular metabasalts, metapyroclastic rocks and granophytic metagabbros as the main host rocks in the Igarapé Bahia deposit, even though they are strongly hydrothermally altered and ductilely deformed (Ferreira Filho 1985, Sachs 1993, Althoff et al. 1994, Lindenmayer 1998, Almada and Villas 1999, Dreher et al. 2005). Metaarenites, metasiltites, metaargilites were considered subordinate host rocks (Althoff et al. 1994), occurring in the upper part of the deposit and collectively interpreted as turbidite sequences (Dreher et al. 2005, 2008). Most of these studies were performed over the Acampamento Norte, Acampamento Sul and Furo 30 orebodies, whilst the geology of the Alemão orebody, discovered later, is still poorly known. Dreher et al. (2008) considered the Alemão orebody as a down-faulted segment of the Acampamento Norte orebody.

The circular shape of the Igarapé Bahia deposit could point to the presence of an ancient volcanic caldera in the area (Almada and Villas 1999). In contrast, Tallarico et al. (2005) suggested that this shape is an evidence for a granitic or alkaline intrusive body at depth.

Several authors have recognized the importance of breccias within the central zone of the deposit (e.g. Almada and Villas 1999, Dreher et al. 2005, Tallarico et al. 2005). However, their origin is controversial. According to Almada and Villas (1999) and Dreher et al. (2005), these breccias are syngenetic and formed during the collapse of the volcano-sedimentary material of the Igarapé Bahia Group. These breccias were named as fragmental rocks, and described as polymitic matrix-supported breccias consisting of basalt, BIF and chert clasts set within a matrix of magnetite, siderite, chlorite and chalcopyrite (Dreher et al. 2005). In contrast, the same breccias were assigned as hydraulic breccias resulting of hydrothermal processes (Lindenmayer et al. 1998).

According to Dreher et al. (2008), the copper-gold mineralization is restricted to the Igarapé Bahia Group and does not transect the upper Águas Claras Formation.

The Igarapé Bahia deposit was first described as stringer ore formed in the late Archean to the Paleoproterozoic (Ferreira Filho 1985). Similarly, Almada and Villas (1999) and Villas and Santos (2001) suggested that copper-gold mineralization in the Igarapé Bahia deposit was syngenetic and related to a volcanic-exhalative system, analogous to the Besshy-type VHMS deposits (Almada and Villas, 1999). Key points for this model include (i) the dominant presence of submarine mafic volcanic rocks and the presence of exhalative rocks (i.e. BIF and chert); and (ii) the significant occurrence of terrigenous material (Almada and Villas 1999). An oceanic hydrothermal system at 400 °C and fluids circulating through the volcanosedimentary rocks was interpreted as responsible for the copper–gold mineralization during the fracturing of the host rocks (Althoff et al. 1994). The uncommon geochemical signature of the volcano-exhalative ore, with significant enrichment in U, F, P and LREE, was attributed to late hydrothermal events (Almada and Villas 1999, Villas and Santos 2001). This model was endorsed by Dreher et al. (2008), who considered the mineralized fragmental rocks formed synchronously to the volcanosedimentary sequence of the Igarapé Bahia Group.

Alternatively, Hunh and Nascimento (1997) first suggested that the iron oxide-rich copper–gold systems at Carajás could be similar to those of the iron oxide–copper–gold deposit class (IOCG; Hitzman et al. 1992). Supporting this model, Tallarico et al. (2005) obtained a SHRIMP U–Pb monazite age of $2,575 \pm 12$ Ma, considered as related to the timing of the epigenetic IOCG mineralization at Igarapé Bahia. This age, also recorded in the giant Salobo IOCG deposit ($2,576 \pm 8$ Ma, Re–Os in molybdenite, Réquia et al. 2003), was correlated with a single mineralization event and with the emplacement of the ca. 2.57 Ga granites (e.g. Old Salobo granite).

4. Analytical techniques

4.1 Drill Core description, petrographic studies and SEM

Field trip was performed in the Igarapé Bahia mine surroundings, including the visiting to the open pit and the description of eight drill holes (F30-DH01, F30-DH02, F30-DH03, ALM-FD067, ALM-FD068, ALM-FD073, ALM-FD173, ACPS F382, ACPN F328). Systematic description of the drill cores focused on determination of the host rocks, spatial distribution and types of hydrothermal alteration, and styles of copper-gold mineralization.

Petrographic studies and Energy Dispersive X-Ray Spectrometer (EDS) analyses on Scanning Electron Microscope (SEM) were performed on representative samples of

least altered host rocks, different hydrothermally altered zones and copper–gold mineralization styles. These analyses were carried out at the Microscope Laboratory of the Institute of Geosciences, University of Campinas (UNICAMP), Brazil.

4.2 LA-SF-ICP-MS U-Pb zircon geochronology

Zircon grains were separated from crushed rocks at the Institute of Geosciences, University of Campinas (UNICAMP, Brazil), using gravimetric and magnetic separation techniques. They were later mounted on a 1 inch round epoxy mount resin, polished using diamond paste and cleaned using 10% v/v HNO₃ followed by de-ionized water. SEM and cathodoluminescence images were taken of selected zircons in the separates.

Geochronological data were obtained at the Isotope Geology Laboratory of the Institute of Geoscience, University of Campinas (UNICAMP), Brazil. A full description of the analytical approach is reported in Navarro et al. (2015). An ICP-MS Element XR (Thermo Scientific), coupled with an Excite.193 (Photon Machines) laser ablation system was used to collect the isotope data. The acquisition protocol adopted was: 30 s of a gas blank acquisition followed by the ablation of the sample for 60 s in ultrapure He (laser frequency at 10 Hz, spot size of 40 µm). Data were collected for masses 202, 204, 206, 207, 208, 232, 235 and 238 using the ion counting modes of the SEM detector, except for masses 232 and 238, which were analyzed in combined ion counting and analogue mode. Four points were measured per mass peak, and the respective dwell times per mass were 4, 8, 4, 16, 3,3,3 and 4 ms. Data were reduced off-line using Iolite software (version 2.5) following the method described by Paton et al. 2010, which involves subtraction of gas blank followed by downhole fractionation correction comparing with the behavior of the 91500 reference zircon (Wiedenbeck et al. 1995). Common Pb correction was accomplished using VizualAge version 2014.10 (Petrus and Kamber 2012) when necessary. Zircon reference samples included Peixe and Temora standards. The programs Isoplot (Ludwig, 2003, 2009) and DensityPlotter (Vermeesch 2012) were also used for data processing. Data-point error ellipses are 2σ.

4.3 SHRIMP U-Pb monazite geochronology

The SHRIMP analyses were performed on a SHRIMP II instrument at the Jonh de Laeter Centre, at Curtin University, Australia. The monazite analytical procedure applied in the Curtin consortium SHRIMP II has been described by Fletcher et al.

(2010). A 10–15 μm diameter spot is used, with a mass-filtered O₂-primary beam of ~0.6–0.7 nA on monazite from samples FD67/225 and 80,10. Data for each spot is collected in sets of 8 scans on the monazite through the mass range of $^{196}\text{LaPO}_2^+$, $^{203}\text{CePO}_2^+$, $^{204}\text{Pb}^+$, Background, NdPO_2^+ , $^{206}\text{Pb}^+$, $^{207}\text{Pb}^+$, $^{208}\text{Pb}^+$, $^{232}\text{Th}^+$, $^{245}\text{YCeO}^+$, $^{254}\text{UO}^+$, $^{264}\text{ThO}_2^+$ and $^{270}\text{UO}_2^+$. The $^{206}\text{Pb}/^{238}\text{U}$ age standard and U content standard used is French (514 Ma and 1000 ppm U and 6.3% Th; Fletcher et al., 2010). The $^{207}\text{Pb}/^{206}\text{Pb}$ standard used to monitor instrument induced mass fractionation is Z2908 (1796 ± 2 Ma; Fletcher et al., 2010). The $^{207}\text{Pb}/^{206}\text{Pb}$ ratios obtained on Z2908 monazites during the SHRIMP sessions slightly differ from the $^{207}\text{Pb}/^{206}\text{Pb}$ TIMS ratios and a fractionated correction was applied to the standard monazite (French) and the unknowns. The common Pb correction was based on the measured ^{204}Pb -correction. “Negative” $^{204}\text{Pb}/^{206}\text{Pb}$ ratios were occasionally obtained, although their values were almost negligible, and the ^{204}Pb corrected and uncorrected $^{207}\text{Pb}^*/^{206}\text{Pb}^*$, $^{235}\text{U}/^{207}\text{Pb}^*$ and $^{238}\text{U}^*/^{206}\text{Pb}^*$ ratios matched within uncertainty. The programs SQUID II and Isoplot (Ludwig, 2003, 2009) were also used for data processing.

4.4 Sulfur Isotopes in Sulfides

Chalcopyrite separates were extracted from mineralized rocks of the Alemão, Furo 30 and Acampamento Sul orebodies in the Igarapé Bahia deposit. For sulfur isotope analysis, SO₂ production was obtained from the combustion of sulfides with excess oxygen in tin capsules at 1080 °C. The gas produced from the combustion was brought through a stream of helium to tungsten and zirconium catalysts for reduction in a high purity copper filament. The separation of SO₂ took place in a gas chromatograph. Stable isotope ratios were analyzed using MC–ICP–MS Neptune (Thermo Finnigan) coupled with laser New Wave UP213 Nd:YAG, in the Geochronology Laboratory of the University of Brasília. The $\delta^{34}\text{S}$ values have an accuracy of 0.01 ‰ and were reported in relation to the Canyon Diablo Troilite (CDT) standard.

4.5 Trace Elements in Chalcopyrite

The same chalcopyrite separates utilized for sulfur isotopes were also subjected to *in situ* trace element analyses. The samples were dissolved using nitric, chloridric and fluoridric acids in the microwaves oven. All the dissolutions were performed with ultra-pure water (18,2 MΩ.cm), obtained from the Milli-Q system. The nitric acid was purified via sub-boiling. The bottles were previously cleaned with a 5% HNO₃ and

rinsed with ultra-pure water. The detection limit (DL) was determined as the average (\bar{x}) plus 3 standard deviation (s) from ten blank samples ($DL = \bar{x} + 3s$).

The analyses were carried out in the ICP–MS XseriesII (Thermo) coupled with a CCT (Collision Cell Technology). The calibration of the instrument was done with multielementary solutions via 100 mg/L monoelementary standard-solutions (AccuStandards). Quality control was assured using the WMS-1 (sulfide ore powder) standard reference material.

5. Geology of the Igarapé Bahia deposit

The Igarapé Bahia deposit consists of four orebodies, from south to north: Furo 30, Acampamento Sul, Acampamento Norte and Alemão. The deposit is mainly hosted by the metavolcanosedimentary sequence of the Igarapé Bahia Group and the metasedimentary rocks of the Águas Claras Formation (Fig. 2 A, B, C, D, E).

The preserved sequence of the Igarapé Bahia Group is recognized particularly along the Furo 30 and Acampamento Sul orebodies, whereas the overlying metasedimentary Águas Claras Formation is best seen along the Alemão orebody (Fig. 3). Primary sedimentary bedding (S_0) and structures are preserved within sequences from the Igarapé Bahia Group and Águas Claras Formation.

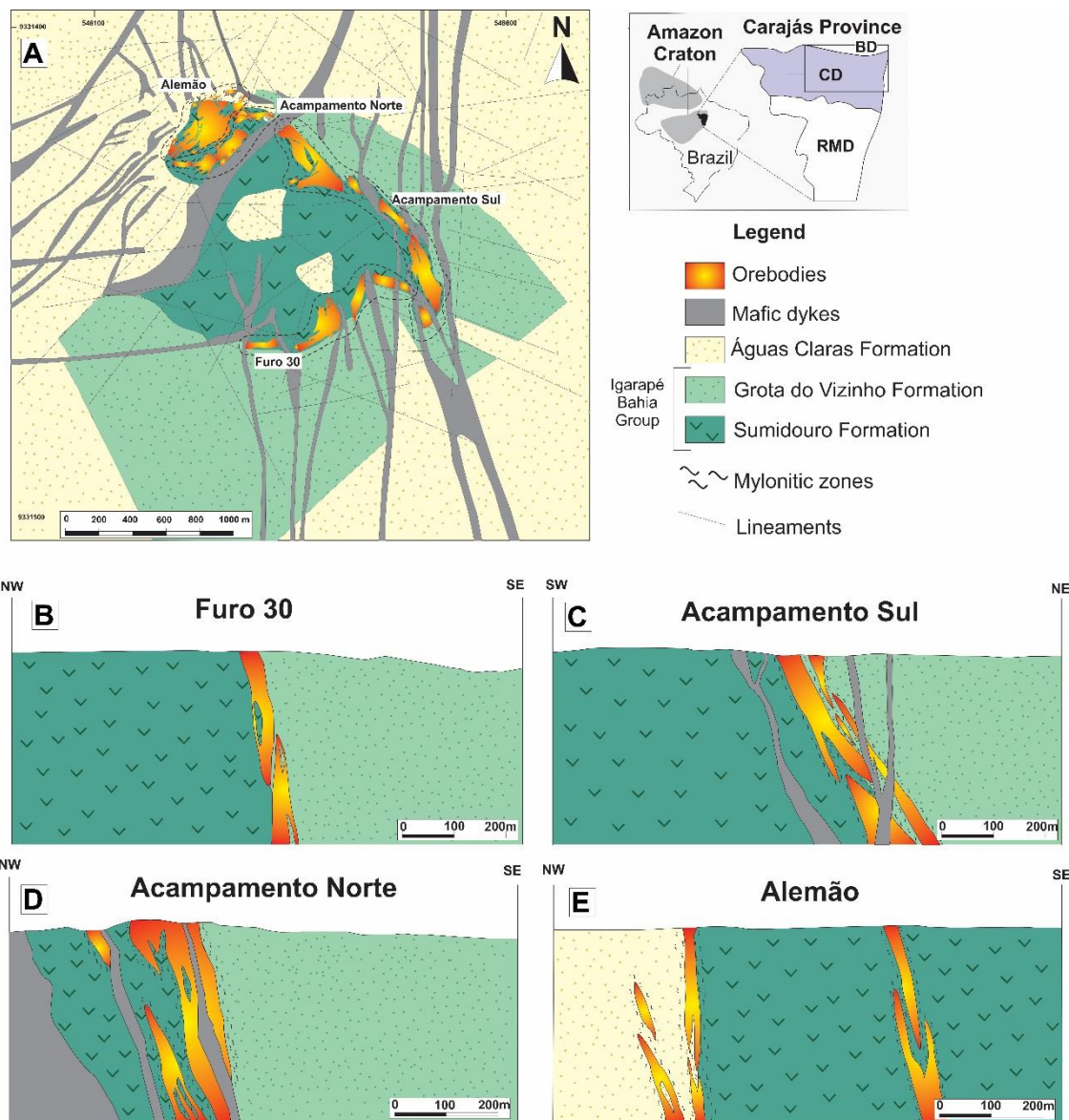


Fig. 2. a) Geological map of the Igarapé Bahia deposit. Cross-section of the b) Furo 30, c) Acampamento Sul, d) Acampamento Norte and e) Alemão orebodies. Orebodies are steeply dipping lenses with mylonitic foliation and/or hydrothermal breccias. Modified from VALE.

Brittle-ductile deformation with the development of mylonitic foliation and hydrothermal brecciation is observed in all orebodies with a substantial increase in its intensity towards the northern part of the deposit (i.e. Alemão and Acampamento Norte orebodies). Deformation imparted an anastomosed subvertical foliation (S_n) that tilted the primary S_0 structures and juxtaposed different lithotypes in the inner part of the orebodies.

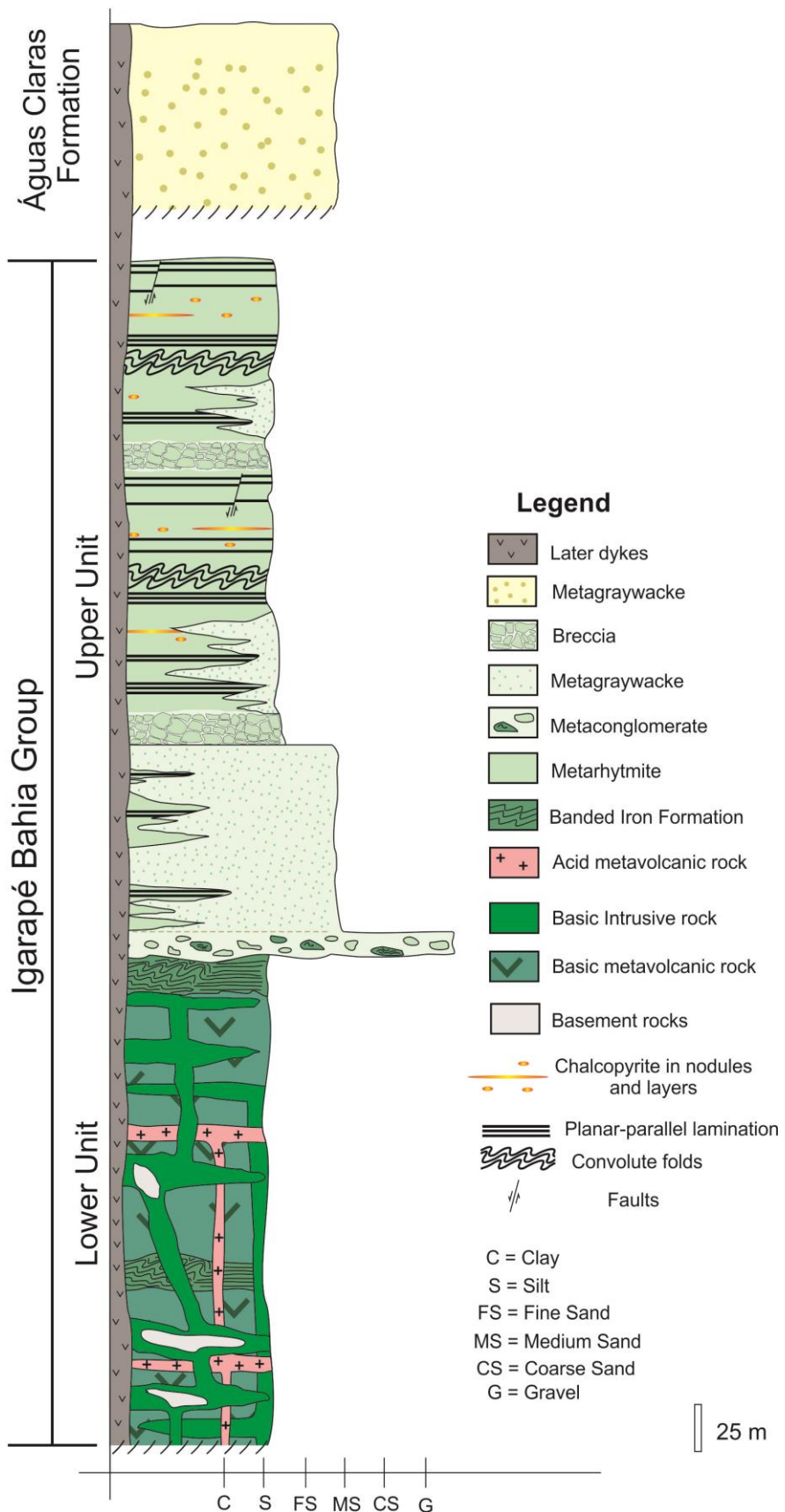


Fig. 3. Schematic stratigraphic column of the Igarapé Bahia Group and Águas Claras Formation within the Igarapé Bahia deposit.

5.1 Lower Unit of the Igarapé Bahia Group

The lower unit of the Igarapé Bahia Group comprises mainly mafic metavolcanic and intrusive rocks, and banded iron formation. Blocks of a felsic rock, interpreted as a possible xenolith, also occur within the mafic intrusive rocks from the lower unit. The felsic rock has granitic composition, is fine-grained and dominantly composed of quartz, potassium feldspar and minor plagioclase (Fig. 4A). Polycrystalline quartz, subgrains in quartz and bending of plagioclase twins are commonly observed. This indicates that this rock underwent recrystallization and metamorphic reequilibration. Most of its quartz is the product of silicification, which was accompanied by sericite, carbonate and chlorite formation (Fig. 4E).

The mafic metavolcanic rocks of the lower unit are aphanitic and in general strongly altered to chlorite (Fig. 4B). Nevertheless, least altered samples consist dominantly of plagioclase and pyroxene with a subophitic texture (Fig. 4D). Mafic intrusions of the lower unit are medium-grained phaneritic rocks and comprise the main bulk of the lower unit (Fig. 4C). These rocks are isotropic, composed of plagioclase laths and amphibole with rare relict pyroxene (augite-pigeonite), suggesting a gabbroic protolith (Fig. 4E). Chlorite, titanite and epidote are also present in mafic metavolcanic and intrusive rocks. However, it is difficult to distinguish a metamorphic or hydrothermal origin for these minerals. Intense hydrothermal alteration seems to have overprinted the low-grade metamorphic paragenesis, if present.

Felsic metavolcanic rocks are of very restricted occurrence in this formation. They are characterized by the presence of beta-quartz phenocrysts set in an aphanitic matrix (Fig. 4F). Hydrothermal chlorite and carbonate commonly replaces the matrix and obliterate their geological contacts with other lithotypes (Fig. 4G).

Meter-thick banded iron formations with layers of chert and magnetite frequently occur within mafic metavolcanic rocks, but also as clasts within hydrothermal breccias.

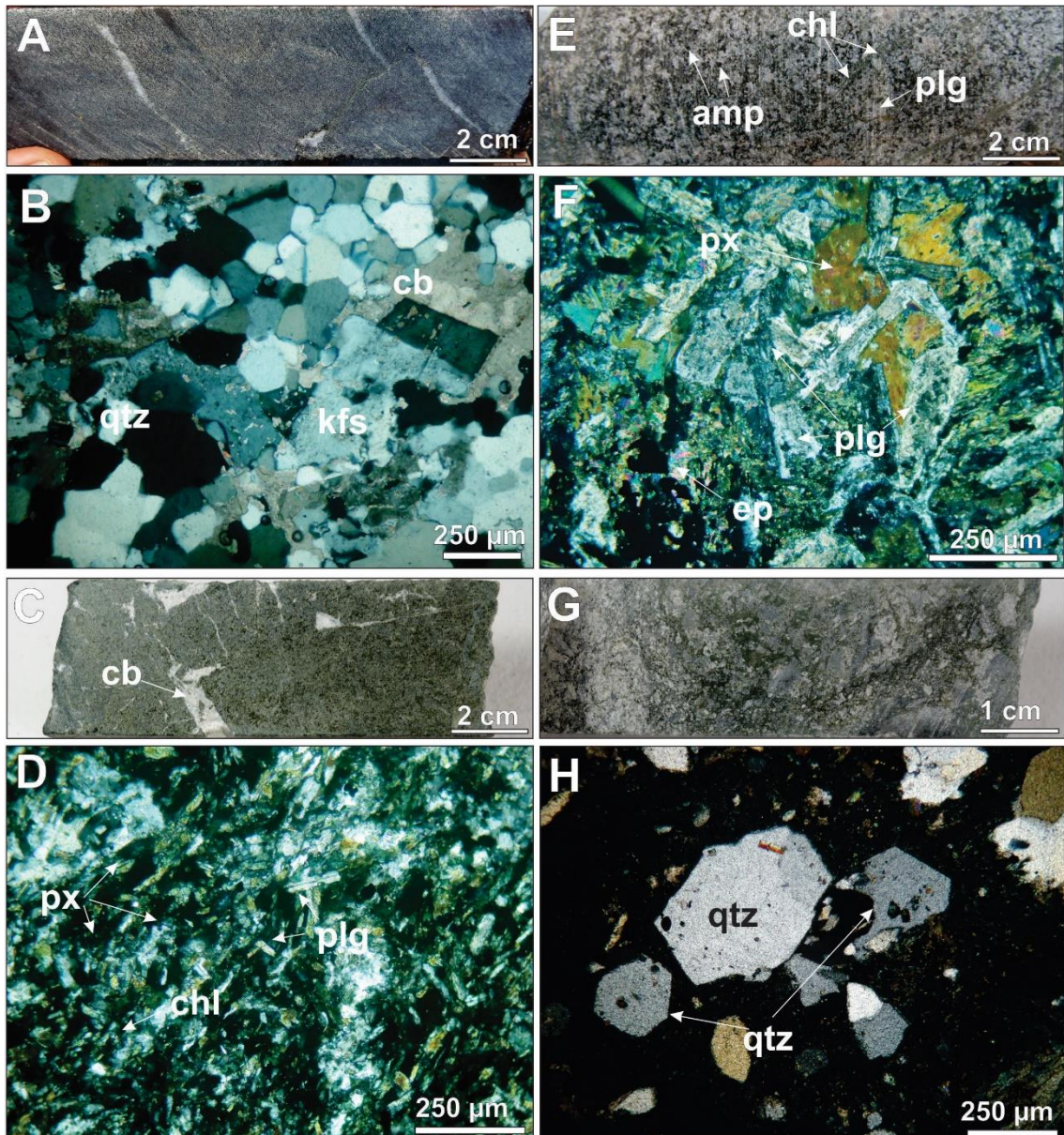


Fig. 4. Main lithotypes of the lower unit of the Igarapé Bahia Group. a) Fine-grained granite as xenoliths within the lower unit. b) Fotomicrograph of the fine-grained granite from the basement with quartz and K-feldspar with carbonate in their interstices. c) Fine-grained mafic metavolcanic rock with intense chlorite formation cut by later carbonate veinlets. d) Fotomicrograph of the basic metavolcanic rock with relicts of pyroxene, with intense chlorite formation. e) Metagabbro of the lower unit with amphibole, plagioclase and chlorite. f) Fotomicrograph of the metagabbro with partial replacement of the pyroxene by amphibole and preservation of the plagioclase laths. g) Felsic metavolcanic rock with intense chlorite formation. h) Felsic metavolcanic rock of the lower unit with beta-quartz phenocrysts set in a fine-grained matrix composed of fine-grained hydrothermal chlorite. Photos B, F, D and H are polarized light images. Mineral abbreviations: amp: amphibole, cb = carbonate, chl = chlorite, ep = epidote, plg = plagioclase, px = pyroxene, qtz = quartz, tur = tourmaline.

5.2 Upper Unit of the Igarapé Bahia Group

The upper unit of the Igarapé Bahia includes, from bottom to top, banded iron formation (BIF), metagraywackes and metarhytmites.

The banded iron formation is a 10-meter-thick layer that marks the transition from the volcanic environment of the lower unit to the chemical-siliciclastic deposition of the upper unit (Fig. 5A). The banded iron formation consists of alternation of millimeter-thick layers of magnetite with centimeter-thick chert layers. Pyrite and chalcopyrite also occur associated with magnetite. Intense hydrothermal chlorite alteration in the chert interstices is observed in the BIF.

Conglomerate is sitting stratigraphically above the BIF. It is matrix-supported, polyitic, and dominated by sub-angular clasts of BIF and metarhytomite (Fig. 5B). The conglomerate shows a gradational contact with the upper metagraywacke rocks. The clasts of the conglomerate become less abundant in the upward sequence, whereas the metagraywacke with massive texture begins to predominate.

The metagraywacke has the same mineralogical composition and textures of the conglomerate matrix (Fig. 5C). This rock is poorly-sorted and immature. It comprises medium to coarse quartz grains, which ranges from 0,8 mm to 7 mm, set in a very fine-grained matrix (>15 vol%). Quartz clasts are commonly monocrystalline, subangular to angular with well-developed facets and straight extinction, but polycrystalline quartz also occurs (Fig. 5D, E). Some rare feldspar grains are also recognized in these rocks. X-ray diffraction analyses in the matrix reveal the predominance of illite and sericite as its main constituents. Coarse muscovite grains occur within the matrix and exhibit bending cleavages, but its presence is restricted.

At stratigraphically higher levels, interlayering of metarhytmites and metagraywackes becomes frequent, but in the upper parts the former predominate over the latter lithotype. In these upper zones, metarhytomite rip up clasts within metagraywacke flows are very common. Fluidized flow structures of the metagraywackes rocks within metarhytmites are also observed (Fig. 5F, G).

The metarhytmites display thin plan-parallel bedding consisting of the interleaving of millimetric to centimetric layers of pelitic material and very fine sand (Fig. 5H, I). X-ray diffraction analyses of the metarhytmites indicate the presence of illite and sericite. Convoluted folds are recognized in the whole rhytomite sequence. Later faults offset plan-parallel bedding and convolute folds.

Clast-supported sedimentary breccias within the sequence of metarhytmites are common. These breccias are composed of disrupted metarhytomite clasts set in a metagraywacke matrix (Fig. 5J).

5.3 *Águas Claras Formation*

The Águas Claras Formation is best recognized within the Alemão orebody, in the northwestern portion of the deposit, where it sits right in contact with the lower unit of the Igarapé Bahia Group.

In this sector of the deposit, the Águas Claras Formation comprises a metagraywacke with moderately-sorted massive rocks composed of coarse-grained quartz within a very fine-grained matrix (>15%; Fig. 5K). Quartz grains are subrounded to subangular, have size of coarse- to very coarse sand, are monocrystalline with straight extinction, and some of them display well-developed facets (Fig. 5L, M). The matrix is composed primarily of illite and sericite. Bended coarse muscovite and zircon grains are also present in the matrix.

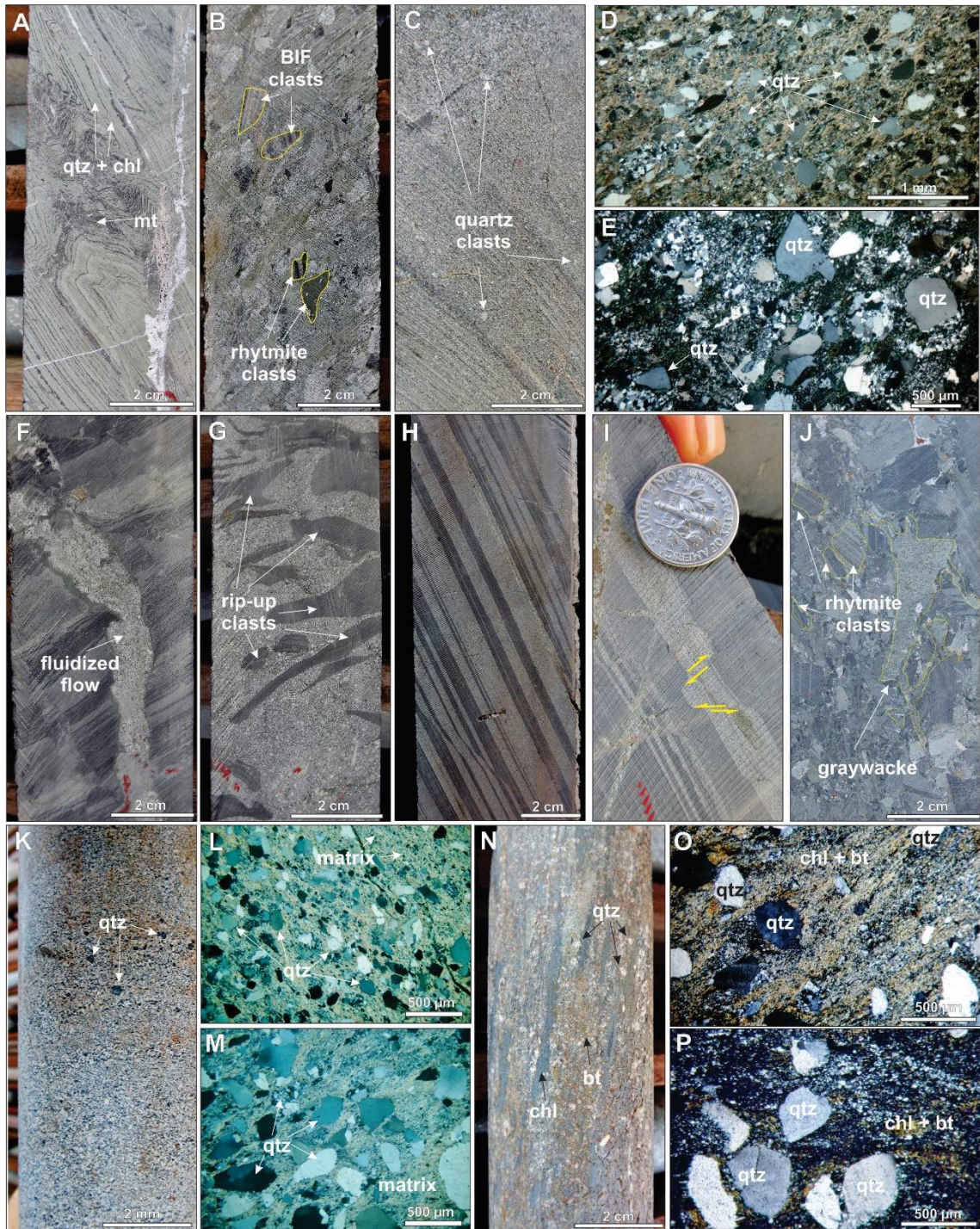


Fig. 5. Main lithotypes of the upper unit of the Igarapé Bahia Group and Águas Claras Formation. a) Banded iron formation at the bottom of upper unit showing convolute folds cut by late calcite veinlets. b) Basal metaconglomerates with BIF and metarhytmite clasts. c) Massive metagraywacke rock of the upper unit with scattered coarser quartz clasts in the matrix. d) Fotomicrograph of the upper unit metagraywacke with coarse quartz grains set in a matrix of illite and sericite. e) Same as d) but showing monocrystalline quartz grains in the metagraywacke with well-developed facets. f) Fluidized sediment flow of the metagraywacke cutting the metarhytmite sequence. g) Rip-up metarhytmite clasts within the metagraywacke sequence. h) Plan-parallel bedding with the interleaving of millimetric to centimetric layers of pelitic material and very fine sand of the metarhytmites rock in the drill core. i) Normal faults

displacing layers of the metarhytmites. j) Breccias within the metarhytomite sequence showing metarhytomite clasts cemented by metagraywacke flows. k) Metagraywackes from the Águas Claras Formation, with quartz grains set in a very fine-grained matrix with illite and scarce sericite. l) Fotomicrograph of unaltered rock of the Águas Claras formation, with quartz grains set in a sericitic matrix. m) Metagraywackes with coarse monocrystalline quartz grains in a sericitic matrix. n) Chloritized Águas Claras metagraywacke with mylonitic foliation and preservation of some quartz grains. o) Fotomicrograph of chloritized Águas Claras formation, with quartz grains set in foliated matrix of chlorite and minor biotite. p) Preservation of coarse quartz grains in mylonitized metagraywackes from the Águas Claras Formation. Photos D, E, L, M, O and P are polarized light images. Mineral abbreviations: bt = biotite, chl = chlorite, qtz = quartz, mt = magnetite.

This rock is commonly intercalated with hydrothermally altered and mylonitized facies, but the preservation of some features is evident, as suggested by the presence of coarse quartz grains in these zones (Fig. 5N, O). Hydrothermal chlorite, biotite and tourmaline replace illite and sericite and define the mylonitic foliation of these rocks (Fig. 5P).

5.4 Later mafic dykes

Later phaneritic, fine-grained, undeformed mafic dykes crosscut the main host rocks, hydrothermally altered zones and copper-gold mineralization, but their absolute age is still unknown.

6. Chalcopyrite nodules and layers within the upper unit of the Igarapé Bahia Group

Chalcopyrite nodules and layers occur within the metarhytomite sequence. They appear concordant with the bedding planes (S_0) and preferentially confined within very fine-grained sandy layers (Fig. 6A, B, C).

The average size of the sulfide nodules is 0.4 cm, but coarser nodules with up to 3 cm width, as well as smaller nodules with sizes <0.05 mm, are also recognized disseminated in the metarhytomite matrix (Fig. 6C). Chalcopyrite layers up to 1 cm also occur parallel to the bedding. Chalcopyrite nodules and layers have both inclusions and rims of quartz and chlorite (Fig. 6E, F). These rims also consist of tiny chalcopyrite grains intergrown with chlorite and quartz (Fig. 6G).

Chalcopyrite nodules are also encountered within conglomerate, breccia clasts and rip-up clasts (Fig. 6D), whereas the layers are commonly disrupted by faults, which

suggest formation prior to slumping and deformation of the metarhytmite. This chalcopyrite generation is overprinted by ductile deformation and hydrothermal alteration.

Scanning Electron Microscope (SEM) with coupled Energy Dispersive X-Ray Spectrometer (EDS) allowed the recognition of abundant monazite and xenotime as tiny inclusions within chalcopyrite nodules and layers (Fig. 6H). Subordinate amounts of galena, cobaltite, molybdenite and baddeleyite were also recognized (Fig. 6I).

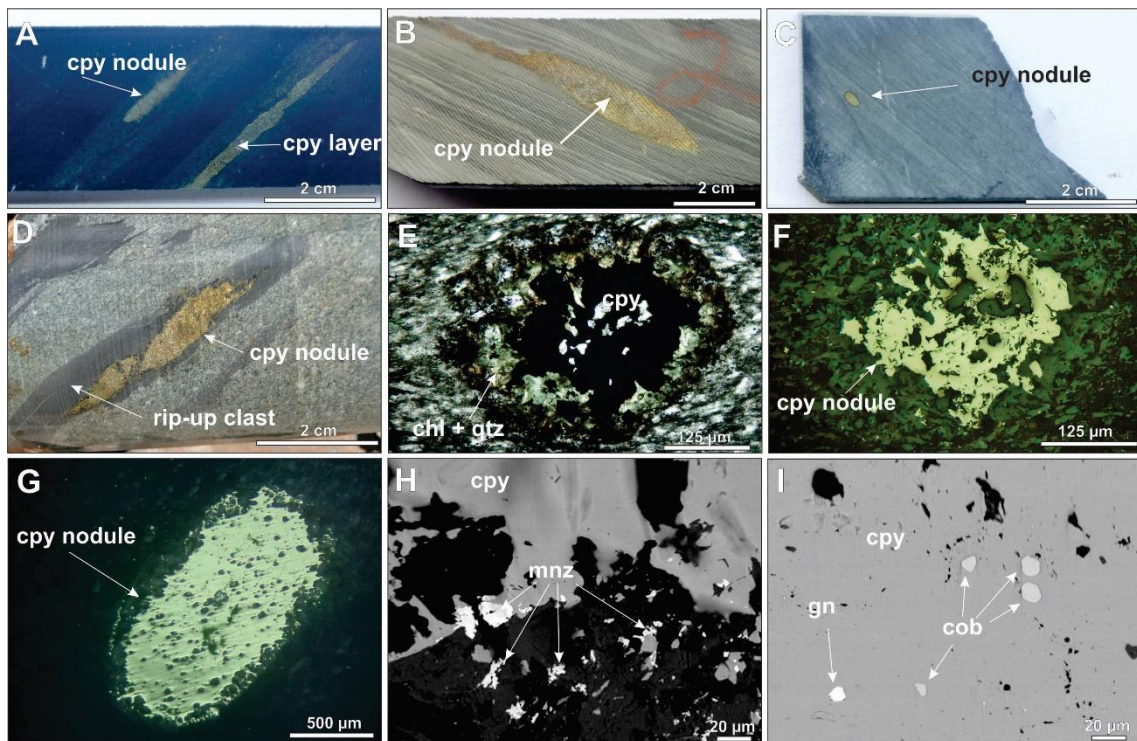


Fig. 6. Features of the chalcopyrite nodules and layers in the metarhytmites of the upper unit of the Igarapé Bahia. a) and b) Chalcopyrite nodules and layers concordant with the finely-laminated primary bedding in metarhytmite. c) Chalcopyrite nodule immersed in the metarhytmite matrix. d) Chalcopyrite nodules within metarhytmites rip-up clasts from the metagraywackes. Fotomicrographs of chalcopyrite nodules enveloped by chlorite and quartz under e) transmitted light and f) reflected light. g) Chalcopyrite nodule with a rim of chalcopyrite, chlorite and quartz. h) Monazite crystals along and near the edges of chalcopyrite nodules. i) Inclusions of galena and cobaltite in chalcopyrite nodule. Photos H and I are backscattered electron images. Mineral abbreviations: Chl = chlorite, Cpy = chalcopyrite, Cob = cobaltite, Gn = galena, Mnz = monazite, Qtz = quartz.

7. Hydrothermal Alteration

The sequence of hydrothermal alteration and the associated paragenetic evolution is similar in the four orebodies (Fig. 7). The nature of the host rocks is less discernible due to the intensity of hydrothermal alteration in the northern parts of the Igarapé Bahia deposit, in the Alemão and Acampamento Norte orebodies. In the Furo 30 orebody, hydrothermal alteration is weaker and the primary structures and textures of the host rocks are better preserved.

Calcic-sodic alteration is distal and spatially restricted, while potassic-(ferric) alteration with biotite is well developed in metabasic rocks. Tourmaline and carbonate formation followed potassic-(ferric) alteration and was pre- to syn-ore precipitation. Chlorite formation is late in the hydrothermal evolution and represents the most widespread hydrothermal alteration stage at Igarapé Bahia deposit. These hydrothermal alteration zones grade spatially from outer chlorite-rich zones to proximal carbonate-magnetite-sulfide-bearing zones.

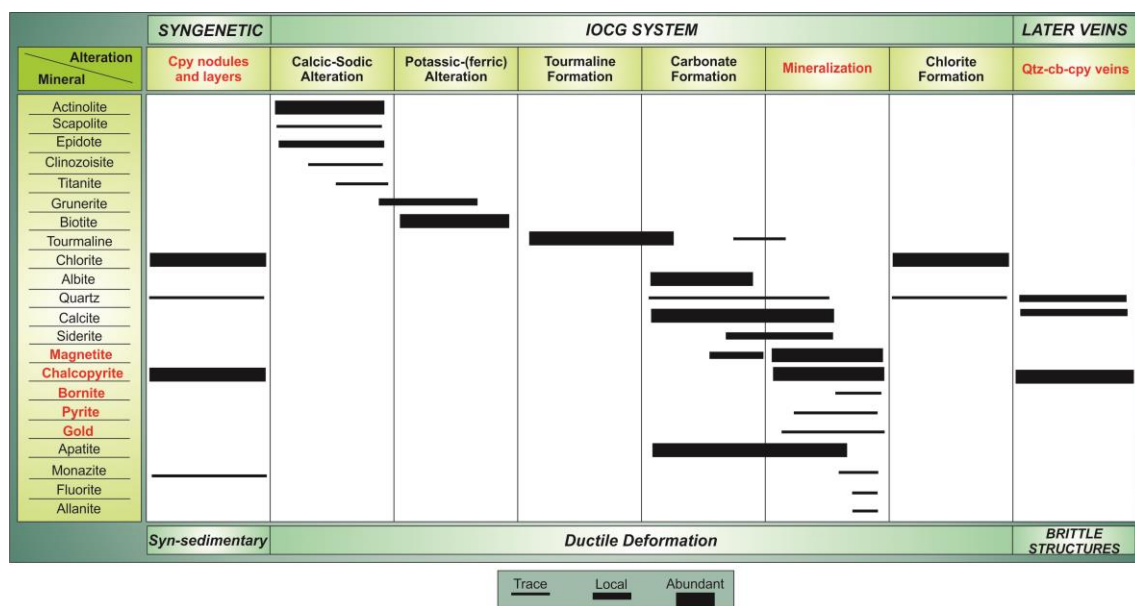


Fig. 7. Paragenetic table of the Igarapé Bahia deposit showing the evolution of the hydrothermal system and different styles of mineralization with their main constituents.

Mylonitic rocks composed of different hydrothermal minerals are conspicuous in the Igarapé Bahia deposit. These rocks show structures of shearing associated with the development of hydrothermal minerals. These coupled processes result in (tourmaline)-carbonate-magnetite, (tourmaline)-carbonate-chlorite and (tourmaline)-(biotite)-chlorite mylonites and breccias (Fig. 8A, B, C, D).

Hydrothermal breccias are expressive at Igarapé Bahia. These breccias are matrix-supported, polymitic and welded predominantly by carbonate and chlorite, and minor chalcopyrite and magnetite (Fig. 8E). The clasts comprise mainly coarse and rounded lithic fragments that include metasomatized metavolcanic rocks and BIF (Fig. 8F). Both mylonites and breccias host copper-gold mineralization.

7.1 Calcic-Sodic Alteration

Calcic-sodic alteration is distal, spatially restricted and mainly developed over the mafic lithotypes. It is represented predominantly by actinolite and more subordinately scapolite, clinozoisite, epidote and minor titanite (Fig. 8G).

Actinolite comprises needle-shaped crystals that have commonly been replaced by biotite and later carbonate. Scapolite crystals are coarse-grained and usually display acicular-fibrous texture dispersed in the rock (Fig. 8H). In the mafic rocks, it is encountered in the interstices of the minerals or replacing plagioclase. Epidote, clinozoisite and titanite are medium-grained crystals set in a matrix of later biotite.

7.2 Potassic-(ferric) Alteration

Potassic-(ferric) alteration is represented by widespread biotite formation that is best developed over mafic rocks. Biotite delineates the mylonitic foliation or composes part of hydrothermal breccia matrix. In less deformed zones, biotite displays radial-fibrous arrangements. Biotite is often replaced completely or partially by later chlorite.

Grunerite is of restricted occurrence and occurs as needle-shaped crystals within the mylonitic foliation, together with biotite (Fig. 8I).

7.3 Tourmaline Formation

Tourmaline is a conspicuous mineral in the Igarapé Bahia deposit where it occurs as very thin to coarse grains of up to 0.5 centimeters dispersed in the carbonate-chlorite-rich alteration zones. It is commonly replaced by chlorite and quartz (Fig 8J, K). Tourmaline relicts are also common within magnetite-chalcopyrite-rich zones. Most of tourmaline grains are aligned with stretched carbonate along the foliation. However, minor later tourmaline grains are recognized orthogonal to the mylonitic foliation (Fig 8K).

Optical characteristics under transmitted light of the microscope, which include pleochroism and birefringence, suggest that tourmaline composition ranges from dravite to shorl. Tourmaline crystals are frequently zoned, likely evidencing different composition from rim to core (Fig. 8J).

7.4 Carbonate–(Magnetite) Formation

Carbonate formation is a very pervasive and widespread hydrothermal stage in the Igarapé Bahia deposit, although it is better recognized in the central parts of the orebodies. This stage is defined by a mineral assemblage essentially dominated by calcite, together with variable amounts of siderite, apatite, chlorite, magnetite I and chalcopyrite.

Calcite takes place as mineral aggregates, either as stretched crystals performing the mylonitic foliation or as idioblastic grains in isotropic portions (Fig. 8K). Coarse-grained calcite crystals are surrounded by chlorite forming strain shadows (Fig. 8L). Siderite has the same spatial distribution, but is less abundant than calcite. It is recognized due to its red color under transmitted light in the microscope, likely as a result of its oxidation.

In addition, some albite porphyroblasts are recognized in these zones. Fine idioblastic apatite crystals are dispersed within carbonate zones. Apatite is associated with sulfides and magnetite or is aligned along mylonitic foliation with carbonates (Fig. 8M).

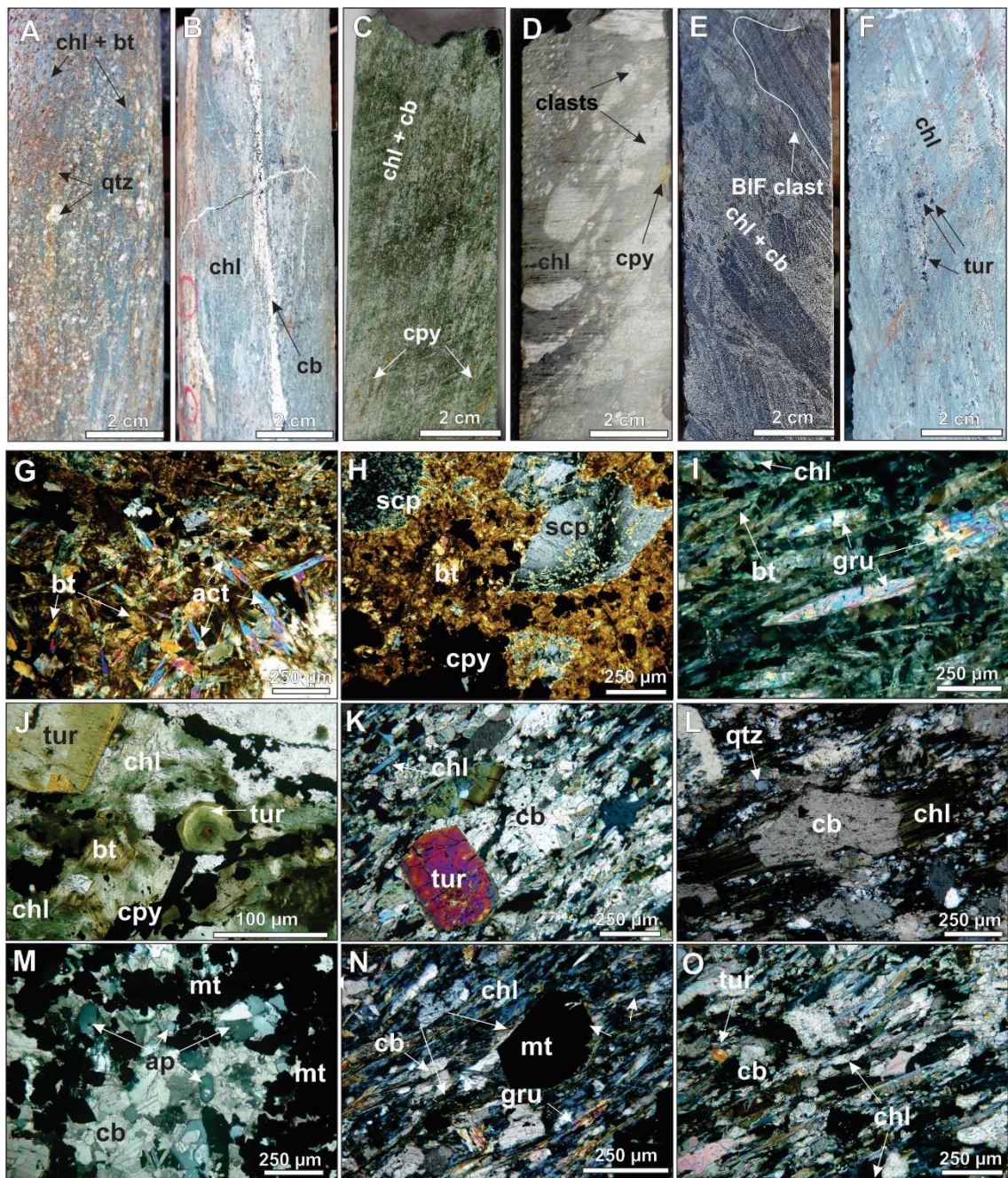


Fig. 8. Main hydrothermal alteration features of the Igarapé Bahia deposit. a) Biotite-chlorite mylonite with preservation of the quartz grains from the Águas Claras Formation. b) Drill core of zones with intense chlorite and carbonate formation performing the mylonitic foliation in the metagraywackes of the Águas Claras Formation. c) Mylonite with chlorite and carbonate along the foliation and stretched chalcopyrite. d) Hydrothermal breccias with clasts of metavolcanic rocks welded by chlorite and minor chalcopyrite. e) Hydrothermal breccia with BIF clasts cemented by a matrix of chlorite and carbonate in the mafic metavolcanic rocks. f) Chlorite-rich alteration zone containing disseminated tourmaline grains. g) Calcic-sodic alteration with needle-shaped actinolite crystals. h) Scapolite formation with radial fibrous texture partially replaced by biotite. i) Grunerite crystals associated with biotite. Photos G to I are polarized light images. j) Zoned tourmaline porphyroblasts immersed in a chlorite-rich matrix with chalcopyrite. Photo J is natural light image. k) Carbonate formation in mylonitic rock with scattered tourmaline. l) Chlorite-rich alteration zone with scattered tourmaline. m) Tourmaline, apatite, and carbonatite in a chlorite-rich matrix. n) Chlorite, tourmaline, and grunerite in a chlorite-rich matrix. o) Tourmaline, carbonatite, and chlorite in a chlorite-rich matrix.

tourmaline grains. l) Carbonate porphyroblasts with chlorite alteration along the rims. m) Apatite grains within a carbonate-magnetite alteration zone. n) Chlorite and carbonate formation in strongly mylonitized zones associated with magnetite. o) Typical texture of mylonitic hydrothermally altered rocks with stretched carbonate and lepidoblastic chlorite. Photos K to O are polarized light images. Mineral abbreviations: ab = albite, act = actinolite, ap = apatite, bt = biotite, cb = carbonate, chl = chlorite, cpy = chalcopyrite, gru = grunerite, mt = magnetite, qtz = quartz, scp = scapolite, tur = tourmaline.

7.5 Chlorite Alteration

Chlorite formation was the most widespread hydrothermal alteration in all four orebodies and represents the last stage of the hydrothermal alteration at Igarapé Bahia. This alteration stage is structurally controlled and related to the mylonitic foliation development.

Chlorite clearly replaces some of the previous hydrothermal minerals. Optical characteristics suggest that most of chlorite formation is represented by Fe-chlorite, although Mg-chlorite is recognized in some portion.

Chlorite and carbonate are the most common minerals that compose the mylonitic foliation with stretched crystals. In these zones, lepidoblastic chlorite is interleaved with carbonate and minor tourmaline, magnetite I and chalcopyrite (Fig. 8N, O). Chlorite also outlines the carbonate crystals and ore minerals, usually exhibiting strain shadows (Fig. 8L). Stretched quartz often accompanies chlorite formation along the mylonitic foliation.

8. Copper-Gold Mineralization

The Alemão, Acampamento Norte and Acampamento Sul orebodies are steeply dipping and confined to mylonitic zones and hydrothermal breccias, spatially related to banded iron formations of the lower unit of the Igarapé Bahia Group. At the Alemão orebody, the ore is dominantly composed of massive chalcopyrite-magnetite lenses (Fig. 9A), together with hydrothermal breccias (Fig. 9B, C, E). At the Acampamento Sul and Acampamento Norte orebodies, breccias are ubiquitous (Fig. 9D); whereas at the Furo 30 orebody, tourmaline-carbonate-magnetite-chalcopyrite mineralization develops preferably at the contact of the lower and upper units of the Igarapé Bahia Group (Fig. 9F). In this case, breccias and mylonites are not usual.

Ore mineral association is similar in all the orebodies, including chalcopyrite as the main sulfide, accompanied by coarse-grained pyrite and large amounts of

subdioblastic magnetite II, which comprise up to 60% of the rocks (Fig. 9G, H). Chalcopyrite is often stretched along the foliation within breccias or mylonitic rocks, although undeformed chalcopyrite also occurs in some parts. Bornite occurs locally intergrown or in the edges of chalcopyrite (Fig. 9H), in the same way as covellite (Fig. 9G). The main gangue minerals include carbonates (i.e. calcite and siderite), apatite, tourmaline, chlorite and fluorite.

Numerous microscopic inclusions within the orebodies were identified under the Scanning Electron Microscope (SEM). Uraninite, galena, cobaltite and molybdenite are very common in the ore association (Fig. 9K). In addition, ETR-rich minerals also occur and include monazite $[(Ce, Nd)(PO_4)]$, xenotime $[Y(PO_4)]$, allanite $(\{CaCe\} \{Al_2Fe^{2+}\}(Si_2O_7)(SiO_4)O(OH))$ and petersenite $[Na_4(Ce, La, Nd)_2(CO_3)_5]$ (Fig. 9L). Besides the high content of apatite within the ore, other phosphates, including cheralite $[CaTh(PO_4)_2]$ and autunite $[Ca(UO_2)_2(PO_4)_2 \cdot 11H_2O]$, are also present. A remarkable feature of the copper-gold ore at the Igarapé Bahia is the high content of sheelite $[Ca(WO_4)]$, cassiterite (SnO_2), pyrochlore ($Ca_2Nb_2O_6OH$) and subordinated contents of wolframite ($Fe^{2+}WO_4$) and fergusonite ($YNbO_4$) (Fig. 9K, L, M).

Gold is found as tiny crystals ($<10 \mu m$) within the ore zones, spatially associated with chalcopyrite, and rare crystals can be recognized under the optical microscope. It is often associated with hessite (Ag_2Te), cobaltite ($CoAsS$) and gersdorffite ($NiAsS$) (Fig. 9N, O).

9. Late quartz–carbonate–chalcopyrite veins

Late quartz–carbonate–chalcopyrite veins filling brittle structures are widely recognized in all four orebodies of the Igarapé Bahia deposit (Fig. 9P, Q). These veins cross cut all the previous stages of hydrothermal alteration and related orebodies and display no hydrothermal alteration halos.

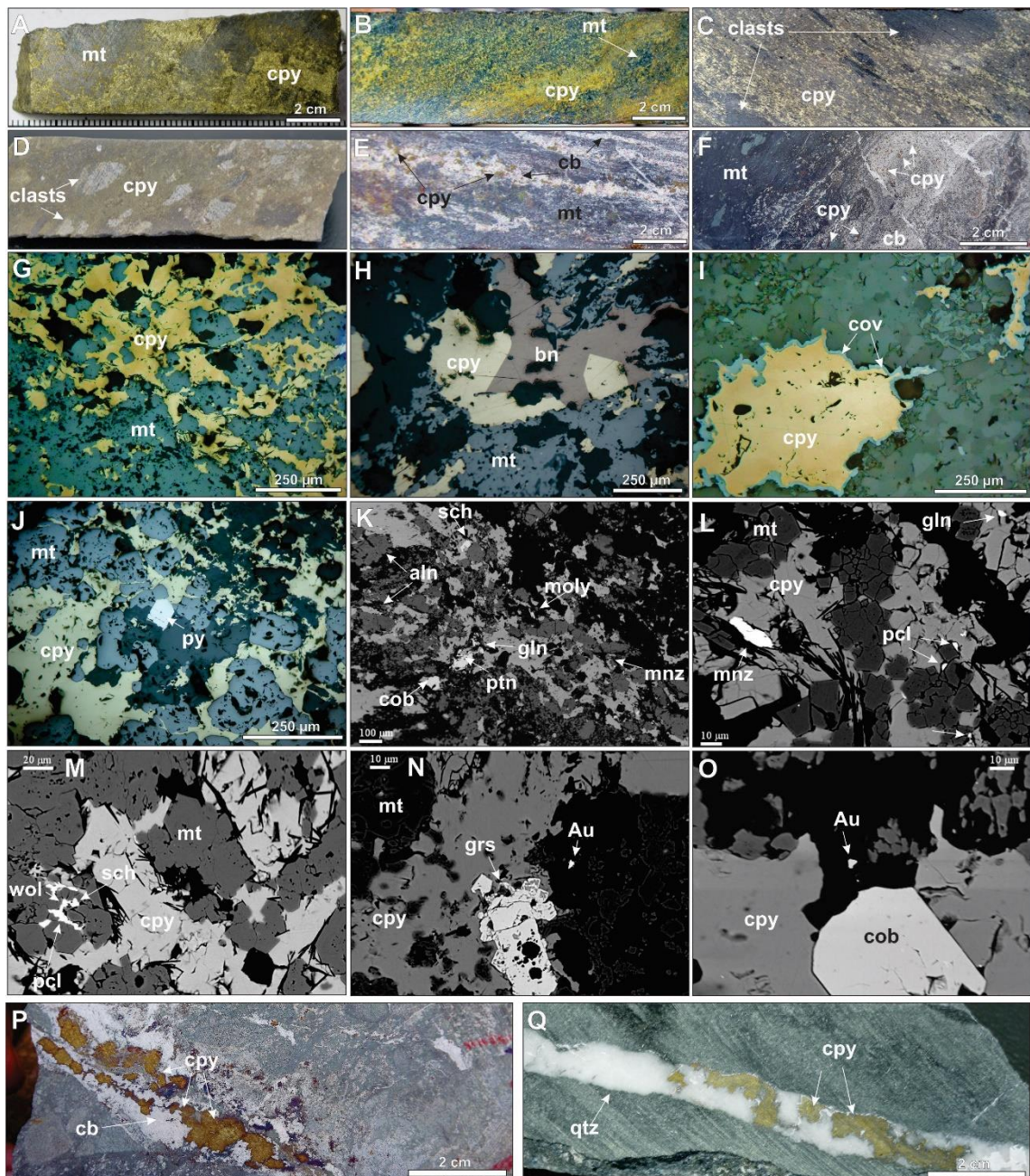


Fig. 9. Main styles of mineralization and ore associations at Igarapé Bahia deposit. a) Massive ore with chalcopyrite and magnetite in the Alemão orebody. b) Slightly foliated chalcopyrite-magnetite ore of the Alemão orebody. c) Hydrothermal breccia with foliated matrix composed of chalcopyrite and magnetite and clasts of metavolcanic rocks at the Alemão orebody. d) Hydrothermal breccia with BIF and metavolcanic clasts set in a foliated chalcopyrite matrix in the Acampamento Norte orebody. e) Mylonitic mineralized rocks with chalcopyrite, magnetite and large contents of carbonate at the Alemão orebody. f) Hydrothermal breccia of the Furo 30 orebody with chalcopyrite within magnetite-carbonate-rich zones. g) Intergrowth of chalcopyrite and magnetite crystals in mineralized zones of the Alemão orebody. h) Rare bornite crystals associated with chalcopyrite. i) Covellite replacing chalcopyrite in its edges. j) Idioblastic pyrite within mineralized zones with chalcopyrite and magnetite. Photos G to J are reflected light image. k) Tiny inclusions of scheelite, allanite, molybdenite, galena, cobaltite, monazite and pentlandite in mineralized zones. l) Monazite crystals in paragenesis with chalcopyrite. m) and

Chalcopyrite and magnetite zones with inclusions of wolframite, scheelite, and pyrochlore. Gold associated with precipitation of n) gersdorffite and o) cobaltite. Photos K to O are backscattered electron images. p) Later quartz-carbonate-chalcopyrite veinlets cutting previous stages of hydrothermal alteration. q) Quartz-rich veinlets with chalcopyrite crosscutting a metavolcanic rock. Mineral abbreviations: aln = allanite, ap = apatite, Au = ouro, bn = bornite, cb = carbonate, cob = cobaltite, cov = covellite, cpy = chalcopyrite, gln = galena, grs = gersdorffite, mnz = monazite, moly = molybdenite, mt = magnetite, ptm = pentlandite, plc = pyrochlore, py = pyrite, qtz = quartz, sch = scheelite, wol = wolframite.

In these veins, calcite is predominant and frequently displays open-space filling textures (e.g. comb texture), indicating emplacement at shallow crustal levels. Some quartz associated with calcite is observed and the ratio of quartz/carbonate varies in the veins. These veins contain idioblastic, well-formed chalcopyrite II crystals but conspicuously lack any iron oxide.

10. U–Pb Geochronology

10.1 LA–SF–ICP–MS U–Pb zircon dating

Four samples from the main host units of the Igarapé Bahia deposit were selected for dating by LA–SF–ICP–MS at the Institute of Geosciences of the University of Campinas (Table 1).

At the Furo 30 orebody, samples from the fine-grained granite xenoliths within the lower unit (DH01/347,70), and from metagraywackes of the upper unit (DH02/407,70) were selected. Detrital zircon populations were analyzed from the metagraywacke.

In the Alemão orebody, dated samples included the metagraywackes from the Águas Claras Formation (FD67/132,65) and low-grade ore zones (FD73/330,25). The age of the Águas Claras Formation remains uncertain. The youngest detrital zircon population could better constrain the maximum depositional age of this unit. The low-grade ore samples can reveal the age of the host rock at Alemão, where primary textures have been obliterated.

Table 1. Selected samples of the Igarapé Bahia deposit from which zircon and monazite grains were extracted to be analyzed by LA–SF–ICP–MS and U–Pb SHRIMP in zircon and monazite

Sample	Description	Unit	Mineral	Method	Age (Ma)
DH01/347,70	Xenoliths of weakly-altered deformed granitoids within the upper unit	Basement xenolith	Zircon	LA-SF-ICP-MS	$2,935 \pm 36$ Ma
DH02/407,70	Weakly chlorite-altered metagraywacke with preserved primary textures	Upper unit	Detrital zircon	LA-SF-ICP-MS	- 2.82 – 2.88 Ga - 2.94 – 2.99 Ga
FD67/132,65	Unaltered metagraywacke	Águas Claras Formation	Detrital zircon	LA-SF-ICP-MS	- 2.82 – 2.88 Ga - 2.91 – 2.96 Ga
FD73/330,25	Carbonate-chlorite mylonite with minor chalcopyrite	Águas Claras Formation (?)	Detrital zircon	LA-SF-ICP-MS	- 2.81 – 2.89 Ga - 2.91 – 3.03 Ga
FD57/225	Chlorite-carbonate mylonite containing magnetite and chalcopyrite	Low grade ore	Hydrothermal Monazite	U-Pb SHRIMP	$2,559 \pm 34$ Ma

Zircon grains from the fine-grained granite xenolith within the lower unit (DH01/347,70) are murky pink to yellowish, fairly fractured, with predominance of rounded grains. Crystal length ranges from 100 to 300 μm and elongation ratio (length/width) varies from 1:1 to 2:1. Weak oscillatory zoning is observed in several grains, but most of grains exhibit metamictic texture, with low to moderate luminescence in CL images (Fig. 10A). The majority of concordant grains (>95% of concordance, 14 grains) are older than ca. 2.8 Ga and yielded an upper intercept age of $2,935 \pm 36$ Ma (MSWD = 0.85) (Fig. 11A). Two grains display older $^{207}\text{Pb}/^{206}\text{Pb}$ ages of $3,147 \pm 22$ Ma (101% concordant) and $3,138 \pm 24$ Ma (103% concordant) and are possibly inherited.

Metagraywacke (DH02/407,70) exhibits pinkish rounded zircon grains with the presence of some fragmental grains. Crystal length ranges from 50 to 200 μm and elongation ratio (length/width) varies from 1:1 to 2:1. Oscillatory zoning with high luminescence in CL images is very common, with the exception of some metamictic grains (Fig. 10B). Twenty-nine zircon analyses revealed the presence of detrital zircon population with most of grains (>85% of concordance) fixed at ca. 2.82 – 2.88 Ga and

ca. 2.94 – 2.99 Ga, and peak at 2,965 Ma (Fig. 11B). The youngest zircon grain shows a $^{207}\text{Pb}/^{206}\text{Pb}$ age of $2,784 \pm 27$ Ma.

The metagraywackes from the Águas Claras Formation (FD67/132,65) shows predominantly murky pink zircon grains, subrounded to rounded, with length ranging from 100 to 300 μm with aspect ratios (length/width) around 2:1. Only zircon grains with concordance greater than 85% were plotted in the DensityPlotter software to trace zircon sources. CL images revealed that majority of zircon grains with medium to high luminescence (Fig. 10C) yielded a predominant population with ages in ca. 2.82 – 2.88 Ga and secondary population at ca. 2.91 – 2.96 Ga, with peak at 2,874 Ma (Fig. 11C). Zircon grains with low luminescence in the CL images display older ages between ca. 3.18 Ga and 3.29 Ga. The youngest zircon crystal yielded a $^{207}\text{Pb}/^{206}\text{Pb}$ age of $2,763 \pm 32$ Ma.

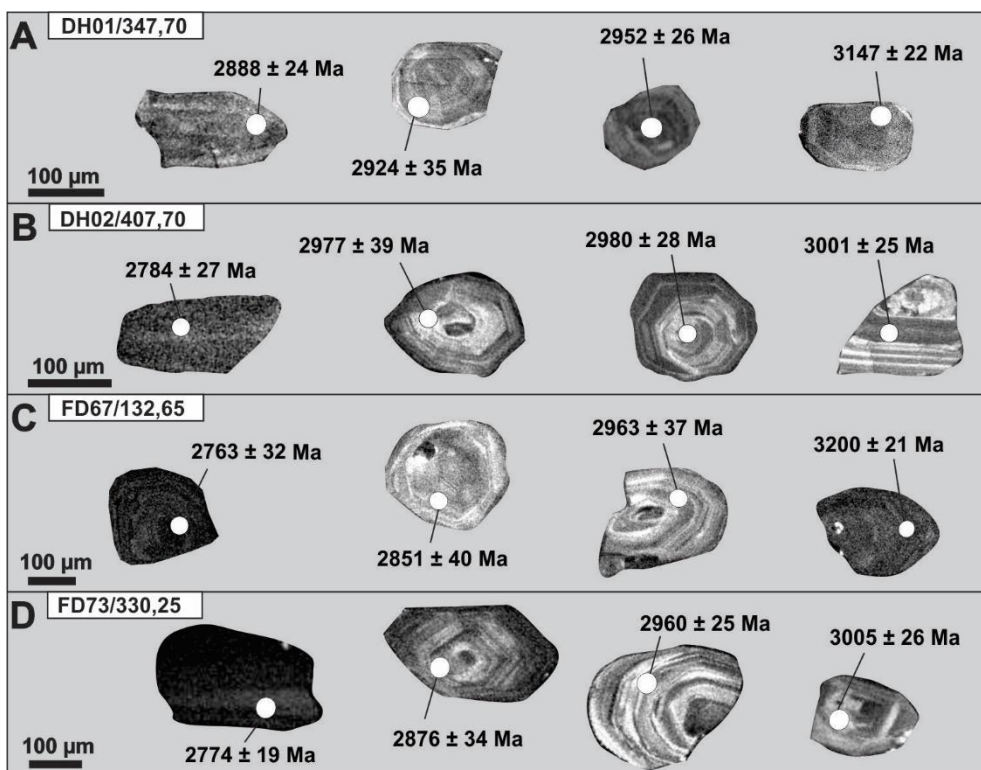


Fig. 10. CL images of zircon grains from the main host rocks of the Igarapé Bahia, including a) fine-grained granite (DH01/347,70) b) metagraywackes from the upper unit (DH02/407,70), c) metagraywackes from the Águas Claras Formation (FD67/132,65) and d) low-grade ore samples (FD73/330,25). $^{207}\text{Pb}/^{206}\text{Pb}$ ages are indicated in the image where spot analyses were carried out.

Zircon grains from the Alemão low-grade ore sample (FD73/330,25) are murky pink, with subrounded to rounded habit, and length ranging from 100 to 300 μm with aspect ratios (length/width) around 2:1. Only zircon grains with concordance greater than 85% were plotted in the DensityPlotter software to trace zircon sources. CL images revealed zircons grains with intermediate to high luminescence (Fig. 10D). Zircon populations are fixed at 2.81 – 2.89 Ga and 2.91 – 3.03 Ga, with peak at 2,898 Ma, although some zircon grains are older than ca. 3.1 Ga (Fig. 11D). The youngest zircon crystal yielded a $^{207}\text{Pb}/^{206}\text{Pb}$ age of $2,774 \pm 19$ Ma.

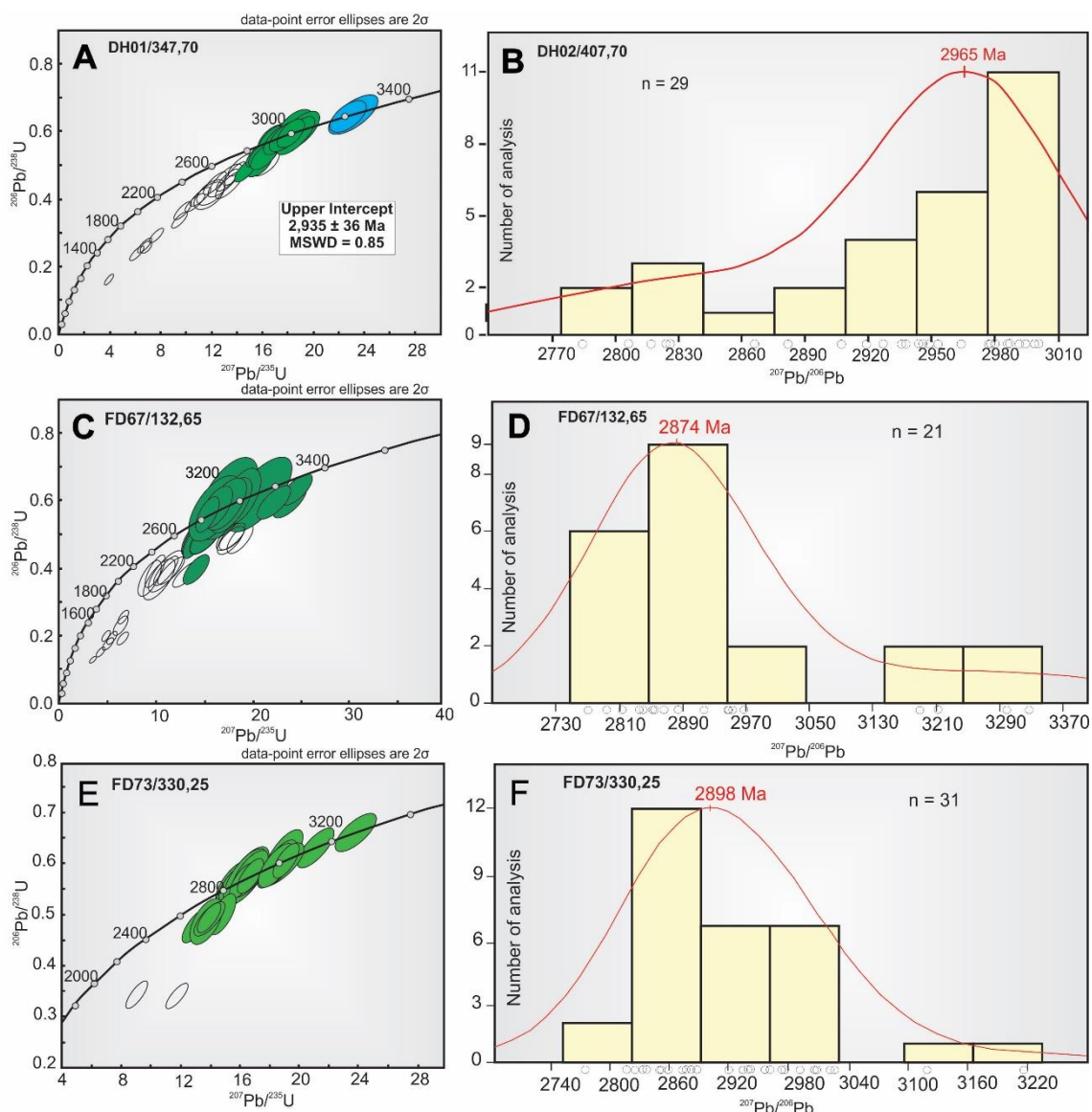


Fig. 11. U-Pb LA-ICP-MS zircon ages of the Furo 30 and Alemão orebodies. a) $^{206}\text{Pb}/^{238}\text{U}$ vs. $^{207}\text{Pb}/^{235}\text{U}$ diagrams for fine-grained granite. b) Probability density plot for the metagraywacke of the upper unit in the Furo 30 orebody. c) $^{206}\text{Pb}/^{238}\text{U}$ vs. $^{207}\text{Pb}/^{235}\text{U}$ and d) probability density plots for the Águas Claras Formation. e) $^{206}\text{Pb}/^{238}\text{U}$ vs. $^{207}\text{Pb}/^{235}\text{U}$ and f) probability density plots for low-grade ore samples.

10.2 In situ SHRIMP IIe U–Pb monazite dating

Monazite crystals are ubiquitous in hydrothermally altered and mineralized zones. The average size of the monazite grains ranges from 15 to 50 μm , but some coarser grains of up to 150 μm are recognized. The scarcity of coarser monazite grains hampers the acquisition of more analyzes. One spot yielded a $^{207}\text{Pb}/^{206}\text{Pb}$ age of 2,559 ± 34 Ma (Fig. 10g).

This data is not reliable to interpret and constrain the exactly age of the mineralization at the Alemão orebody. However, this is a valuable data to compare with previous U-Pb geochronological data of the mineralized zones of the Igarapé Bahia deposit (i.e. ca. 2.57 Ga, U-Pb in monazite, Tallarico et al. 2005).

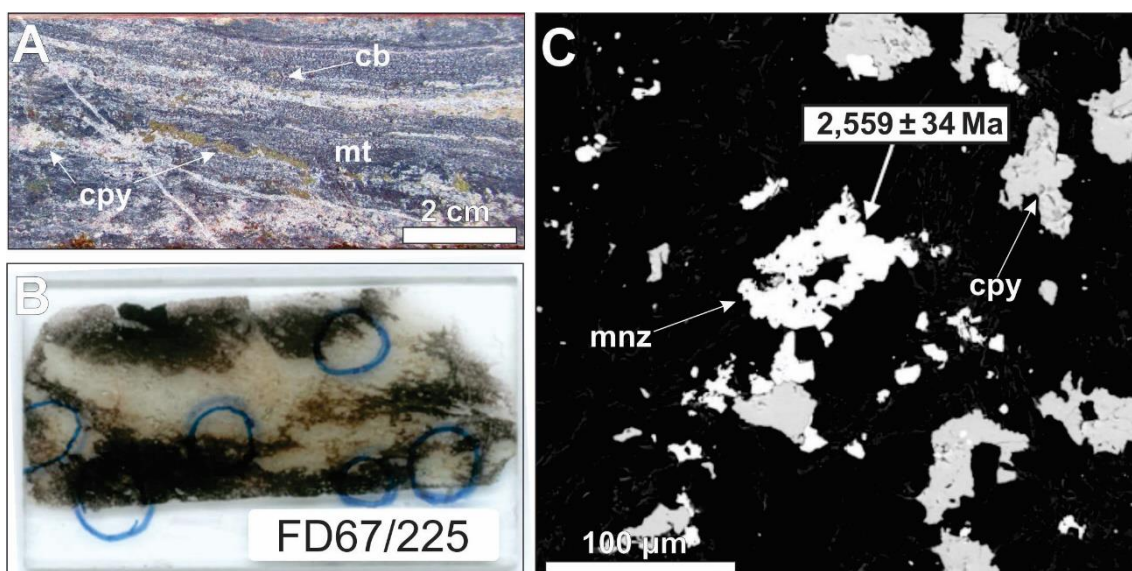


Fig. 12. Images of the SHRIMP IIe U-Pb monazite dating in the Alemão orebody. a) Magnetite-rich rocks with stretched carbonate and chalcopyrite from the Alemão orebody, where U-Pb dating was performed. b) Thin section of the dated samples with the location of possible monazite grains. c) Backscattered electron images of the in situ SHRIMP analyses with associated $^{207}\text{Pb}/^{206}\text{Pb}$ age of monazite grain.

11. Sulfur Isotopes

Sulfur isotope analyses were carried out in different generations of chalcopyrite from the Igarapé Bahia deposit (Table 2). Sulfur isotope compositions ($\delta^{34}\text{S}_{\text{VCDT}}$) were determined in chalcopyrite from nodules and layers within the upper unit in the Acampamento Sul ($\delta^{34}\text{S}_{\text{VCDT}} = +0.29\text{\textperthousand}$) and Furo 30 ($\delta^{34}\text{S}_{\text{VCDT}} = +1.04$ to $+1.56\text{\textperthousand}$) orebodies, and in chalcopyrite from magnetite-rich ore zones in the Alemão ($\delta^{34}\text{S}_{\text{VCDT}} = +1.36$ to $+5.35\text{\textperthousand}$) and Furo 30 orebodies ($\delta^{34}\text{S}_{\text{VCDT}} = +2.25$ to $+4.13\text{\textperthousand}$).

Table. 2. Sulfur isotope data of chalcopyrite from distinct types and orebodies of the Igarapé Bahia deposit. Abbreviations: cpy = chalcopyrite, mt = magnetite.

Sample	Orebody	Type	$\delta^{34}\text{S}$
DH03/179.10	Furo 30	Cpy layer	+1.04
DH03/145.90	Furo 30	Cpy layer	+1.56
DH03/181.40	Furo 30	Cpy nodule	+1.24
DH03/192.80	Furo 30	Cpy nodule	+1.24
DH03/326.50	Furo 30	Cpy nodule	+1.10
DH03/187.80	Furo 30	Cpy nodule	+1.46
F353/158.40	Acampamento Sul	Cpy nodules	+0.29
FD173/110.75	Alemão	Cpy in mt-rich zones	+2.07
FD68/393.80	Alemão	Cpy in mt-rich zones	+3.45
FD68/345.70	Alemão	Cpy in mt-rich zones	+3.22
Al68/485.60	Alemão	Cpy in mt-rich zones	+1.64
FD67/215.80	Alemão	Cpy in mt-rich zones	+5.35
FD68/417.85	Alemão	Cpy in mt-rich zones	+1.86
FD68/461.80	Alemão	Cpy in mt-rich zones	+1.36
DH03/317.05	Furo 30	Cpy in mt-rich zones	+2.78
DH03/315.75	Furo 30	Cpy in mt-rich zones	+2.25
DH03/456	Furo 30	Cpy in mt-rich zones	+4.13
DH01/413.90	Furo 30	Cpy in mt-rich zones	+2.58

$\delta^{34}\text{S}_{\text{VCDT}}$ values display a narrow variation for chalcopyrite nodules and layers ($\delta^{34}\text{S}_{\text{VCDT}} = +0.29$ to $+1.56\text{\textperthousand}$) with compositions spanning that of the magmatic field. Chalcopyrite from magnetite-rich ore zones in the Alemão and Furo 30 orebodies display a wider variation of the $\delta^{34}\text{S}_{\text{VCDT}}$ values ($\delta^{34}\text{S}_{\text{VCDT}} = +1.36$ to $+5.35\text{\textperthousand}$; Fig. 13).

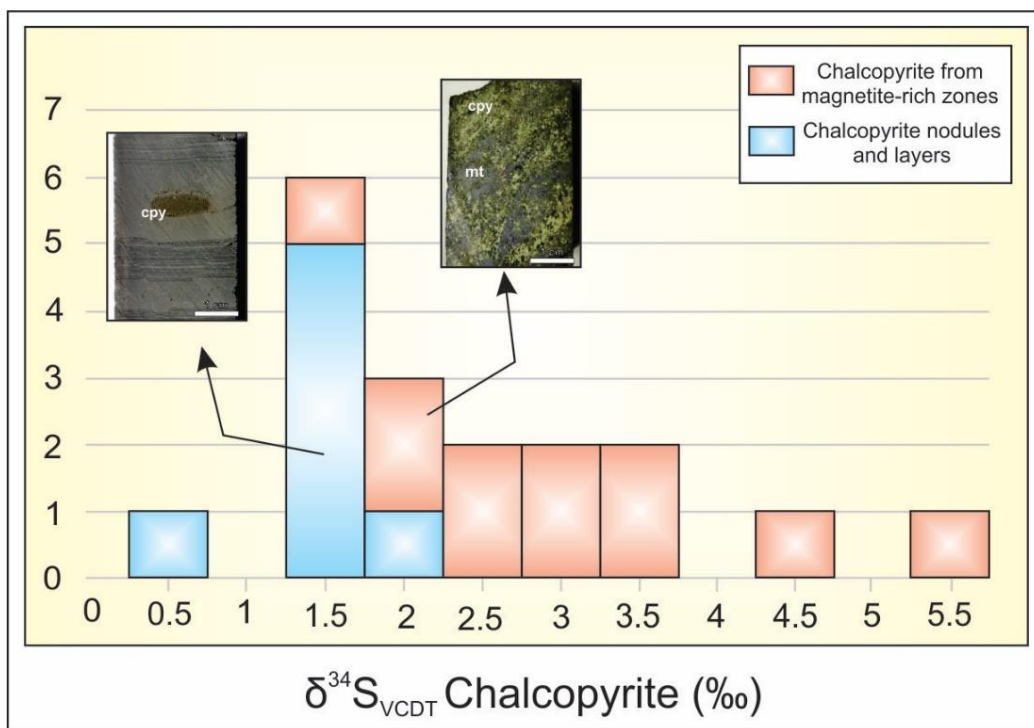


Fig. 13. Histogram displaying the sulfur isotope compositions of chalcopyrite nodules and layer (blue boxes) and chalcopyrite from magnetite-rich zones (red boxes).

12. Chemical composition of chalcopyrite

Trace element analyses were performed in chalcopyrite from nodules and layers and from magnetite-rich zones (IOCG system). Chalcopyrite from magnetite-rich zones exhibits positive anomalies of U, La, Pb and Nd and negative Sr anomalies in comparison to the primitive mantle (McDounough and Sun 1995). A remarkable characteristic of the chalcopyrite from magnetite-rich zones is its strong negative Zr anomaly (Fig. 14A). Chalcopyrite nodules and layers has positive Rb, Th, U, Pb, La and Nd anomalies, and negative Nb, Sr and Zr anomalies. However, U and Zr anomalies are less pronounced in chalcopyrite nodules and layers than in chalcopyrite from magnetite-rich zones.

Chalcopyrite from nodules and layers shows fractionation of light rare earth elements (LREE) in relation to heavy rare earth elements (HREE), with $(\text{La/Yb})_N$ ranging from 10.95 to 586.94. However, chalcopyrite from magnetite-rich zones have a slightly less fractionated pattern ($(\text{La/Yb})_N = 6.35$ to 35.85) and higher ΣREE contents (36.64 to 767.96 ppm) when compared to chalcopyrite from nodules and layers ($\Sigma\text{REE} = 8.48$ to 424.09 ppm). In the latter, negative Eu anomalies were characterized in some samples ($\text{Eu/Eu}^* = 0.61$ to 1), whereas chalcopyrite from magnetite-rich zones shows

negative or positive Eu anomalies ($\text{Eu}^*/\text{Eu} = 0.61$ to 1.96; Fig 14B). Positive anomalies of cerium are quite subtle and were observed in only two samples.

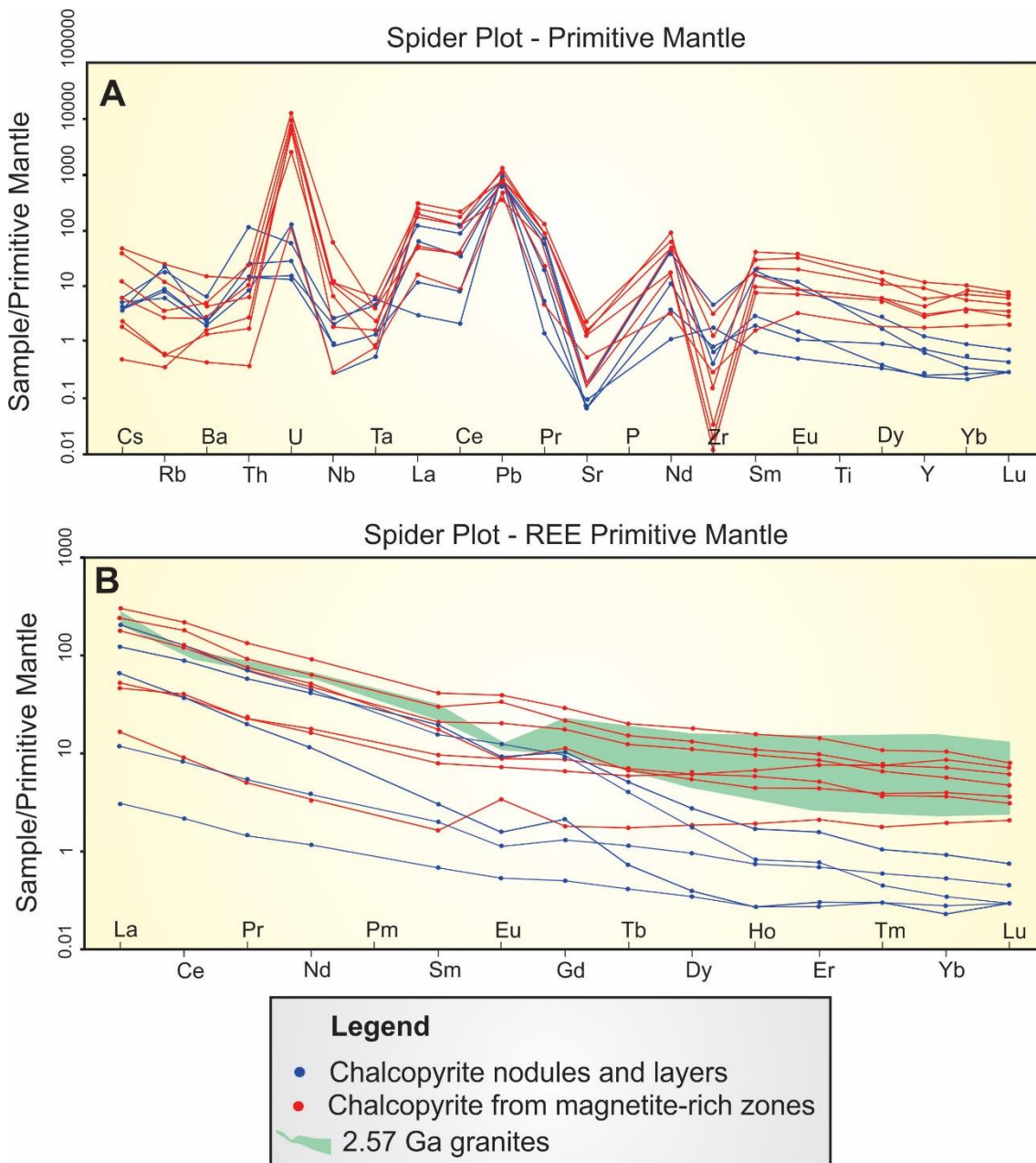


Fig. 14. Trace element composition of chalcopyrite from the Igarapé Bahia deposit, showed by a) a multivariant plot and b) spider diagram.

The diagrams of Figure 15 use a combination of trace elements, some in combination with $\delta^{34}\text{S}$ values, in attempt to compositionally discriminate both generations of chalcopyrite. Elevated contents of Ni (14.6 – 7,136 ppm), Co (10.7 – 3,846 ppm), Bi (36.4 – 136 ppm) and Zr (7.1 – 48 ppm) are characteristic of chalcopyrite nodules and layers. In contrast, chalcopyrite from magnetite-rich zones

displays higher values of U (2.22 – 247 ppm), Sn + W (9.85 – 54.26 ppm), Y + Nb (8.1 – 61.2 ppm) and Sr (3.23 – 46.3 ppm), as well as higher $\delta^{34}\text{S}$ values.

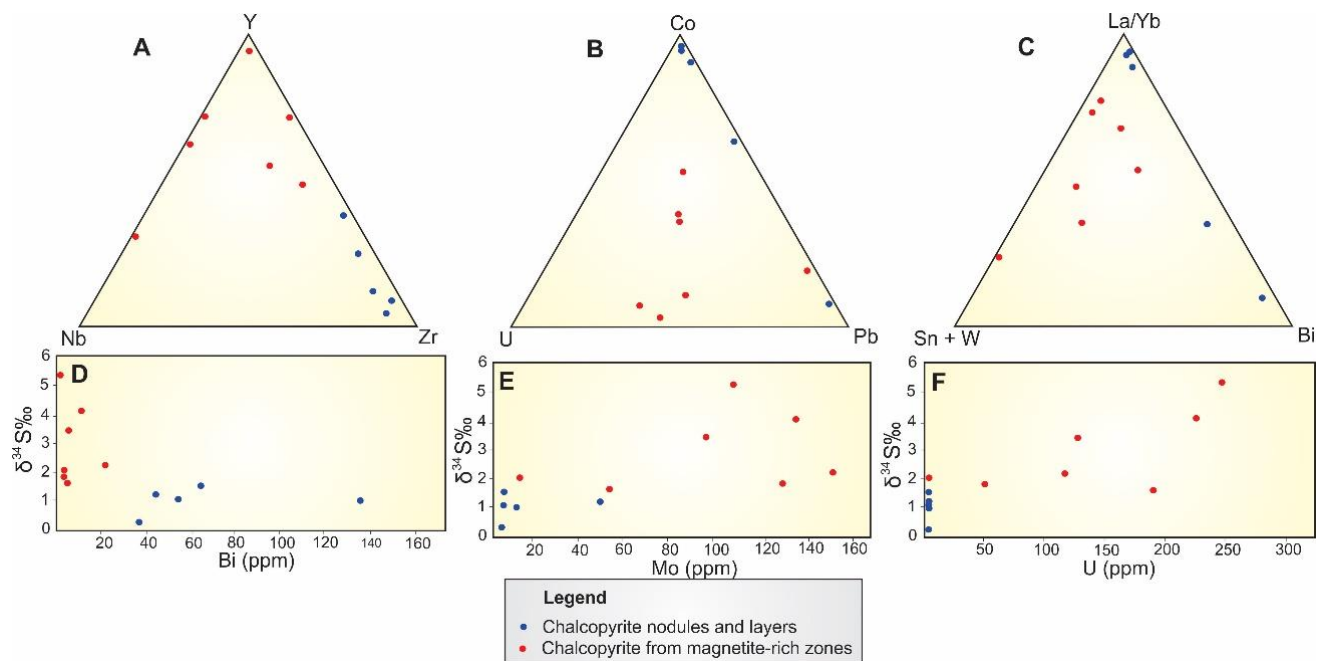


Fig. 15. Trace element composition of chalcopyrite from the Igarapé Bahia deposit. Ternary diagrams at a, b) and c) discriminate chalcopyrite nodules from chalcopyrite from magnetite-rich zones using a combination of (a) Y – Nb – Zr, (b) Co – U – Pb, and (c) La/Yb – Sn+W – Bi. Plots of $\delta^{34}\text{S}$ values versus d) Bi, e) Mo and f) U in chalcopyrite.

13. Discussions

13.1 Origin of the host rocks and regional implications

The main host rocks of the Igarapé Bahia deposit include mainly mafic and felsic metavolcanic rocks, metagabbro and banded iron formation of the lower unit, metagraywackes, metarhytmites and banded iron formation of the upper unit of the Igarapé Bahia Group, and metagraywackes of the Águas Claras Formation.

Bimodal magmatism in the lower unit is characterized by mafic and felsic metavolcanic rocks, though geological contacts between these units are hard to distinguish due to strong hydrothermal alteration. The presence of amygdaloidal metabasalts, autobreccias, hyaloclastites and pillow lava structures suggests that the lower unit formed in a submarine environment (Tallarico et al. 2005, Dreher et al. 2008). The majority of the lower unit comprises metagabbroic rocks, intrusive into the metavolcanic rocks. These metagabbros can represent volcanic conduits. The mafic magmatism was dated by U–Pb in zircon at $2,748 \pm 34$ Ma (SHRIMP, Tallarico et al.

2005). This age constrains the timing of volcanism of the lower unit and represents a reliable age for the deposition of the Igarapé Bahia Group during the Neoarchean.

Xenoliths of a fine-grained granite within the metagabbro intrusions of the lower unit yielded an upper intercept age of $2,935 \pm 36$ Ma (MSWD = 0.85). This age is correlated with those of the Xingu Complex (i.e. 2.95 and 2.86 Ga, Machado et al. 1991) and suggests that basement rocks are present in the Igarapé Bahia deposit as xenoliths within the lower unit.

The upper unit of the Igarapé Bahia Group represents the establishment of a chemical-siliciclastic depositional setting. Banded iron formations occur in basal parts of the upper unit and represent an Algoma-type oxide facies iron formation and were deposited during the hiatus of the volcanism of the lower unit of the Igarapé Bahia Group. Algoma-type iron formations, in most cases, were likely formed due to exhalative hydrothermal processes close to volcanic centers (Bekker et al. 2010). Coeval volcanism and sea floor hydrothermal systems in the Igarapé Bahia Group might have provided the dissolved iron for the precipitation of these BIF (Isley 1995), but also conditions for the precipitation of chalcopyrite nodules and layers.

Metagraywackes sequences are ubiquitous in the basal portions of the upper unit. They occur as sediment flows within metarhytmites or as massive layers. The presence of euhedral, monocrystalline, angular quartz grains with well-developed crystal faces are typical of volcanic or volcaniclastic rocks (Leyrit & Montenat 2000). Brecciated layers, convolute folds and rip-up clasts found in these rocks are evidence of reworked pyroclastic rocks (Leyrit & Montenat 2000). U–Pb zircon dating of this rock, however, does not support a single source for the zircon grains. Zircon populations of ca. 2.82 – 2.88 Ga and ca. 2.94 – 2.99 Ga suggest most of the grains are from Mesoarchean basement rocks, which have ages coeval to known crystallization and metamorphism ages of the Xingu Complex rocks (i.e. ca. 2.96 Ga and 2.86 Ga, Machado et al. 1991). Scarce zircon grains show ages close to that of the volcanism of the Itacaiúnas Supergroup (i.e. 2.76 – 2.73 Ga). The youngest zircon grain at $2,784 \pm 27$ Ma represents the maximum depositional age. Collectively, these features suggest that metagraywackes rocks represent reworked pyroclastic rocks or, more likely, epiclastic ones due to the scarcity of Neoarchean zircon grains.

Within the upper unit, the metarhytmites represent a sequence of pelagic sediments deposited in a low energy depositional environment during tectonic stable periods. However, these rocks were continuously disturbed by repetitive greywacke

fluxes. These fluxes were considered by Dreher et al. (2008) as turbiditic flows, which may have formed by slumps or during small earthquakes (Posamentier 2006). The widespread presence of faults is compatible with tectonic instability during sediment deposition in a submarine environment. The interfingering of metavolcaniclastic rocks and metarhytmites of the upper unit is a result of this process, which involved deposition of rhytmite sequence continuously affected by the graywacke turbiditic flows.

The bimodal magmatism character, the tectonic instability, the immature terrigenous clastic sedimentary rocks and the presence of a consolidated basement are compatible with a continental rift development (Wilson 1993). The basement xenoliths within the lower sequence also evidence the existence of an older sialic crust. The sequence of the Igarapé Bahia Group and likely the whole Itacaiúnas Supergroup were, therefore, deposited in an ensialic rift basin, as also pointed by other authors (e.g. Gibbs *et al.* 1986, DOCEGEO 1988, Tavares 2015). Recent studies demonstrated that mafic volcanic rocks from the Grão Pará Group were formed during the rifting of an older continental crust due to post-orogenic extension in the passage from the Mesoarchean to the Neoarchean (Martins *et al.* 2017).

Concordant detrital zircon grains (>95% concordant) with $^{207}\text{Pb}/^{206}\text{Pb}$ ages older than 3.1 Ga are encountered in fine-grained granite ($3,138 \pm 24$ and $3,147 \pm 22$ Ma) and in metagraywackes of the Águas Claras Formation ($3,118 \pm 18$ Ma, $3,215 \pm 18$ Ma, $3,299 \pm 21$ Ma). They represent the oldest U–Pb zircon ages reported in the Carajás Domain. Similar T_{DM} ages of up to 3,162 Ma in the Mesoarchean Canaã dos Carajás granite and Campinas Verde tonalite, and up to 3,136 Ma in the Neoarchean Planalto and Pedra Branca granitoids (Feio *et al.* 2013) have also been obtained. Together, these detrital zircon ages and the T_{DM} ages reveal that there was continental crust formed prior to 3.1 Ga in the Carajás Domain, as already proposed by Feio *et al.* (2013).

The origin and depositional processes for the formation of the metagraywackes of the Águas Claras Formation are still poorly understood. The different facies of the Águas Claras Formation could represent sequences formed in different depositional settings (Nogueira *et al.* 1995). At the Igarapé Bahia mine surroundings, however, only massive metagraywackes were recognized. If these metagraywackes represent the bottom or top sequences of the Águas Claras Formation remains uncertain. The petrographic features of the quartz grains suggest a volcanic origin for them. Given that no volcanism is reported during the timing of the Águas Claras Formation deposition

(Nogueira et al. 1995), these rocks probably are epiclastic and formed from the erosion of volcanic rocks, with a large contribution of terrigenous material reflected in the different sources of zircon grains.

The Águas Claras Formation was also ductilely deformed and strongly hydrothermally altered within the Alemão orebody, at the northwestern part of the deposit. This has important implications for its age. It means that the Águas Claras formation does host the mineralization at the Igarapé Bahia deposit and, therefore, is older than the age of the IOCG epigenetic mineralization (i.e. $2,575 \pm 12$ Ma, Tallarico et al. 2005). Zircon grains from the low-grade ore samples (FD73/330,25), which are similar in texture and age to those of the Águas Claras Formation, reinforce its presence within the deposit. Sources for zircon grains (see Figure 10E) might include mainly basement rocks from the Xingu Complex, with zircon population in $2.81 - 2.89$ Ga and $2.91 - 3.03$ Ga. Maximum age of deposition can be constrained by the youngest zircon grains at $2,763 \pm 32$ Ma and $2,774 \pm 19$ Ma.

The timing of deposition of the Águas Claras Formation remains very speculative. Pb–Pb zircon ages in metagabbros sills that crosscut the sequence of the Águas Claras Formation yielded ages of $2,645 \pm 12$ Ma, which is interpreted as the minimum age of its deposition (Dias et al. 1996). Likewise, Trendall et al. (1998) considered that the deposition of the Águas Claras Formation occurred at ca. $2,681 \pm 5$ Ma, according to U–Pb ages in detrital zircon. Pb–Pb dating of diagenetic pyrite, otherwise, yielded ages of 2.06 Ga, suggesting that the deposition of the Águas Claras Formation would be Rhyacian (Mougeot et al. 1996).

In addition, near-zero $\Delta^{33}\text{S}$ values in diagenetic pyrite within the Águas Claras Formation are consistent with its origin after the Great Oxidation Event (GOE) (Fabre et al. 2011). Due to the absence of mass-independent sulfur fractionation (MIF-S), its age was considered in agreement with that of the diagenetic pyrite (e.g. Pb–Pb; ca. 2.06 Ga). However, according to Cabral et al. (2017), sulfides within black shales associated with banded iron formations from the Neoarchean Grão Pará Group (Itacaiúnas Supergroup) have no mass-independent fractionation of sulfur (MIF-S). Thus, the absence of MIF-S in the sulfides of the Itacaiúnas Supergroup and Águas Claras Formation does not represent evidence to constrain the age of these metasedimentary sequences.

Conversely, we cannot rule out the possibility that the metagraywackes attributed to the Águas Claras Formation are part of the uppermost part of the Neoarchean Igarapé Bahia Group or even the base of the Grão Pará Group.

13.2 Syngenetic copper mineralization

Chalcopyrite nodules and layers occur within the metarhytmites of the upper unit of the Igarapé Bahia Group. They likely represent an early syngenetic copper mineralization at Igarapé Bahia, associated with the deposition of Igarapé Bahia Group. The key points to distinguish this early copper mineralization from the IOCG one include (i) the absence of iron oxide, (ii) the lack of hydrothermal alteration halos, and (iii) the stratabound character of the mineralization.

The volcanic setting and the presence of a wide sea floor hydrothermal system during the establishment of the Igarapé Bahia Group could explain the occurrence of a primary, syngenetic copper mineralization in the deposit. This mineralization could have been formed by processes similar to those responsible for VHMS deposits, which involve shallow subseafloor replacement (Galley et al. 2007). This copper mineralization does not show the typical morphology expected for VHMS deposits, which commonly includes: (i) stockwork zones in the footwall and (ii) massive sulfide lenses (or mounds) and related chimneys in the hangingwall (Franklyn et al. 2005, Galley et al. 2007, Tornos et al. 2015). The presence of banded iron formation spatially associated with this mineralization may point to a distal setting in relation to exhalative centers. Chert-magnetite iron formations are frequently associated with VHMS systems and comprise products of distal low temperature hydrothermal discharge (Gross 1995). The large extension of the banded iron formations at Carajás suggests that precipitation occurred from a metal-rich hydrothermal buoyant vent (Peter 2003).

Nevertheless, chalcopyrite nodules and layers occurrences at Igarapé Bahia may represent a disseminated mineralization in distal parts of an exhalative system, likely associated with dispersion of hydrothermal buoyant vents. Chalcopyrite precipitation may have occurred by both particle fallout and subseafloor replacement. Fluid infilling within open spaces of the sedimentary sequence while the sediment was still porous and permeable resulted in the precipitation of hydrothermal chalcopyrite nodules and layers concordant to primary structures (Dreher & Xavier 2001, Galley et al. 2007). In this case, the interaction of ore-bearing hydrothermal fluids with cooler trapped fluids triggered chalcopyrite precipitation (Gibson et al. 2005).

Sulfur isotope compositions of chalcopyrite nodules and layers range from +0.29 to +1.56‰, and are distinct from that of the chalcopyrite from the magnetite-rich zones. If chalcopyrite nodules and layers were formed as part of an exhalative system, their formation is due to the convection of evolved seawater that has reacted with host rocks

along the flow path and extracted heat, metals and sulfur from them. Although, sulfur may be derived from sulfates dissolved in the seawater, in Precambrian VHMS deposits, the $\delta^{34}\text{S}$ values of sulfides are typically close to 0‰ (Sangster 1968, Huston 1999), similar to those reported for chalcopyrite layers and nodules at Igarapé Bahia. This may reflect the low sulfate concentration in the oceans during the Archean. This may evidence that sulfur was likely extracted from volcanic rocks of the Igarapé Bahia Group due to fluid-rock interaction.

Trace elements in chalcopyrite nodules and layers display high contents of Ni, Co, Bi and Zr. With the exception of Zr, the other elements are compatible with mafic rocks and could also suggest that most of the components of this copper mineralization, including sulfur, are derived from the metavolcanic sequence of the lower unit. The high La/Yb ratios of chalcopyrite in comparison to those of chalcopyrite from magnetite-rich zones suggest that hydrothermal fluids responsible for the precipitation of chalcopyrite nodules and layers were not able to transport the relatively immobile heavy rare earth elements. It can suggest that hydrothermal fluids were cooler and more diluted when compared to fluids that formed the IOCG mineralization (Yongliang & Yusheng 1991). This is corroborated by the ΣREE content, which is lower than that of chalcopyrite from magnetite-rich zones.

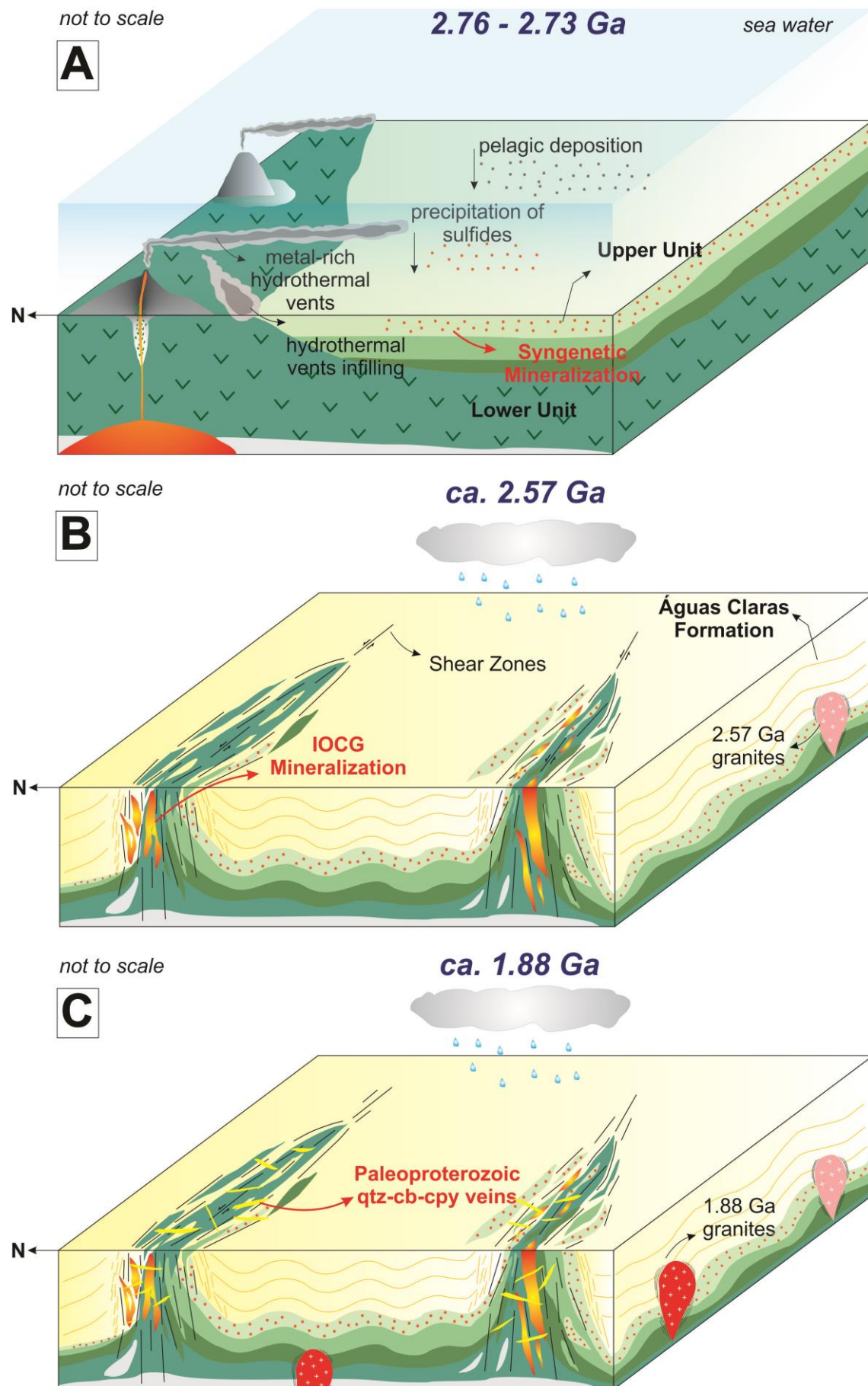


Fig. 16. Geological evolution of the Igarapé Bahia deposit. a) Syngenetic, stratabound copper mineralization coeval with deposition of the Igarapé Bahia Group. b) Structural-controlled IOCG mineralization at Igarapé Bahia. c) 1.88 Ga granite emplacement with associated qtz-cb-cpy veins crosscutting host rocks and previous mineralization.

A volcano-exhalative origin was already proposed for the Igarapé Bahia deposit (Almada and Villas 1999, Dreher et al. 2008), but in this case the authors did not envisage a syngenetic copper mineralization stage overprinted by an IOCG event. Schwarz and Frantz (2013) suggested that the Cu–Zn Pojuca deposit, located 15 km northeastern of the Igarapé Bahia deposit, also contains a primary exhalative mineralization coeval with the deposition of the Grão Pará Group overprinted by a later IOCG event.

Even though it is not dated, relative age of the syngenetic mineralization might be synchronous with that of the Igarapé Bahia Group (i.e. 2.76 – 2.73 Ga). This primary source of copper might be important for the formation of later epigenetic hydrothermal copper systems at Carajás. The precipitation of early sulfides within the Itacaiúnas Supergroup created fertile sequences that was later remobilized and generated the broad group of IOCG deposits of Carajás.

13.3 The IOCG hydrothermal system and copper-gold mineralization

The temporal and spatial distribution of the hydrothermal alteration types revealed that the Igarapé Bahia orebodies share a similar evolution within the hydrothermal system. This includes the Alemão orebody, considered a down-faulted part of the Acampamento Norte and previously interpreted to represent a different hydrothermal system (Tallarico et al. 2005, Dreher et al. 2008).

The orebodies show an early and spatially restricted calcic-sodic alteration (i.e. actinolite–epidote–scapolite) followed by potassic–(ferric) alteration (biotite). In contrast to calcic–sodic and potassic–(ferric) alteration, carbonate and chlorite formation are widespread in the deposit. The precipitation of large amounts of calcite, siderite and magnetite precedes the chalcopyrite precipitation. Chlorite formation is ubiquitous even in the distal portion of the deposit and formed during the latest stages of hydrothermal alteration. This alteration type reflects the gradual cooling of the hydrothermal system likely due to the influx of external and colder fluids.

Chalcopyrite represents the most common ore mineral, however minor bornite is also present in some zones. Gold is intrinsically associated with As- and Ag-rich minerals.

The hydrothermal breccias described as fragmental rocks in previous works (Dreher et al. 2005, 2008) are not interpreted here as syngenetic in relation to the upper unit, since these rocks and the related hydrothermal alteration were controlled by ductile shear zones, as already suggested by other authors (e.g. Tallarico et al. 2005). Hydrothermal breccias and mylonites represent the locus of the most intense hydrothermal fluid flow. Fluid pressure fluctuations and opening of dilatant sites due to faulting represent the major mechanisms that triggered brecciation (Clark and James 2003) and allowed the precipitation of hydrothermal minerals. Those minerals (e.g. biotite–carbonate–chlorite–chalcopyrite–magnetite) comprise the main matrix of these breccias in the Igarapé Bahia deposit. The importance of hydraulic breccias have already been reported in other important IOCG deposits in the world (e.g. Olympic Dam deposit in the Gawler Craton, Oreskes et al. 1990; Sossego deposit at Carajás Province, Monteiro et al. 2008). In some orebodies (e.g. Furo 30), the mineralized breccias, although scarce, are concordant to primary S_0 structures, especially at the contact of lower and upper sequences. These zones represent weak structural boundaries and geochemical barriers, which facilitated the fluid circulation and metal precipitation.

Chalcopyrite associated with magnetite-rich zones (i.e. IOCG system) shows $\delta^{34}\text{S}$ values from +1.36 to +5.35‰. Dreher et al. (2008) and Galarza et al. (2008) also obtained similar intervals for $\delta^{34}\text{S}$ in chalcopyrite, ranging from +0.5 to +5.6‰ and from -0.3 to +4.2‰, respectively. These slightly positive $\delta^{34}\text{S}$ values (1–5‰) suggest that, in addition to magmatic sulfur sources, sulfate could have been incorporated in sulfides via thermochemical sulfate-reduction reactions at high temperatures (Ono et al. 2007).

Trace elements in chalcopyrite from magnetite-rich zones endorse the IOCG origin for this type of mineralization. Chalcopyrite from these zones is enriched in REE, Mo and U, which can be a direct evidence of the typical geochemical signature of the IOCG ore-forming fluids (Hitzman et al. 2000). In addition, Y, Nb, Sn and W are also present in the chalcopyrite. The higher LREE fractionation patterns in comparison to HREE and positive Eu anomalies indicate that these elements behave as relatively mobile elements within the ore-forming fluids. This can be facilitated by chloride- and fluoride-rich fluids (Williams-Jones et al. 2012; Migdisov and William-Jones 2014).

The positive Eu anomalies could also suggest presence of high-temperature hydrothermal up flow of relatively reduced fluids (Bau, 1991). Even in these conditions, the strong negative Zr anomalies suggest that zirconium was not partitioned to the fluid and remains as immobile elements in the source. Even though some of these elements are encountered in mineral inclusions within chalcopyrite, these results clearly distinguish chalcopyrite from magnetite-rich zones from chalcopyrite nodules and layers. Additionally, these mineral inclusions are coeval with the host mineral and can provide, therefore, important information of the ore signature. Thus, different fluids and metal sources might have contributed to the formation of chalcopyrite nodules and layers, and chalcopyrite from magnetite-rich zones.

Metalliferous highly saline fluids ($\text{H}_2\text{O} + \text{NaCl} + \text{CaCl}_2$, >45% wt% NaCl) coexisting with carbonic fluids ($\text{CO}_2 \pm \text{CH}_4$) were responsible for the IOCG mineralization at Igarapé Bahia (Dreher et al. 2008). The participation of low salinity fluids (6 wt% NaCl, Dreher et al. 2008) provide evidence for fluid mixing that may have triggered ore precipitation by dilution and cooling of the ore-forming fluids.

The uncommon ore geochemical signature with high contents of W, Sn and Nb, due to the presence of scheelite, cassiterite, wolframite, pyroclore and fergusonite, is a remarkable feature at the Igarapé Bahia deposit. This signature is not usual of all IOCG deposits of the Carajás Province (Xavier et al. 2012), although U, Mo and REE also characterizes Igarapé Bahia IOCG mineralization. This geochemical signature could be assigned to ca. 2.57 Ga A-type, peralkaline (to metaluminous) granites. In general, A-type granites display elevated contents of HFSE and REE; whereas more fractionated peralkaline granites tend to be enriched specifically in Zr, REE, Y, Nb, Ta, U and Th, although Sn and W can also be observed (Cerný et al. 2005). Therefore, the geochemical signature of Igarapé Bahia IOCG mineralization could have been formed due to hydrothermal fluids exsolved from the highly fractionated 2.57 Ga A-type granites, what could also explain the CO_2 -fluids.

In addition, geochemical signature data of these granites in the Carajás Domain, although scarce, have similar REE patterns to that of chalcopyrite from the magnetite-rich zones (see Figure 14). The Eu positive anomaly of the chalcopyrite in comparison to Eu negative anomaly of these granites might be explained to the partitioning of europium to the hydrothermal fluid instead of granitic melt. However, tracing the sources of metals and likely the ore-forming fluids demand more investigation.

This signature is also typical of Paleoproterozoic A-type granite-related deposits, such as the Cu–Au–(Mo–W–Bi–W) Breves and Estrela deposits (Tallarico et al. 2004, Volp 2005). Thus, a Paleoproterozoic overprinting at the Igarapé Bahia deposit cannot be precluded and the Carajás A-type granite magmatism may have been a triggering factor.

The IOCG mineralization system overprints the syngenetic copper mineralization and its age has been constrained at $2,575 \pm 12$ Ma (Tallarico et al. 2005). U–Pb monazite age in one single crystal of the Alemão orebody performed in this study yielded a $^{207}\text{Pb}/^{206}\text{Pb}$ age of $2,559 \pm 34$ Ma. Although this age is not reliable enough to constrain the timing of mineralization at Igarapé Bahia deposit, it reinforces the previous age of 2.57 Ga in the deposit. Together with the giant Salobo deposit, the Igarapé Bahia deposit represents at the ca. 2.57 Ga IOCG deposits mineralization systems, contrasting with the ca. 2.71–2.68 Ga and 1.88 Ga IOCG systems reported in the Southern Copper Belt of the Carajás Province (Moreto et al. 2015a, b).

Isochron Pb–Pb ages in gold ($2,744 \pm 12$ Ma, MSWD = 12.5; Galarza et al. 2008) and in chalcopyrite ($2,772 \pm 46$ Ma, MSWD = 7,839; $2,754 \pm 36$ Ma, MSWD = 1566; $2,756 \pm 24$ Ma, MSWD = 509; $2,777 \pm 22$ Ma, MSWD = 55; Galarza et al. 2008) display large errors and MSWD values. However, these ages may reflect the timing of Pb removal from its source region (Faure 1986) during the syngenetic copper mineralization event. In any case, disturbance in the Pb–Pb isotopic system is also suggested by younger Pb–Pb ages at $2,521 \pm 56$ Ma and $2,595 \pm 200$ Ma in gold (Santos 2002), which are close to those estimated for the IOCG mineralization timing.

The metallogenetic event at ca. 2.5 Ga recorded at Igarapé Bahia and Salobo was assigned to granite intrusions of similar ages (i.e. Old Salobo granite; Réquia et al. 2003, Tallarico et al. 2005). The link between the emplacement of ca. 2.5 Ga granites and the formation of IOCG deposits at Carajás, however, is still controversial. The Cu–Au mineralization at the Igarapé Bahia deposit shows no spatial relationship with any intrusion in the deposit, but it is also located along the regional-scale Carajás Fault system. In the case of Salobo, a protracted tectono-thermal event with successive reactivations of the Cinzento Shear Zone near ca. 2.5 Ga have been proposed for the origin of the Cu–Au mineralization, but granite magmatism in this period cannot be ruled out (Melo et al. 2016).

13.4 Later quartz–carbonate–chalcopyrite veins

A remarkable characteristic of the Igarapé Bahia deposit is the widespread presence of later quartz–carbonate–chalcopyrite veins that crosscut previous hydrothermal alteration stages. These veins represent an economically important type of ore, but lack the iron oxide content that characterizes the IOCG style mineralization.

These veins and veinlets might be emplaced under lower crustal levels in a brittle regime. Similar veins were recognized in other IOCG deposits at Carajás, such as Bacuri deposit at the Southern Copper Belt and Grotta Funda (Melo et al. 2014, Hunger 2017).

Sulfur isotopes in chalcopyrite of these veins yielded $\delta^{34}\text{S}$ values between -0.3 and $+4\text{\textperthousand}$ (Dreher et al. 2008), very similar to that of chalcopyrite from the IOCG system. They may represent a remobilization of the Neoarchean IOCG sulfides and bear a genetic link with the Paleoproterozoic metallogenetic event (Fig. 17). A-type anorogenic magmatism in ca. 1.88 Ga may be the responsible for this remobilization.

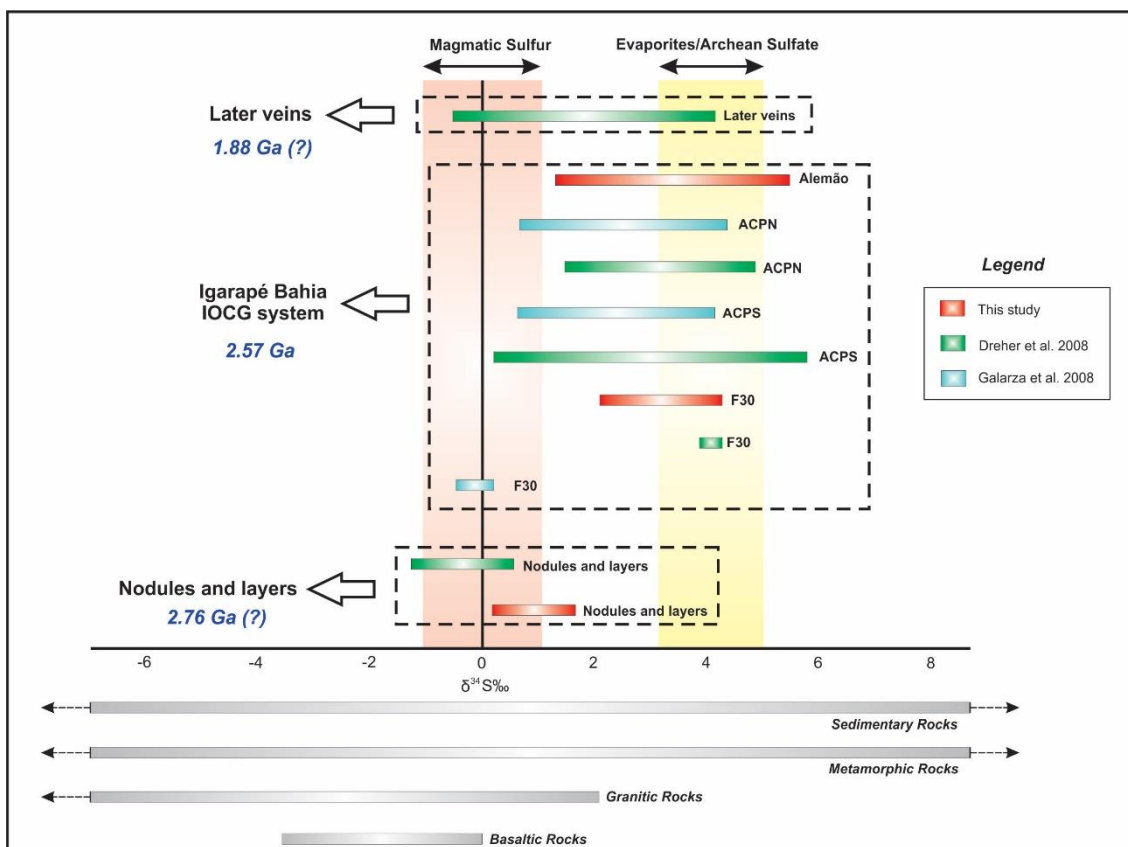


Fig. 17. Sulfur isotope composition of distinct styles of chalcopyrite at the different orebodies in the Igarapé Bahia deposit, showing that the generation of chalcopyrite might show different ages. Evaporites/achean sulfate field are from Ohmoto and Goldhaber (1997); magmatic sulfur field is from Eldridge et al. (1991).

14. Conclusions

The Igarapé Bahia deposit reveals a complex and protracted metallogenetic evolution. Host rocks comprise mainly metavolcanic rocks, metagabbros and metasedimentary rocks (metarhytmites, epiclastic rocks and banded iron formation) formed in deep-seated ocean water in a rift basin. The maximum deposition age of the upper unit of the Igarapé Bahia Group is constrained at $2,784 \pm 27$ Ma. Xenoliths of fine-grained granites within the lower unit, dated at $2,935 \pm 36$ Ma, reveal the presence of a sialic crust prior to rifting. Geological relationship within the Igarapé Bahia deposit suggests that the controversial Águas Claras Formation might have been deposited in the Neoarchean, but its age should be better investigated. U–Pb dating of detrital zircon yielded the maximum deposition age of the Águas Claras Formation at $2,763 \pm 32$ Ma and $2,774 \pm 19$ Ma.

Early syngenetic mineralization was coeval with the deposition of the upper unit (i.e. 2.76 – 2.73 Ga). Chalcopyrite nodules and layers formed by a sub-sea floor hydrothermal system, which permitted infilling of open spaces within the sedimentary sequence and its replacement. Sulfur and likely metals were mainly extracted from the metavolcanic sequence, as indicated by trace element signature (e.g. Ni, Co and Bi) and $\delta^{34}\text{S}$ values (+0.29 to +1.56‰) of chalcopyrite.

The IOCG mineralization overprints the syngenetic mineralization. It was strictly associated with ductile deformation and hydrothermal brecciation. Widespread hydrothermal alteration grades outwards from chlorite-rich zones to proximal carbonate–magnetite–sulfide-bearing zones. The ore zones comprise chalcopyrite–magnetite-rich mylonite and breccias, with minor other sulfides and gangue minerals (e.g. tourmaline, carbonate, apatite and chlorite). $\delta^{34}\text{S}$ values (+1.36 to +5.35‰) in this chalcopyrite generation suggest participation of magmatic and externally-derived sulfur sources. The latter may reflect sulfate thermochemical reduction at high temperatures. Trace element geochemistry shows high ΣREE values associated with large contents of U, Mo, Sn, W, Y, Nb and Sr, contrasting with chalcopyrite nodules and layers. This ore signature might point to a genetic link with highly fractionated ca. 2.57 Ga peralkaline granites. Timing of the IOCG mineralization is constrained at $2,559 \pm 34$ Ma, in agreement with previous data for Igarapé Bahia deposit ($2,575 \pm 12$ Ma, Tallarico et al. 2005). An important tectonic event at ca. 2.5 Ga possibly associated with granite

magmatism may have generated the necessary conditions for the IOCG mineralization at this period.

The Igarapé Bahia deposit, therefore, represents the first example in the Carajás Domain revealing the overprinting of different Cu–Au mineralization styles. Exhalative systems and syngenetic copper mineralization might be important for the formation of later epigenetic IOCG deposits, likely providing part of their metals and sulfur.

15. Acknowledgments

This work was supported by the National Council for Scientific and Technological Development [CNPq; 481969/2013-6; 308365/2014-3, 457689/2014-5] and by the São Paulo Research Foundation (2016/13162-7]. We are very grateful to VALE and their geologists for the continuous support in the field.

16. References

- Almada, M.C.O., Villas, R.N., 1999. O depósito Bahia: um possível exemplo de depósito vulcanogenênico tipo Besshi arqueano em Carajás. Revista Brasileira de Geociências. 29, 579-592.
- Althoff, A.M.R., Villas, R.N.; Giuliani, G.A., 1994. Mineralização cuprífera da área Bahia, Serra dos Carajás (PA): Evolução dos fluidos hidrotermais e modelo metalogenético. Geochimica Brasiliensis. 8, 135 - 155.
- Araújo O.J.B., Maia, R.G.N., 1991. Serra dos Carajás: folha SB.22-Z-A. Estado do Pará. Escala 1:250.000. Texto explicativo. DNPM/CPRM, 164 p.
- Barros, C.E.M., Macambira M.J.B., Barbey P., Scheller T., 2004. Dados isotópicos Pb-Pb em zircão (evaporação) e Sm-Nd do Complexo granítico Estrela, Província Mineral de Carajás, Brasil: implicações petrológicas e tectônicas. Revista Brasileira de Geociências. 34, 531–538.
- Bau, M., 1991. Rare-Earth element mobility during hydrothermal and metamorphic fluid-rock interaction and the significance of the oxidation state of europium. Chemical Geology. 93, 219–230.
- Bekker, A., Slack, F.F., Planavsky, N., Krapez, B., Hofmann, A., Konhauser, K.O., Rouxel, O.J., 2010. Iron Formation: The sedimentary product of a complex interplay among mantle, tectonic, oceanic, and biospheric processes. Economic Geology. 105, 467 – 508.

- Cerný, P., Bleven, P.L., Cuney, M., London, D., 2005. Granite-related ore deposits, in: Hedenquist, J.W., Thompson, J.F.H., Goldfarb, R.J., Richards, J.P., (eds), *Economic Geology, 100th anniversary volume*, pp. 337–370.
- Cabral, A.R., Buhn, B., Gomes Jr., A.A.S., Galbiatti, H.F., Lehmann, B., Halder, S., 2017. Multiple sulfur isotopes from the Neoarchean Serra Sul black shale, Carajás Mineral Province, northern Brazil. *Journal of South American Earth Sciences*. 79, 377–383.
- Clark, C., James, P., 2003. Hydrothermal brecciation due to fluid pressure fluctuations: examples from the Olary Domain, South Australia. *Tectonophysics*. 366, 187 – 206.
- Dardenne, M.A., Ferreira Filho, C.F., Meirelles, M.R., 1988. The role of shoshonitic and calc-alkaline suites in the tectonic evolution of the Carajás district, Brazil. *Journal of South American Earth Sciences*. 1, 363-372.
- Delinardo da Silva, M.A., 2014. Metatexitos e diatexitos do Complexo Xingu na região de Canaã dos Carajás: Implicações para a evolução mesoarqueana do Domínio Carajás, PA. Master Thesis, University of Campinas, pp. 119.
- Dall'Agnol R., Cunha, I.R.V., Guimarães F.V., Oliveira, D.C., Teixeira, M.F., Feio, G.R.L., Lamarão, C.N., 2016. Mineralogy, geochemistry, and petrology of Neoarchean ferroan to magnesian granites of Carajás Province, Amazonian Craton: The origin of hydrated granites associated with charnockites. *Lithos*. In press
- Dias, G.S., Macambira, M.B., Dall'Ágnol, R., Soares, A.D.V. Barros, C.E.M., 1996. Datações de zircões de sill de metagabro: comprovação de idade arqueana da Formação Águas Claras, Carajás, Pará. In: Simp. Geol. Amaz., 5, SBG, Belém, pp. 376-378.
- DOCEGEO 1988. Revisão litoestratigráfica da Província Mineral de Carajás - Litoestratigrafia e principais depósitos minerais, in: 35º Congresso Brasileiro de Geologia, Belém. (Proceedings).
- Dreher, A.M., Xavier, R.P., Taylor, B.E., Martini, S. 2008. New geologic, fluid inclusion and stable isotope studies on the controversial Igarapé Bahia Cu-Au deposit, Carajás province, Brazil. *Mineralium Deposita*. 43, 161–184.
- Dreher, A.M., Xavier, R.P., Taylor, B.E., Martini, S. 2005. Fragmental rocks of the Igarapé Bahia Cu-Au deposit, Carajás Mineral Province, Brazil. *Revista Brasileira de Geociências*. 35, 359–368.
- Dreher, A.M., Xavier, R.P., 2001. Provável origem e processo de mineralização das brechas do depósito de Igarapé Bahia, Carajás, in: 7º Simpósio de Geologia da Amazônia, Belém. (Proceedings).

- Eldridge, C.S., Compston, W., Williams, I.S., Harris, J.W., Bristow, J.W., 1991. Isotope evidence for the involvement of recycled sediments in diamond formation. *Nature*. 353, 649–653.
- Fabre, S., Nédélec, A., Poitrasson, F., Strauss, H., Thomazo, C., Nogueira, A., 2011. Iron and Sulphur isotopes from the Carajás mining province (Pará, Brazil): implications for the oxidation of the ocean and the atmosphere across the Archaean-Proterozoic transition. *Chem. Geol.* 289, 124–139.
- Faure, G., 1986. Principles of Isotope Geology, New York, John Wiley & Sons, 589 p.
- Feio, G.R.L., Dall'Agnol, R., Dantas, E.L., Macambira, M.J.B., Gomes, A.S., Sardinha, D.C., Oliveira, D.C., Santos, R.D., Santos, P.A. 2012. Geochemistry, geochronology, and origin of the Neoarchean Planalto Granite suite, Carajás, Amazonian craton: A-type or hydrated charnockitic granites? *Lithos*. 151, 57–73.
- Feio, G.R.L., Dall'Agnol R., Dantas, E.L., Macambira, M.J.B., Santos, J.O.S., Althoff, F.J., Soares J.E.B., 2013. Archean granitoid magmatism in the Canaã dos Carajás area: implications for crustal evolution of the Carajás province, Amazonian craton, Brazil. *Precambrian Research*. 227, 157–185.
- Ferreira Filho, C.F. 1985. Geologia e mineralizações sulfetadas do Prospecto Bahia, Província Mineral de Carajás. Unpublished Master Thesis, University of Brasilia.
- Fletcher, I.R., McNaughton N.J., William, J.D., Rasmussen, B., 2010. Matrix effects and calibration limitations in ion probe U-Pb and Th-Pb dating of monazite. *Chemical Geology*. 270, 31–44.
- Franklyn, J.M., Gibson, H.L., Jonasson, I.R., Galley, A.G., 2005. Volcanogenic massive sulfide deposits. In: Hedenquist, J.W., Thompson, J.F.H., Goldfarb, R.J., Richards, J.P., (eds) *Economic Geology 100th Aniverssary Volume*. pp. 523–560.
- Galarza, M.A., Macambira M.J.B., Villas R.N. 2008. Dating and isotopic characteristics (Pb and S) of the Fe oxide–Cu–Au–U–REE Igarapé Bahia ore deposit, Carajás mineral province, Pará state, Brazil. *Journal of South American Earth Sciences*. 25, 377–397.
- Galley, A.G., Hannington, M.D., Jonasson, I.R., Volcanogenic massive sulphide deposits, *in* Goodfellow, W.D., ed., *Mineral Deposits of Canada: A Synthesis of Major Deposit-Types, District Metallogeny, the Evolution of Geological Provinces, and Exploration Methods*: Geological Association of Canada, Mineral Deposits Division, Special Publication No. 5, p. 141–161.
- Gibbs, A.K., Wirth, K.R., Hirata, W.K., Olszewski Jr., W.J., 1986. Age and composition of the Grão Pará Group volcanics, Serra dos Carajás. *Revista Brasileira de Geociências*. 16, 201–211.

- Gibson, H.L., Morton, R.L., Hudak, G.J., 2005. Submarine volcanic processes, deposits and environments favorable for the location of volcanic-associated massive sulfide deposits. In: *Reviews in Economic Geology, Volcanic-associated massive sulfide deposits: processes and examples in modern and ancient settings.* 8, 13–48.
- Gross, G.A., 1995. Stratiform iron: Geological Survey of Canada, *Geology of Canada.* 8, 41 – 54.
- Hirata, W.K., Rigon, J.C., Kadekaro, K., Cordeiro, A.A.C., Meireles E.A., 1982. *Geologia Regional da Província Mineral de Carajás.* In: *1º Simpósio de Geologia da Amazônia, Belém.* (Proceedings)
- Hitzman, M.W., 2000. Iron oxide–Cu–Au deposits: what, where, when, and why, in: Porter T.M. (Eds.), *Hydrothermal iron oxide copper-gold and related deposits: a global perspective* Austral Miner Fund, Adelaide, pp. 9–25.
- Hitzman, M.W., Oreskes, N., Einaudi, M.T., 1992. Geological characteristics and tectonic setting of Proterozoic iron oxide (Cu-U-Au-REE) deposits. *Precambrian Research.* 58, 241–287.
- Huhn, S.R.B., Nascimento, J.A.S., 1997. São os depósitos cupríferos de Carajás do tipo Cu-Au-U-ETR? In: Costa, M.L., Angélica, R.S., Contribuições a geologia da Amazônia, SBG, Belém, pp. 143-160.
- Hunger, R.B., 2016. O depósito de óxido de ferro-cobre-ouro (IOCG) Grota Funda, Domínio Carajás (PA): alteração hidrotermal, regime de fluidos e idade da mineralização. Unpublished Master Dissertation, Campinas, University of Campinas, p. 91.
- Huston, D.L., 1999. Stable isotopes and their significance for understanding the genesis of volcanic-hosted massive sulfide deposits: a review. *Reviews in Economic Geology.* 8, 157-179
- Isley, A.E., 1995. Hydrothermal plumes and the delivery of iron to banded iron formation. *Journal of Geology.* 103, 169–185.
- Lindenmayer, Z.G., Fleck, A., Gomes, C.H., Santos, A.B.S., Caron, R., Paula, F. de C., Laux, J.H., Pimentel, M.M., Sardinha, A.S., 2005. Caracterização geológica do Alvo Estrela (Cu-Au), Serra dos Carajás, Pará. In: Marini, O.J., Ramos, B.W., Queiroz, E.T., (Eds.). *Caracterização de Depósitos Minerais de Distritos Mineiros da Amazônia.* Brasília. DNPM-CT-Mineral-FINEP-ADIMB, pp. 137-205.
- Lindenmayer, Z.G., Ronchi, L.H., Laux, J.H., 1998. Geologia e geoquímica da mineralização de Cu-Au primária da mina de Au do Igarapé Bahia, Serra dos Carajás. *Revista Brasileira de Geociências.* 28, 257-268.
- Leyrit, H., Montenat, C., 2000. *Volcaniclastic Rocks, from Magmas to Sediments,* Gordon and Breach Science Publishers, Amsteldijk. p. 270.

- Ludwig, K.R., 2003. User's manual for isoplot/ex v. 3.00. In: A geochronological toolkit for Microsoft Excel, Berkeley, BGC Special Publication. 4, 1-71.
- Ludwig, K.R., 2009. SQUID II., a user's manual, Berkeley Geochronology Center Special Publication 2, 2455 Ridge Road, Berkeley, CA 94709, USA 22.
- Machado, N., Lindenmayer, D.H., Kroug, T.E., Lindenmayer, Z.G., 1991. U-Pb geochronology of Archean magmatism and basement reactivation in the Carajás Area, Amazon Shield, Brazil. *Precambrian Research*. 49, 1–26.
- Martins, P.L.G., Toledo, C.L.B., Silva, A.M., Chemale Jr., F., Santos, J.O.S., Assis, L.M., 2018. Neoarchean magmatism in the southeastern Amazonian Craton, Brazil: Petrography, geochemistry and tectonic significance of basalts from the Carajás Basin. *Precambrian Research*. 302, 340-357.
- McDonough, W.F., Sun, S.S., 1995. Composition of the Earth. *Chemical Geology*. 120, 223–253.
- Migdisov, A.A., Williams-Jones, A.E., 2014. Hydrothermal transport and deposition of the rare earth elements by fluorine-bearing aqueous fluids. *Mineralium Deposita*. 49, 987–997
- Mougeot, R., Respaut, J.P., Briquel, L., Ledru, P., Milesi, J.P., Macambira, M.J.B., Huhn, S.B., 1996. Geochronological constraints for the age of the Águas Claras Formation (Carajás Province, Pará, Brazil). In: 39º Congresso Brasileiro de Geologia, Salvador. (Proceedings).
- Moreto, C.P.N., Monteiro, L.V.S., Xavier, R.P., Creaser, R.A., Dufrane, S.A., Tassinari, C.C.G., Sato, K., Kemp, A.I.S., Amaral, W.S., 2015b. Neoarchean and Paleoproterozoic Iron Oxide-Copper-Gold events at the Sossego deposit, Carajás Province, Brazil, Re-Os and U-Pb geochronological evidence. *Economic Geology*. 110, 809–835.
- Moreto, C.P.N., Monteiro L.V.S., Xavier R.P., Creaser R.A., Dufrane S.A., Melo, G.H.C., Delinardo da Silva, M.A., Tassinari, C.C.G., Sato, K., 2015a. Timing of multiple hydrothermal events in the iron oxide–copper–gold deposits of the Southern Copper Belt, Carajás Province, Brazil. *Mineralium Deposita*. 50, 517-546.
- Moreto, C.P.N., Monteiro, L.V.S., Xavier, R.P., Amaral, W.S., Santos, T.J.S., Juliani, C., Souza Filho, C.R., 2011. Mesoarchean (3.0 and 2.86 Ga) host rocks of the iron oxide-Cu-Au Bacaba deposit, Carajás Mineral Province: U-Pb geochronology and metallogenetic implications. *Mineralium Deposita*. 46, 789-811.
- Nogueira, A.C.R., Truckenbrodt, W., Pinheiro, R.V.L., 1995. Formação Águas Claras, Pré-Cambriano da Serra dos Carajás: redescricão e redefinição litoestratigráfica. *Boletim do Museu Paraense Emilio Goeldi*. 7, 177-277.

- Ohmoto, H., Goldhaber, M.B., 1997. Sulfur and carbon isotopes. In: Barnes HL (ed) *Geochemistry of hydrothermal ore deposits*, 3rd edn. Wiley, New York, pp. 517–611.
- Oreskes, N., Einaudi, M.T., 1990. Origin of rare earth element-enriched hematite breccias at the Olympic Dam Cu-U-Ag deposit, Roxby Downs, South Australia: *Economic Geology*. 85, 1 – 28.
- Peter, J.M., 2003. Ancient iron-rich metalliferous sediments (iron formations): Their genesis and use in the exploration for stratiform base metal sulphide deposits, with examples from the Bathurst Mining Camp in: Lentz, D.R., (eds) *Geochemistry of Sediments and Sedimentary Rocks: Evolutionary Considerations to Mineral Deposit-Forming Environments*, GEOText 4: Geological Association of Canada, p. 145-173.
- Petrus, J.A., Kamber, B.S., 2012. VizualAge: A novel approach to Laser Ablation ICP-MS U-Pb Geochronology Data Reduction. *Geostandards and Geoanalytical Research*. 36, 247-270.
- Pidgeon, R.T., Macambira, M.J.B., Lafon, J.M., 2000. Th–U–Pb isotopic systems and internal structures of complex zircons from an enderbite from the Pium Complex, Carajás Province, Brazil: evidence for the ages of granulite facies metamorphism and the protolith of the enderbite. *Chemical Geology*. 166, 159–171.
- Pinheiro, R.V.L., 2013. Carajás, Brazil – A short tectonic review. In: 13th Simpósio de Geologia da Amazônia, Belém. (Proceedings).
- Pinheiro, R.V.L., Holdsworth, R.E., 1997. Reactivation of Archean strike-slip fault systems, Amazon region, Brazil. *Journal of the Geological Society*. 154, 99–103.
- Posamentier, H.W., Walker, R.G., 2006. Deep-water turbidites and submarine fans, in: Facies model, Society for Sedimentary Geology, pp. 532.
- Réquia, K., Stein, H., Fontboté, L., Chiaradia, M., 2003. Re–Os and Pb–Pb geochronology of the Archean Salobo iron oxide copper–gold deposit, Carajás Mineral Province, northern Brazil. *Mineralium Deposita*. 38, 727–738.
- Sachs, L.L.B. 1993. O magmatismo associado ao depósito mineral cupro-aurífero do Igarapé Bahia, Carajás, PA, Brasil. Master dissertation, University of Campinas, 142p.
- Sangster, D.F. 1968. Relative sulfur isotope abundances of ancient seas and stratabound sulfide deposits. *Geol. Assoc. Can.*, 17, pp. 79-91
- Santos, M.N.S., Oliveira, D.C., 2016. Rio Maria granodiorite and associated rocks of Ourilândia do Norte – Carajás province: Petrography, geochemistry and implications for sanukitoid petrogenesis. *Journal of South American Earth Sciences*. 72, 279-301.

- Santos, J.O.S., 2003. Geotectônica do Escudo das Guianas e Brasil-Central. In: Bizzi LA,(ed) Geologia, tectônica e recursos minerais do Brasil: texto, mapas e SIG. Brasília, CPRM, pp. 169-226.
- Santos, M.G.S., 2002. Estudo dos isótopos de Pb e Nd do depósito de Cu-Au (U-ETR) Alemão, Província Mineral de Carajás (PA). Unpublished Master Dissertation, University of Pará, Belém, p. 121
- Souza, S.R.B., Macambira, M.J.B., Sheller, T., 1996. Novos dados geocronológicos para os granitos deformados do Rio Itacaiúnas (Serra dos Carajás, PA), implicações estratigráficas, in: 5th Simposio de Geologia da Amazônia, Belém. (Proceedings).
- Schwarz, M., Frantz, J.C., 2013. Depósito de Cu-Zn Pojuca Corpo Quatro: IOCG ou VMS? Pesquisas em Geociências. 40, 05 - 19.
- Shanks, W.C., 2001. Stable isotopes in seafloor hydrothermal systems-Vent fluids, hydrothermal deposits, hydrothermal alteration, and microbial processes. In: Valley, J.W., Cole, D.R., (Eds), Stable isotope geochemistry, Reviews in Mineralogy and Geochemistry. pp. 469-525.
- Shanks, W.C. III, Bohlke J.K., Seal R.R., 1995. Stable isotopes in mid-ocean ridge hydrothermal systems: Interaction between fluids, minerals and organisms, in: Humphris, S.E., Zierenberg, R.A., Mullineaux, L.S., Thomson, R.E. (eds) Seafloor Hydrothermal Systems: Physical, Chemical, Biological, and Geological Interactions. Am Geophys Union, Washington, DC, p. 194–221.
- Tallarico, F.H.B., Figueiredo, B.R., Groves, D.I., Kositcin, N., McNaughton, N.J., Fletcher, I.R., Rego, J.L., 2005. Geology and SHRIMP U-Pb geochronology of the Igarapé Bahia deposit, Carajás copper-gold belt, Brazil: an Archean (2.57 Ga) example of iron-oxide Cu-Au-(U-REE) mineralization. Economic Geology. 100, 7-28.
- Tallarico F.H.B., McNaughton N.J., Groves D.I., Fletcher I.R., Figueiredo B.R., Carvalho B.J., Rego L.J. e Nunes A.R., 2004. Geological and SHRIMP II U-Pb constraints on the age and origin of the Breves Cu-Au-(W-Bi-Sn) deposit, Carajás, Brazil. Mineralium Deposita. 39, 68–86.
- Tallarico F.H.B. 2003. O cinturão cupro-aurífero de Carajás, Brasil. Tese de Doutorado, UNICAMP, 229p.
- Teixeira J.B.G. 1994. Geochemistry, petrology, and tectonic setting of archean basaltic and dioritic rocks from the N4 Iron deposit, Serra dos Carajás, Pará, Brazil. 1994. Thesis (Doctor of Philosophy). Department of Geosciences, Penn State University.

- Tassinari, C.C.G., Macambira, M.J.B., 1999. Geochronological Provinces of the Amazonian Craton. *Episodes*. 22, 174-182.
- Tavares, F., 2015. Evolução Geotectônica do nordeste da Província Carajás. Unpublished PhD Thesis, Rio de Janeiro, University of Rio de Janeiro. pp. 130.
- Tornos, F., Peter, J.M., Allen, R., Conde, C., 2015. Controls on the siting and style of volcanogenic massive sulphides deposits. *Ore Geology Reviews*. 68, 142–163.
- Trendall, A.F., Basei M.A.S., De Laeter J.R., Nelson D.R. 1998. SHRIMP U-Pb constraints on the age of the Carajás formation, Grão Pará Group, Amazon Craton. *Journal of South American Earth Sciences*. 11, 265-277.
- VALE, 2002. Nova Fase da mina de Igarapé Bahia. VALE information Market, press releases. <http://www.vale.com/brasil/PT/investors/information-market/press-releases/Paginas/nova-fase-da-mina-de-igarape-bahia.aspx>. Accessed 04 november 2016.
- Vasquez, M.L., Sousa, C.S., Carvalho, J.M.A. (Orgs), 2008. Mapa Geológico e de Recursos Minerais do Estado do Pará, escala 1:1.000.000. Programa Geologia do Brasil (PGB), Integração, Atualização e Difusão de Dados da Geologia do Brasil, Mapas Geológicos Estaduais. CPRM – Serviço Geológico do Brasil, Superintendência Regional de Belém.
- Vermeesch, P., 2012. On the visualisation of detrital age distributions. *Chemical Geology*. 312-313, 190-194.
- Villas, R.N.N., Santos, M.D., 2001. Gold deposits of the Carajás Mineral Province: deposit types and metallogenesis. *Mineralium Deposita*. 36, 300–331.
- Volp, K.M., 2005. The Estrela copper deposit, Carajás, Brazil: Geology and implications of a Proterozoic copper stockwork. In: 8th Biennial SGA Meeting Beijing, China. Pp. 1085–1088.
- Wiedenbeck, M., Alle, P., Corfu, F., Griffin, W.L., Meier, M., Oberli, F., Von Quadt, A., Roddick, J.C., Spiegel, W., 1995. Three natural zircon standards for U-Th-Pb, Lu-Hf, trace element and REE analyses. *Geostandards Newsletter*. 19, 1-23.
- Williams-Jones, A.E., Migdisov, A.A., Samson, I.M., 2012. Hydrothermal mobilization of the rare earth elements—a tale of Ceria and Yttria. *Elements*. 8, 355–360
- Wilson, M., 1993. Magmatism and the geodynamics of basin formation. *Sedimentary Geology*. 86, 5-29.
- Wirth, K.R, Gibbs, A.K., Olszewski, W.J., 1986. U-Pb ages of zircons from the Grão Pará Group and Serra dos Carajás Granite, Pará, Brazil. *Revista Brasileira de Geociências*. 16, 195-200.

- Xavier, R.P., Monteiro, L.V.S., Souza Filho, C.R., Torresi, I., Carvalho, E.R., Dreher, A.M., Wiedenbeck, M., Trumbull, R.B., Pestilho, A.L.S., Moreto, C.P.N., 2012. The iron oxide copper–gold deposits of the Carajás Mineral Province, Brazil, in: Geology and Genesis of Major Copper Deposits and Districts of the World: A Tribute to Richard H. Sillitoe, Chapter: pp 618.
- Yongliang, X., Yusheng, Z., 1991. The mobility of rare-earth elements during hydrothermal activity: a review. Chinese Journal of Geochemistry. 10, 295-306.

Appendix

Supplementary Table 1. Summary of U-Pb LA-SF-ICP-MS zircon data of the Igarapé Bahia deposit.

Zircon grain	Sample DH01/347,70												Ages				
	Isotopic Ratios																
	% ²³⁸ U com m	U (pp m)	Th (pp m)	²³² Th/ ²³⁸ U	²⁰⁷ Pb/ ²³⁵ U	1 σ	²⁰⁶ Pb/ ²³⁸ U	1 σ	err corr	²⁰⁷ Pb/ ²⁰⁶ Pb	2 σ	²⁰⁶ Pb/ ²³⁸ U	2 σ	²⁰⁷ Pb/ ²³⁵ U	2 σ	% corr	
DH34770_1	0.24	70	31	0.44	17,700	0.600	0.6020	0.0230	0.5522	2924	35	3015	91	2967	32	103	
DH34770_2	0.16	141	183	1.29	12,310	0.360	0.4470	0.0140	0.7182	2750	22	2349	62	2611	28	85	
DH34770_3	0.16	175	213	1.22	10,680	0.320	0.3890	0.0120	0.7564	2736	22	2094	57	2473	28	77	
DH34770_4	0.48	54	94	1.73	11,720	0.430	0.4090	0.0160	0.5973	2843	34	2178	71	2556	35	77	
DH34770_5	0.23	78	110	1.41	16,190	0.560	0.5650	0.0200	0.6498	2835	28	2848	83	2868	33	100	
DH34770_6	0.20	116	80	0.69	13,160	0.390	0.4590	0.0150	0.6993	2818	24	2405	67	2694	28	85	
DH34770_7	0.15	171	64	0.37	13,130	0.350	0.4310	0.0120	0.7239	2880	19	2287	55	2685	26	79	
DH34770_8	0.12	155	157	1.01	17,030	0.530	0.5760	0.0200	0.6237	2804	27	2926	81	2929	30	104	
DH34770_9	0.27	73	128	1.76	15,210	0.470	0.5230	0.0170	0.6376	2847	27	2690	71	2813	30	94	
DH34770_10	0.08	199	158	0.79	17,780	0.640	0.5790	0.0230	0.7462	2888	24	2958	92	2949	37	102	
DH34770_11	0.42	59	23	0.38	11,970	0.450	0.4180	0.0160	0.5914	2862	32	2227	71	2579	36	78	
DH34770_12	0.25	75	93	1.24	15,940	0.500	0.5650	0.0190	0.6245	2814	31	2861	77	2861	31	102	
DH34770_13	0.17	100	153	1.54	22,730	0.600	0.6450	0.0190	0.6488	3147	22	3180	74	3212	26	101	
DH34770_14	0.13	204	160	0.79	11,150	0.310	0.4060	0.0120	0.6786	2721	22	2179	54	2525	26	80	
DH34770_15	0.12	243	214	0.88	9,780	0.280	0.3660	0.0110	0.6989	2666	22	1998	52	2399	26	75	
DH34770_16	0.15	134	132	0.98	14,770	0.390	0.5230	0.0150	0.6943	2784	23	2685	65	2788	25	96	
DH34770_17	0.22	98	103	1.06	14,500	0.410	0.5010	0.0160	0.6609	2805	25	2610	69	2773	27	93	
DH34770_18	0.21	96	93	0.97	14,080	0.470	0.5000	0.0170	0.7160	2774	26	2597	72	2742	33	94	
DH34770_19	0.12	134	44	0.33	23,150	0.800	0.6480	0.0240	0.7145	3138	24	3235	94	3231	34	103	
DH34770_20	0.13	297	338	1.14	6,170	0.230	0.2409	0.0090	0.8195	2600	26	1369	46	1956	32	53	
DH34770_21	0.18	100	43	0.43	17,350	0.460	0.5860	0.0170	0.6487	2854	22	2956	70	2958	26	104	
DH34770_22	0.21	112	122	1.09	13,450	0.400	0.4670	0.0150	0.6707	2803	26	2459	66	2692	29	88	
DH34770_23	0.13	335	273	0.81	6,820	0.160	0.2596	0.0070	0.6799	2645	24	1480	36	2086	21	56	
DH34770_24	0.22	104	114	1.10	14,850	0.450	0.4980	0.0160	0.6685	2866	25	2594	70	2786	29	91	
DH34770_25	0.14	569	401	0.70	3,970	0.130	0.1625	0.0055	0.8255	2535	22	961	30	1602	25	38	
DH34770_26	0.12	349	343	0.98	9,480	0.250	0.3381	0.0098	0.7234	2733	21	1862	47	2372	24	68	
DH34770_27	0.20	168	102	0.61	12,600	0.370	0.4360	0.0130	0.6676	2813	24	2310	59	2641	28	82	
DH34770_28	0.34	83	42	0.51	15,990	0.510	0.5670	0.0180	0.5554	2815	31	2875	75	2871	30	102	
DH34770_29	0.16	265	178	0.67	13,590	0.380	0.4500	0.0140	0.7353	2867	21	2366	59	2703	26	83	
DH34770_30	0.19	199	132	0.66	15,300	0.460	0.5200	0.0160	0.7134	2824	22	2685	68	2823	29	95	
DH34770_31	0.24	206	70	0.34	13,390	0.460	0.4520	0.0170	0.7495	2828	27	2374	73	2687	33	84	
DH34770_32	0.11	456	235	0.51	13,790	0.370	0.4770	0.0140	0.7719	2787	19	2499	62	2724	26	90	
DH34770_33	0.24	196	133	0.68	16,370	0.470	0.5650	0.0180	0.6131	2842	27	2877	74	2898	28	101	
DH34770_34	0.28	168	87	0.52	16,050	0.510	0.5090	0.0170	0.6388	2952	26	2639	72	2854	30	89	
DH34770_35	0.23	313	300	0.96	6,790	0.220	0.2613	0.0093	0.6047	2620	28	1484	47	2075	29	57	
DH34770_36	0.18	306	307	1.00	7,690	0.220	0.2918	0.0092	0.7098	2675	23	1629	45	2181	25	61	
DH34770_37	0.15	147	71	0.49	18,160	0.640	0.5950	0.0230	0.6295	2902	31	2966	92	3001	34	102	

Supplementary Table 1. (continued)

Zircon grain	Isotopic Ratios											Ages					
	% $^{206}_{\text{Pb}}$ com m	U (pp m)	Th (pp m)	^{232}Th / ^{238}U	$^{207}\text{Pb}/$ ^{235}U	1 σ	$^{206}\text{Pb}/$ ^{238}U	1 σ	err corr	$^{207}\text{Pb}/$ ^{206}Pb	2 σ	$^{206}\text{Pb}/$ ^{238}U	2 σ	$^{207}\text{Pb}/$ ^{235}U	2 σ	% conc.	
	Sample DH02/407,70																
DH40770_1	0,14	78	54	0,69	19,680	0,520	0,6500	0,0180	0,6449	2964	24	3189	70	3056	26	108	
DH40770_2	0,09	138	114	0,82	15,740	0,480	0,5590	0,0180	0,6980	2826	23	2843	73	2842	29	101	
DH40770_3	0,07	167	174	1,04	15,590	0,490	0,5570	0,0180	0,6497	2784	27	2842	73	2844	31	102	
DH40770_4	0,12	122	87	0,71	15,490	0,520	0,4940	0,0160	0,6925	2999	23	2574	69	2830	33	86	
DH40770_5	0,08	155	82	0,53	17,860	0,570	0,5930	0,0210	0,7608	2938	21	2975	83	2975	31	101	
DH40770_6	0,09	132	111	0,84	18,090	0,580	0,5980	0,0210	0,6932	2949	25	2977	86	2983	32	101	
DH40770_7	0,10	116	63	0,54	18,130	0,470	0,5920	0,0160	0,6769	2946	21	2973	67	2976	24	101	
DH40770_8	0,07	179	123	0,68	18,630	0,470	0,5980	0,0170	0,6408	2978	22	3014	67	3014	24	101	
DH40770_9	0,11	148	219	1,48	11,900	0,350	0,3960	0,0120	0,6652	2894	24	2139	56	2591	27	74	
DH40770_10	0,24	54	72	1,35	15,090	0,500	0,5520	0,0200	0,5754	2817	35	2803	80	2805	32	100	
DH40770_11	0,18	69	29	0,43	18,710	0,600	0,5910	0,0200	0,6242	2986	27	2955	78	3027	31	99	
DH40770_12	0,16	74	60	0,82	17,430	0,570	0,5890	0,0210	0,5438	2946	32	2940	87	2939	32	100	
DH40770_13	0,11	109	58	0,53	17,770	0,520	0,5860	0,0170	0,6987	2927	22	2949	70	2954	28	101	
DH40770_14	0,15	124	155	1,25	10,960	0,430	0,3920	0,0160	0,5794	2815	33	2095	75	2501	37	74	
DH40770_15	0,07	240	238	0,99	10,750	0,420	0,3990	0,0140	0,8705	2705	22	2124	64	2445	33	79	
DH40770_16	0,11	106	118	1,12	18,780	0,600	0,6020	0,0210	0,6628	2992	27	3012	84	3016	30	101	
DH40770_17	0,17	101	128	1,26	10,990	0,330	0,3900	0,0130	0,6050	2824	26	2102	59	2514	27	74	
DH40770_18	0,22	68	62	0,91	13,980	0,530	0,4880	0,0200	0,6750	2866	31	2506	84	2729	36	87	
DH40770_19	0,17	70	41	0,58	20,060	0,810	0,6210	0,0270	0,6301	2987	35	3070	110	3068	40	103	
DH40770_20	0,41	33	21	0,65	15,240	0,650	0,5000	0,0210	0,6086	2977	39	2556	88	2779	41	86	
DH40770_21	0,16	70	66	0,95	18,850	0,620	0,6100	0,0220	0,7067	2980	28	3027	86	3026	32	102	
DH40770_22	0,08	161	111	0,69	18,590	0,550	0,5940	0,0180	0,7065	2999	25	2967	72	3016	28	99	
DH40770_23	0,06	195	60	0,31	18,030	0,530	0,6000	0,0200	0,6421	2919	24	2992	78	2992	28	103	
DH40770_24	0,24	72	74	1,03	12,200	0,460	0,3940	0,0150	0,7721	2987	27	2099	68	2582	35	70	
DH40770_25	0,10	130	103	0,80	17,090	0,570	0,6140	0,0230	0,6099	2824	30	3039	88	2925	32	108	
DH40770_26	0,15	85	109	1,28	16,960	0,520	0,5880	0,0190	0,5988	2882	27	2958	77	2912	29	103	
DH40770_27	0,24	50	31	0,62	19,080	0,590	0,6110	0,0190	0,6172	3001	25	3021	75	3017	30	101	
DH40770_28	0,12	96	48	0,50	17,950	0,570	0,5930	0,0210	0,6797	2980	27	2982	83	2980	31	100	
DH40770_29	0,11	128	48	0,38	15,010	0,500	0,4980	0,0170	0,7151	2944	23	2564	73	2775	32	87	
DH40770_30	0,09	135	91	0,67	15,940	0,480	0,5660	0,0180	0,7101	2806	23	2861	74	2860	29	102	
DH40770_31	0,16	76	66	0,86	17,940	0,640	0,5910	0,0230	0,7338	2953	29	2962	90	2954	36	100	
DH40770_32	0,21	54	34	0,64	18,620	0,660	0,6090	0,0220	0,6840	2995	28	2987	84	2986	33	100	
DH40770_33	0,11	126	189	1,50	14,040	0,530	0,4880	0,0200	0,7469	2907	30	2535	89	2756	37	87	
DH40770_34	0,20	87	99	1,14	10,910	0,610	0,3890	0,0220	0,7228	2847	42	2080	100	2466	55	73	
DH40770_35	0,22	62	35	0,56	17,570	0,660	0,5920	0,0240	0,6618	2936	30	2938	95	2942	35	100	
DH40770_36	0,19	77	70	0,92	12,570	0,560	0,4980	0,0250	0,6750	2667	38	2580	100	2634	43	97	

Supplementary Table 1. (continued)

Zircon grain	Sample FD73/330,25											Ages				
	%	Isotopic Ratios										2 _g		2 _g		% conc
	²⁰⁶ U com m	U (pp m)	Th (pp m)	²³² Th / ²³⁸ U	²⁰⁷ Pb/ ²³⁵ U	1 _σ	²⁰⁶ Pb/ ²³⁸ U	1 _σ	err corr	²⁰⁷ Pb/ ²⁰⁶ Pb	2 _σ	²⁰⁶ Pb/ ²³⁸ U	2 _σ	²⁰⁷ Pb/ ²³⁵ U	2 _σ	% conc
FD33025_1	0.04	260	146	0.56	21,090	0.520	0.6300	0.0160	0.7573	3118	18	3134	62	3139	24	101
FD33025_2	0.12	86	114	1.33	18,420	0.600	0.5980	0.0190	0.6760	2990	27	2996	75	3006	31	100
FD33025_3	0.18	71	105	1.49	13,860	0.380	0.4880	0.0130	0.6288	2851	23	2556	59	2732	26	90
FD33025_4	0.25	43	55	1.29	16,380	0.580	0.5720	0.0220	0.6652	2881	31	2899	88	2890	33	101
FD33025_5	0.11	107	94	0.87	16,380	0.400	0.5700	0.0140	0.6500	2872	19	2908	59	2899	23	101
FD33025_7	0.11	96	71	0.75	18,790	0.440	0.5980	0.0140	0.6052	3007	19	3021	58	3024	22	100
FD33025_8	0.06	244	190	0.78	13,040	0.380	0.4790	0.0140	0.6653	2774	19	2514	60	2677	27	91
FD33025_9	0.07	258	211	0.82	9,040	0.330	0.3430	0.0110	0.7620	2714	19	1881	52	2318	34	69
FD33025_10	0.10	113	100	0.88	15,450	0.400	0.5530	0.0160	0.8608	2835	20	2830	65	2831	25	100
FD33025_11	0.19	57	28	0.48	18,940	0.530	0.6000	0.0170	0.6685	3025	20	3029	68	3027	27	100
FD33025_12	0.08	128	125	0.98	17,990	0.400	0.5880	0.0130	0.7155	2960	17	2984	54	2982	21	101
FD33025_13	0.09	126	48	0.38	18,050	0.430	0.5890	0.0150	0.6764	2972	18	2990	60	2986	23	101
FD33025_14	0.29	38	35	0.93	18,380	0.530	0.5970	0.0170	0.6816	3005	26	2987	69	2985	28	99
FD33025_15	0.06	183	171	0.93	15,560	0.380	0.5590	0.0140	0.6550	2824	17	2838	58	2839	23	100
FD33025_16	0.16	80	67	0.83	14,840	0.390	0.5000	0.0160	0.7406	2933	23	2594	69	2798	25	88
FD33025_17	0.08	146	49	0.33	18,430	0.410	0.5950	0.0130	0.6546	2955	18	2993	55	3000	21	101
FD33025_18	0.15	75	45	0.61	16,940	0.480	0.5770	0.0180	0.6372	2887	23	2920	75	2924	28	101
FD33025_19	0.22	50	38	0.77	19,280	0.440	0.6070	0.0140	0.7101	3020	21	3047	58	3053	22	101
FD33025_20	0.09	141	111	0.79	14,720	0.390	0.4900	0.0140	0.6263	2940	18	2554	58	2786	26	87
FD33025_21	0.00	306	93	0.30	18,100	0.420	0.5910	0.0140	0.7438	2938	18	2983	55	2989	22	102
FD33025_23	0.10	118	110	0.93	17,370	0.410	0.5790	0.0140	0.6942	2919	17	2946	57	2954	23	101
FD33025_24	0.07	158	62	0.40	23,830	0.530	0.6600	0.0150	0.8293	3215	18	3256	58	3251	22	101
FD33025_25	0.28	40	51	1.29	16,530	0.600	0.5770	0.0230	0.6844	2876	34	2889	91	2888	34	100
FD33025_26	0.39	34	23	0.68	13,770	0.460	0.4860	0.0180	0.6824	2858	35	2518	77	2728	32	88
FD33025_27	0.17	69	67	0.97	15,540	0.470	0.5580	0.0190	0.6826	2849	27	2843	79	2840	29	100
FD33025_28	0.13	94	122	1.30	16,140	0.380	0.5640	0.0150	0.5132	2886	20	2869	61	2868	23	99
FD33025_29	0.09	124	256	2.06	16,500	0.450	0.5720	0.0150	0.6485	2851	21	2901	60	2902	25	102
FD33025_30	0.12	98	70	0.71	19,020	0.520	0.6170	0.0200	0.6702	2960	25	3073	78	3035	27	104
FD33025_31	0.12	93	60	0.64	19,010	0.430	0.6040	0.0140	0.6954	2975	20	3029	57	3029	21	102
FD33025_32	0.07	163	121	0.74	16,210	0.390	0.5660	0.0130	0.6361	2832	18	2883	56	2888	23	102
FD33025_33	0.13	96	79	0.82	16,950	0.500	0.5810	0.0180	0.6846	2872	26	2930	73	2929	28	102
FD33025_34	0.08	173	266	1.53	13,950	0.340	0.4920	0.0120	0.7041	2816	17	2576	52	2734	23	91
FD33025_35	0.11	188	192	1.02	11,750	0.300	0.3411	0.0098	0.5579	3149	20	1874	47	2571	24	60

Supplementary Table 1. (continued)*Sample FD67/132,65*

Zircon grain	Isotopic Ratios										Ages					
	% ²⁰⁶ com m	U (pp m)	Th (pp m)	²³² Th / ²³⁸ U	²⁰⁷ Pb/ ²³⁵ U	1 σ	²⁰⁶ Pb/ ²³⁸ U	1 σ	err corr	²⁰⁷ Pb/ ²⁰⁶ Pb	2 σ	²⁰⁶ Pb/ ²³⁸ U	2 σ	²⁰⁷ Pb/ ²³⁵ U	2 σ	% conc
FD13265_1	0,08	181	138	0,76	13,740	0,490	0,4860	0,0190	0,7720	2787	26	2522	82	2727	34	90
FD13265_2	0,14	109	78	0,71	13,920	0,450	0,4820	0,0170	0,6706	2806	26	2518	75	2728	31	90
FD13265_3	0,09	171	54	0,32	17,870	0,510	0,4910	0,0140	0,7185	3200	21	2542	62	2962	27	79
FD13265_4	0,06	320	133	0,42	11,680	0,480	0,3790	0,0170	0,7895	2920	27	2037	75	2539	38	70
FD13265_5	0,08	180	105	0,58	15,370	0,520	0,5590	0,0210	0,6677	2763	32	2829	86	2829	32	102
FD13265_7	0,13	143	90	0,63	11,210	0,450	0,3980	0,0170	0,5820	2780	22	2112	75	2484	38	76
FD13265_8	0,17	94	96	1,01	14,200	0,470	0,4900	0,0180	0,8362	2833	26	2561	78	2759	31	90
FD13265_9	0,17	79	33	0,41	22,220	0,710	0,5950	0,0210	0,7267	3210	23	2986	84	3178	31	93
FD13265_10	0,18	95	64	0,67	13,840	0,470	0,4880	0,0180	0,7610	2829	30	2544	75	2717	32	90
FD13265_11	0,16	87	67	0,78	24,610	0,640	0,6330	0,0180	0,6424	3299	21	3142	69	3286	26	95
FD13265_12	0,37	36	16	0,44	18,170	0,730	0,6030	0,0270	0,5538	2943	36	2990	110	2987	39	102
FD13265_13	0,21	72	43	0,59	17,140	0,530	0,5790	0,0190	0,6731	2878	29	2919	77	2922	29	101
FD13265_14	0,22	65	41	0,63	18,330	0,490	0,6060	0,0190	0,6218	2942	27	3004	75	2999	26	102
FD13265_15	0,43	54	45	0,83	11,140	0,400	0,3860	0,0150	0,6076	2848	34	2090	70	2509	32	73
FD13265_16	0,22	103	42	0,41	11,610	0,320	0,3930	0,0120	0,5656	2867	28	2127	57	2570	25	74
FD13265_17	0,33	64	32	0,49	11,190	0,430	0,3940	0,0150	0,6244	2802	36	2109	68	2520	36	75
FD13265_18	0,15	282	116	0,41	6,650	0,260	0,1957	0,0078	0,5751	3089	23	1138	42	2033	36	37
FD13265_19	0,15	145	96	0,66	10,930	0,570	0,3810	0,0200	0,8159	2811	31	2042	96	2451	55	73
FD13265_20	0,11	122	66	0,54	23,880	0,730	0,6000	0,0200	0,8188	3327	22	2998	78	3253	30	90
FD13265_21	0,31	49	52	1,06	16,120	0,610	0,5730	0,0270	0,7221	2878	40	2870	110	2874	38	100
FD13265_23	0,18	118	130	1,11	13,190	0,590	0,3860	0,0160	0,5264	3112	27	2071	74	2648	43	67
FD13265_24	0,11	166	73	0,44	17,830	0,610	0,4940	0,0160	0,7013	3116	22	2575	68	2957	33	83
FD13265_25	0,09	167	113	0,68	17,070	0,510	0,5830	0,0190	0,8182	2845	25	2931	77	2935	29	103
FD13265_26	0,27	154	85	0,55	4,890	0,160	0,2030	0,0071	0,7483	2518	29	1179	38	1771	28	47
FD13265_27	0,47	98	35	0,36	5,070	0,210	0,1788	0,0078	0,6387	2866	39	1047	42	1793	35	37
FD13265_28	0,37	42	23	0,55	17,500	1,300	0,6070	0,0490	0,6991	2943	62	2960	190	2955	72	101
FD13265_29	0,26	55	15	0,27	20,800	1,400	0,6170	0,0450	0,6406	3187	47	2990	170	3072	66	94
FD13265_30	0,17	85	39	0,46	30,790	0,940	0,6020	0,0210	0,5775	3719	22	2973	83	3492	31	80
FD13265_31	0,19	175	100	0,57	6,680	0,220	0,2585	0,0085	0,7287	2633	26	1466	43	2045	29	56
FD13265_32	0,15	126	84	0,67	18,770	0,570	0,4880	0,0160	0,7882	3247	21	2568	67	3014	30	79
FD13265_33	0,33	207	157	0,76	3,490	0,110	0,1326	0,0046	0,7239	2716	33	799	26	1509	26	29
FD13265_34	0,24	99	91	0,92	10,890	0,360	0,3950	0,0140	0,7446	2759	28	2119	64	2493	30	77
FD13265_35	0,40	137	43	0,31	4,340	0,170	0,1551	0,0063	0,6070	2840	32	917	35	1673	33	32
FD13265_36	0,28	72	24	0,33	11,810	0,560	0,3920	0,0190	0,7173	2920	35	2100	87	2541	49	72
FD13265_37	0,12	179	97	0,54	10,040	0,440	0,3940	0,0200	0,7236	2645	36	2100	91	2420	42	79
FD13265_38	0,35	133	91	0,68	5,520	0,210	0,1968	0,0077	0,7329	2738	30	1141	41	1873	34	42
FD13265_39	0,35	51	41	0,81	16,560	0,590	0,5770	0,0220	0,7139	2848	35	2897	90	2901	34	102
FD13265_40	0,18	100	38	0,38	17,910	0,610	0,4890	0,0180	0,7317	3189	25	2551	80	2961	34	80
FD13265_41	0,44	54	40	0,74	11,510	0,480	0,3920	0,0170	0,5398	2851	40	2108	77	2520	41	74
FD13265_42	0,56	41	29	0,72	11,670	0,550	0,4080	0,0200	0,7309	2938	45	2150	92	2548	46	73
FD13265_43	0,46	39	10	0,25	17,610	0,840	0,5730	0,0280	0,6432	2948	43	2860	110	2933	46	97
FD13265_44	0,15	182	53	0,29	9,470	0,530	0,3710	0,0220	0,6133	2679	50	2020	100	2373	54	75
FD13265_45	0,51	73	53	0,72	6,310	0,310	0,2330	0,0120	0,6466	2808	45	1318	60	1961	43	47
FD13265_46	0,33	56	29	0,51	15,310	0,660	0,4960	0,0210	0,6848	2963	37	2561	93	2794	43	86
FD13265_47	0,50	37	15	0,41	17,370	0,860	0,5930	0,0300	0,7294	2879	49	2940	120	2935	50	102
FD13265_48	0,26	89	48	0,54	10,470	0,530	0,3810	0,0210	0,6125	2865	43	2020	97	2428	49	71
FD13265_49	0,26	69	57	0,82	18,860	0,860	0,6090	0,0340	0,5420	2911	48	3020	130	3023	45	104
FD13265_50	0,54	35	10	0,29	16,200	1,100	0,5770	0,0390	0,7657	2860	61	2860	150	2861	70	100
FD13265_51	0,20	113	86	0,76	10,400	0,690	0,3700	0,0250	0,5321	2811	46	1980	120	2414	64	70
FD13265_52	0,49	54	30	0,55	14,160	0,520	0,3970	0,0180	0,6153	3271	39	2109	81	2736	35	64

Supplementary Table 2. Summary of U–Pb SHRIMP monazite data of the Igarapé Bahia deposit.

Sample FD67/132,65

Monazite grain	Isotopic Ratios								Ages					
	% $^{206}_{\text{U}}$ comm	U (ppm)	Th (ppm)	$^{232}\text{Th}/$ ^{238}U	$^{207}\text{Pb}/$ ^{235}U	$1\ \sigma$	$^{206}\text{Pb}/$ ^{238}U	$1\ \sigma$	err corr	$^{207}\text{Pb}/$ ^{206}Pb	$1\ \sigma$	$^{206}\text{Pb}/$ ^{238}U	$1\ \sigma$	% conc
N16-14.19-1	0,06	2554	5,9	0,002	2,6	8,3	0,109	8	0,97	2559	34	668	51	78

Supplementary Table 3. Trace elements data for chalcopyrite from the Igarapé Bahia deposit.

	Chalcopyrite from IOCG system							Chalcopyrite nodules and layers				
	FD68/ 393.80	FD173 /110.75	FD68/ 417.85	AL69/ 485.60	DH03/ 456.00	F353/158 .40	DH03/ 315.75	DH03/ 145.90	DH03/ 192.80	DH03/ 179.10	DH02/ 326.50	ED67/ 215.80
Li	0,80	0,23	1,44	1,26	2,66	1,12	0,85	3,38	2,00	2,78	1,00	0,56
Be	0,27	0,28	0,98	0,18	0,39	0,10	1,22	0,05	0,16	0,42	0,10	0,70
Sc	2,45	2,74	8,22	1,03	7,01	1,46	10,2	4,73	5,96	1,07	1,79	1,98
V	77,5	48,1	116	24,9	57,0	7,97	25,2	18,8	23,4	3,53	6,54	99,6
Cr	0,41	1,74	26,0	0,37	11,8	7,50	4,18	22,2	17,6	13,5	7,03	0,61
Co	33,4	17,8	123	214	14,1	1728	149,1	3846,0	10,7	3511,3	248,4	34,4
Ni	48,6	113,5	138	227	72,4	168	55,4	7136	14,6	3925	51,2	81,1
Cu	240615	285134	210450	213743	92950	337484	130329	9934	364127	199780	383426	98686
Zn	93,8	103	69,0	114	21,1	58,9	36,7	26,7	72,3	51,1	67,0	28,7
Ga	3,95	6,30	8,26	4,39	9,00	2,14	6,87	5,26	3,94	2,63	1,73	10,4
Rb	2,13	0,36	14,8	7,27	1,64	4,79	0,35	11,3	3,82	13,3	5,46	0,21
Sr	3,23	10,7	31,5	3,69	46,3	1,28	28,9	3,24	3,91	1,81	1,39	27,7
Y	19,2	7,95	39,1	12,4	26,1	1,05	50,1	5,40	2,87	1,10	3,18	13,6
Zr	0,21	2,96	33,4	0,12	13,4	7,10	1,56	48,0	4,45	19,4	8,72	0,35
Nb	42,0	0,19	7,59	4,56	7,28	0,59	1,28	1,75	0,18	1,37	0,57	7,94
Mo	94,0	11,0	128	51,3	134	3,53	150	4,50	47,3	9,39	3,82	106
Cd	<LD	<LD	<LD	<LD	<LD	0,05	<LD	0,05	<LD	0,01	0,31	<LD
Sn	7,38	9,48	15,2	11,6	7,35	8,07	10,6	<LD	3,11	0,93	5,99	3,48
Sb	0,64	0,35	0,32	0,81	0,32	7,72	0,79	1,50	1,78	6,09	0,80	0,89
Cs	0,26	0,05	1,00	0,79	0,14	0,09	0,04	0,13	0,11	0,08	0,08	0,01
Ba	32,7	2,80	101	29,0	19,5	15,0	9,18	41,2	12,9	15,5	15,1	10,9
La	33,8	10,6	131	115	153	41,3	195	78,6	127	1,95	7,60	29,5
Ce	61,2	14,8	203	208	294	57,8	359	146	209	3,54	13,4	65,5
Pr	5,75	1,28	17,5	19,0	23,1	4,93	33,7	14,5	17,9	0,36	1,34	5,75
Nd	20,2	4,13	58,2	63,6	78,9	14,0	114	50,7	55,0	1,43	4,72	22,0
Sm	3,12	0,65	8,31	6,93	12,0	1,20	16,7	7,77	6,24	0,27	0,80	3,91
Eu	1,11	0,51	3,08	1,35	5,06	0,24	5,92	1,39	1,89	0,08	0,17	1,33
Gd	3,51	0,96	9,50	6,08	11,6	1,12	15,6	5,50	5,03	0,27	0,70	4,73
Tb	0,57	0,17	1,21	0,65	1,49	0,07	1,96	0,50	0,39	0,04	0,11	0,68
Dy	4,24	1,24	7,40	3,58	8,84	0,26	11,9	1,83	1,17	0,23	0,64	4,03
Ho	0,98	0,28	1,41	0,65	1,59	0,04	2,29	0,25	0,12	0,04	0,11	0,86
Er	3,27	0,90	3,68	1,89	4,21	0,12	6,21	0,68	0,33	0,13	0,30	2,23
Tm	0,50	0,12	0,44	0,26	0,51	0,02	0,73	0,07	0,03	0,02	0,04	0,25
Yb	3,68	0,87	2,48	1,71	3,12	0,10	4,56	0,40	0,15	0,12	0,23	1,61
Lu	0,48	0,14	0,32	0,24	0,41	0,02	0,54	0,05	0,02	0,02	0,03	0,21
Hf	0,03	0,09	0,78	0,02	0,36	0,16	0,09	1,00	0,09	0,42	0,20	0,01
Ta	0,16	0,03	0,24	0,03	0,15	0,05	0,06	0,17	0,02	0,22	0,05	0,09
W	3,68	0,37	0,68	2,58	4,59	0,73	4,02	0,21	0,97	3,33	0,19	50,8
Pb	138	70,7	54,9	187	174	132	113	95,6	121	266	132	144
Bi	5,01	2,95	2,78	4,48	10,9	36,4	21,5	64,2	43,9	136	54,1	0,05
Th	1,94	0,03	1,06	0,50	0,86	2,03	0,14	9,14	0,67	1,14	1,21	0,22
U	128	2,22	50,7	190	225	0,57	117	1,19	2,57	0,31	0,27	247

**Anexo II – “Tracing fluid sources for
Salobo and Igarapé Bahia IOCG
deposits, Carajás Province: implications
for the genesis of the IOCG deposits”**

Tracing fluid sources for the Salobo and Igarapé Bahia deposits, Carajás Province: implications for the genesis of the IOCG deposits

GUSTAVO H. C. DE MELO¹; LENA V. S. MONTEIRO²; ROBERTO P. XAVIER¹,
CAROLINA P. N. MORETO¹; KURT KYSER³

¹Institute of Geosciences, University of Campinas (UNICAMP), R. João Pandiá Calógeras, 51, 13083-870 Campinas (SP), Brazil

²Institute of Geosciences, University of São Paulo (USP), Rua do Lago, 562, 05508-080 São Paulo (SP), Brazil

³Department of Geological Sciences and Geological Engineering Queen's University, Kingston, Ontario, Canada

Abstract

The Salobo and Igarapé Bahia iron oxide–copper–gold (IOCG) deposits stand out as economically important Cu–Au deposits in the Carajás Province. While Salobo is mainly hosted by basement gneisses and ca. 2.76 Ga deformed granitoids, the Igarapé Bahia deposit has the metavolcanosedimentary sequence of the Igarapé Bahia Group as the main hosts. Paragenetic evolution of the IOCG alteration–mineralization evidences higher temperature conditions at Salobo with assemblages composed of hastingsite–actinolite, almandine–grunerite–tourmaline, and almandine–grunerite–biotite–(magnetite). At Igarapé Bahia, in contrast, hydrothermal assemblages are represent by (tourmaline)–carbonate–magnetite, (tourmaline)–carbonate–chlorite and (tourmaline)–(biotite)–chlorite. Even though these deposits have different geological attributes, their timing of mineralization was likely synchronous at ca. 2.57 Ga. However, the origin of ore-forming fluids in these deposits and their link with the tectono-magmatic evolution of Carajás Province remain uncertain. Stable isotope analyses carried out on hydrothermal minerals permitted unravel the fluid evolution in each deposit. At Salobo, iron-enrichment was formed at 429 ± 45 °C with involvement of hydrothermal fluids with magmatic compositions, as estimated from grunerite ($\delta^{18}\text{O}_{\text{H}_2\text{O}} = +6.66$ to $+7.96\text{\textperthousand}$, $\delta\text{D}_{\text{H}_2\text{O}} = -10.65$ to $-1.33\text{\textperthousand}$), garnet ($\delta^{18}\text{O}_{\text{H}_2\text{O}} = +6.88$ to $+7.77\text{\textperthousand}$) and tourmaline ($\delta^{18}\text{O}_{\text{H}_2\text{O}} = +4.11$ to $+6.41\text{\textperthousand}$, $\delta\text{D}_{\text{H}_2\text{O}} = -15.40$ to $+5.12\text{\textperthousand}$). Fluids associated with potassic alteration, at 520 ± 45 °C, also have typical magmatic composition, as indicated by biotite ($\delta^{18}\text{O}_{\text{H}_2\text{O}} = +7.16$ to $+7.96\text{\textperthousand}$, $\delta\text{D}_{\text{H}_2\text{O}} = -36.96$ to $-21.93\text{\textperthousand}$) and quartz ($\delta^{18}\text{O}_{\text{H}_2\text{O}} = +6.88 \pm 0.35\text{\textperthousand}$). Sulfur isotope signatures for chalcopyrite and bornite range from $+0.81$ to $+1.28\text{\textperthousand}$ and -0.37 to $+1.63\text{\textperthousand}$, respectively, what suggests a magmatic sulfur source at Salobo. In the Igarapé Bahia deposit, fluids associated with tourmaline display magmatic signatures ($\delta^{18}\text{O}_{\text{H}_2\text{O}} = +5.54$ to $+6.24\text{\textperthousand}$, $\delta\text{D}_{\text{H}_2\text{O}} = -46.98$ to $-32.70\text{\textperthousand}$, at 398 ± 85 °C). Fluids in equilibrium with calcite ($\delta^{18}\text{O}_{\text{H}_2\text{O}} = +1.68$ to $3.10\text{\textperthousand}$, 398 ± 85 °C) and later chlorite ($\delta^{18}\text{O}_{\text{H}_2\text{O}} = +2.13$ to $+3.41\text{\textperthousand}$, $\delta\text{D}_{\text{H}_2\text{O}} = -57.69$ to $-21.67\text{\textperthousand}$, 255 ± 15 °C) evidence that input of ^{18}O -depleted fluids might have contributed to the hydrothermal system. $\delta^{13}\text{C}_{\text{CO}_2}$ values (-9.04 to $-4.65\text{\textperthousand}$) for fluids in equilibrium with calcite, however, imply in magmatic source for carbon. The highest $\delta^{18}\text{O}_{\text{H}_2\text{O}}$ values recorded from magnetite ($+11.71 \pm 0.16\text{\textperthousand}$) might point to intense fluid–rock interaction. Collectively, oxygen, hydrogen, carbon, and sulfur isotope data reinforce that magmatic fluids played an important role in the early stages of the IOCG hydrothermal system evolution in both deposits. Crystallization of ca. 2.5 granites (e.g.

Old Salobo) and exsolution of magmatic brines represent the main source of the ore-forming fluids. These fluids were exsolved in deeper crustal levels and ascended through shear zones. However, the influx of ^{18}O -depleted fluids in the later stages at Igarapé Bahia suggests that formation water might be important for its formation. These results reveal the complexity of these deposits, which had hybrid sources, with predominance of those magmatic, during the evolution of a long-lived and wider mineral system.

Introduction

Since the discovery of the outstanding Olympic Dam deposit in Australia, in 1975, and the definition of the iron oxide–copper–gold (IOCG) deposit class (Hitzman et al., 1992), similar deposits have been target of mineral exploration and academic research. However, despite of advances in scientific investigation, the origin of the hypersaline ore-forming fluids of the IOCG deposits is still controversial. In part, it is due to the remarkable variability in geological features, tectonic setting and ages of the IOCG deposits worldwide. There are those who argue in favor of a magmatic origin for the hydrothermal fluids (e.g. Sillitoe 2003, Pollard 2006) and those who propose that brines were mainly derived from evaporites (e.g. Barton and Jonson 1996, Haynes 2000, Xavier et al. 2008). However, the IOCG deposits could represent hybrid systems with different contribution for the ore-forming fluids reflecting their distinct geological settings.

In the Carajás Province, Amazon Craton, Brazil, an important cluster of high-tonnage IOCG deposits were formed during multiple hydrothermal events in the Neoarchean (2.72 – 2.68 Ga and ca. 2.57 Ga) and Paleoproterozoic (ca. 1.88 Ga) (Réquia et al. 2003, Tallarico et al. 2005, Moreto et al. 2015a, b). The IOCG deposits that record the ca. 2.57 Ga hydrothermal event are likely restricted to the northern sector of Carajás Domain, including Salobo and Igarapé Bahia deposits.

The Salobo (1,112 Mt @ 0.69% Cu and 0.43 g/t Au, VALE 2012) and Igarapé Bahia (219 Mt @ 1.4% Cu and 0.86 g/t Au, Tallarico et al. 2005) deposits stand out in the world as economically and scientifically important IOCG deposits. Although these deposits have different geological attributes (i.e. host rocks, hydrothermal alteration patterns and ore mineralogy; Réquia et al. 2003, Tallarico et al. 2005, Dreher et al. 2008, Melo et al. 2016, Melo et al. in prep), they might share a common metallogenic evolution. Their association with a wide magmatic–hydrothermal system developed at ca. 2.57 Ga has been proposed based on the similar age of copper–gold mineralization and granite emplacement (e.g. Old Salobo granite; Réquia et al., 2003, Tallarico et al. 2005, Groves et al., 2010). The importance of externally-derived fluids including association with bittern fluids has also been demonstrated from boron isotopes and halogen chemistry (Xavier et al. 2008, 2009). However, the relative contribution of these distinct fluid sources and their regional importance in the metallogenetic evolution of the Carajás Province should be better evaluated.

In addition, the complex and controversial evolution of the Carajás Domain in the Neoarchean hampers a more detailed characterization of possible sources for the ore-forming fluids of the IOCG deposits. In ca. 2.5 Ga, for instance, an important tectono-magmatic event has been recognized in the northern sector of the Carajás Domain (Machado et al. 1991, Barbosa 2004, Melo et al. 2016, Toledo 2017). This tectonic event was likely associated with granite magmatism and may have generated a fertile scenario for Cu–Au mineralization. This metallogenetic event could also be responsible for remobilization of the Cu–Au ore formed in 2.71 – 2.68 Ga, which is well documented in the Southern Copper Belt of the Carajás Province (e.g. Sequeirinho, Cristalino, Bacuri and Bacaba deposits; Moreto et al. 2015a, b), but it remains very speculative.

In this paper, we report new O, H, C and S stable isotope data for the Salobo and Igarapé Bahia deposits. These data can provide important information on the isotopic signature of the ore-forming fluids, their diverse origin, temperature of alteration-mineralization and on physicochemical conditions of mineral precipitation in the Salobo and Igarapé Bahia deposits. In addition, these data are evaluated and discussed according to the tectono-magmatic evolution of the Carajás Domain and the main metallogenetic episodes recognized in the province.

Regional Geological Setting

The Carajás Province, located at the southeastern part of the Amazon Craton, represents an Archean block and comprises one of the most important mineral provinces in the world (Tassinari et al. 1999, Santos 2003). This province is divided into two tectonic domains: (i) Rio Maria, at south, with a typical granite-greenstone belt sequence, including TTG and sanukitoids, and (ii) Carajás, represented by Mesoarchean basement rocks and Neoarchean supracrustal sequences (Santos 2003, Vasquez et al. 2008).

The Carajás Domain hosts an important concentration of high-tonnage IOCG deposits (Fig. 1). These deposits include mainly Salobo, Igarapé Bahia, GT 46, Paulo Alfonso and Furnas in the northern sector, and Sossego, Cristalino and Alvo 118 in the Southern Copper Belt (Huhn et al. 1999, Réquia et al. 2003, Tallarico et al. 2005, Monteiro et al. 2008a, b, Torresi et al. 2011, Moreto et al. 2015a, b).

Basement rocks encompass gneisses and migmatites of the Xingu Complex, granulites ($3,002 \pm 14$ Ma, Pidgeon et al. 2000), calc-alkaline granites and undifferentiated TTG (Moreto et al. 2011, Feio et al. 2013, Dall'Agnol et al. 2016).

Overlying the basement rocks there are metavolcanosedimentary sequences of the Rio Novo Group and the Itacaiúnas Supergroup. The Rio Novo Group comprises amphibolite, schist, metagraywacke, metavolcanic rocks and gabbro (Hirata et al. 1982). The Itacaiúnas Supergroup (2.76 – 2.74 Ga) consists mainly of metavolcanic, metavolcaniclastic and metasedimentary rocks, including banded iron formations (DOCEGEO 1988). It is divided into the Igarapé Salobo, Igarapé Pojuca, Grão Pará and Igarapé Bahia groups.

Two models have been proposed for the deposition of the supracrustal sequences of the Carajás Domain. These models include: (i) a continental rift with an associated bimodal magmatism and tholeiitic character for the metabasalts of the Grão Pará Group (Gibbs et al 1986, Wirth et al. 1986, DOCEGEO 1988, Tallarico 2003); and (ii) an arc-related setting, with high potassium calc-alkaline signature for the metabasalts from the Itacaiúnas Supergroup (Dardenne et al. 1988, Texeira 1995, Lindenmayer et al. 2005)

The Águas Claras Formation comprises a low-grade metasedimentary sequence deposited in shallow marine to continental fluvial environment. The minimum age of deposition is constrained in $2,708 \pm 37$ Ma, by the dating of intrusive mafic dykes within the Águas Claras Formation (U–Pb in zircon, Mousseot et al., 1996a). However, Pb–Pb ages in diagenetic pyrite from the Águas Claras Formation yielded ages of 2.06 Ga (Mousseot et al. 1996b), evidencing that the Águas Claras deposition may have been younger.

Mafic-ultramafic layered complexes of ca. 2.76 to 2.74 Ga in the Carajás Domain are represented mainly by the Luanga and Vermelho bodies (Machado et al. 1991, Ferreira Filho et al. 2007).

Granitic magmatism occurred in three events in the Carajás Domain. The 2.76 – 2.73 Ga granites encompass Planalto, Plaquê, Serra do Rabo, Cristalino, Estrela and Igarapé Gelado suites (Huhn et al. 1999a, 1999b, Avelar et al. 1999, Sardinha et al. 2006, Barros et al. 2004, 2009; Feio et al. 2012, Melo et al. 2016). These granites are, in general, A-type, alkaline to metaluminous, and considered syn-tectonic in relation to the shear zones development. The Old Salobo and Itacaiúnas granites represent the restricted granite magmatism in ca. 2.57 Ga at the northern sector of Carajás Domain (Machado et al. 1991; Souza et al. 1996, Melo et al. 2016). They are A-type peralkaline

to metaluminous granites. Anorogenic magmatism in 1.88 Ga is widespread in the Carajás Domain and expressed by the Central de Carajás, Cigano, Pojuca, and Breves granites (Machado et al. 1991; Lindenmayer and Teixeira 1999; Tallarico 2003).

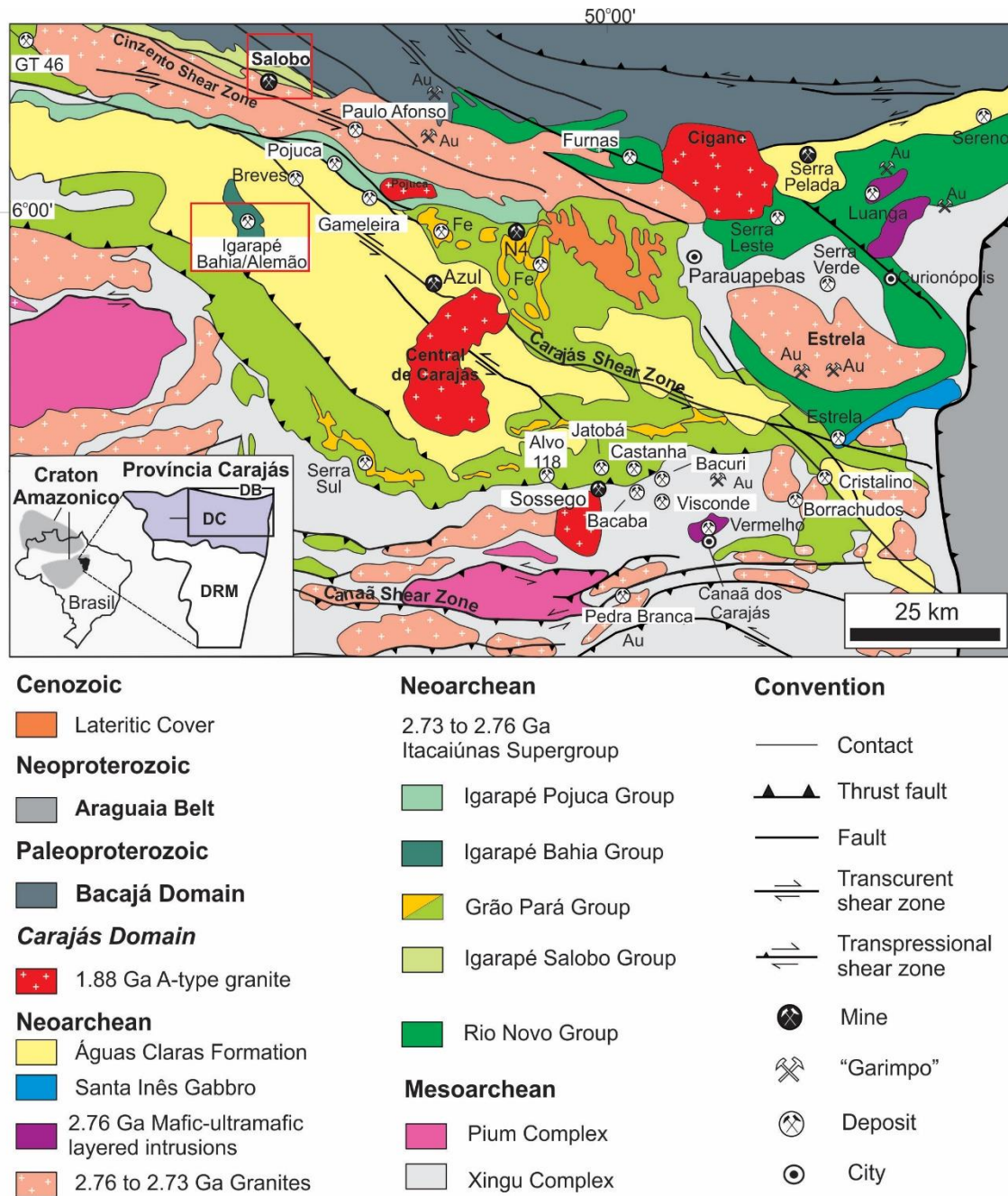


Fig. 1. Geological map of the Carajás Domain with the location of the main ore deposits. The red boxes show the location of Salobo and Igarapé Bahia deposits (modified from Vasquez et al. 2008, Dall'Agnol et al. 2016, Santos e Oliveira 2016).

According to Araújo et al. (1998), the structural framework of the Carajás Domain developed in a dextral transtension regime, allowing the deposition of the sediments from the Rio Novo Group and Itacaiúnas Supergroup. This basin was later inverted by sinistral transpression (Araújo et al. 1998, Pinheiro and Holdsworth 1997, Holdsworth and Pinheiro 2000). The Carajás Domain was divided into three structural domains: the (i) Carajás, (ii) Cinzento and (iii) Canaã domains, with ages ranging from 2.7 to 2.5 Ga (Pinheiro et al. 2013). The Carajás and Cinzento systems correspond to regional-scale WNW-ESE shear zones, whereas in the Southern Copper Belt the Canaã system encompass E-W-strike shear zones developed over the basement rocks (Pinheiro et al. 2013).

Geology of the Salobo and Igarapé Bahia Deposits

Salobo deposit

The Salobo deposit lies in the WNW–ESE Cinzento Shear Zone, where basement rocks from the Xingu Complex ($2,950 \pm 25$ and $2,857 \pm 6.7$ Ma; U–Pb zircon; Melo et al., 2016) and deformed granitoids from the Igarapé Gelado suite ($2,763 \pm 4.4$ Ma; U–Pb zircon; Melo et al. 2016) represent the main host units (Fig. 2; 3A, B; Melo et al. 2016). Remnants of the Itacaiúnas Supregroup metavolcanosedimentary sequence are also recognized in the southwestern part of the deposit. These rocks were intensely ductile deformed and hydrothermally altered, generating mylonitic rocks with variable amounts of actinolite, garnet, grunerite, almandine, tourmaline, biotite and magnetite (Réquia et al. 2003, Melo et al. 2016).

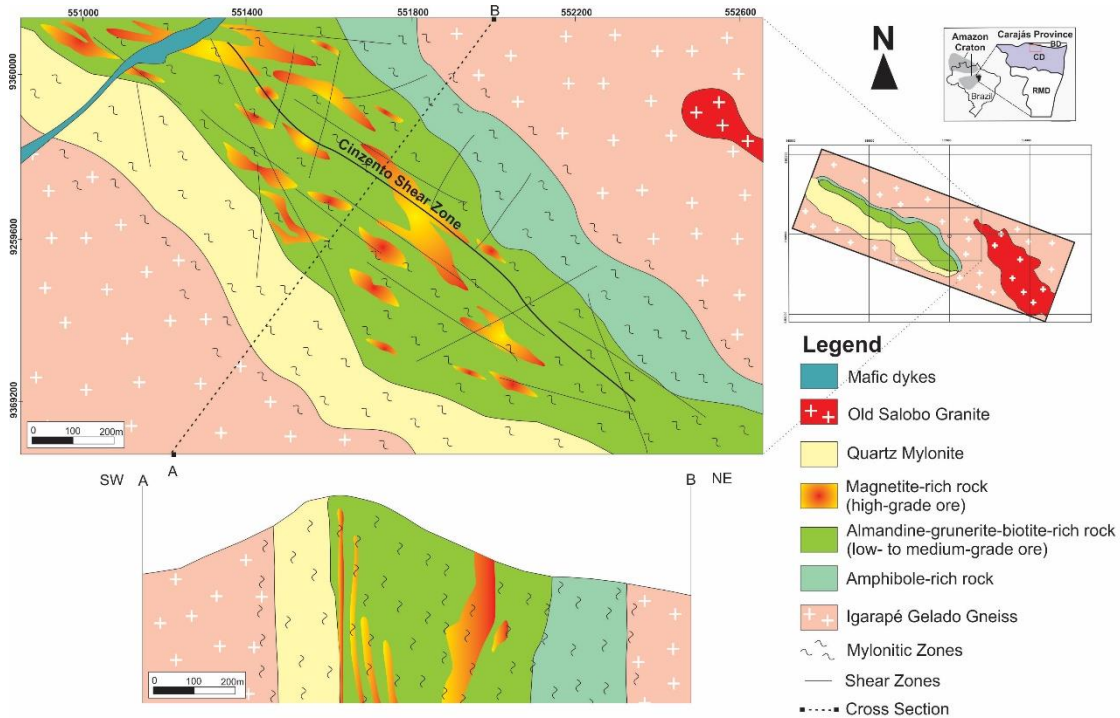


Fig. 2. Geological map and cross section of the Salobo deposit, showing the host rocks, hydrothermally altered zones and the steeply dipping ore lenses (modified from VALE).

The host rocks are crosscut by several intrusions. The Old Salobo granite is an A-type, syntectonic, peralkaline to metaluminous granite (Lindenmayer 2003) and was dated in $2,573 \pm 2$ Ma and $2,547 \pm 5.3$ Ma (Machado et al. 1991, Melo et al. 2016, Fig. 3C). A Paleoproterozoic (ca. 1.88 Ga) anorogenic, metaluminous, isotropic granite was also recognized at Salobo deposit and named as Young Salobo granite. Late dolerite dikes crosscut the sequence of host and mineralized rocks (Lindenmayer 1990; Machado et al. 1991).

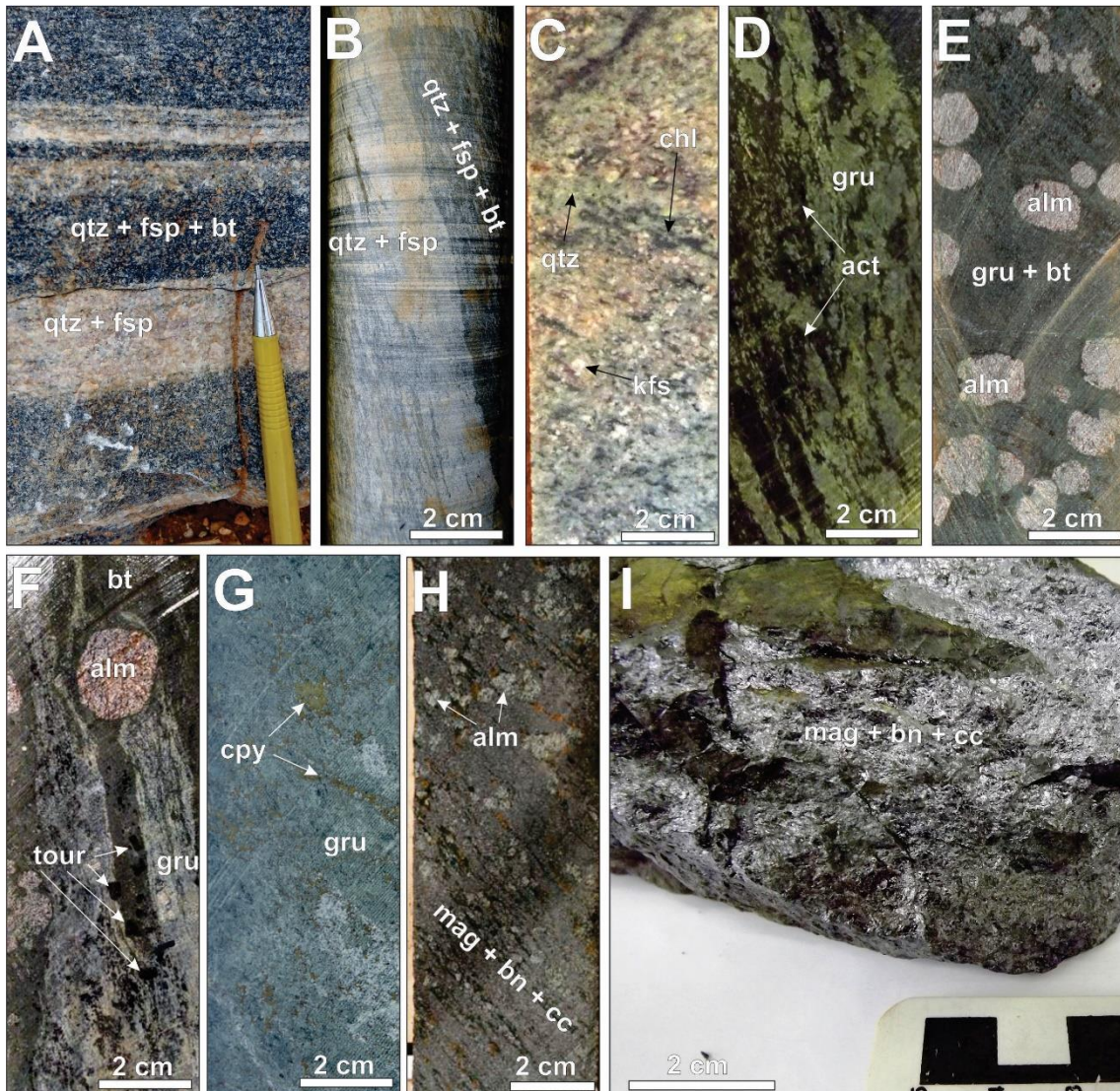


Fig. 3. General aspects of the host rocks and hydrothermal alteration zones of the Salobo deposit. a) Igapé Gelado gneiss with compositional banding. b) Drill core sample of the Igapé Gelado gneiss with a well-developed mylonitic foliation. c) Typical aspect of the Old Salobo granite with hydrothermal alteration with chlorite and potassic feldspar. d) Na-Ca alteration with actinolite replaced by later grunerite. e) Grunerite-almandine-biotite rich rocks in the central zone of Salobo. f) Almandine-grunerite-biotite-(tourmaline)-rich rocks widely recognized in the central part of the deposit. g) Zones of iron-enrichment with grunerite with disseminated chalcopyrite. h) Foliated samples of the central portion of the deposit with massive development of magnetite and relicts of almandine-(biotite-grunerite). i) Massive ore at Salobo with magnetite, bornite and chalcocite. Abbreviations: Act = actinolite, Alm = almandine, Bn = bornite, Bt = biotite, Cc = chalcocite, Chl = chlorite, Cpy = chalcopyrite, Fsp = feldspar, Gru = grunerite, Kfs = potassium feldspar, Mag = magnetite, Qtz = quartz, Tour = tourmaline.

The mineral assemblages in the central zone of the Salobo deposit represent products of hydrothermal alteration, which precludes the recognition of the protolith features in these portions (Xavier et al. 2012, Melo et al. 2016). Na-Ca alteration occurs

in the outer zones of the deposit, where protolith textures are still preserved. The main hydrothermal alteration encompasses a widespread iron-enrichment (almandine–grunerite–magnetite) and tourmaline formation (Melo et al. 2016; Fig. 8). Almandine forms (i) clean porphyroblasts and (ii) poikiloblastic crystals with fine-grained grunerite inclusions aligned with foliation (Fig. 4A). Grunerite crystals define the mylonitic foliation (Fig. 4B), replace early actinolite and surrounds almandine porphyroblasts. Almandine and grunerite are synchronous, whereas magnetite is late in comparison to them (Melo et al. 2016). Schorl tourmaline is also widespread within these zones (Fig. 4C). Tourmaline crystals are temporally associated with grunerite, but they are replaced by biotite and quartz performing shadow pressure around tourmaline (Fig. 4D).

Potassic alteration with biotite is broadly recognized in the central parts of the deposit. Biotite replaces grunerite, crosscut almandine (Fig. 4E), and was coeval with the ore precipitation. Biotite and associated quartz commonly define the mylonitic foliation, with strain shadow around almandine and tourmaline (Fig. 4F). A later low-temperature assemblage (stilpnomelane-greenalite-chamosite-Fe-pyrosmalite) overprints previous stages (Melo et al. 2016).

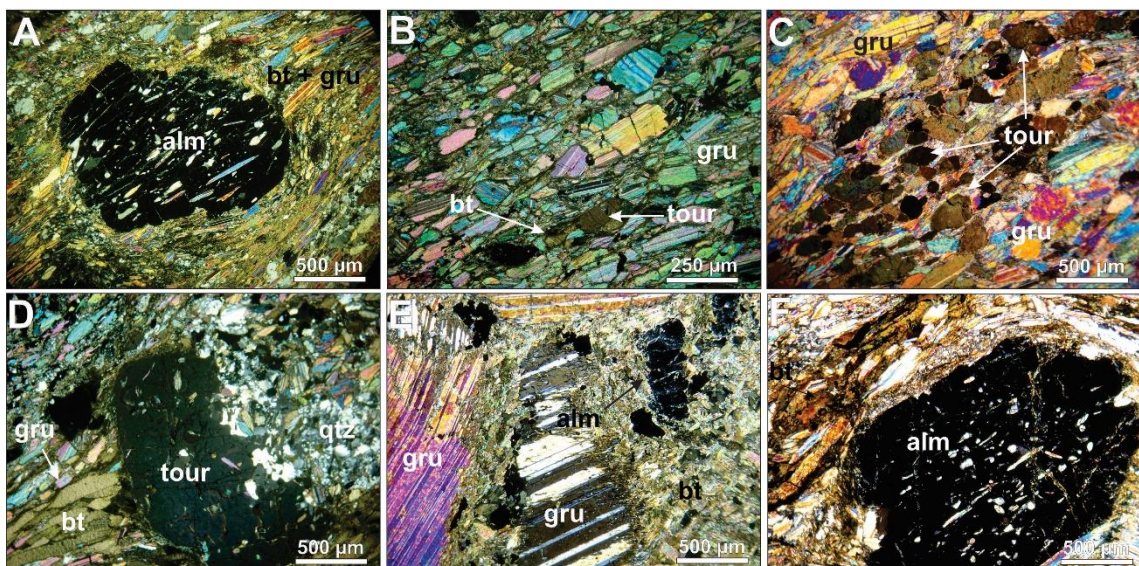


Fig. 4. Photomicrograph of different hydrothermal mineral assemblages at Salobo under transmitted light and crossed polars. a) Almandine porphyroblast with poykilitic texture recording the mylonitic foliation associated with grunerite and replaced by biotite; b) Oriented grunerite crystals perfoming the mylonitic foliation associated with fine-grained tourmaline crystals; c) Aggregates of tourmaline crystals aligned with grunerite; d) Tourmaline porphyroblast replaced by biotite and quartz; e) Relicts of grunerite and almadine porphyroblasts replaced by later biotite. f) Almandine porphyroblast with biotite crystals forming shadow pressure around it. Abbreviations: Alm = almandine, Bt = biotite, Gru = grunerite, Qtz = quartz, Tour = tourmaline.

The Cu–Au ore is represented by NW–SE steeply dipping lenses or elongated bodies along the mylonitic foliation associated with magnetite-rich rocks (Fig. 3H, I; Melo et al. 2016). Bornite and chalcocite with minor chalcopyrite represent the main ore minerals, but significant contents of Co, Ni, As, Ag, Au, Mo, F, REE, and U are characteristic of the Salobo ore. Features of extreme shearing in the hydrothermally altered rocks and in the ore point to the important role of the Cinzento Shear Zone coeval with metasomatism (Melo et al. 2016).

Re–Os molybdenite dating in the samples of the Salobo ore yielded an age of $2,576 \pm 8$ Ma (Réquia et al. 2003), which might reflect the main stage of mineralization. This age was genetically linked to the Old Salobo granite crystallization (Réquia et al. 2003). However, a monazite U–Pb age of $2,452 \pm 14$ Ma suggests that successive reactivations of the Cinzento Shear Zone associated with hydrothermal activity affected the Salobo deposit even during the Siderian (Melo et al. 2016).

Igarapé Bahia deposit

The Igarapé Bahia deposit is located in an erosional window within the Águas Claras Formation close to the extensive Carajás Shear Zone. The deposit is hosted by metavolcanosedimentary rocks of the Neoarchean Igarapé Bahia Group and metasedimentary rocks of the Águas Claras Formation (Fig. 5A). The deposit is divided into four orebodies from south to north: Furo 30, Acampamento Sul, Acampamento Norte and Alemão orebodies (Fig. 5B, C, D, E).

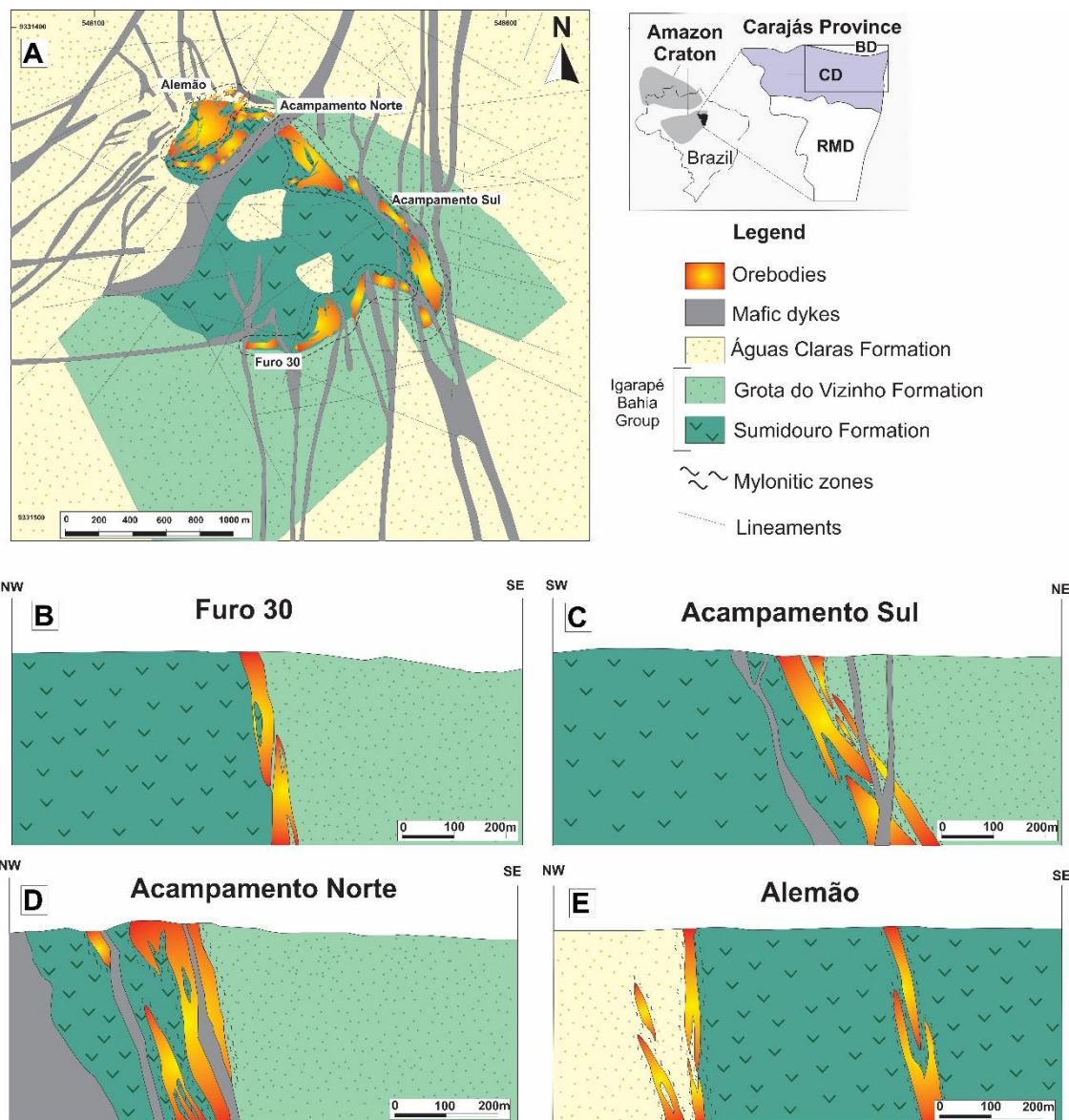


Fig. 5. a) Geological map of the Igarapé Bahia deposit showing the main host units and projection of the orebodies. Geological profile of the a) Furo 30, b) Acampamento Sul, c) Acampamento Norte and d) Alemão orebodies (modified from VALE).

The metavolcanosedimentary units of the Igarapé Bahia Group includes mafic and acid metavolcanic rocks and metagabbros (lower unit), and banded iron formation, metagraywackes and metarhytmites (upper unit; Fig. 6A, B, C, D, E; Lindenmayer et al 1998, Tallarico et al. 2005, Dreher et al. 2008, Melo et al. in prep). Metagraywackes of the Águas Claras Formation also host the mineralization, especially in the Alemão orebody (Fig. 6F, G). Most of these rocks preserve S_0 structures, but they are strongly affected by ductile deformation, which imparted a Sn mylonitic foliation within these rocks (Fig. 6G, H, I, K, L).

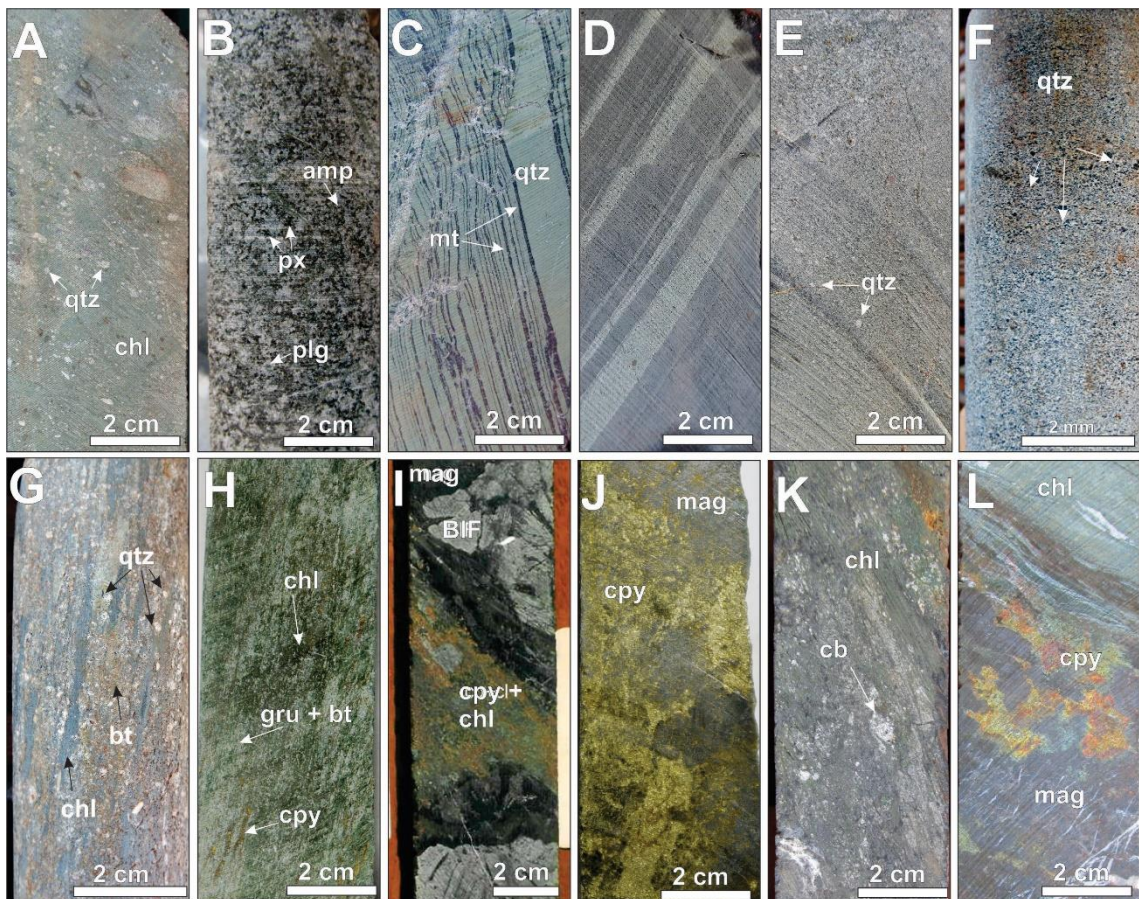


Fig. 6. General aspects of the host rocks and hydrothermal alteration zones of the Igarapé Bahia deposit. a) Chlorite alteration in metavolcanic rocks of the lower unit of the Igarapé Bahia Group. b) Chlorite-alteration in metagabbroic rocks with rare relicts of pyroxene. c) Banded Iron Formation formed by magnetite and quartz and cut by late calcite veinlets in the transition of the lower unit and upper unit of the Igarapé Bahia Group. d) Metarhytmites with plan-parallel bedding and normal faults in the upper unit. e) Massive metagraywacke rocks of the upper unit. f) General aspect of the Águas Claras Formation metagraywackes. g) Sheared and hydrothermally altered metagraywackes of the Águas Claras Formation. h) Grunerite–chlorite–biotite-rich rocks with mylonitic foliation and some stretched chalcopyrite grains. i) Hydrothermal breccia with BIF clast cemented by chalcopyrite and chlorite. j) Typical aspect of copper–gold ore from the Alemão orebody composed of chalcopyrite. k) Zone with intense chlorite and carbonate formation, where features of the host are not recognized. l) Mylonitic rocks with chlorite formation and magnetite–chalcopyrite-rich zones. Abbreviations: Amp = amphibole, Cb = carbonate, Chl = chlorite, Cpy = chalcopyrite, Gru = grunerite, Kfs = potassium feldspar, Mag = Magnetite, Px = pyroxene, Qtz = quartz, Tour = tourmaline.

Hydrothermal alteration is conspicuous in the four orebodies with no significant differences among them (Melo et al. in prep). Na–Ca alteration (actinolite–epidote–scapolite) and K–(Fe) alteration with biotite and minor grunerite is early and spatially restricted in the deposit (Fig. 8).

Carbonate formation is widespread and characterized by stretched crystals performing the mylonitic foliation of the rocks (Fig. 7A, B, D). Although calcite prevails, siderite and ankerite can also be present. In general, carbonate–chlorite, tourmaline–carbonate–chlorite and/or magnetite–carbonate–chlorite mylonitic rocks are recognized in carbonate alteration zones (Fig. 7D). Tourmaline porphyroblasts occur within the carbonate matrix (Fig. 7A, B). These minerals are widely recognized both in outer and inner zones of the orebodies.

Magnetite (I) formation precedes chalcopyrite precipitation and is commonly observed intergrown with carbonate and relicts of tourmaline as idiomorphic crystals (Tallarico et al. 2005, Dreher et al. 2008, Melo et al. in prep). However, most of magnetite is represented by magnetite (II) within the ore zones as xenomorphic crystals, where chalcopyrite is already observed.

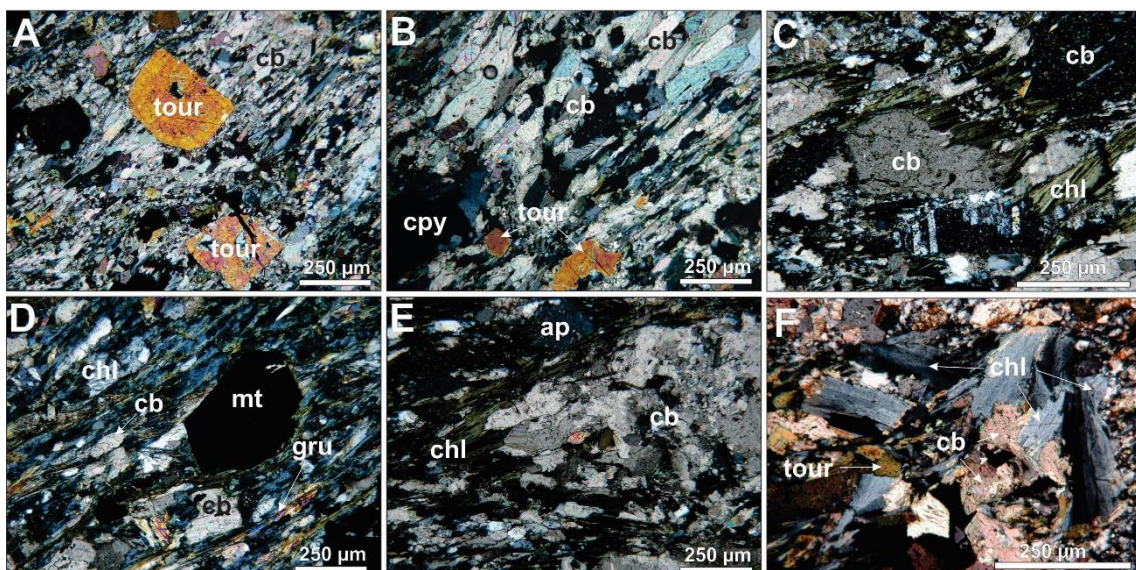


Fig. 7. Photomicrograph of different hydrothermal mineral assemblages at Igarapé Bahia. a) Tourmaline porphyroblasts set in the foliated carbonate matrix; b) Zones of carbonate alteration with stretched crystals of carbonate associated with tourmaline and chalcopyrite; c) Calcite porphyroblasts replaced by chlorite in their rims. d) Magnetite (I) crystals set in a carbonate matrix and replaced by later chlorite; e) Zones with carbonate formation and apatite surrounded and replaced by chlorite. f) Later chlorite crystals within calcite-tourmaline matrix.

Steeply dipping mylonitic rocks and hydrothermal breccias represent the locus of mineralization at Igarapé Bahia (Fig. 6I, J, K, L; Melo et al. in prep). Hydrothermal breccias are composed of altered clasts of the host rocks cemented by hydrothermal minerals (i.e. carbonate, chlorite and chalcopyrite). Massive ore is also observed at Igarapé Bahia, but mainly in the Furo 30 orebody (Melo et al. in prep). Ore mineralogy

includes mainly chalcopyrite and pyrite as the main sulfides with large contents of magnetite, reaching up to 60% of the ore. The ore geochemistry signature at Igarapé Bahia usually includes U (uraninite), REE (monazite, allanite, xenotime, petersinit), P (apatite, cheralite, autunite), Nb (pyrochlore, fergusonite), W (sheelite and wolframite), Sn (cassiterite) (Melo et al. *in prep*). Gold is often found associated with hessite, cobaltite and gersdorffite.

Chlorite formation was the most widespread hydrothermal alteration at Igarapé Bahia but it was late in relation to the ore precipitation (Fig. 7D, E, F; Tallarico et al. 2005, Dreher et al. 2008, Melo et al. *in prep*). Streched chlorite crystals are oriented according to the mylonitic foliation of the rocks and commonly replace previous carbonate and tourmaline (Fig. 7E, F). Chlorite also makes pressure shadow around carbonate grains (Fig. 7C).

Timing of mineralization in the Acampamento Sul orebody was constrained at $2,575 \pm 12$ Ma (SHRIMP U–Pb in monazite, Tallarico et al. 2005). Recent geochronological studies in the Alemão orebody yielded ages of $2,559 \pm 34$ Ma (U–Pb in hydrothermal monazite), showing that the timing of mineralization in the distinct orebodies was coeval at Igarapé Bahia (Melo et al. *in prep*). These ages are quite similar to the mineralization age obtained in the Salobo deposit ($2,576 \pm 8$ Ma, Re–Os in molybdenite, Réquia et al. 2003) and in the Old Salobo granite ($2,573 \pm 2$ Ma, $2,547 \pm 5.3$ Ma; U–Pb in zircon; Machado et al. 1991, Melo et al. 2016), pointing to a synchronous event in both deposits associated with granitic magmatism emplacement (Réquia et al. 2003, Tallarico et al. 2005).

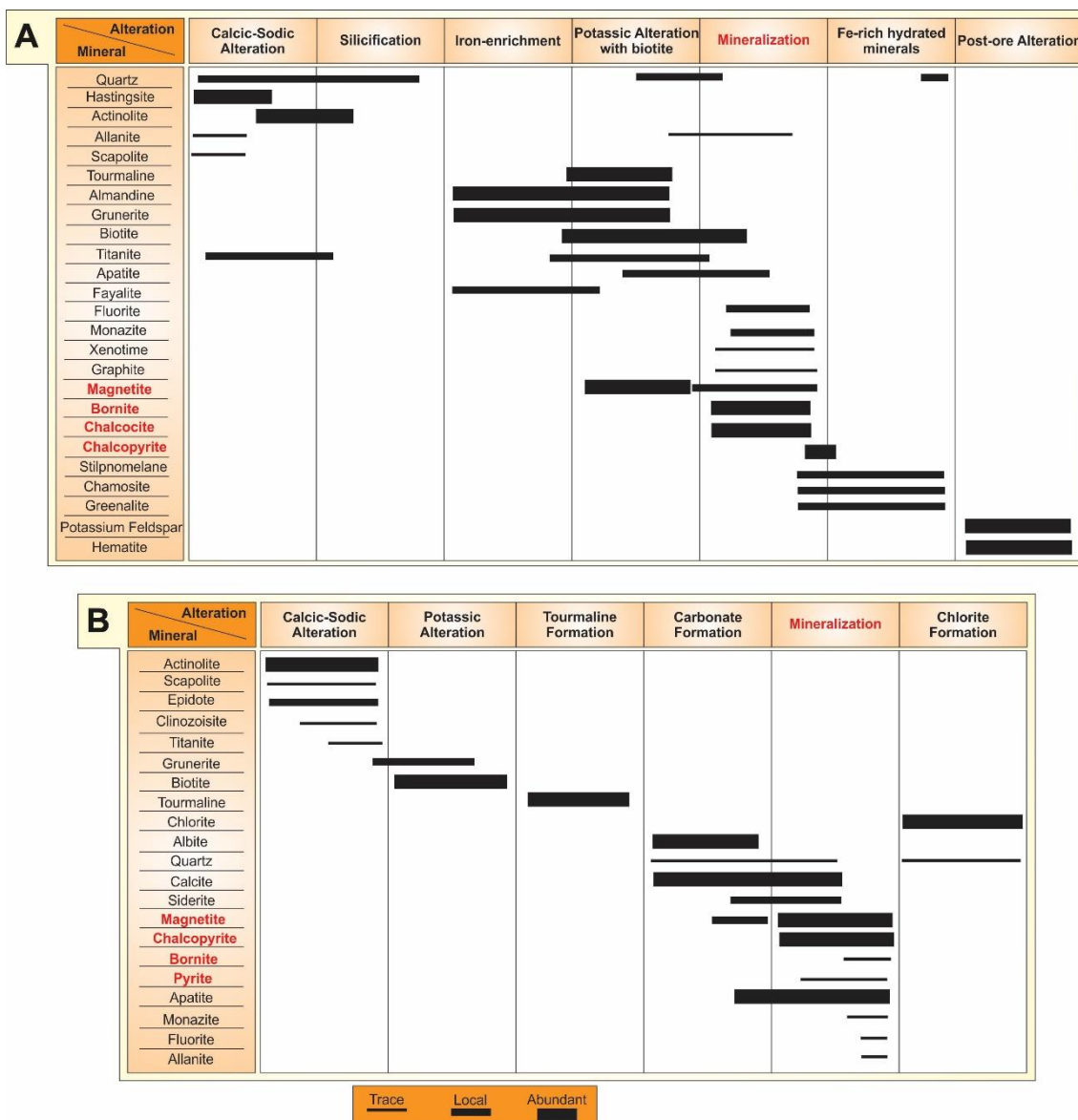


Fig. 8. Paragenetic table showing the evolution of the hydrothermal system at a) Salobo and b) Igarapé Bahia (modified from Melo et al. 2016, Melo et al. in prep.).

Analytical Procedures

Oxygen, hydrogen, carbon and sulfur isotope analysis

Oxygen stable isotope analyses were carried out on biotite, calcite, chlorite, garnet, grunerite, magnetite, quartz, and tourmaline from Salobo and Igarapé Bahia deposits. Hydrogen isotope analyses were obtained for biotite, chlorite, grunerite, and tourmaline samples. Minerals were extracted from drill core samples and crushed into an agate mortar with a pestle to remove all the mineral inclusions. Mineral separates amount range from 20 to 50 mg. The isotopic composition of oxygen in garnet was determined at the Center for Granite Research, Stable Isotope Laboratory (NEG-

LABISE) of the Federal University of Pernambuco. Oxygen isotope analysis in silicates, carbonates and oxide, and hydrogen analysis in silicates were determined at the Queen's Facilities for Isotope Research (QFIR) at Queen's University (Canada). The $\delta^{18}\text{O}$ ratio of calcite was determined by reacting approximately 1 mg of powdered material with 100% anhydrous phosphoric acid at 72°C for 4 hours. The CO₂ released was analyzed using a Thermo-Finnigan Gas Bench coupled to a Thermo-Finnigan DeltaPlus XP Continuous-Flow Isotope-Ratio Mass Spectrometer (CF-IRMS). $\delta^{18}\text{O}$ values are reported using the delta (δ) notation in permil (‰), relative to Vienna Standard Mean Ocean Water (VSMOW), with a precision of 0.2‰. Oxygen in silicates was extracted from 5mg samples at 550-600°C according to the conventional BrF5 procedure of Clayton and Mayeda (1963) and analyzed via dual inlet on a Thermo-Finnigan DeltaPlus XP Isotope-Ratio Mass Spectrometer (IRMS). $\delta^{18}\text{O}$ values are reported using the delta (δ) notation in units of permil (‰) relative to Vienna Standard Mean Ocean Water (VSMOW) international standard, with a precision of 0.1‰. For hydrogen in silcates, samples were weighed into silver capsules, degassed for 1 hour at 100°C then crushed and loaded into a zero-blank auto sampler. The hydrogen isotopic composition was measured using a Thermo-Finnigan thermo-combustion elemental analyzer (TC/EA) coupled to a Thermo-Finnigan DeltaPlus XP Continuous-Flow Isotope- Ratio Mass Spectrometer (CF-IRMS). $\delta^2\text{H}$ values are reported using delta (δ) notation in permil (‰), relative to Vienna Standard Mean Ocean Water (VSMOW), with a precision of 3‰.

In addition, five calcite samples were analyzed to obtain oxygen and carbon isotope compositions in the Centro de Pesquisas Geocronológicas (CPGeo), at University of São Paulo. The oxygen and hydrogen isotopic compositions are reported in relation to Vienna Standard Mean Ocean Water (VSMOW) and carbon isotopic compositions in relation to Pee Dee Belemnite (PDB).

Bornite and chalcopyrite mineral separates were extracted from mineralized rocks of the Salobo deposit. The sulfur isotope analysis were performed in a MC-ICP-MS Neptune (Thermo Finnigan) coupled with laser New Wave UP213 Nd:YAG, in the Geochronology Laboratory of the University of Brasilia. Sulfur values are reported in relation to Vienna Canyon Diablo Troilite (VC DT).

Results

Oxygen Isotopes

Oxygen isotope analyses were carried out on minerals representative of different stages of hydrothermal alteration at Salobo and Igarapé Bahia deposits. In the Salobo deposit, the oxygen isotope analysis included biotite ($\delta^{18}\text{O}_{\text{VSMOW}} = +4.7$ to $+5.9\text{\textperthousand}$; $n = 3$), grunerite ($\delta^{18}\text{O}_{\text{VSMOW}} = +5.5$ to $+6.8\text{\textperthousand}$; $n = 3$), garnet ($\delta^{18}\text{O}_{\text{VSMOW}} = +4.2$ to $+6.8\text{\textperthousand}$; $n = 5$), quartz ($\delta^{18}\text{O}_{\text{VSMOW}} = +9.5\text{\textperthousand}$; $n = 1$) and tourmaline ($\delta^{18}\text{O}_{\text{VSMOW}} = +4.9$ to $+7.2\text{\textperthousand}$; $n = 3$). Calcite ($\delta^{18}\text{O}_{\text{VSMOW}} = +3.9$ to $+5.3\text{\textperthousand}$; $n = 6$), chlorite ($\delta^{18}\text{O}_{\text{VSMOW}} = +2.5$ to $+3.7\text{\textperthousand}$; $n = 4$), magnetite ($\delta^{18}\text{O}_{\text{VSMOW}} = +3.8\text{\textperthousand}$; $n = 1$) and tourmaline ($\delta^{18}\text{O}_{\text{VSMOW}} = +6.9$ to $+7.6\text{\textperthousand}$; $n = 2$) were analyzed in the Igarapé Bahia deposit. The $\delta^{18}\text{O}_{\text{VSMOW}}$ values display a narrow variation in both deposits. The exceptions are garnet and tourmaline at Salobo with a fairly variation in the $\delta^{18}\text{O}_{\text{VSMOW}}$ values.

Temperature Conditions

Temperature conditions for the Salobo deposit were calculated for mineral pairs with evidences of textural equilibrium using their oxygen isotope composition. Estimates were done using oxygen isotope fractionation factors of Zheng (1993) for quartz-biotite and quartz-grunerite. In addition, for the Igarapé Bahia deposit, temperature conditions estimated by fluid inclusion studies by Dreher et al. (2008) were considered. The temperature data were integrated to those estimated based on mineral chemistry data (Réquia 1995, Zang and Fyfe 1994) and summarized in the table 1.

In the Salobo deposit, the grunerite-garnet and quartz-biotite pairs gave temperatures of 429°C and 475 to 565 °C for potassic alteration and iron-enrichment stage, respectively.

In the Igarapé Bahia, temperatures estimated for magnetite-quartz pairs vary from 483 to 313 °C (Dreher et al. 2008), whereas mineral chemistry in chlorite yielded a temperature of 270 °C for the latest stages of hydrothermal alteration.

Table 1. Compilation of temperatures estimated from oxygen isotopic composition and mineral chemistry from Salobo and Igarapé Bahia. Abbreviations: Bt = biotite, Gru = grunerite, Mag = magnetite, Qtz = quartz, Tour = tourmaline.

Deposit	Hydrothermal Alteration	Temperature (°C) – Stable Isotopes	Temperature (°C) – Mineral Chemistry	References
<i>Salobo</i>				
	Iron-enrichment	429 (Grt-gru pair)		This study
	Potassic Alteration	565 (Qtz-bt pair)		This study
	Potassic Alteration	495 (Qtz-bt pair)		This study
	Potassic Alteration	475 (Qtz-bt pair)		This study
	Later Fe-hydrated		347 (Chlorite geothermometer)	Réquia et al. 1995
<i>Igarapé Bahia</i>				
	Ore precipitation	313 (Qtz-mag pair)		Dreher et al. 2008
	Ore precipitation	416 (Qtz-mag pair)		Dreher et al. 2008
	Ore precipitation	453 (Qtz-mag pair)		Dreher et al. 2008
	Ore precipitation	403 (Qtz-mag pair)		Dreher et al. 2008
	Ore precipitation	323 (Qtz-mag pair)		Dreher et al. 2008
	Ore precipitation	349 (Qtz-mag pair)		Dreher et al. 2008
	Ore precipitation	483 (Qtz-mag pair)		Dreher et al. 2008
	Chlorite Formation		240 – 270 (Chlorite geothermometer)	Zang and Fyfe (1994)

Oxygen isotope composition of the hydrothermal fluids

Oxygen isotope composition of the hydrothermal fluids in equilibrium with minerals formed in different alteration stages was estimated, at the temperature intervals listed in Table 2. For the Salobo deposit, temperature intervals of 429 ± 45 °C for iron-enrichment stage and 520 ± 45 °C for potassic alteration were considered. For the Igarapé Bahia deposit, temperature intervals of 398 ± 85 °C for carbonate and tourmaline formation, and 255 ± 15 °C for chlorite formation were used.

Oxygen isotope composition of fluids was calculated using isotope fractionation factor for biotite–H₂O (Botting and Javoy 1973), calcite–H₂O (O’Neil et al 1969), chlorite–H₂O (Zheng 1993), garnet–H₂O (Zheng 1993), grunerite–H₂O (Zheng 1993), magnetite–H₂O (Zheng 1991), quartz–H₂O (Clayton et al. 1972), tourmaline–H₂O (Zheng 1993) (Fig. 7, 8).

In the Salobo deposit, fluids associated with iron-enrichment stage, at 429 ± 45 °C, have calculated $\delta^{18}\text{O}_{\text{H}_2\text{O}}$ values from +6.66 to +7.96‰ (grunerite), and from +6.88 to +7.77‰ (almandine). Oxygen isotope composition of fluids in equilibrium with tourmaline ($\delta^{18}\text{O}_{\text{H}_2\text{O}} = +4.11$ to +6.41‰), at 429 ± 45 °C, is slightly ¹⁸O-depleted. During potassic alteration with biotite, at 520 ± 45 °C, fluids show $\delta^{18}\text{O}_{\text{H}_2\text{O}}$ values from +7.16 to +7.96‰ (biotite) and $\delta^{18}\text{O}_{\text{H}_2\text{O}} = +6.88 \pm 0.35$ ‰ (quartz).

In the Igarapé Bahia deposit fluids associated with tourmaline have $\delta^{18}\text{O}_{\text{H}_2\text{O}}$ values from +5.54 to +6.24‰, at $398 \pm 85^\circ\text{C}$. At similar temperatures, fluids in equilibrium with calcite display ^{18}O -depleted values ($\delta^{18}\text{O}_{\text{H}_2\text{O}} = +1.68$ to +3.1‰), whereas $\delta^{18}\text{O}_{\text{H}_2\text{O}}$ values of fluids associated with magnetite formation reveal a relatively heavy oxygen isotope signature ($+11.71 \pm 0.165$). During the chlorite formation stage, fluids had lower $\delta^{18}\text{O}_{\text{H}_2\text{O}}$ values from +2.13 to +3.41‰, at $255 \pm 15^\circ\text{C}$.

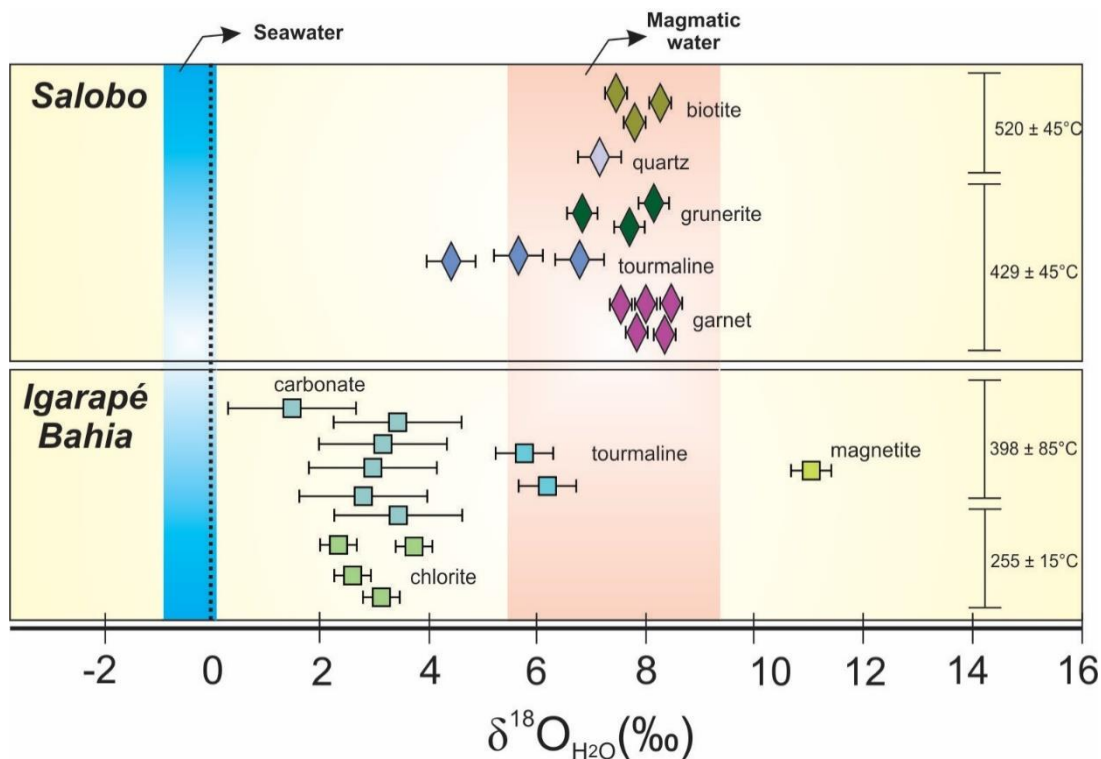


Fig. 9. Oxygen isotopic composition of hydrothermal fluids in equilibrium with silicates, carbonates and oxides from the Salobo and Igarapé Bahia deposits. Seawater and magmatic water fields are from Taylor (1997).

Hydrogen Isotopes

Hydrogen isotope analyses were carried out on hydrated minerals of different stages of hydrothermal alteration at Salobo and Igarapé Bahia deposits (Table 2). These include biotite ($\delta\text{D} = -74$ to $-59\text{\textperthousand}$; $n = 3$), grunerite ($\delta\text{D} = -52$ to $-43\text{\textperthousand}$; $n = 3$) and tourmaline ($\delta\text{D} = -43$ to $-23\text{\textperthousand}$; $n = 3$) in the Salobo deposit and tourmaline ($\delta\text{D} = -82$ to $-68\text{\textperthousand}$; $n = 2$) and chlorite ($\delta\text{D} = -95$ to $-59\text{\textperthousand}$; $n = 4$) at Igarapé Bahia.

Hydrogen isotope compositions of the hydrothermal fluids were calculated using fractionation factors for biotite– H_2O (Suzuki and Epstein 1976), chlorite– H_2O (Graham et al. 1993) and tourmaline– H_2O (Kotzer et al. 1993), following the same procedures of oxygen isotopes and using the same temperature intervals. In the case of

grunerite, the fractionation factor of hornblend–H₂O (Suzuoki and Epstein 1976) was used to calculate the hydrogen isotopic composition of the fluid in equilibrium with this mineral.

Table 2. Oxygen and hydrogen isotope composition of distinct minerals and associated hydrothermal fluids from the Salobo and Igarapé Bahia deposits.

Samples	Hydrothermal Alteration	Mineral	$\delta^{18}\text{O}_{\text{min}}$	T(°C)	$\delta^{18}\text{O}_{\text{H}_2\text{O}}$	$\delta\text{D}_{\text{min}}$	$\delta\text{D}_{\text{H}_2\text{O}}$
<i>Salobo</i>							
FD329/85,25	Potassic Alteration	Biotite	+4.9	520 ±45	+7.36 ±0.04	-74	-36.93 ±2.2
Salore 8b	Potassic Alteration	Biotite	+5.5	520 ±45	+7.96 ±0.04	-59	-21.93 ±2.2
FD177/276,50	Potassic Alteration	Biotite	+4.7	520 ±45	+7.16 ±0.04	-71	-33.38 ±2.2
Salore 8a	Iron-enrichment	Grunerite	+6.4	429 ±45	+7.56 ±0.3	-52	-10.65 ±6.27
FD177/512,50	Iron-enrichment	Grunerite	+5.5	429 ±45	+6.66 ±0.3	-43	-1.33 ±6.27
FD189/453,50	Iron-enrichment	Grunerite	+6.8	429 ±45	+7.96 ±0.3	-46	-4.76 ±6.27
FD189/439	Tourmaline Formation	Tourmaline	+6.1	429 ±45	+5.3 ±0.46	-32	-4.06 ±7.13
FD177/328a	Tourmaline Formation	Tourmaline	+7.2	429 ±45	+7.12 ±0.46	-23	+5.12 ±7.13
FD177/205,25	Tourmaline Formation	Tourmaline	+4.9	429 ±45	+4.11 ±0.46	-43	-15.40 ±7.13
FD177/328b	Iron-enrichment	Garnet	+4.2	429 ±45	+6.89 ±0.16		
146/329-249	Iron-enrichment	Garnet	+6.8	429 ±45	+9.49 ±0.16		
277/249	Iron-enrichment	Garnet	+5.1	429 ±45	+7.77 ±0.16		
1775KA	Iron-enrichment	Garnet	+4.6	429 ±45	+7.27 ±0.16		
329/349	Iron-enrichment	Garnet	+4.9	429 ±45	+7.58 ±0.16		
Salore 8c	Potassic Alteration	Quartz	+9.5	429 ±45	+6.88 ±0.35		
<i>Igarapé Bahia</i>							
FD173/299,45	Tourmaline Formation	Tourmaline	+7.6	398 ±85	+6.24 ±0.33	-82	-46.98 ±4.66
FD173/191,05	Tourmaline Formation	Tourmaline	+6.9	398 ±85	+5.54 ±0.33	-68	-32.70 ±4.66
FD173/118,50 ^a	Carbonate Formation	Calcite	+3.9	398 ±85	+1.68 ±1.44		
FD73/658,05	Carbonate Formation	Calcite	+4.9	398 ±85	+2.70 ±1.44		
FD73/418,20	Carbonate Formation	Calcite	+5.3	398 ±85	+3.10 ±1.44		
FD68/706,10	Carbonate Formation	Calcite	+5.3	398 ±85	+3.07 ±1.44		
FD73/406,35	Carbonate Formation	Calcite	+4.7	398 ±85	+2.43 ±1.44		
FD73/245,05	Carbonate Formation	Calcite	+4.8	398 ±85	+2.62 ±1.44		
FD173/118,50 ^b	Carbonate Formation	Magnetite	+3.8	398 ±85	+11.71 ±0.17		
FD73/305,70	Chlorite Formation	Chlorite	+3.7	255 ±15	+3.41 ±0.34	-59	-21.67 ±0.75
FD68/706,10	Chlorite Formation	Chlorite	+2.5	255 ±15	+2.13 ±0.34	-95	-57.69 ±0.75
FD73/406,35	Chlorite Formation	Chlorite	+2.7	255 ±15	+2.37 ±0.34	-60	-22.25 ±0.75
FD73/418,20	Chlorite Formation	Chlorite	+3.0	255 ±15	+2.69 ±0.34	-62	-25.12 ±4.65

The calculated δD_{H_2O} values for fluids in equilibrium with grunerite and tourmaline at Salobo, at 429 ± 45 °C, are -10.65 to $-1.33\text{\textperthousand}$ and -15.40 to $+5.12\text{\textperthousand}$, respectively. Fluids in equilibrium with biotite show lower δD_{H_2O} values (-36.96 to $-21.93\text{\textperthousand}$) than those associated with grunerite and tourmaline.

For the Igarapé Bahia deposit, δD_{H_2O} values for fluids in equilibrium with tourmaline, at 398 ± 85 °C, are -46.98 to $-32.70\text{\textperthousand}$. During the latest stages of chlorite formation, at 255 ± 15 °C, fluids display higher δD_{H_2O} ($-23.01 \pm 0.75\text{\textperthousand}$) and lower ($-57.69 \pm 0.75\text{\textperthousand}$) values than fluids responsible for tourmaline formation.

Carbon Isotopes

Carbon isotope studies were carried out on calcite from carbonate–magnetite (with chlorite) mylonitic rocks from the Igarapé Bahia deposit. Calcite from the carbonate alteration stage displays $\delta^{13}C_{VPDB}$ values ranging from -11.50 to $-7.12\text{\textperthousand}$.

Carbon isotope composition of the hydrothermal fluids was calculated using fractionation factors for calcite–CO₂ (Ohmoto & Rye 1979). These calculations were performed using temperature and isotope composition intervals in the same procedure reported for oxygen and hydrogen isotope composition of the fluids.

Hydrothermal fluids associated with calcite during the carbonate alteration stage, at 398 ± 85 °C, display $\delta^{13}C_{CO_2}$ values from -9.04 to $-4.65\text{\textperthousand}$.

Table 3. Carbon isotope composition of calcite associated with hydrothermal fluids from the Igarapé Bahia deposit.

Sample	Hydrothermal Alteration	Mineral	$\delta^{13}\text{C}_{\text{VPDB}}$	T(°C)	$\delta^{13}\text{C}_{\text{CO}_2}$
FD73/658,05	Carbonate Formation	Calcite	-8.25	398±85	-5.79±0.63
FD73/418,20	Carbonate Formation	Calcite	-7.69	398±85	-5.23±0.63
FD68/706,10	Carbonate Formation	Calcite	-7.12	398±85	-4.65±0.63
FD73/406,35	Carbonate Formation	Calcite	-8.71	398±85	-6.24±0.63
FD73/245,05	Carbonate Formation	Calcite	-11.50	398±85	-9.04±0.63

Sulfur Isotopes

Sulfur isotope analyses were performed on bornite ($\delta^{34}\text{S}_{\text{VCDT}} = -0.37$ to $+1.63$; n = 3) and chalcopyrite ($\delta^{34}\text{S}_{\text{VCDT}} = +0.81$ to $+1.28$; n = 3) from mineralized zones of the Salobo deposit. These data was integrated and compared with available data for the Igarapé Bahia deposit (Dreher et al 2008, Galarza et al. 2008, Melo et al. in prep).

Table 4. Sulfur isotope data for sulfides from the Salobo deposit. Abbreviations: Bn = bornite, Bt = biotite, Cc = chalcocite, Cpy = chalcopyrite, Grt = garnet, Gru = grunerite.

Sample	Mineral	Description	$\delta^{34}\text{S}$
FD177/83,1	Chalcopyrite	Cpy in grt-gru-bt-rich rocks	+0.91
FD177/575,55	Chalcopyrite	Cpy in grt-gru-bt-rich rocks	+0.81
FD177//103	Chalcopyrite	Cpy in grt-gru-bt-rich rocks	+1.28
Sal.Ore-7	Bornite	Massive ore with bn and cc	+1.63
Sal.Ore-6	Bornite	Massive ore with bn and cc	-0.37
Sal.Ore-5	Bornite	Massive ore with bn and cc	+1.04

There is no compelling difference between $\delta^{34}\text{S}_{\text{VCDT}}$ values of bornite and chalcopyrite. Both minerals show a narrow variation in the $\delta^{34}\text{S}_{\text{VCDT}}$ values.

Discussions

Comparing the geology of Salobo and Igarapé Bahia deposits

Geological attributes are distinct in the Salobo and Igarapé Bahia deposits. The main differences lies in the host rocks and paragenetic evolution of their hydrothermal systems. At Salobo, host rocks comprises primarily basement gneisses ($2,950 \pm 25$ and $2,857 \pm 6.7$ Ma; U–Pb zircon; Melo et al., 2016) and Neoarchean ($2,763 \pm 4.4$ Ma; U–

Pb zircon; Melo et al. 2016) deformed granitoids, whereas metavolcanosedimentary units are subordinate. In contrast, the Igarapé Bahia deposit is hosted by the metavolcanosedimentary sequence of the Igarapé Bahia Group (2.76 – 2.73 Ga) and the metasedimentary units of the Águas Claras Formation.

Hydrothermal alteration and ductile deformation associated with shear zones development were coeval in both deposits. The IOCG alteration–mineralization is also distinct. Hydrothermal assemblages with hastingsite–actinolite, almandine–grunerite–tourmaline, and almandine–grunerite–biotite–(magnetite) are common at Salobo. The Igarapé Bahia deposit, in turn, exhibits hydrothermal mineral associations with (tourmaline)–carbonate–magnetite, (tourmaline)–carbonate–chlorite and (tourmaline)–(biotite)–chlorite. These associations and the paragenetic evolution of these deposits suggest higher temperature conditions at Salobo compared to Igarapé Bahia.

However, these deposits are linked with the same metallogenetic event at 2.57 Ga (Réquia et al. 2003, Tallarico et al. 2005, Melo et al. 2016). The ca. 2.57 Ga granites are recognized within the Salobo deposit (i.e. Old Salobo granite), but at Igarapé Bahia these granites have not been characterized yet.

Evolution and sources of the hydrothermal fluids

The evolution of the hydrothermal system was distinct in the Salobo and Igarapé Bahia deposits. Temperature conditions were higher at Salobo than at Igarapé Bahia. The main hydrothermal alteration stages at Salobo, iron-enrichment and potassic alteration might have been formed at elevated temperatures, 429 ± 45 °C and 520 ± 45 °C, respectively. Ore precipitation occurred at lower temperatures (334 to 366 °C; Réquia 1995). Later chlorite, formed syn to post ore precipitation, was formed in similar conditions (e.g. 347 °C, Réquia 1995), evidencing that even in the latest stages of hydrothermal alteration at Salobo the temperatures were relatively high. The Igarapé Bahia deposit, in turn, exhibits relatively lower temperatures preceding ore precipitation, reaching 483 to 313 °C during magnetite formation (Dreher et al. 2008). Widespread chlorite formation evidences a sharp temperature decrease, with temperatures of 255 ± 15 °C (Zhang and Fyfe, 1995).

The $\delta^{18}\text{O}_{\text{H}_2\text{O}}$ values for the hydrothermal fluids during iron-enrichment (grunerite–almandine–tourmaline) in the Salobo deposit, at 429 ± 45 °C, range from +4.88 to +9.49‰. During potassic alteration, at 520 ± 45 °C, the $\delta^{18}\text{O}_{\text{H}_2\text{O}}$ values for the hydrothermal fluids reveal a narrow variation (+7.16 to +7.96‰). With the exception of

fluids in equilibrium with a tourmaline with $\delta^{18}\text{O}$ -depleted values (+4.11‰), the other results fall within the magmatic fluid field. Thus, magmatic sources are consistent with the $\delta^{18}\text{O}_{\text{H}_2\text{O}}$ values for the main hydrothermal alteration stages (i.e. iron enrichment and potassic alteration) at Salobo.

Regarding the $\delta\text{D}_{\text{H}_2\text{O}}$ values, Salobo displays a fairly variation in its values, ranging from -36.93 to +5.12‰. Fluids associated with potassic alteration with biotite show lower δD values (-36.93 to -21.93‰) in comparison to fluids that precipitated tourmaline (-15.40 to -5.12‰) and grunerite (-10.65 to -1.33‰).

The $\delta^{18}\text{O}_{\text{H}_2\text{O}}$ and $\delta\text{D}_{\text{H}_2\text{O}}$ values for the hydrothermal fluids at Salobo clearly constrain the ore-forming fluids into the field of felsic magmatic water, which have D-enriched values similar to those of the volcanic vapor field. There is no apparent dislocation of the values towards neither to the meteoric water line nor to the seawater and formation water fields. Nevertheless, low temperature mineral assemblages (e.g. chlorite) were not analyzed in this study, then the isotopic behavior of the hydrothermal fluids under lower temperatures conditions at Salobo might be disguised and should be interpreted with caution.

In the Igarapé Bahia deposit, at $398 \pm 85^\circ\text{C}$, the $\delta^{18}\text{O}_{\text{H}_2\text{O}}$ values show a wide variation between +1.68 and +11.63‰. Whereas relatively high $\delta^{18}\text{O}_{\text{H}_2\text{O}}$ were calculated for fluids associated with magnetite (+11.63‰), calcite shows the lowest $\delta^{18}\text{O}_{\text{H}_2\text{O}}$ values (+1.68 to +3.1‰). The fluids associated with tourmaline, in turn, exhibit $\delta^{18}\text{O}_{\text{H}_2\text{O}}$ values (+5.54 to +6.24‰) spanning those of the magmatic field. The later stages of hydrothermal alteration, represented by a widespread chlorite formation, at $255 \pm 15^\circ\text{C}$, display a narrow variation with values ranging from +2.13 to +3.41‰.

At Igarapé Bahia, $\delta\text{D}_{\text{H}_2\text{O}}$ values are fairly lower during tourmaline formation (-46.98 to -32.70‰) than that of the fluids in equilibrium with chlorite (-25.12 to -21.67‰). The exception is fluid in equilibrium with a chlorite sample with very low $\delta\text{D}_{\text{H}_2\text{O}}$ values (-57.69‰).

In sync, $\delta^{18}\text{O}_{\text{H}_2\text{O}}$ and $\delta\text{D}_{\text{H}_2\text{O}}$ suggest that Igarapé Bahia copper-gold mineralization was formed primarily by magmatic water with the latest stages recording the influx of ^{18}O -depleted fluids (Fig. 10). These ^{18}O -depleted fluids could be assigned as: (i) formation water (i.e. evolved meteoric water) or even (ii) evolved seawater. The high $\delta^{18}\text{O}_{\text{H}_2\text{O}}$ recorded in fluids associated with magnetite is probably a result of intense interaction of the hydrothermal fluids with metasedimentary sequences in the Igarapé Bahia deposit.

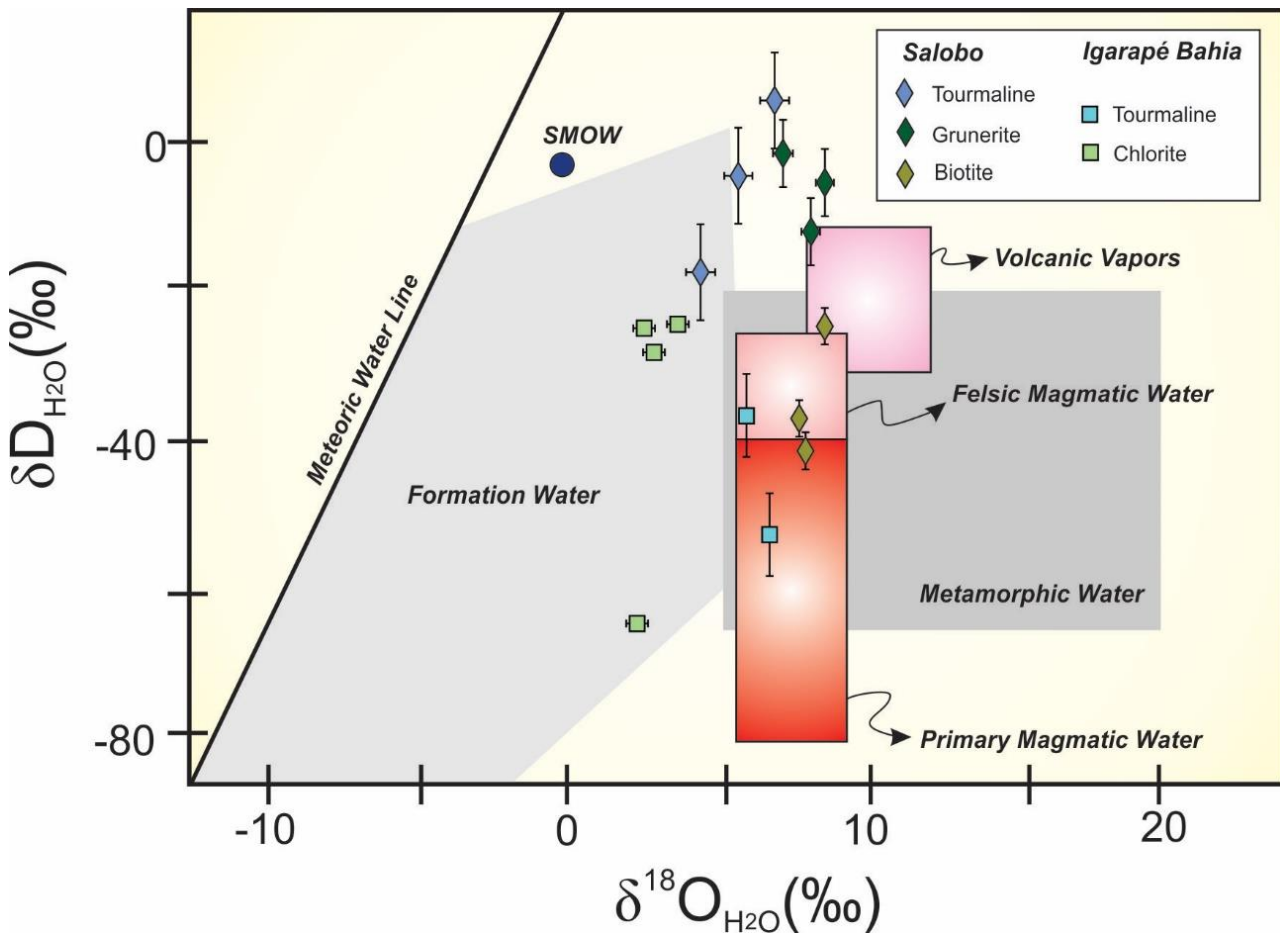


Fig. 10. Oxygen-hydrogen diagram for fluids associated with different stages of hydrothermal alteration at Salobo and Igarapé Bahia deposits. The andesitic volcanic vapor, felsic magmatic water, primary magmatic water, metamorphic water and formation water fields are from Giggenbach (1992), Taylor (1992), Taylor (1974), Sheppard (1986) and Taylor (1997), respectively.

Sulfur and Carbon Sources

In the Salobo deposit, the sulfides show a narrow variation of sulfur isotopic composition ($\delta^{34}\text{S}_{\text{VCDT}} = -0.37$ to $+1.63\text{\textperthousand}$) very close to the magmatic field (Ohmoto & Goldhaber 1997). The $\delta^{34}\text{S}$ values obtained in this and previous studies (Réquia and Fontboté 2001) point to a single magmatic source as the main source for the sulfur at Salobo. Although there are some values greater than $+1\text{\textperthousand}$, external sources for sulfur at Salobo might have been minimum or absent.

The chalcopyrite from IOCG mineralization at Igarapé Bahia show variable $\delta^{34}\text{S}$ values, ranging from -0.3 to $+5.6\text{\textperthousand}$. Apparently, there are no differences between the orebodies: Alemão ($\delta^{34}\text{S}_{\text{VCDT}} = +1.36$ to $+5.35\text{\textperthousand}$), Furo 30 ($\delta^{34}\text{S}_{\text{VCDT}} = -0.3$ to $+4.13\text{\textperthousand}$), Acampamento Norte ($\delta^{34}\text{S}_{\text{VCDT}} = +0.9$ to $+4.7\text{\textperthousand}$) and Acampamento Sul

($\delta^{34}\text{S}_{\text{VCDT}} = +0.5$ to $+5.6\text{\textperthousand}$; Dreher et al 2008, Galarza et al. 2008, Melo et al. in prep.).

Comparatively, Salobo has lower values and a narrower variation of the sulfur isotopic composition of sulfides than Igarapé Bahia (Fig. 11). It is quite similar to what is observed in relation to $\delta^{18}\text{O}_{\text{H}_2\text{O}}$ and $\delta\text{D}_{\text{H}_2\text{O}}$ values for both deposits. Magmatic sources for sulfur might have contributed in both deposits, but at Igarapé Bahia, in addition to magmatic sources, isotopically heavy sulfur may be also derived from preexisting sulfides or sulfates within the metasedimentary sequence of the Itacaiúnas Supergroup or the Águas Claras Formation.

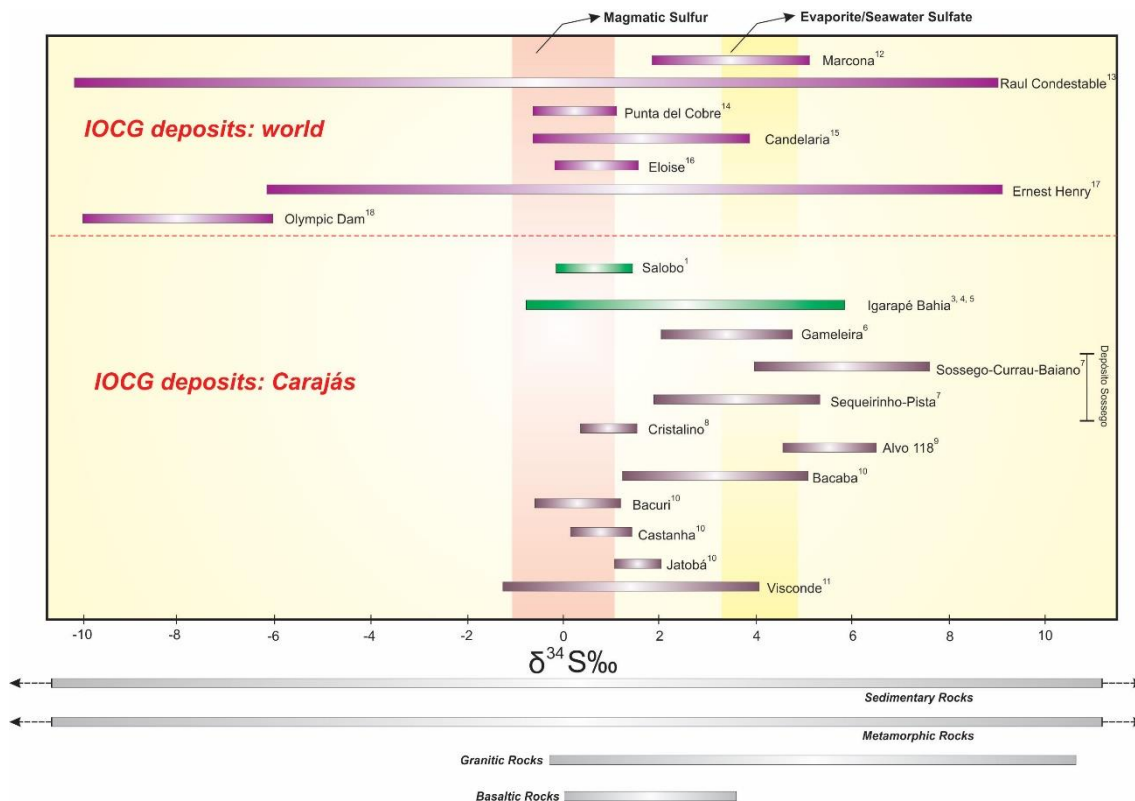


Fig. 11. Sulfur isotope composition of sulfides from the Salobo, Igarapé Bahia (green boxes) and other IOCG deposits in the Carajás Province and in the world. Data extracted from: 1 – This study, 2 – Dreher et al. (2008), 3 – Galarza et al. (2008), 4 – Melo et al. in prep, 6 – Fleck e Lindenmayer (2003), 7 – Monteiro et al. (2008), 8 – Ribeiro et al. (2008), 9 – Torresi et al. (2011), 10 – Pestilho (2011), 11 – Silva et al. (2015), 12 – Chen et al. (2011), 13 – Haller et al. (2003), 14 – Marschik et al. (2000), 15 – Marschik and Fontboté (2001), 16 – Rotherham et al. (1998), 17 – Twyerould (1997), 18 – Perring et al. (2003). Magmatic and Archean evaporites/seawater sulfate fields are from Ohmoto & Goldhaber (1997) and Eldridge et al. (1991), respectively.

Calculated $\delta^{13}\text{C}_{\text{CO}_2}$ values for calcite from carbonate alteration zones range from -9.04 to $-4.65\text{\textperthousand}$. These values are very similar to those of magmatic carbon derived from carbonatites and MORB (Ohmoto 1986, Mattey 1987). Although oxygen isotopes in the same minerals ($\delta^{18}\text{O}_{\text{H}_2\text{O}} = +2.43$ to $+3.10\text{\textperthousand}$) point to externally-derived sources, the carbon at Igarapé Bahia is, indeed, magmatic in origin (Fig. 12), suggesting a fluid mixing. This is similar to that observed for other IOCG deposits in the Southern Copper Belt (e.g. Sossego and Sequeirinho orebodies at Sossego deposit, Bacaba and Castanha deposits; Monteiro et al. 2008a, Pestilho 2011).

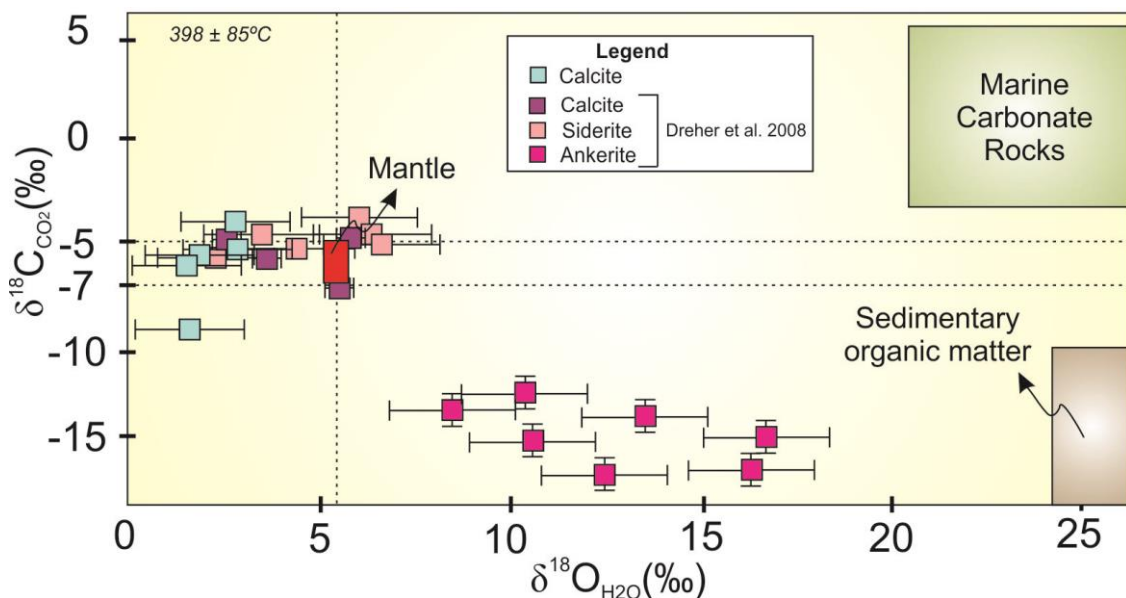


Fig. 12. Oxygen-carbon diagram for fluids associated carbonate formation and $\delta^{13}\text{C}$ and $\delta^{18}\text{O}$ for different carbonates at Igarapé Bahia (Dreher et al. 2008). Mantle, marine carbonate rocks and sedimentary organic matter fields are extracted from Hoefs (2009), Veizer and Hoefs (1976) and Liu and Jiu (1997), respectively.

Fluids and tectono-magmatic evolution of the Carajás Province

Oxygen, hydrogen, carbon and sulfur isotope results point to an important participation of magmatic fluids for the genesis of the Salobo and Igarapé Bahia deposits. However, an externally-derived source of fluids and sulfur was also present, especially in the latter.

The importance of a magmatic component in both deposits is clear. Thus, it is essential to figure out where these fluids exsolved from. Granitic magmatism coeval with the timing of mineralization in both deposits (i.e. 2.57 Ga; Réquia et al. 2003, Tallarico et al. 2005, Melo et al. in prep) is confined to two small ca. 2.5 Ga granitic

bodies: Old Salobo and Itacaiúnas granites (Machado et al. 1991, Souza et al. 1996, Melo et al. 2016). Although this magmatism is not widespread in the province, the existence of other 2.5 Ga granitic bodies and the occurrence of an important magmatic event in this period cannot be ruled out (Melo et al. 2016) and must be better investigated.

Silicate magmas can saturate in volatiles and exsolve a fluid phase to form chloride-enriched aqueous liquidus, hypersaline brines and water-bearing salt melts; with or without coexisting aqueous vapor (Webster 2004). As the fractional crystallization evolves and magmas reach the near-solidus temperatures, liquid immiscibility and exsolution of coexisting fluids strongly increase (Veksler 2004). This is more common in peralkaline acid to intermediate magmas due to (i) the high contents of volatile components (F, Cl, B, Li) and (ii) earlier saturation in immiscible fluids phases (Veksler 2004, Webster 2004). The presence of CO₂ as a magmatic volatile phase or in hydrothermal systems also induces immiscibility even in deeper crustal levels (Lowestern 1999).

At Salobo, CO₂–(CH₄)-rich fluids were recognized and assigned to dehydration of metamorphic rocks in amphibolite facies, and interpreted as the highest temperature fluid (Réquia 1995). H₂O–NaCl–(CaCl₂) fluids with homogenization temperatures up to 485 °C and salinities ranging from 30.6 to 58.4 wt% NaCl were interpreted as later introduced to the system (Réquia 1995). In the Igarapé Bahia deposit, H₂O–NaCl–CaCl₂–(± FeCl₂) and CO₂–(CH₄)-rich fluids were also identified and considered to be simultaneously trapped at the same timeframe of the Cu–Au mineralization, with a minimum trapping temperature of 330 °C and with salinities up to 45 wt% NaCl (Dreher et al. 2008).

The unmixing from a single homogeneous H₂O–CO₂–(±CH₄)–NaCl–CaCl₂–(± FeCl₂) could have generated the variety of fluid inclusions recognized at Igarapé Bahia and similarly at Salobo. Thus, the hydrothermal fluids characterized at Salobo and Igarapé Bahia can be a result of exsolution of magmatic brines closely related to iron metasomatism in both deposits. This is in agreement with δ¹⁸O_{H₂O} and δD_{H₂O} data obtained in this study for the higher temperature mineral assemblages (i.e. grunerite, tourmaline and biotite at Salobo, and tourmaline at Igarapé Bahia).

Crystallization of ca. 2.57 Ga granites and exsolution of H₂O–CO₂– NaCl–(CaCl₂–CH₄) fluids can represent the main source for ore-forming fluids for Salobo and Igarapé Bahia. These deposits do not seem to have direct spatial association of their

hydrothermal alteration zones with granite cupolas, as it would be expected for a proximal hydrothermal–magmatic system (i.e. porphyry Cu, skarns and greisen deposits). On the contrary, these granites crystallized in depth, where mechanical energy was insufficient to fracture the host rocks (Fig. 13; Pollard 2006). The CO₂-rich magmas may exsolve a fluid phase under higher pressure conditions and in deeper portions of the crust (Pollard 2006). These fluids were, then, channeled and ascended through crustal-scale shear zones (i.e. Cinzento and Carajás Shear Zones). The exsolution of these magmatic fluids can also explain the high content of CO₂-rich fluids in both deposits (Réquia 1995, Dreher et al. 2008). Sulfur, especially at Salobo deposit, has been also derived from magma.

The expression of these granites in surface might be minimum compared to what might be in depth; or they are still poorly recognized. The Old Salobo granite comprises an A-type peralkaline granite and is one of the representative of crystallized granites at this timing. Similar granites are represented by the Itacaiúnas granite and granites from the GT-46 deposit (Toledo 2017).

Peralkaline granites are strongly enriched in Zr, REE, Y, Nb, Ta, U, and Th and can even form mineralization of these elements (Cerný et al. 2005). This geochemical signature might have formed due to highly fractionated and volatile-rich residual magmas, which crystallized small bodies (Schmitt et al. 2002).

The presence of an important, regional-scale, tectono-thermal event (Machado et al. 1991, Barbosa 2004, Melo et al. 2016) associated with granitic magmatism created a fertile scenario for the formation of IOCG deposits in the northern sector of the Carajás Domain.

One of the reasons that could explain the differences in the geological attributes of these deposits is that Salobo lies within the basement and Neoarchean deformed granitoids, whereas Igarapé Bahia is hosted by the metavolcanosedimentary sequence of the Igarapé Bahia Group and metasedimentary units of the Águas Claras Formation. Fluid/rock ratio are larger at Salobo and likely more channeled within the shear zones in comparison to Igarapé Bahia.

Hydrothermal fluids from the Igarapé Bahia deposit do not seem to be stucked strictly to the magmatic field. The circulation of formation fluids could explain the wide variation of the oxygen and hydrogen isotope signatures at Igarapé Bahia. In this case, the migration of meteoric water within the metavolcanosedimentary sequences explains the presence of δ¹⁸O-depleted fluids in the latest stages at Igarapé Bahia. The intense

interaction of these mixed fluids with the country rocks, in turn, is recorded by the higher $\delta^{18}\text{O}_{\text{H}_2\text{O}}$ values estimated from magnetite.

The presence of ^{18}O -depleted fluids in the Igarapé Bahia deposit could also be attributed to seawater. Once no active basin is reported at ca. 2.5 Ga, this possibility is more restricted. However, it is possible that isotopic signatures related to evolved seawater can reflect an older environment, likely associated with the deposition of the metavolcanosedimentary sequences.

The Salobo and Igarapé Bahia deposits, in spite of recording a mineralization stage at ca. 2.57 Ga, likely have relicts of older hydrothermal events. This is not only recorded in the ages, as previously suggested by geochronological data (Pb–Pb in gold, $2,772 \pm 46$ Ma, $2,754 \pm 36$ Ma, $2,756 \pm 24$ Ma, $2,777 \pm 22$ Ma; Galarza et al. 2008; Pb–Pb in chalcocite, $2,705 \pm 42$ Ma), but also in the boron isotopic composition of tourmaline minerals (e.g. core crystals; Melo et al., in prep), what makes the comprehension of these deposits a more complex challenge. This possibility must be better investigated, once most of the components of the ca. 2.5 Ga IOCG deposits could be inherited from the Neoarchean (2.71 – 2.68 Ga) IOCG deposits or even from the metavolcanosedimentary sequences.

The Neoarchean (Sequeirinho orebody at Sossego deposit and Visconde deposit, Monteiro et al. 2008a, Silva et al. 2015, Moreto et al 2015a,b) and Paleoproterozoic (Sossego orebody at Sossego deposit and Alvo 118, Monteiro et al. 2008a, Torresi et al. 2011, Moreto et al 2015a,b) IOCG deposits at the Southern Copper Belt show multiple sources for the ore-forming fluids. ^{18}O -enriched signatures were characterized in these deposits and assigned to metamorphic or magmatic fluids (Monteiro et al. 2008a, Torresi et al. 2011, Silva et al. 2015). These systems were later fed with influx of $\delta^{18}\text{O}$ -depleted fluids, likely due to the participation of meteoric fluids or seawater (Monteiro et al. 2008a, Torresi et al. 2011, Silva et al. 2015). Similarly, Salobo and Igarapé Bahia show a primary magmatic source for ore-forming fluids with a significant contribution of formation fluids in the latter.

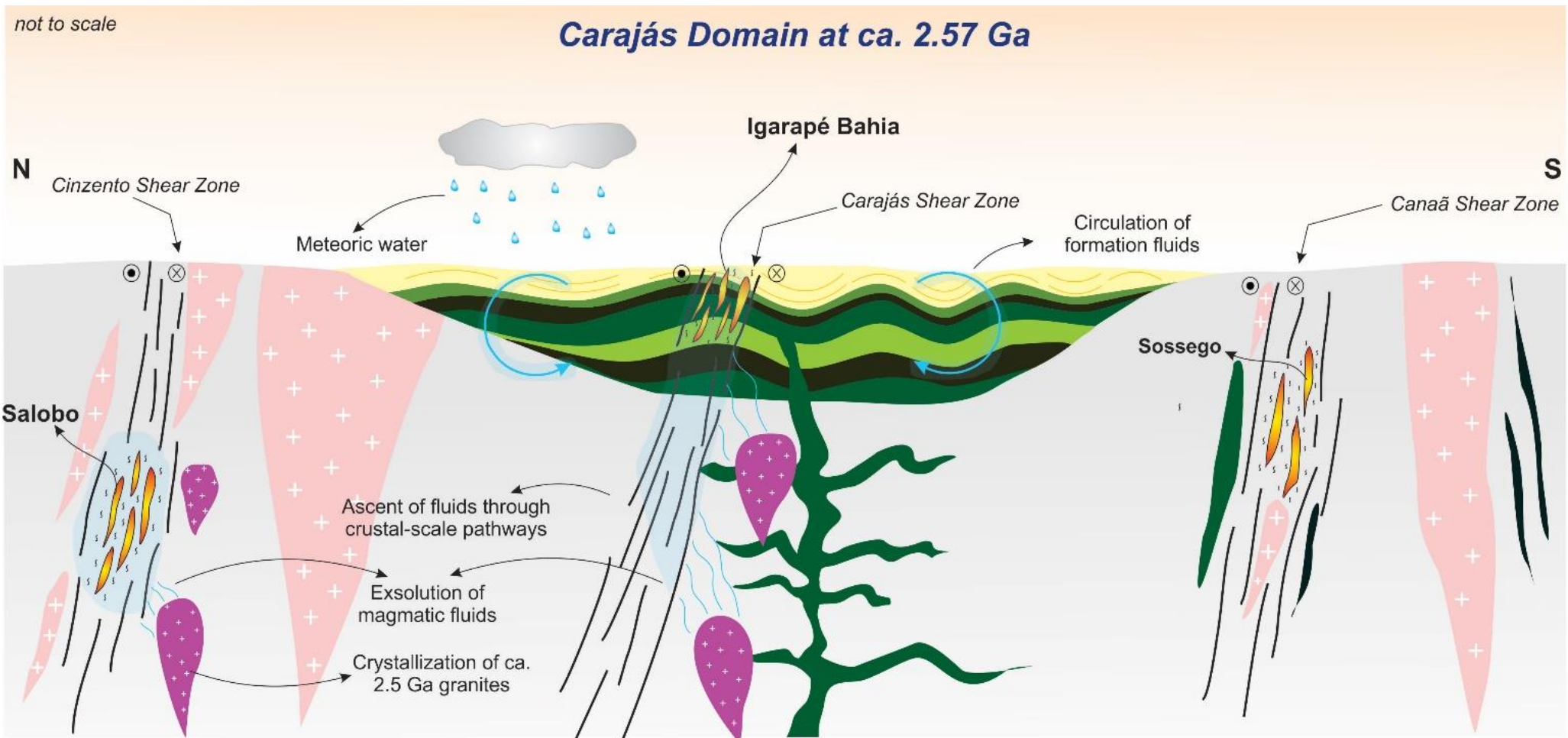


Fig. 13. Metallogenetic model for the genesis of ca. 2.57 Ga Salobo and Igarapé Bahia deposits.

Implications for fluid reservoirs in the IOCG deposits

Despite of different genetic models, all IOCG deposits require hypersaline, sulfide-poor and relatively oxidized fluids (Barton and Johnson 2004). If these fluids involve magmatic (e.g., granitic intrusions; Sillitoe 2003, Pollard 2006) or non-magmatic (e.g., marine or terrestrial brines; Barton and Johnson, 1996) source remains very controversial in the IOCG deposits worldwide.

The importance of the Salobo and Igarapé Bahia deposits in a global scenario as important representatives of the IOCG class bring up new perspectives regarding ore-forming fluids of such deposits. Our data show that even though externally-derived fluids might be present in these deposits, especially at Igarapé Bahia, the importance of magmatic fluids exsolved from granites is evident.

Recent discoveries in the El Laco magnetite–apatite deposit, in Chilean Andes, show that it was formed due to the separation of an iron-rich melt from a silicate-rich melt with andesitic composition (Tornos et al. 2016). Coexisting hydrothermal fluids exsolved from iron-rich melts reached temperature up to 900 °C (Tornos et al. 2016). If magnetite–apatite deposits are end-members of the IOCG clan (Hitzman et al. 1992, Barton and Johnson 1996), it is possible that there is a genetic link between magmatic fluids, magnetite-apatite deposits and IOCG deposits. A similar approach have been proposed for the M-III and M-IV magnetite mineralization stages at the giant Marcona IOCG deposit, where iron oxide melt and magmatic fluids were the responsible for the formation of these stages, respectively (Chen et al. 2011).

One remarkable point of the IOCG deposits might be the mixing of a high temperature, ^{18}O -rich fluids in the early stages of the hydrothermal system with medium- to low-temperature ^{18}O -poor fluids (Fig. 14). The former is usually derived from magmatic sources. This is well-recorded at Olympic Dam (early stages: $\delta^{18}\text{O} = +8$ to $+10\text{\textperthousand}$ at 400 °C; latest stages: $\delta^{18}\text{O} = -2.5$ to $4.5\text{\textperthousand}$ at 400 to 200 °C; Oreskes and Einaudi 1992), Ernest Henry (ore stage: $\delta^{18}\text{O} = +7$ to $+10\text{\textperthousand}$; Mark et al. 2010), Candelaria (early stages: $\delta^{18}\text{O} = +7\text{\textperthousand}$ at 400°C, latest stages: $\delta^{18}\text{O} = -0.2\text{\textperthousand}$ at 275°C; Ullrich et al. 2001), Marcona (M-III stage: $\delta^{18}\text{O} = +5.2$ to $+7.7\text{\textperthousand}$ at 700 to 800°C, M-IV stage: $\delta^{18}\text{O} = -9.6$ to $+12.2\text{\textperthousand}$ at 600 to 430°C; Chen et al. 2011) and at Sossego (Sequeirinho orebody, early stages: $+6.9 \pm 0.9\text{\textperthousand}$, at $550 \pm 25^\circ\text{C}$, latest stages: $-1.8 \pm 3.4\text{\textperthousand}$, at 400 – 200°C; Sossego orebody, early stages: $8.4 \pm 1.6\text{\textperthousand}$, at 450°C, latest stages: $-3.3 \pm 3.2\text{\textperthousand}$ to $1.5 \pm 2.1\text{\textperthousand}$, at 300°C; Monteiro et al., 2008) deposits. Into them, even though external fluids are invoked for the latest stages, magmatic fluids are the

main and primary source for fluids. The magmatic component might be essential to form a world-class IOCG deposit.

On the other hand, the importance of externally-derived fluids must not be ruled out. The Wernecke IOCG deposit, at Yukon Territory, Canada, is a typical non-magmatic IOCG deposit (Hunt et al. 2007). Brines derived from evaporitic sequences are considered the main ore-forming fluids (Hunt et al. 2007). Likewise, Xavier et al. (2008) demonstrated that the high $\delta^{11}\text{B}$ values could be assigned to the participation of marine evaporites as the source of boron and high saline fluids of the IOCG systems of Carajás. Halogens ratios of Cl/Br and Na/Cl carried out at Salobo, Igarapé Bahia, Sossego, Gameleira and Alvo 118, however, highlight the importance of residual evaporated seawater (bittern fluids) with magma-derived brines to form the IOCG deposits of Carajás (Xavier et al. 2009).

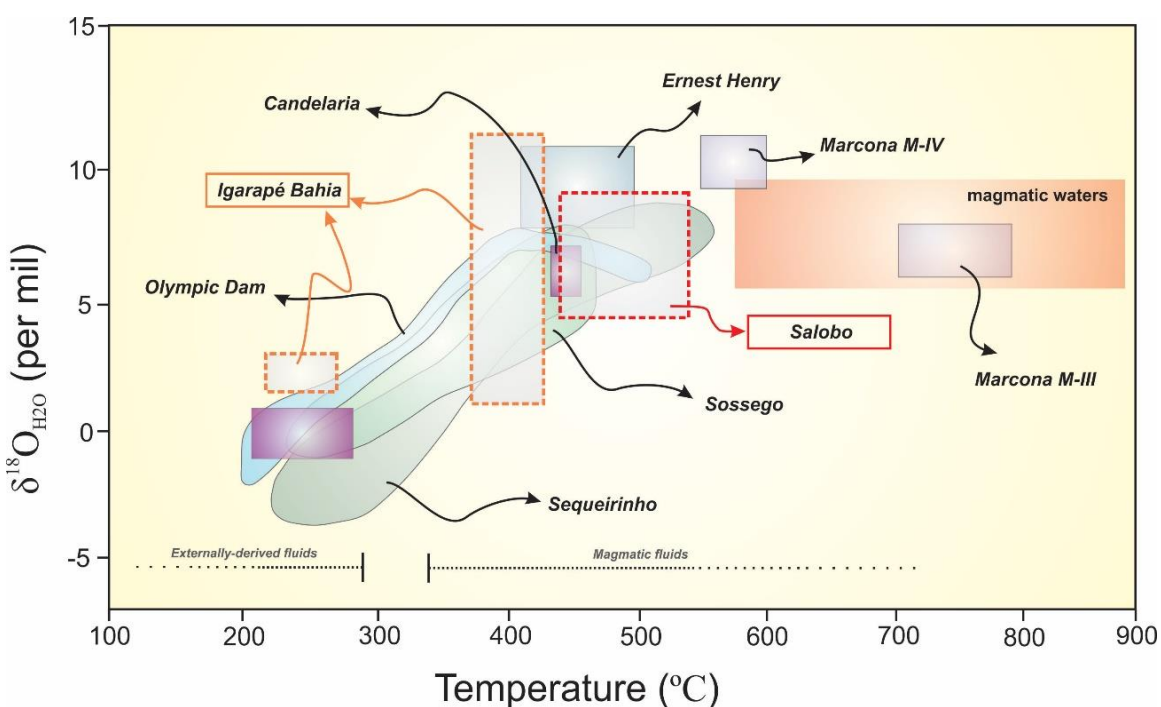


Fig. 14. $\delta^{18}\text{O}_{\text{H}_2\text{O}}$ -temperature diagram showing the characteristic of fluids in different IOCG deposits in the world (modified from Chen et al. 2011). Red and orange dotted boxes outline Salobo and Igarapé Bahia positions, respectively. Data obtained from Oreskes and Einaudi 1992, Mark et al. 2000, Ullrich et al. 2001, Monteiro et al. 2008, Chen et al. 2011. Magmatic waters field are from Taylor (1997).

Conclusions

The investigation of the geology and the application of stable isotope geochemistry in different minerals at Salobo and Igarapé Bahia deposits provided new insights for these IOCG systems:

- Temperatures conditions of the hydrothermal systems are higher at Salobo than Igarapé Bahia, reaching 520 ± 45 °C in the former and ranging from 483 to 313 °C in the later;
- $\delta^{18}\text{O}_{\text{H}_2\text{O}}$ and $\delta\text{D}_{\text{H}_2\text{O}}$ values for the early stages of hydrothermal fluids at Salobo and Igarapé Bahia clearly constrain the ore-forming fluids into the felsic magmatic water. Fluid inclusion studies corroborate with isotopic data, pointing to exsolution of $\text{H}_2\text{O}-\text{CO}_2-\text{NaCl}-(\text{CaCl}_2-\text{CH}_4)$ fluids from the granite magmatism at Carajás Domain. Magmatic sulfur correspond to the main sulfur source at Salobo deposit;
- Whereas at Salobo hydrothermal fluids are dominantly magmatic, at Igarapé Bahia deposit the influx of ^{18}O -depleted fluids in the latest stages of its hydrothermal system may suggest the involvement of formation water. At Igarapé Bahia sulfur from preexisting sulfides of the metasedimentary sequence of the Itacaiúnas Supergroup is likely the main sulfur source. These sulfides might have precipitated by thermochemical reactions of the sulfate seawater at ca. 2.76 – 2.74 Ga;
- The IOCG metallogenetic event diverges in age and in geological context from the 2.71 to 2.68 Ga IOCG deposits in the Southern Copper Belt. The ca. 2.5 Ga metallogenetic event was strongly linked with fluids derived from granitic magmatism, but also formation water. This event could have been associated with a regional-scale tectono-thermal event, which created a fertile scenario for the IOCG formation especially in the northern sector of the Carajás Domain;
- The Salobo and Igarapé Bahia deposits might represent different portions within a wide mineral system, in which local fluid-rock processes were responsible for the diversity in their geological attributes.

References

- Almada, M.C.O., Villas, R.N., 1999, O depósito Bahia: um possível exemplo de depósito vulcanogenênico tipo Besshi arqueano em Carajás: Revista Brasileira de Geociências, v. 29, p. 579-592.
- Araújo, O.J.B., Maia, R.G.N., 1991, Serra dos Carajás: folha SB.22-Z-A, Estado do Pará, Escala 1:250.000. Texto explicativo. DNPM/CPRM. 164 p.
- Barbosa, J.P.O., 2004, Geologia estrutural, geoquímica, petrografia e geocronologia de granitóides da região de Igarapé Gelado, Norte da Província Mineral de Carajás. Unpublished MSc. Dissertation, University of Pará.
- Barros, C.E.M., Sardinha A.S., Barbosa J.P.O., Macambira M.J.B., 2009, Structure, Petrology, Geochemistry and zircon U/Pb and Pb/Pb geochronology of the synkinematic Archean (2.7 Ga) A-type granites from the Carajás Metallogenic Province, northern Brazil: Canadian Mineralogist, v. 47, p. 1423-1440.
- Barton, M..D., Johnson, D.A., 1996, Evaporitic-source model for igneous-related Fe oxide-(REE-Cu-Au-U) mineralization: Geology, v. 24, p. 259–262.
- Bottinga, Y., and Javoy, M., 1973, Comments on oxygen isotope geothermometry: Earth Planetary Science Letters, v. 20, p. 250-265.
- Cerný, P., Blevin, P.L., Cuney, M., London, D., 2005. Granite-related ore deposits. Economic Geology, 100th anniversary volume, pp. 337-370.
- Chen, H., Kyser, T.K., Clark, A.H., 2011, Contrasting fluids and reservoirs in the contiguous Marcona and Mina Justa iron oxide-Cu (-Ag-Au) deposits, south-central Perú: Mineralium Deposita, v. 46, p. 677-706.
- Clayton; R.N.; O'Neil, J.R.; Mayeda, T.K., 1972, Oxygen isotope exchange between quartz and water: Journal of Geophysics Research, v. 77, p. 3057-3067.
- Clayton, R., Mayeda, T.K., 1963, The use of bromine pentafluoride in the extraction of oxygen from oxides and silicates for isotopic analysis: Geochimica et Cosmochimica Acta, v. 27, p. 43–52
- Dardenne, M.A., Ferreira Filho, C.F., Meirelles, M.R., 1988, The role of shoshonitic and calc-alkaline suites in the tectonic evolution of the Carajás district, Brazil: Journal of South American Earth Sciences, v. 1, p. 363-372.
- Delinardo da Silva, M.A., 2014, Metatexitos e diatexitos do Complexo Xingu na região de Canaã dos Carajás: Implicações para a evolução mesoarqueana do Domínio Carajás, PA. Unpublished MSc. Thesis, Campinas, University of Campinas.

- Dall'Agnol, R., Cunha, I.R.V., Guimarães, F.V., Oliveira, D.C., Teixeira, M.F., Feio, G.R.L., Lamarão, C.N., 2016, Mineralogy, geochemistry, and petrology of Neoarchean ferroan to magnesian granites of Carajás Province, Amazonian Craton: The origin of hydrated granites associated with charnockites: *Lithos*, v. 277, p. 3-32.
- DOCEGEO, 1988, Revisão litoestratigráfica da Província Mineral de Carajás - Litoestratigrafia e principais depósitos minerais: 35th Congresso Brasileiro de Geologia, Belém. (Proceedings).
- Dreher, A.M., Xavier, R.P., Taylor, B.E., Martini, S., 2008, New geologic, fluid inclusion and stable isotope studies on the controversial Igarapé Bahia Cu-Au deposit, Carajás province, Brazil: *Mineralium Deposita*, v. 43, p. 161–184.
- Dreher, A.M., Xavier, R.P., Taylor, B.E., Martini, S., 2005, Fragmental rocks of the Igarapé Bahia Cu-Au deposit, Carajás Mineral Province, Brazil: *Revista Brasileira de Geociências*. v. 35(3), p. 359–368.
- Feio, G.R.L., Dall'Agnol, R., Dantas, E.L., Macambira, M.J.B., Gomes, A.S., Sardinha, D.C., Oliveira, D.c., Santos, R.D., Santos, P.A., 2012, Geochemistry, geochronology, and origin of the Neoarchean Planalto Granite suite, Carajás, Amazonian craton: A-type or hydrated charnockitic granites? *Lithos*, v. 151, p. 57 – 73.
- Feio, GRL, Dall'Agnol R., Dantas, E.L., Macambira, M.J.B., Santos, J.O.S., Althoff, F.J., Soares, J.E.B., 2013, Archean granitoid magmatism in the Canaã dos Carajás area: implications for crustal evolution of the Carajás province, Amazonian craton, Brazil: *Precambrian Research*, v. 227, p. 157-185.
- Ferreira Filho, C.F., 1985, Geologia e mineralizações sulfetadas do Prospecto Bahia, Província Mineral de Carajás: Unpublished MSc. Thesis, Brasilia, University of Brasilia.
- Fleck, A., and Lindenmayer Z.G., 2003, Estudo da interação flui-rocha no depósito de Cu-Au de Gameleira, Serra dos Carajás, com a utilização de isótopos estaveis, in Ronchi, L.H., Althoff, F.J., eds, *Caracterização e modelamento de depósitos minerais.*, 3rd: São Leopoldo, Editora Unisinos, p. 183-198.
- Galarza, M.A., Macambira M.J.B., Villas R.N., 2008, Dating and isotopic characteristics (Pb and S) of the Fe oxide–Cu–Au–U–REE Igarapé Bahia ore deposit, Carajás mineral province, Pará state, Brazil: *Journal of South America Earth Sciences*, v. 25, p. 377-397.
- Gibbs, A.K., Wirth K.R., Hirata W.K., Olszewski Jr., W.J., 1986, Age and composition of the Grão Pará Group volcanics, Serra dos Carajás: *Revista Brasileira de Geociências*, v. 16: p. 201–211.

- Giggenbach, W.F., 1992, Magma degassing and mineral deposition in hydrothermal systems along convergent plate boundaries: *Economic Geology*, v. 87, p. 1927–1944.
- Graham, C.M.; Atkinson, J.; and Harmon, R.S., 1984, Hydrogen isotope fractionation in the system chlorite-water: NERC 6th progress report of research 1981-1984, NERC Pub. Ser. D., 25, 99. 139
- Haller, A., Zúñiga, A.J., Corfu, F., Fontboté, L., 2002, The iron oxide-Cu-Au deposit of Raul-Condestable, Mala, Lima, Peru. Sociedad Geologica del Peru: XI Congreso Peruano de Geología, Lima, Resúmenes, p. 80.
- Hirata, W.K., Rigon, J.C., Kadekaru, K., Cordeiro, A.A.C., Meireles, E.A., 1982, Geologia Regional da Província Mineral de Carajás: 1st Simpósio de Geologia da Amazônia, Belém. (Proceedings)
- Hitzman, M.W., 2000, Iron oxide–Cu–Au deposits: what, where, when, and why: Porter TM (ed) Hydrothermal iron oxide copper-gold and related deposits: a global perspective Austral Miner Fund, Adelaide, pp 9–25.
- Hitzman, M.W., Oreskes, N., Einaudi, M.T., 1992, Geological characteristics and tectonic setting of Proterozoic iron oxide (Cu-U-Au-REE) deposits: *Precambrian Research*, v. 58, p. 241–287
- Huhn, S.R.B., Nascimento, J.A.S., 1997, São os depósitos cupríferos de Carajás do tipo Cu-Au-U-ETR? Costa, M.L., Angélica, R.S., Contribuições a geologia da Amazônia, SBG, Belém, p. 143-160.
- Hunt, J., Baker, T., Thorkelson, D., 2007, A review of iron oxide copper–gold deposits, with focus on the Wernecke Breccias, Yukon, Canada, as an example of a non-magmatic end member and implications for IOCG genesis and classification: *Exploration and Mining Geology*, v. 16, p. 209–232
- Hoefs, J., 2007, Stable Isotope Geochemistry: 7th edition. Springer-Verlag Berlin Heidelberg, pp. 402.
- Kotzer, T.G.; Kyser, T.K.; King, R.W.; and Kerrich, R. (1993) An empirical oxygen- and hydrogen-isotope geothermometer for quartz-tourmaline and tourmaline-water; *Geochim. Cosmochim. Acta* 57, 3421-3426
- Kyser, T.K., Kerrich, R., 1991, Retrograde exchange of hydrogen isotopes between hydrous minerals and water at low temperatures: *Geochemica Society, Special Publication*, v 3, p. 409–422

- Lindenmayer, Z. G., Fleck, A., Gomes, C.H., Santos, A.B.S., Caron, R., Paula, F.C., Laux, J.H., Pimentel, M.M., e Sardinha, A.S. 2005, Caracterização geológica do alvo estrela (Cu-Au), Serra dos Carajás, Pará In: Caracterização de Depósitos Minerais em Distritos Mineiros da Amazônia. DNPM, CT-Mineral / FINEP, ADIMB, CD-ROM, 2005, cap. IV, 1, 137-205.
- Lindenmayer, Z.G, Ronchi LH, Laux JH, 1998, Geologia e geoquímica da mineralização de Cu-Au primária da mina de Au do Igarapé Bahia, Serra dos Carajás: Revista Brasileira de Geociências, v. 28(3), p. 257-268.
- Lindenmayer, Z.G., 1990, Salobo sequence, Carajás, Brasil: Geology, Geochemistry and Metamorphism. Unpublished PhD thesis, Canada, University of Ontario, 407p.
- Lowenstern, J.B., 2001, Carbon dioxide in magmas and implications for hydrothermal systems: Mineralium Deposita, v. 36, p. 490–502
- Machado, N., Lindenmayer, D.H., Krough TE, Lindenmayer, Z.G., 1991, U-Pb geochronology of Archean magmatism and basement reactivation in the Carajás Area, Amazon Shield, Brazil: Precambrian Research, v. 49, p. 1–26.
- Mark, G, Oliver, N.H.S., Williams, P.J., Valenta, R.K., Crookes, R.A., 2000, The evolution of the Ernest Henry Fe-oxide-(Cu-Au) hydrothermal system: Porter TM (ed) Hydrothermal iron oxide-copper-gold and related deposits: a global perspective. Austral Miner Fund, Adelaide, pp 123–136
- Marschik, R., Fontboté, L., 2001, The Candelaria–Punta del Cobre iron oxide Cu–Au (–Zn–Pb) deposits, Chile: Economic Geology, v. 96, p. 1799–1826.
- Marschik, R, Leveille, R.A., Martin, W., 2000, La Candelaria and the Punta del Cobre district, Chile: early Cretaceous iron-oxide Cu– Au(–Zn–Ag) mineralization: Porter TM (ed) Hydrothermal iron oxide cooper-gold and related deposits: a global perspective Austral Miner Fund, Adelaide, pp. 163–176
- Melo, G.H.C., Monteiro, L.V.S., Xavier, R.P., Moreto, C.P.N., In prep, The geology of the Igarapé Bahia deposit: host rocks, hydrothermal alteration and U-Pb geochronology of the Alemão, Acampamento Norte, Acampamento Sul and Furo 30 orebodies, Carajás Province (Brazil). To be submitted to Ore Geology Reviews
- Melo, G.H.C., Monteiro, L.V.S., Xavier, R.P., Moreto, C.P.N., Santiago, E.B.S., Dufrane, S.A., Aires, B., Santos, A.F.F., 2016, Temporal evolution of the giant Salobo IOCG deposit, Carajás Province (Brazil): constraints from paragenesis of hydrothermal alteration and U-Pb geochronology. Mineralium Deposita, v. 52, p. 709-732.

- Mougeot, R., Respaut J.P., Briqueu L., Ledru P., Milesi J.P., Macambira M.J.B., Huhn S.B., 1996, Geochronological constrains for the age of the Águas Claras Formation (Carajás Province, Pará, Brazil). In: Cong. Bras. Geol, 39, Anais., Salvador, SBG. 6:579-581.
- Moreto, C.P.N., Monteiro, L.V.S., Xavier RP, Creaser, R.A., Dufrane, S.A., Tassinari, C.C.G., Sato, K., Kemp, A.I.S., Amaral,W.S., 2015b, Neoarchean and Paleoproterozoic Iron Oxide-Copper-Gold events at the Sossego deposit, Carajás Province, Brazil, Re-Os and U-Pb geochronological evidence: Economic Geology, v. 110, p. 809–835.
- Nogueira, A.C.R., Truckenbrodt W., Pinheiro R.V.L., 1995, Formação Águas Claras, Pré-Cambriano da Serra dos Carajás: redescrição e redefinição litoestratigráfica. Bol. Mus. Par. Em. Goeldi, 7: 177-277.
- Ohmoto, H., 1986, Stable isotope geochemistry of ore deposits. In: Valley JW, Taylor Jr HP, O'Neil JR (eds) Reviews in Mineralogy: Stable isotopes in high temperature geological processes. Mineral Soc Am 16:491–560
- O'Neil, J.R.; Clayton, R.N.; and Mayeda, T.K., 1969, Oxygen isotope fractionation in divalent metal carbonates; Journal of Chemical Physics, v. 51(12), p. 5547-5558.
- Oreskes, N, Einaudi, M., 1992, Origin of hydrothermal fluids at Olympic Dam: preliminary results from fluid inclusions and stable isotopes: Economic Geology, v.87, p. 64–90
- Pestilho, A.L.S., 2011, Sistemática de isótopos estáveis aplicada à caracterização da evolução dos paleo-sistemas hidrotermais associados aos depósitos cupríferos Alvo Bacaba e Alvo Castanha, Província Mineral de Carajás, PA: Unpublished MSc. Dissertation, Campinas, University of Campinas
- Pidgeon, R.T., Macambira, M.J.B., Lafon, J.M., 2000, Th–U–Pb isotopic systems and internal structures of complex zircons from an enderbite from the Pium Complex, Carajás Province, Brazil: evidence for the ages of granulite facies metamorphism and the protolith of the enderbite: Chemical Geology, v. 166, p. 159–171.
- Pinheiro, R.V.L., 2013, Carajás, Brazil – A short tectonic review: 13th Simpósio de Geologia da Amazônia, Belém (Proceedings).
- Pinheiro, R.V.L., Holdsworth, R.E., 1997, Reactivation of Archean strike-slip fault systems, Amazon region, Brazil. Journal of the Geological Society, v. 154, p. 99–103.
- Pollard, J.P., 2006, An intrusion-related origin for Cu-Au mineralization in iron oxide-copper-gold (IOCG) provinces: Mineralium Deposita, v. 41, p. 179.
- Réquia, K, Stein, H., Fontboté, L., Chiaradia, M., 2003, Re–Os and Pb–Pb geochronology of the Archean Salobo iron oxide copper–gold deposit, Carajás Mineral Province, northern Brazil: Mineralium Deposita, v. 38, p. 727–738.

- Requia, K., and Fontbonné, L., 2001, The Salobo iron oxide copper-gold hydrothermal system, Carajás mineral province, Brazil: Geological Society of America, Abstract with Programs, v. 33, p. 2.
- Réquia, K.C.M., 1995, O papel do metamorfismo e fases fluidas na gênese da mineralização de cobre de Salobo, Província Mineral de Carajás, Pará: Unpublished PhD Thesis, Campinas, University of Campinas.
- Ribeiro, A.A. 2008. Litogeоquímica e geologia isotópica estável (C, S, O) do Depósito Cuproaurífero do Alvo Cristalino Sul, Província Mineral de Carajás, Pará. Dissertação de Mestrado, UFOP, 127p.
- Rotherham, J.F., Blake, K.L., Cartwright, I., Williams, P.J., 1998, Stable isotope evidence for the origin of the Mesoproterozoic Starra Au–Cu deposit, Cloncurry district, northwest Queensland: Economic Geology, v. 93, p. 1435–1449
- Santos, M.N.S., Oliveira, D.C., 2016, Rio Maria granodiorite and associated rocks of Ourilândia do Norte – Carajás province: Petrography, geochemistry and implications for sanukitoid petrogenesis: Journal of South American Earth Sciences, v. 72, p. 279-301.
- Santos, J.O.S., 2003, Geotectônica do Escudo das Guianas e Brasil-Central. In: Bizzi LA,(ed) Geologia, tectônica e recursos minerais do Brasil: texto, mapas e SIG. Brasília, CPRM, pp 169-226.
- Schmitt, A.K., Trumbull, R.B., Dulski, P., Emmermann, R., 2002. Zr-Nb-Ree Mineralization in peralkaline granites from the Amis Complex, Brandberg (Namibia): evidence of magmatic pre-enrichment from melt inclusions. Economic Geology, v. 97 (2), p. 399–413.
- Sillitoe, R.H., 2003, Iron oxide–copper–gold deposits: an Andean view: Mineralium Deposita, v. 38, p. 787–812
- Silva, A.R.C., Villas, R.N.N., Lafon, J.M., Craveiro, G.S., Ferreira, V.P., 2015, Stable isotope systematics and fluid inclusion studies in the Cu–Au Visconde deposit, Carajás Mineral Province, Brazil: implications for fluid source generation: Mineralium Deposita, v. 50, p. 547-569
- Souza, S.R.B., Macambira M.J.B., Sheller T., 1996, Novos dados geocronológicos para os granitos deformados do Rio Itacaiúnas (Serra dos Carajás, PA), implicações estratigráficas. In: Simp. Geol. Amaz., 5, Belém, Anais, 380–383.
- Suzuoki, T.; and Epstein, S., 1976, Hydrogen isotope fractionation between OH-bearing minerals and water: Geochim. Cosmochim Acta, v. 40, p. 1229-1240.

- Tallarico, F.H.B., Figueiredo, B.R., Groves, D.I., Kositcin N., McNaughton, N.J., Fletcher, I.R., Rego, J.L., 2005, Geology and SHRIMP U-Pb geochronology of the Igarapé Bahia deposit, Carajás copper-gold belt, Brazil: an Archean (2.57 Ga) example of iron-oxide Cu-Au-(U-REE) mineralization: *Economic Geology*, v. 100, p. 7-28.
- Tallarico, F.H.B., 2003, O cinturão cupro-aurífero de Carajás, Brasil. Unpublished PhD Thesis, Campinas, University of Campinas, 229p
- Tassinari, C.C.G., Macambira, M.J.B., 1999, Geochronological Provinces of the Amazonian Craton: *Episodes*, v. 22, p. 174-182.
- Tavares, F., 2015, Evolução Geotectônica do nordeste da Província Carajás. Unpublished PhD Thesis, Rio de Janeiro, University of Rio de Janeiro. pp. 130.
- Teixeira, J.B.G., 1994, Geochemistry, petrology, and tectonic setting of archean basaltic and dioritic rocks from the N4 Iron deposit, Serra dos Carajás, Pará, Brazil. Tese de doutorado. Instituto de Geociências, Universidade de São Paulo. 161p.
- Taylor, H.P. Jr., 1997, Oxygen and hydrogen isotope relationships in hydrothermal mineral deposits: Barnes HL (ed) *Geochemistry of hydrothermal ore deposits*. Wiley, New York, pp 229–302.
- Taylor, B.E., 1992, Degassing of H₂O from rhyolitic magma during eruption and shallow intrusion, and the isotopic composition of magmatic water in hydrothermal systems: *Geological Survey of Japan Report*, v. 279, p. 190–194.
- Taylor, H.P. Jr., 1974, The application of oxygen and hydrogen isotope studies to problems of hydrothermal alteration and ore deposition: *Economic Geology*, v. 69, p. 843–883.
- Tornos, F., Velasco, F., Hanchar, J.M., 2016, Iron-rich melts, magmatic magnetite, and superheated hydrothermal systems: The El Laco deposit, Chile: *Geology*, v. 44, p. 427-430.
- Twyerould, S.C., 1997, The geology and genesis of the Ernest Henry Fe–Cu–Au deposit, NW Queensland, Australia. Ph.D. thesis, University of Oregon, p 494
- Ullrich, T.D., Clark, A.H., Kyser, T.K., 2001, The Candelaria Cu–Au deposit, III Región, Chile: product of long-term mixing of magmatic-hydrothermal and evaporite-sourced fluids. GSA Annual Meeting, Boston, Abstracts with Programs, p A-3
- VALE, 2002, Nova Fase da mina de Igarapé Bahia. VALE information Market, press releases. <http://www.vale.com/brasil/PT/investors/information-market/press-releases/Paginas/nova-fase-da-mina-de-igarape-bahia.aspx>. Accessed 04 november 2016.
- Veizer, J. and Hoefs, J., 1976, Nature of O₁₈-O₁₆ and C₁₃-C₁₂ Secular Trends in Sedimentary Carbonate Rocks. *Geochimica et Cosmochimica Acta*, 40(11): 387-395.

- Veksler, I.V., 2004, Liquid immiscibility and its role at the magmatic–hydrothermal transition: a summary of experimental studies: *Chemical Geology*, v. 210, p. 7-31.
- Webster, J.D., 2004, The exsolution of magmatic hydrosaline chloride liquidus. *Chemical geology*, v. 210, p. 33-48.
- Wirth, K.R., Gibbs, A.K., Olszewski, W.J., 1986, U-Pb ages of zircons from the Grão Pará Group and Serra dos Carajás Granite, Pará, Brazil: *Revista Brasileira de Geociências* v. 16, p. 195-200.
- Xavier, R.P., Wiedenbeck, M., Trumbull, R.B., Dreher, A.M., Monteiro, L.V.S., Rhede, D., Araújo, C.E.G., Torresi, I., 2008, Tourmaline B-isotopes fingerprint marine evaporites as the source of high-salinity ore fluids in iron oxide-copper-gold deposits, Carajás Mineral Province (Brazil): *Geology*, v. 36, p. 743-746.
- Zang, W., Fyfe, W.S., 1995, Chloritization of the hydrothermally altered bedrock at the Igarapé Bahia gold deposit, Carajás, Brazil: *Mineralium Deposita*, v. 30, p. 30–38.
- Zheng, Y.F., 1993, Calculation of oxygen isotope fractionation in hydroxyl-bearing silicates; *Earth Planetary Science Letters*, v. 120, p. 247-263.
- Zheng, Y.F., 1991, Calculation of oxygen isotope fractionation in metal oxides: *Geochimica et Cosmochima Acta*, v. 55, p. 2299-2307

**Anexo III – “Boron isotopes in
tourmaline of the IOCG deposits in the
northern sector of the Carajás Domain,
Carajás Province (Brazil)”**

**Boron isotopes in tourmaline of the IOCG deposits in the
northern sector of the Carajás Domain, Carajás Province
(Brazil)**

GUSTAVO H. C. DE MELO¹; POLIANA TOLEDO¹, RAPHAEL HUNGER¹,
ROBERTO P. XAVIER¹, LENA V. S. MONTEIRO²; CAROLINA P. N. MORETO¹,
XIN-FU ZHAO³, ZHI-KUN SU³, SILVANDIRA JESUS²

¹*Institute of Geosciences, University of Campinas (UNICAMP), R. João Pandiá
Calógeras, 51, 13083-870 Campinas (SP), Brazil*

²*Institute of Geosciences, University of São Paulo (USP), Rua do Lago, 562, 05508-080
São Paulo (SP), Brazil*

³*State Key Laboratory of Isotope Geochemistry, Guangzhou Institute of
Geochemistry, Chinese Academy of Sciences, Guangzhou 510640, China*

Abstract

The iron oxide–copper–gold (IOCG) deposits located in the northern part of the Carajás Domain in the Carajás Province, Amazon Craton, represent important examples of their class and include Salobo, GT-46, Furnas, Grotá Funda, and Igarapé Bahia. Boron isotope analyses were carried out on tourmaline of different stages of hydrothermal alteration in these five IOCG deposits of the northern sector. At Salobo, $\delta^{11}\text{B}$ values range from +14.9 to +17.0‰ in the tourmaline cores and from +3.4 to +8.2‰ in their rims. At Igarapé Bahia deposit, tourmaline cores (+11.0‰ to +14.6‰) and rims (+3.4 to +9.8‰) also have distinct boron isotopic signatures. Relatively high $\delta^{11}\text{B}$ values are also recorded at tourmaline from the Furnas (+13.1 to +17.2‰) and Grotá Funda (+8.2 to +13.6‰) deposits. The GT-46 deposit tourmaline has the lowest $\delta^{11}\text{B}$ values (+5.4 to +6.4‰). The high $\delta^{11}\text{B}$ values in tourmaline within these deposits evidence the participation of boron derived from submarine hydrothermal fluids or from evaporated seawater brines. The circulation of these fluids might have occurred during the deposition of the ca. 2.76 – 2.73 Ga metavolcanosedimentary sequences of the Itacaiúnas Supergroup. However, the isotopically heavy boron signatures may reflect inheritance from host volcanic rocks, which undergone low-temperature alteration due to interaction with seawater in the ocean floor. Intermediate to lower $\delta^{11}\text{B}$ values, in contrast, are attributed to boron sourced from magmatic brines probably associated with crystallization of granites at ca. 2.57 Ga. These results suggest that seawater and magmatic boron sources took part in the mineral system during distinct Neoarchean tectono-magmatic events separated in time.

Introduction

Tracing fluid sources for IOCG deposits has been a challenge, although a plenty of studies have dealt with this subject in the past few decades. However, the complexity of these systems lead many authors to propose different models to explain their genesis, including: (i) a magmatic-hydrothermal origin (Pollard, 2006; Tornos et al., 2010) or (ii) the large-scale circulation of basinal fluids with igneous rocks acting as heat sources for the hydrothermal system (Barton and Johnson, 1996, 2000).

Tourmaline is a boron silicate mineral with a wide variety in its chemical composition and represents the major boron reservoir in the Earth's crust (Hawthorne and Dirlam, 2011; Dutrow & Henry, 2011). When formed, tourmaline is very stable and has a great capacity to preserve its isotopic signature even in different rock types and P-T conditions (Hawthorne and Dirlam, 2011; Dutrow & Henry, 2011). Hydrothermal tourmaline formation demands boron and other elements from one or multiple fluid sources, and in specific conditions its precipitation can coincide with the deposition of economically valuable metals (Slack and Trumbull, 2011). In this case, tourmaline can represent a sensitive indicator of the chemistry of ore-forming fluids (Slack and Trumbull, 2011).

The application of boron isotopes systematics in the study of hydrothermal ore deposits has shown that tourmaline represents an important tool to trace fluid sources in different mineral systems, including IOCG deposits. Especially in the latter, boron isotopes might help to unravel the participation of magmatic components and/or external brines. However, the current available data for the IOCG deposits worldwide is still limited (e.g. Xavier et al., 2008, Tornos et al., 2012, Zhi-Kun et al., 2016).

The IOCG deposits located in the northern part of the Carajás Domain, in the Carajás Province (Amazon Craton), include the large-tonnage Salobo, GT-46, Furnas, Grota Funda and Igarapé Bahia. Salobo, GT-46 and Furnas deposits are placed along the Cinzento Shear Zone, whereas Grota Funda and Igarapé Bahia deposit occur close to the regional Carajás Strike-Slip Fault System. Collectively, these deposits correspond to more than 2 billion tons of copper-gold ore and represent important examples of their class. Salobo, GT-46, Igarapé Bahia and Grota Funda deposits might share the same timing of mineralization in a single metallogenetic event at ca. 2.57 Ga (Réquia et al., 2003; Tallarico et al., 2005; Melo et al., in prep; Hunger, 2017). This event was

genetically linked with granite emplacement (e.g. Old Salobo Granite; Réquia et al., 2003; Tallarico et al., 2005).

Tourmaline is a conspicuous and important mineral in these deposits formed by hydrothermal processes and can reveal important information about their evolutional history. This paper provides new boron isotopic data of several IOCG deposits in the northern sector of Carajás and may elucidate the boron sources and likely origin of the ore-forming fluids for these deposits.

Geological setting

The Carajás Province is located at the southeastern portion of the Amazon Craton and is divided into two main tectonic domains: the Rio Maria Domain at south, and the Carajás Domain at north (Santos, 2003; Vasquez et al., 2008). The Carajás Domain hosts an important concentration of several types of ore deposits, including large-tonnage iron oxide copper–gold (or IOCG) deposits (Xavier et al., 2012). These deposits are mainly concentrated in the Southern Copper Belt (Moreto et al., 2015a, 2015b) and in the northern sector of the Carajás Domain (Fig. 1)

The basement rocks of the Carajás Domain are represented by orthogneisses and migmatites from the Xingu Complex with crystallization ages at $3,066 \pm 6.6$ Ma (Delinardo da Silva, 2014). Chicrim–Cateté Orthogranulites (previously named as Pium Complex) with crystallization ages of $3,002 \pm 14$ Ma also compose the basement rocks. High-grade metamorphism and deformation associated with migmatization processes affected these rocks at $2,859 \pm 2$ Ma and $2,859 \pm 9$ Ma (Machado et al., 1991; Pidgeon et al., 2000). Mesoarchean undeformed granitoids were characterized in the southern part of the Carajás Domain, and include (1) ca. 3.0 Ga Bacaba Tonalite (Moreto et al., 2011); (2) ca. 2.96 Ga Canaã dos Carajás Granite (Feio et al., 2013); and (3) ca. 2.87 to 2.83 Ga Serra Dourada and Cruzadão granites, and the Rio Verde Trondhjemite (Moreto et al., 2011, Feio et al., 2013).

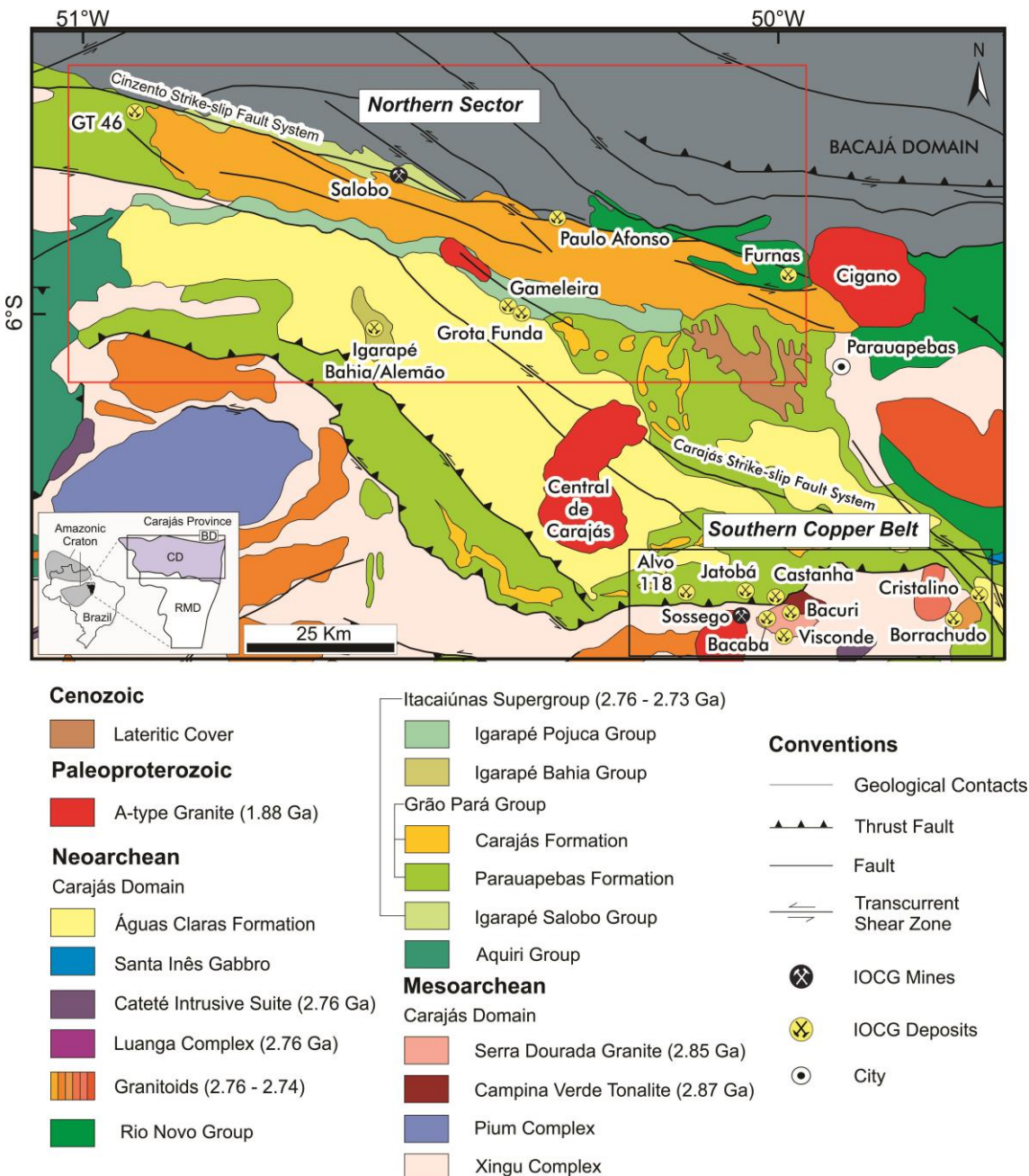


Fig 1. Geological map of the Carajás Domain with the location of the IOCG deposits within the Southern Copper Belt and from the northern sector (red rectangle; deposits (modified from Vasquez et al., 2008; Dall'Agnol et al., 2016; Santos e Oliveira, 2016).

The basement is overlain by the metavolcanosedimentary sequences of the Rio Novo Group and Itacaiúnas Supergroup. The Rio Novo Group, of uncertain age, is composed by amphibolites, schists, metagraywackes, metavolcanic rocks and metagabbros (Hirata et al., 1982). The Neoarchean (2.76 – 2.73 Ga) Itacaiúnas Supergroup encompasses, from bottom to top, metavolcanic and metapyroclastic rocks, banded iron formations and metasedimentary units (Tavares, 2015). These sequences

are grouped into Igarapé Salobo, at the base, Igarapé Pojuca, Grão Pará and Igarapé Bahia groups (DOCEGEO, 1988). Geochemical tholeiitic signature of the metabasalts from the Grão Pará Group suggests that these sequences formed in an intracontinental rift (Wirth et al., 1986; Gibbs et al., 1986; DOCEGEO, 1988; Olszewski et al., 1989). However, the calc-alkaline signature attributed for the same rocks may also evidence they formed in an arc magmatic setting (Meirelles & Dardenne, 1991; Teixeira, 1994; Lindenmayer et al., 2005; Lobato et al., 2005).

These metavolcanosedimentary sequences were covered by the Águas Claras Formation, which comprises a low-grade metasedimentary sequence deposited in a fluvial to shallow marine environment (Nogueira et al., 1995). The age of the Águas Claras Formation remains discussable, although dating of metagabbro sills point to its age at $2,645 \pm 12$ Ma (Dias et al., 1996). Younger ages are also considered for the Águas Claras Formation due to Pb–Pb ages in diagenetic pyrite at ca. 2.06 Ga and the absence of mass independent fractionation of sulfur (MIF-S) in these sulfides (Mougeot et al., 1996; Fabre et al., 2011).

Mafic-ultramafic and felsic magmatism are widely recognized in the domain. At 2.76 to 2.73 Ga mafic-ultramafic layered intrusions intrude basement and supracrustal sequences and include mainly Luanga and Vermelho Complexes (Ferreira Filho et al., 2007). In this same period, a set of syntectonic, foliated, alkaline and metaluminous granites are broadly recognized in the Carajás Domain, which include Planalto, Plaquê, Estrela, Serra do Rabo, Igarapé Gelado, and Pedra Branca suites (Huhn et al., 1999b; Sardinha et al., 2006; Barros et al., 2009; Feio et al., 2012). A-type peralkaline granites of ca. 2.55 to 2.57 Ga are represented only by small granite bodies, the Old Salobo, Itacaiúnas and GT-46 granites (Machado et al., 1991; Souza et al., 1996; Toledo, 2017). Anorogenic granitic magmatism in 1.88 Ga is represented by the Serra dos Carajás suite and includes Central de Carajás, *Young* Salobo, Cigano, Pojuca and Breves granites (Machado et al., 1991; Lindenmayer & Teixeira, 1999; Tallarico, 2003).

The structural framework of the Carajás Domain comprises WNW–ESE striking structures, which have been formed due to a NNE–SSW shortening. According to Araújo et al. (1988), this structural framework developed in response to dextral transtension, creating the Carajás and Cinzento shear zones. The basin was later inverted by sinistral transpression, which last from 2.7 to 2.6 Ga (Araújo et al., 1988; Domingos, 2009). Alternatively, dextral transtension was late in comparison to the Itacaiúnas Supergroup deposition and was responsible for the formation of the Carajás

and Cinzento shear zones (Pinheiro & Holdsworth, 1997; Holdsworth & Pinheiro, 2000). In this model, the basin was inverted only in ca. 2.6 Ga due to dextral transpression (Pinheiro & Holdsworth, 1997; Holdsworth & Pinheiro, 2000).

Geology of the Carajás IOCG deposits

The IOCG deposits of the northern sector analyzed in this study are located in two main zones: (i) along the Cinzento Shear Zone, including Salobo, GT-46 and Furnas, where basements rocks, metagranitoids and metavolcanosedimentary sequences occur, and (ii) placed within the metavolcanosedimentary sequence of the Itacaiúnas Supergroup, represented by the Grotá Funda and Igarapé Bahia deposits, also affected by regional-scale shear zones (i.e. Carajás Shear Zone).

Salobo

The Salobo deposit, with estimated reserves of 1,112 Mt @ 0.69 wt% Cu, 0.43 g/t Au, 55 g/t Ag (VALE, 2012), is located along the WNW–ESE Cinzento Shear Zone, close to northern limit of the Carajás Domain with the Paleoproterozoic Bacajá Domain.

The deposit is hosted by orthogneissic rocks from the Xingu Complex ($2,950 \pm 25$ and $2,857 \pm 6.7$ Ma) and the Igarapé Gelado suite ($2,763 \pm 4.4$ Ma; Melo et al., 2016). Remnants of a metasedimentary sequence, represented by a quartz mylonite, are preserved in the southwestern portion of the deposit (Fig. 2A). The Old Salobo granite crosscut the main host rocks in the northeastern portion of the deposit. It was dated at $2,573 \pm 2$ Ma and $2,547 \pm 5.3$ Ma (Machado et al., 1991; Melo et al., 2016).

These rocks were intensely ductilely deformed within the Cinzento Shear Zone, which imparted a steeply dipping mylonitic foliation in the inner parts of the deposit. This deformation was accompanied by pervasive hydrothermal alteration (Réquia et al., 2003; Melo et al., 2016). In these portions, rare relicts of texture and structures of protoliths are preserved. The A-type anorogenic Young Salobo granite intercepted the whole sequence at 1.88 Ga.

Hydrothermal alteration encompasses early distal Na–Ca alteration with hastingsite–actinolite followed by widespread iron enrichment (Fig. 3A). The latter comprises paragenesis with almandine–grunerite–magnetite–(fayalite). Tourmaline porphyroblasts are also recognized within zones of iron enrichment. Potassic alteration with biotite and associated quartz replace grunerite, almandine and tourmaline, and occurred pre to syn ore precipitation. The copper–gold mineralization is associated with

magnetite–(biotite)-rich rocks in deformed lenses and massive orebodies. Bornite and chalcocite compose the main ore minerals and display a mirmekitic-symplectite texture. The geochemical ore signature includes high contents of Co, Ni, As, Ag, Au, Mo, F, REE and U due to numerous mineral inclusions (e.g. cobaltite, safflorite, hessite, Co-pentlandite, nickeline, monazite, xenotime, synchisite, fluorite, molybdenite, uraninite) in the sulfides (Melo et al., 2016).

Re–Os molybdenite ages in the samples of the Salobo ore yielded an age of $2,576 \pm 8$ Ma (Réquia et al., 2003). This age is interpreted as the age of mineralization at Salobo, even though younger ages are also recorded in the deposit (e.g. U–Pb in monazite, $2,452 \pm 14$ Ma, Melo et al., 2016). The genetic model for Salobo was linked with the Old Salobo granite emplacement at ca. 2.57 Ga (Réquia et al., 2003; Tallarico et al., 2005). A Pb–Pb isochron age in chalcocite, however, might show that Salobo records an older mineralization event at $2,705 \pm 42$ Ma (Tassinari et al., 2003).

GT-46

The GT-46 deposit occurs along the WNW–ESE Cinzento Shear Zone, to the west of the Salobo deposit. The deposit is hosted by a metavolcanosedimentary sequence containing amphibolites (U–Pb in zircon, $2,774 \pm 19$ Ma), actinolite–biotite schists, (almandine)–biotite schists, and metamorphosed banded iron formations (Silva et al., 2005; Toledo, 2017). These rocks are located along the subvertical limbs of a folded structure (Fig. 2B). Foliated tonalites to granodiorites (U–Pb in zircon, $2,532 \pm 26$ Ma), pegmatite bodies (U–Pb in zircon, $2,562 \pm 39$ Ma), porphyritic granites (U–Pb in zircon, $2,557 \pm 26$ Ma), and diabase dykes crosscut the whole sequence (Silva et al., 2005; Toledo, 2017).

Microstructural analysis allowed the identification of distinct foliations: (i) S_{n-1} planes, preserved as mineral inclusion trails (e.g. tourmaline (I), apatite, quartz) within poikiloblastic almandine; (ii) S_n foliation, represented by a set of spaced foliation that varies from roughly parallel to anastomosing; (iii) S_{n+1} foliation, observed as axial planes on folded S_n , or as a continuous schistosity or mylonitic foliation, developed during deformation in shear zones (Toledo, 2017).

Hydrothermal alteration was coeval to S_{n+1} development. The alteration sequence is characterized by an early regional sodic–calcic alteration (hastingsite, albite), followed by potassic alteration (biotite), iron-enrichment (magnetite) and copper mineralization (I) with chalcopyrite–bornite–magnetite (Fig 3B) (Silva et al., 2005;

Toledo, 2017). Molybdenite, pyrite, sphalerite, pentlandite and cassiterite are associated with the copper sulfides in the first mineralization stage (Toledo, 2017). Veins and breccias with chalcopyrite (II), magnetite (II), chlorite, carbonate, quartz and albite comprise the late copper mineralization (II). The latter crosscut S_{n+1} foliation planes (Toledo, 2017). The last alteration stage is represented by chlorite halos and coarse-grained almandine, quartz and biotite crystals spatially associated with pegmatitic intrusions ($2,562 \pm 39$ Ma; Toledo, 2017). Tiny hydrothermal tourmaline (II) crystals occur infilling coarse garnet fractures.

The Re–Os molybdenite age of $2,718 \pm 56$ Ma is accounted for the main stage of ore formation (mineralization I). Younger ages (Re–Os in molybdenite, $2,600 \pm 8$ Ma, $2,557 \pm 8$ Ma and $2,554 \pm 8$ Ma; Silva et al., 2005; Re–Os in molybdenite, $2,503 \pm 51$ Ma, $2,449 \pm 44$ Ma; Toledo, 2017) represent possible evidence of recurrence of hydrothermal events in the GT–46 deposit, likely associated with mineralization stage (II). Paleoproterozoic ages (Ar–Ar in biotite, $1,854 \pm 5$ Ma, 1809 ± 6 Ma) were also obtained in the GT-46 deposit and assigned to the main mineralization stage (Silva et al. 2005).

Furnas

The Furnas deposit, with estimated reserves of 500 Mt @ 0.7% Cu, comprises a WNW–ESE mineralized trend with 9 km of extension within the Cinzento Transcurrent Shear Zone. The host rocks include andalusite–muscovite–biotite schist with staurolite at the footwall zone and amphibole–almandine–biotite schist in the hanging wall zone (Fig. 2C, Jesus, 2016). Slices of the intensely hydrothermally altered Furnas granite are also recognized in drill cores (Jesus, 2016). The ca. 1.88 Ga Cigano granite crosscuts the sequence of the host rocks on the eastern deposit limit (Jesus, 2016).

The zone between footwall and hanging wall is characterized by intense ductile deformation associated with hydrothermal alteration. This alteration processes were responsible by formation of quartz mylonite and biotite-, almandine-, grunerite-, and magnetite-rich rocks (Jesus, 2016).

Metamorphic foliation (S_n) is preserved in mineral trails within garnet and andalusite porphyroblasts, which are recognized in the footwall and hanging wall zones. The shear zone development resulted in mylonitic foliation (S_{n+1}) and was associated with most of the hydrothermal mineral growing (Jesus, 2016).

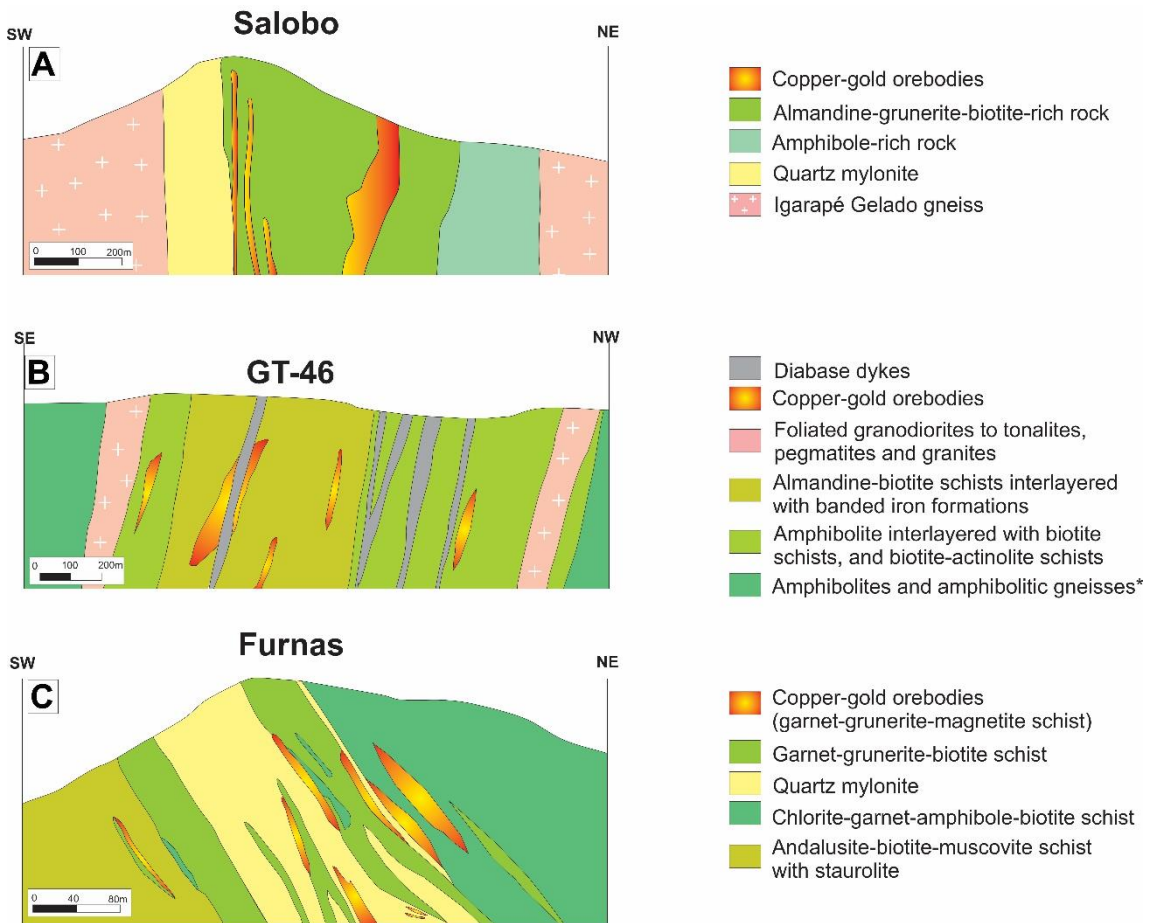


Fig 2. Geological cross sections with the mains host rocks and the location of the orebodies at a) Salobo, b) GT 46 and c) Furnas deposits. Modified from VALE.

Several stages of hydrothermal alteration were recognized at Furnas by Jesus (2016; Fig. 3C). Sodic alteration with albite and silicification are early and synchronous with mylonitization (S_{n+1} foliation). Tourmaline (I) is recognized within these silified zones. This was followed by potassic alteration with biotite, tourmaline (II) and garnet formation. Iron metasomatism is widespread and represented by almandine–grunerite–magnetite. Coalescent almandine and coarse-grained grunerite crystals develop along the mylonitic foliation. Later stages of hydrothermal alteration encompass zones with coarse-grained hastingsite with external chlorite halos and quartz veins.

The copper–gold mineralization (I) is composed of chalcopyrite and bornite in (i) alteration fronts within the garnet–grunerite–magnetite-rich rocks, (ii) veins, (iii) stockwork zones, and (iv) hydrothermal breccias (Jesus, 2016). Later subordinated copper mineralization (II) with chalcopyrite–bornite was associated with the late hastingsite-bearing alteration and with quartz–hastingsite–chlorite–albite–carbonate veins with open-space filling textures (Jesus, 2016).

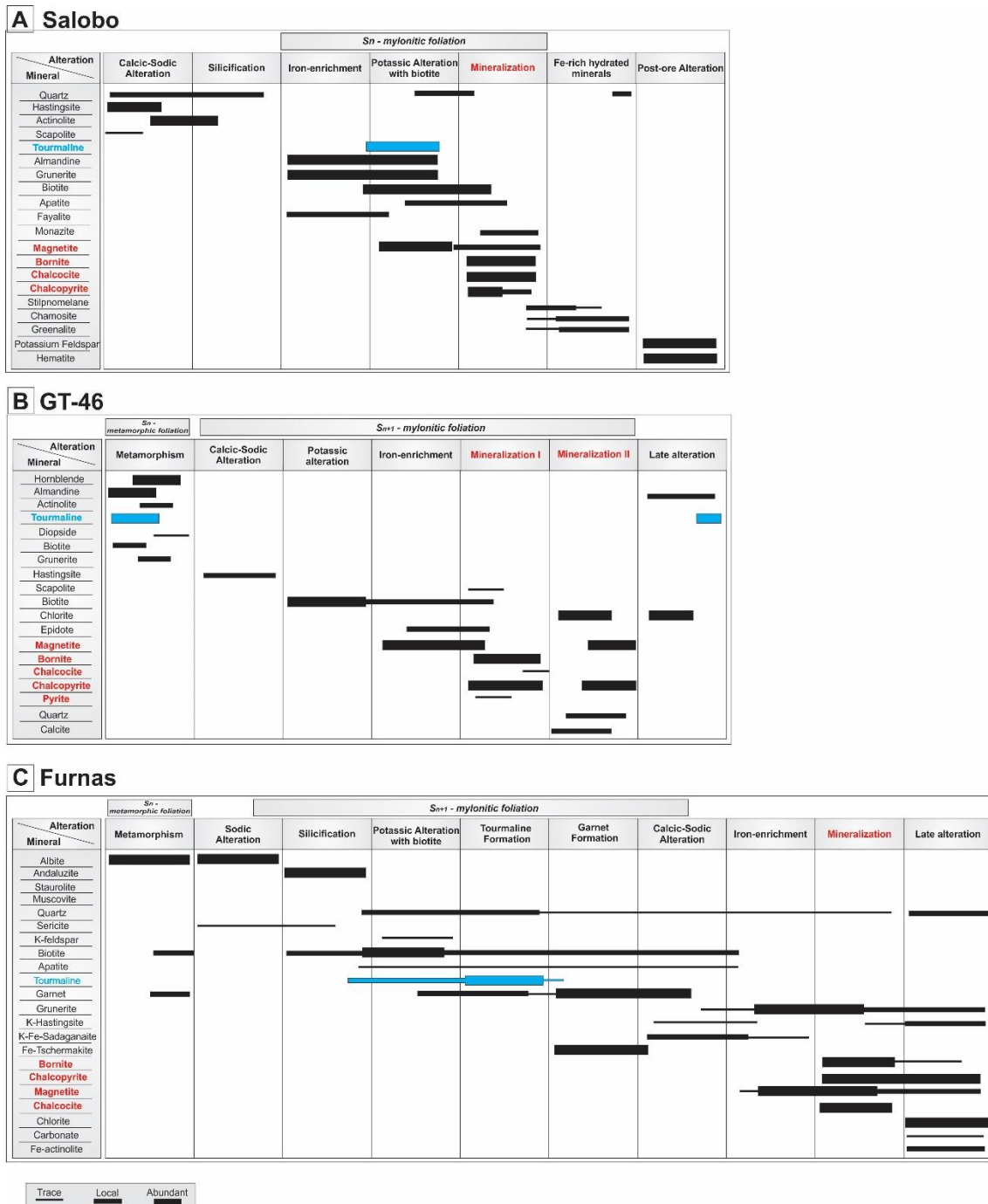


Fig. 3. Paragenetic tables with evolution of the hydrothermal systems at a) Salobo, b) GT 46 and c) Furnas deposits. Blue bars highlight the temporal position of tourmaline. Modified from Melo et al. (2016), Toledo (2017), Jesus (2016).

Grota Funda

The Grota Funda deposit occurs in the northwestern portion of the Carajás Domain along the regional-scale Cinzento WNW–ESE shear zone (Pojuca Fault System). NW–SE and E–W-trending subsidiary faults are also recognized in the deposit.

Mafic volcanic rocks, including basalts and diabases, represent the main hosts of the Cu–Au mineralization (Fig. 4A). Amygdaloidal textures are fairly preserved in the basalts. Gabbros, felsic subvolcanic rocks, and banded iron formations (BIF) represent subordinate lithotypes. Original textures and mineralogy of these rocks were partial to completely obliterated by intense hydrothermal alteration and brittle–ductile deformation (Hunger, 2017).

Na–Ca alteration encompasses pervasive zones with albite, hastingsite, scapolite and quartz (Hunger, 2017). The central zone of the deposit records intense iron-rich metasomatism with formation of magnetite (I)–grunerite–almandine with minor chlorite (I)–quartz. In this stage, zones with more than 55% of magnetite are associated with disseminated chalcopyrite (I), which was formed in the early mineralization stage (mineralization I). Widespread potassic alteration followed the iron-rich metasomatism (Fig. 5A). Biotite and quartz with minor tourmaline (I) are commonly found as stretched crystals defining the mylonitic foliation. Subordinated amounts of apatite, allanite, and ilmenite are common within these zones.

The main mineralization (II) is coeval with potassic alteration and it is represented by breccias composed of chalcopyrite (II), magnetite (II), pyrrhotite, pentlandite, and sphalerite as the main ore minerals. Apatite, quartz, biotite, chlorite and allanite are the main gangue minerals within the breccia orebodies (Hunger, 2017). Late chlorite alteration is also widespread containing variable amounts of chlorite (II), tourmaline (II), magnetite (III), carbonate and actinolite. Massive chalcopyrite (III) also comprise these zones (mineralization III).

Re–Os molybdenite ages from grunerite–magnetite veins, related to iron metasomatism, yielded ages of $2,530 \pm 60$ Ma. This age is interpreted as the timing of the first stage of IOCG mineralization (mineralization I) in the Grota Funda deposit (Hunger, 2017).

Igarapé Bahia

The Igarapé Bahia deposit (219 Mt @ 1.4% Cu and 0.86 g/t Au; Tallarico et al., 2005) lies in an erosional window within the Águas Claras Formation. The deposit comprises, from north to south, the Alemão, Acampamento Norte, Acampamento Sul and Furo 30 orebodies.

Host rocks are mainly represented by the Igarapé Bahia Group. This includes metavolcanic and metapyroclastic rocks and banded iron formation from the lower unit, and metarhytmites and metagraywackes from the upper unit (Fig. 4B, C; Lindenmayer et al., 1998; Tallarico et al., 2005; Dreher et al., 2008). Metagraywackes from the Águas Claras Formation also host the IOCG mineralization at Igarapé Bahia (Melo et al., in prep.). These rocks preserve most of their primary structures and textures in the outwards of the deposit, but inboard shearing associated with hydrothermal alteration overprints most of these features.

Na–Ca hydrothermal alteration with actinolite–epidote–scapolite is restricted and distal to the mineralization. potassic–(ferric) alteration with biotite and grunerite is primarily found in the mafic lithotypes (Melo et al., in prep.). Carbonate–(apatite) formation was coeval with ductile deformation (S_n mylonitic foliation) and precedes magnetite formation (Fig. 5B). Chlorite is widespread in the deposit and envelops the other hydrothermal alteration zones, but it is also recognized in the central part of the deposit. Textures of extreme shearing are also associated with chlorite alteration, forming mylonitic rocks with stretched chlorite crystals. Within these zones, relicts of carbonate, tourmaline and minor biotite and grunerite are preserved.

Copper–gold orebodies are represented by (mylonitic) deformed lenses, hydrothermal breccias or massive bodies (Tallarico et al., 2005; Dreher et al., 2008; Melo et al., in prep.). Ore minerals include mainly chalcopyrite with minor bornite and pyrite. Gold is associated with As- and Ag-bearing minerals. The ore geochemical signature with high contents of W, Sn and Nb, due to the presence of scheelite, cassiterite, wolframite, pyroclore and fergusonite, is a remarkable feature of the Igarapé Bahia deposit.

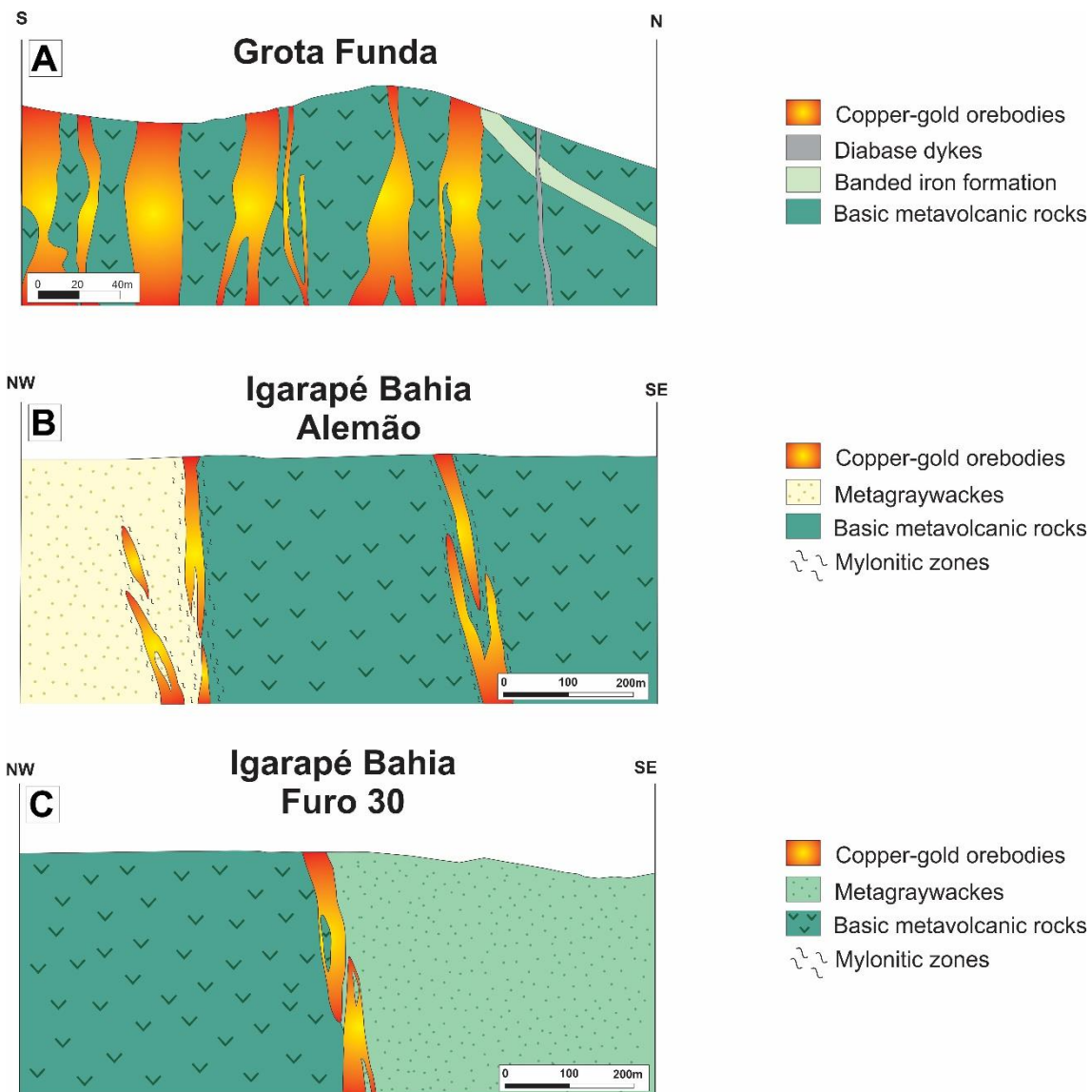
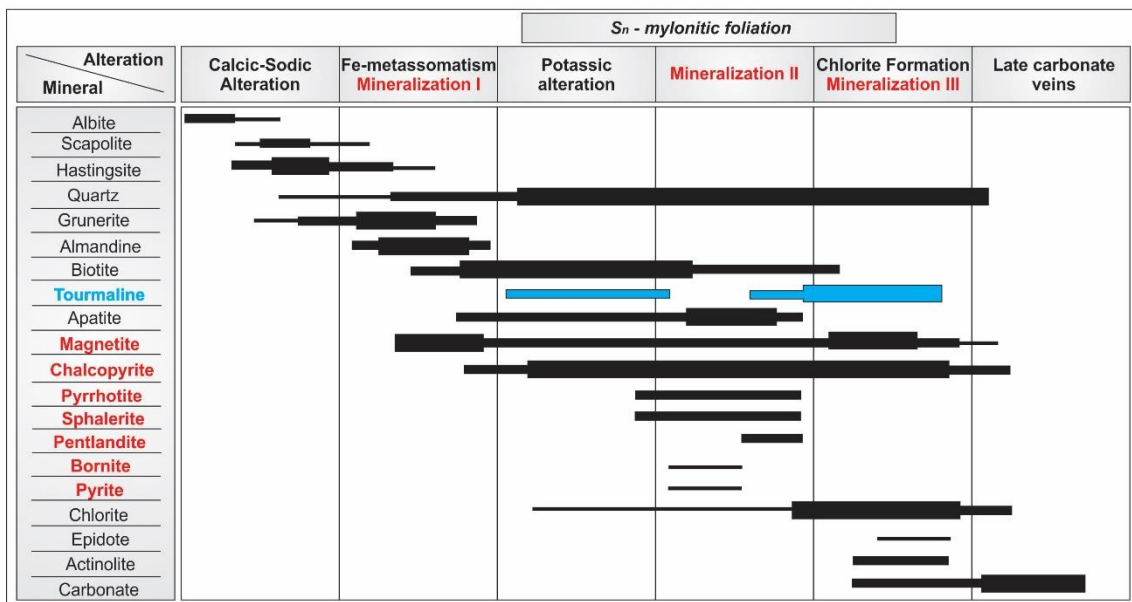


Fig 4. Geological cross sections with the mains host rocks and the location of the orebodies at a) Grota Funda and, b) Alemão and c) Furo 30 orebodies at Igarapé Bahia deposit. Modified from VALE.

Timing of IOCG mineralization is constrained at $2,575 \pm 12$ Ma and $2,559 \pm 34$ Ma at Acampamento Sul and Alemão orebodies, respectively (Tallarico et al., 2005; Melo et al., in prep). These ages overlap in time those of mineralization in the Salobo deposit and granite emplacement (Réquia et al., 2003; Tallarico et al., 2005). Pb–Pb ages in gold ($2,744 \pm 12$ Ma; Galarza et al., 2008) and in chalcopyrite ($2,772 \pm 46$ Ma, $2,754 \pm 36$ Ma, $2,756 \pm 24$ Ma, $2,777 \pm 22$ Ma, Galarza et al., 2008) might point to older stages of mineralization at Igarapé Bahia.

A Grotá Funda



B Igarapé Bahia

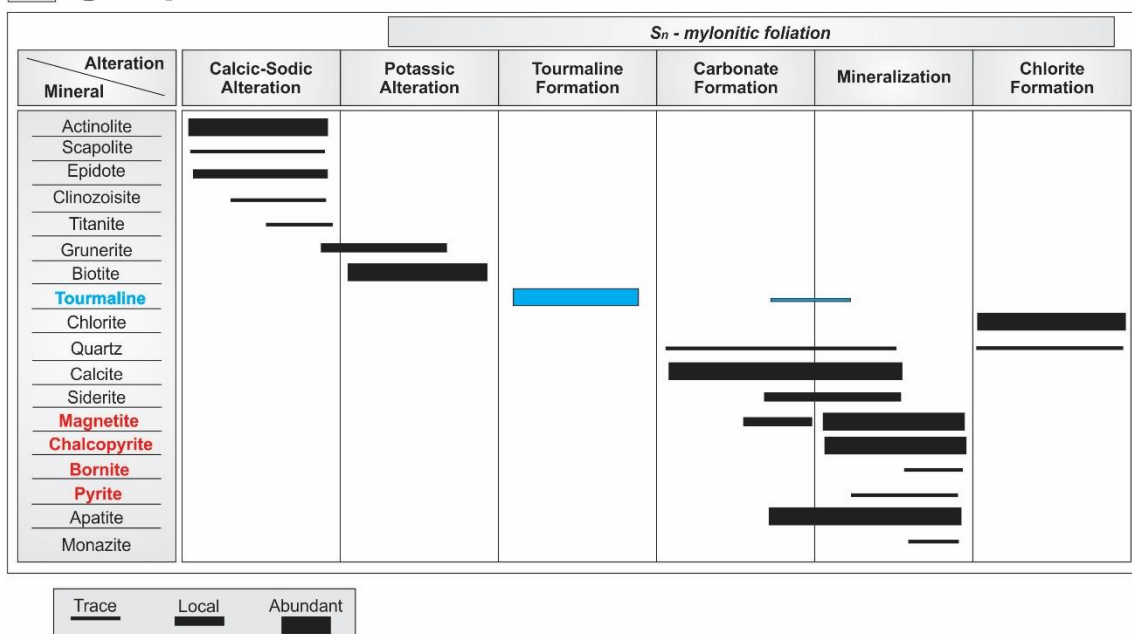


Fig. 5. Paragenetic tables with evolution of the hydrothermal systems at a) Grotá Funda and b) Igarapé Bahia deposits. Blue bars highlight the temporal position of tourmaline. Modified from Hunger (2017), Melo et al. (in prep.).

Tourmaline Occurrences

In the Salobo deposit, tourmaline is a conspicuous mineral within zones of intense iron-enrichment, pre-dating the mineralization. Tourmaline occurs as porphyroblasts within zones with grunerite and minor almandine (Fig. 6A). These tourmaline crystals commonly exhibit poikiloblastic texture with grunerite inclusions.

Biotite and quartz crystals frequently composed shadow pressure around tourmaline. In these zones, tourmaline crystals show corrosion textures and are rotated. Tourmaline composition ranges from schorl to dravite (Xavier et al., 2008). It is common the presence of zoned tourmaline (Fig. 6B). Minor tourmaline is later and synchronous with biotite formation.

Tourmaline (I) grains from the GT-46 deposit commonly occur in almandine–biotite schists, as tiny inclusions in poikiloblastic almandine or, rarely, as fine-grained crystals along S_n foliation. Tourmaline (II) is associated with coarse-grained garnet (II), spatially related with pegmatitic intrusions (Fig 6C), which crosscut all foliation planes and was formed in the latest alteration stage, related to the mineralization stage (II). In the analyzed sample, tourmaline (II) occurs infilling garnet (II) fractures (Fig 6D).

In the Furnas deposit, bluish tourmaline (I) is coeval with silicification. Tourmaline (II) formation is syn to post potassic alteration and temporally associated with tiny coalescent almandine crystals. Tourmaline (II) crystal is brownish, medium-grained and zoned, dispersed within a biotite matrix along the mylonitic foliation (S_{n+1}) (Fig. 6E). Tourmaline (II) was chosen to be analyzed.

Two generations of tourmaline were recognized at Grota Funda. The first generation is associated with potassic alteration with biotite along the mylonitic foliation. Tourmaline (II) is found as coarse-grained grains dispersed within chlorite (II)-rich rocks associated with quartz, magnetite and carbonate (Fig. 6F, G). Massive zones of chalcopyrite (III) are related to this tourmaline generation. The latter was analyzed.

Tourmaline is widespread in outer and inner parts of the Igarapé Bahia deposit and is recognized in its four orebodies. It occurs as fine to medium-grained crystals synchronous with carbonate formation and previous to the mineralization (Fig. 6H). These crystals are often set in the carbonate matrix and replaced by later chlorite and quartz. It is also common the presence of zoned tourmaline crystals. Tourmaline composition usually ranges from schorl to dravite (Xavier et al., 2008). Zonation is clear under transmitted light in the optical microscope (Fig. 6I) and in backscattered images.

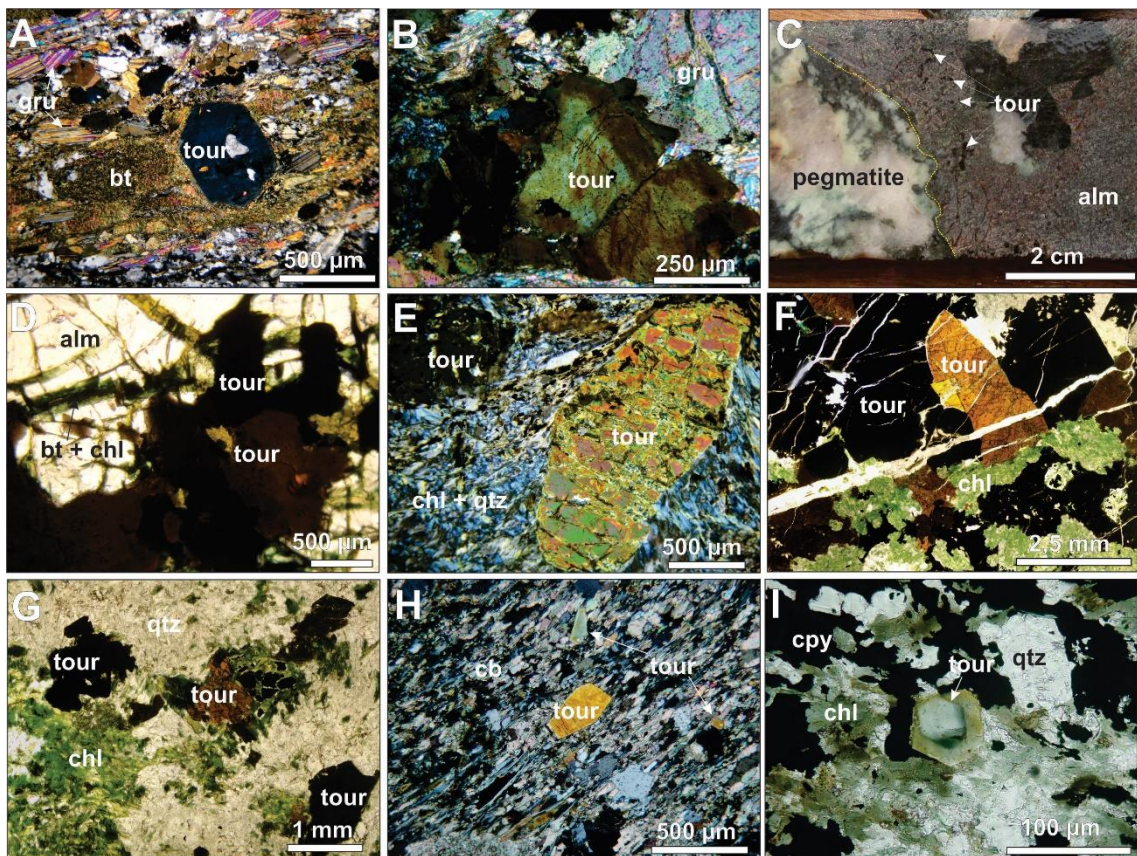


Fig. 6. Fotomicrographs of representative tourmaline crystals within IOCG deposits of the northern sector of the Carajás Province. a) Tourmaline porphyroblast outlined by later biotite at Salobo deposit. b) Zoned tourmaline crystal within Fe-rich zones with grunerite at Salobo deposit. c) Fine tourmaline grains within coarse garnet crystals spatially related to pegmatitic intrusions at GT-46 deposit. d) Tourmaline within fractures in the almandine crystals associated with biotite and chlorite infills in the GT-46 deposit. e) Fractured coarse-grained tourmaline (II) within (biotite)-chlorite-quartz matrix at Furnas deposit. f) Tourmaline-rich rock with coarse-grained tourmaline crystals associated with chlorite at Grota Funda deposit. g) Tourmaline crystals set within zones with chlorite and quartz at Grota Funda deposit. h) Mylonitic carbonate-tourmaline-bearing rocks with tourmaline crystals along the mylonitic foliation at Igarapé Bahia deposit. i) Zoned tourmaline crystal associated with chalcopyrite at Igarapé Bahia. Photos A, B, E and H are polarized light images; photos C, D, F and G are natural light images. Abbreviations: alm = almandine, bt = biotite, cb = carbonate, chl = chlorite, cpy = chalcopyrite, gru = grunerite, qtz = quartz, tour = tourmaline.

Methods

Boron isotope analyses were carried out in the State Key Laboratory of Geological and Mineral Resources (GPMR), China University of Geosciences (CUG), China. A double polished thin section containing tourmaline samples were investigated by optical microscopy and SEM backscattered electron imaging, in order to select spots for laser ablation shots. Boron isotopic compositions of two tourmaline crystals were measured in situ using a Neptune Plus Laser Ablation Multi-Collector Inductively Coupled Plasma Mass Spectrometry (LA–MC–ICP–MS) and a matching New Wave UP193 laser ablation system. Detailed analytical procedures and data reduction followed those of Yang et al., (2015). Operating conditions consist of an energy density of 12 J/cm², 8 Hz repetition rates and spot diameters of 50 µm. Mass bias of the instrument and the fractionation of isotopes were calibrated using the standard-sample-bracketing method (SSB). The tourmaline IAEA B4 (Tonarini et al., 2003) was used as an external standard. Instrumental mass fractionation (IMF) and analytical quality were determined by replicate analyses of international tourmaline reference material IMR RB1 (Hou et al., 2010) and an in-house standard Dai ($\delta^{11}\text{B} = -13.6\text{\textperthousand}$). Individual uncertainty (2σ) for 100-cycle individual analyses was typically around 0.5‰. The reported $\delta^{11}\text{B}$ results were calculated relative to tourmaline IAE B4 of $\delta^{11}\text{B} = -8.71\text{\textperthousand}$ (Tonarini et al., 2003).

Boron isotopic composition of tourmaline

Analysis of boron isotopic composition were carried out on tourmaline from Salobo (n = 20), GT 46 (n = 6), Furnas (n = 17), Grota Funda (n = 15) and Igarapé Bahia (n = 20) deposits. The summary of boron isotope data is shown in table 1.

Table 1. Boron isotope data of tourmaline from Salobo, GT 46, Furnas, Grota Funda and Igarapé Bahia deposits.

Deposit	Spot	Grain	$^{11}\text{B}/^{10}\text{B}$	Error	$\delta^{11}\text{B}$	$2\sigma^2$
Salobo	FD177-1	1	4.6506	0.000195	+17.0	0.04
	FD177-2	1	4.648826	0.000199	+16.6	0.04
	FD177-3	1	4.649275	0.000209	+16.7	0.04
	FD177-4	1	4.599127	0.000216	+5.7	0.05
	FD177-5	1	4.58903	0.000211	+3.4	0.05
	FD177-6	1	4.590275	0.00022	+3.7	0.05
	FD177-7	1	4.610738	0.000224	+8.2	0.05
	FD177-8	1	4.646285	0.000255	+16.7	0.05
	FD177-9	2	4.646825	0.000214	+16.8	0.05
	FD177-10	2	4.638396	0.00022	+14.9	0.05
	FD177-11	2	4.646075	0.000208	+16.6	0.04
	FD177-12	2	4.598732	0.000189	+6.2	0.04
	FD177-13	2	4.597823	0.000204	+6.0	0.04
	FD177-14	3	4.646243	0.000199	+16.3	0.04
	FD177-15	3	4.646254	0.000201	+16.3	0.04
	FD177-16	3	4.64685	0.000221	+16.5	0.05
	FD177-17	3	4.64842	0.000214	+16.8	0.05
	FD177-18	3	4.592198	0.000194	+4.4	0.04
	FD177-19	3	4.601597	0.000252	+6.5	0.05
	FD177-20	3	4.600611	0.000216	+6.3	0.05
GT46	FD39-232-1	1	4.59957	0.00022	+6.4	0.05
	FD39-232-2	1	4.59878	0.00022	+6.2	0.05
	FD39-232-3	1	4.59354	0.00023	+5.1	0.05
	FD39-232-4	1	4.59616	0.00023	+5.7	0.05
	FD39-232-5	2	4.59344	0.00023	+5.1	0.05
	FD39-232-6	2	4.59799	0.00022	+6.1	0.05
Furnas	FD39-119-1	1	4.64196	0.00019	+15.2	0.04
	FD39-119-2	1	4.64317	0.000241	+15.4	0.05
	FD39-119-3	1	4.639779	0.000227	+14.7	0.05
	FD39-119-4	1	4.6378	0.000235	+14.3	0.05
	FD39-119-5	1	4.639401	0.000217	+14.6	0.05
	FD39-119-6	1	4.641474	0.000217	+15.1	0.05
	FD39-119-7	1	4.641745	0.000212	+15.1	0.05
	FD39-119-8	2	4.639369	0.000221	+15.0	0.05
	FD39-119-9	2	4.640624	0.000203	+15.3	0.04
	FD39-119-10	2	4.645408	0.000222	+16.4	0.05
	FD39-119-11	2	4.64125	0.000229	+15.5	0.05
	FD39-119-12	2	4.63736	0.000219	+14.6	0.05
	FD39-119-13	2	4.640434	0.000222	+15.3	0.05
	FD39-119-14	2	4.644818	0.000247	+16.3	0.05
	FD39-119-15	2	4.649257	0.00022	+17.2	0.05
	FD39-119-16	3	4.630424	0.000209	+13.1	0.05
	FD39-119-17	3	4.639549	0.000202	+15.1	0.04

Grota Funda	1093-1	1	4.63897	0.000231	+13.6	0.05
	1093-2	1	4.623945	0.00022	+10.3	0.05
	1093-3	1	4.625591	0.000213	+10.8	0.05
	1093-4	1	4.62179	0.000202	+10.0	0.04
	1093-5	1	4.627106	0.000201	+11.2	0.04
	1093-6	1	4.619879	0.000216	+9.6	0.05
	1093-7	2	4.622403	0.000224	+10.3	0.05
	1093-8	2	4.622117	0.000214	+10.3	0.05
	1093-9	2	4.619563	0.000207	+9.7	0.04
	1093-10	2	4.622221	0.000208	+10.3	0.05
	1093-11	2	4.625029	0.000197	+11.1	0.04
	1093-12	2	4.623277	0.000216	+10.8	0.05
	1093-13	2	4.625459	0.000229	+11.2	0.05
	1093-14	2	4.611471	0.00243	+8.2	0.05
	1093-15	2	4.617163	0.000207	+9.4	0.04
Igarapé Bahia	FD173-1	1	4.640263	0.000178	+8.9	0.04
	FD173-2	1	4.638206	0.000309	+8.7	0.07
	FD173-3	1	4.62466	0.000169	+5.7	0.04
	FD173-4	1	4.648385	0.000206	+11.0	0.04
	FD173-5	1	4.618961	0.000159	+4.5	0.03
	FD173-6	2	4.613943	0.000209	+3.5	0.05
	FD173-7	2	4.66436	0.000179	+14.6	0.04
	FD173-8	2	4.65632	0.000218	+12.8	0.05
	FD173-9	2	4.660758	0.0002	+13.8	0.04
	FD173-10	2	4.642165	0.000309	+9.7	0.07
	FD173-11	3	4.649456	0.000162	+11.6	0.03
	FD173-12	3	4.652475	0.000164	+12.3	0.04
	FD173-13	4	4.622627	0.000187	+5.7	0.04
	FD173-14	4	4.662642	0.00016	+14.5	0.03
	FD173-15	4	4.65857	0.000153	+13.6	0.03
	FD173-16	4	4.612181	0.000162	+3.4	0.04
	FD173-17	5	4.648557	0.000157	+11.4	0.03
	FD173-18	5	4.64108	0.000487	+9.8	0.10
	FD173-19	5	4.633684	0.000183	+8.1	0.04
	FD173-20	5	4.653464	0.000159	+12.5	0.03

In general, positive $\delta^{11}\text{B}$ values (+3.4 to +17.2) in tourmaline are recognized among the deposits (Fig. 7). Considering each deposit, there is no compelling variation of the $\delta^{11}\text{B}$ values in tourmaline. However, in the Salobo and Igarapé Bahia deposits, significant differences in tourmaline core and rim analyses are likely observed.

At Salobo deposit, tourmaline exhibits $\delta^{11}\text{B}$ values ranging from +3.4 to +17.0‰ (Fig. 8A, B). There is a significant difference in the boron isotopic composition of tourmaline core and rim, even though the crystal zonation is not clear in the

petrography. Whereas cores display higher $\delta^{11}\text{B}$ values ranging from +14.9 to +17.0‰, tourmaline rims exhibit $\delta^{11}\text{B}$ values from +3.4 to +8.2‰.

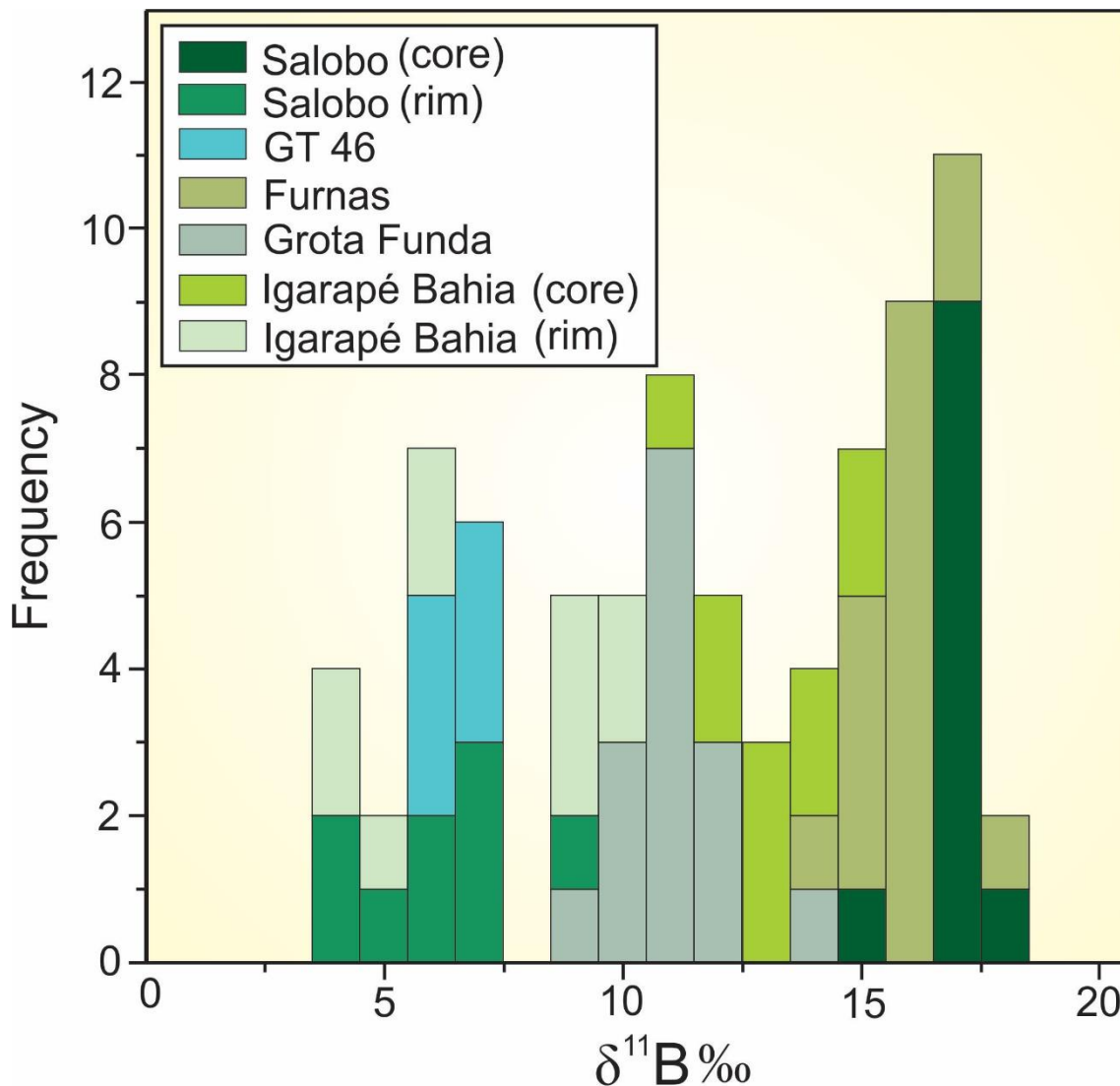


Fig. 7. Histogram with $\delta^{11}\text{B}$ values of tourmaline from the Salobo, GT 46, Furnas, Grota Funda and Igarapé Bahia deposits.

Tourmaline infilling in coarse almandine related to pegmatites from the GT-46 deposit has the narrowest variation of the $\delta^{11}\text{B}$ values (+5.1 to +6.4‰; Fig. 8C, D) of all analyzed samples. In the Furnas deposit, in contrast, the highest $\delta^{11}\text{B}$ values are recorded. The $\delta^{11}\text{B}$ values of tourmaline (II), associated with potassic alteration, range from +13.1 to +17.2‰ (Fig. 8E, F).

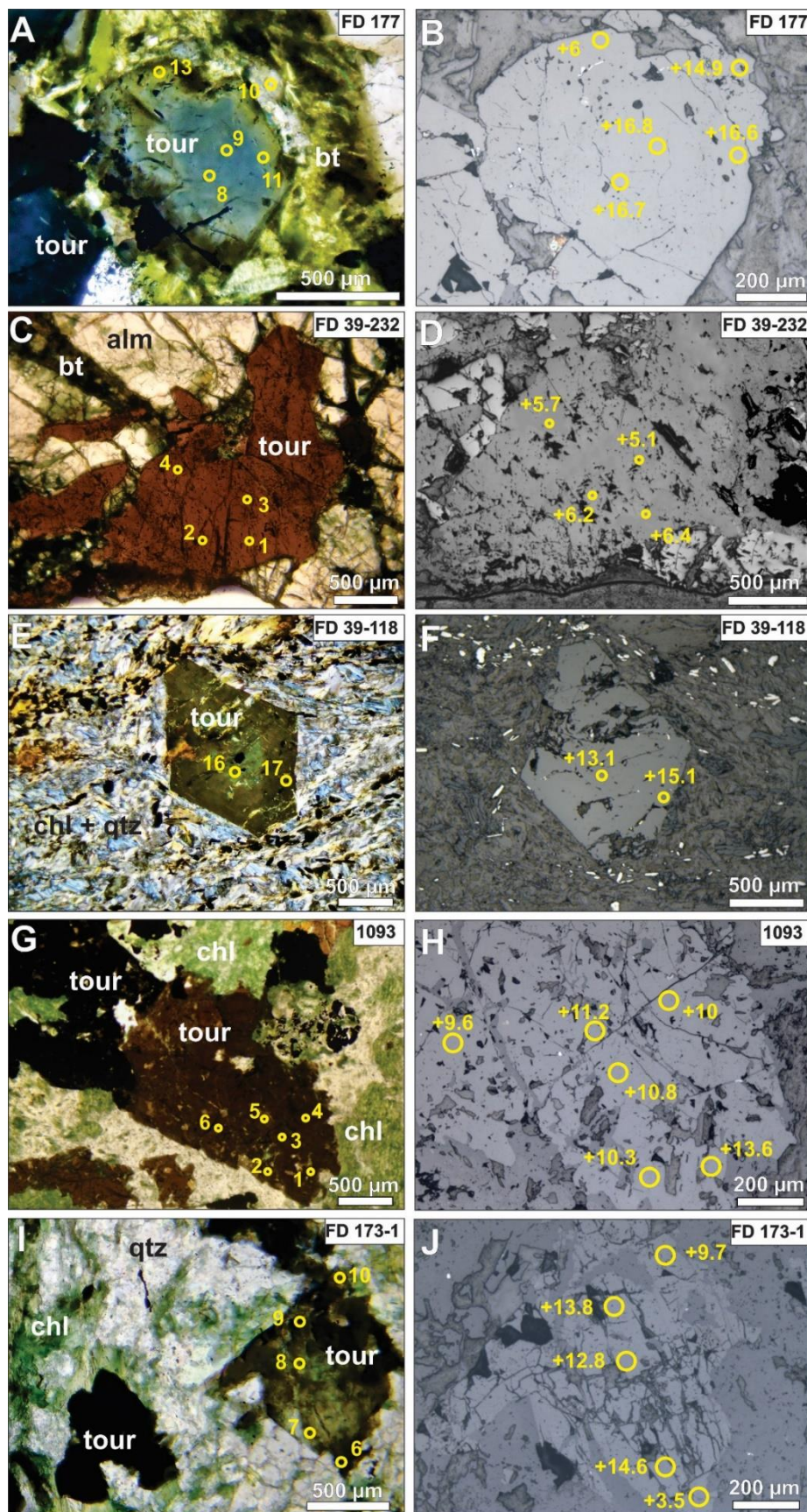


Fig. 8. Polarized light image with spot numbers and backscattered images with $\delta^{11}\text{B}$ values of each spot in a) Zoned tourmaline with later biotite in its rims at Salobo with associated spot

numbers. b) Backscattered image with $\delta^{11}\text{B}$ values of tourmaline in the Salobo deposit. c) Tourmaline within almandine at GT 46 with spot numbers. d) Backscattered image with $\delta^{11}\text{B}$ values of tourmaline in the GT-46 deposit. e) Tourmaline porphyroblast within chlorite–biotite-rich zones with spot numbers at Furnas. f) Backscattered image with $\delta^{11}\text{B}$ values of tourmaline in the Furnas deposit. g) Tourmaline grains within chlorite-rich zones at Grota Funda with spot numbers. h) Backscattered image with $\delta^{11}\text{B}$ values of tourmaline in the Grota Funda deposit. i) Tourmaline crystals replaced by later chlorite in the Igarapé Bahia deposit with spot numbers. j) Backscattered image with $\delta^{11}\text{B}$ values of tourmaline in the Igarapé Bahia deposit.

Abbreviations: *alm* = almandine, *bt* = biotite, *chl* = chlorite, *qtz* = quartz, *tour* = tourmaline.

In the Grota Funda deposit, tourmaline crystals show intermediary $\delta^{11}\text{B}$ values (+8.2 and +13.6‰; Fig. 8G, H). At Igarapé Bahia, tourmaline from the Alemão orebody was chosen to be analyzed. The common zonation observed in the tourmaline crystals is also recorded in their boron isotopic composition. Tourmaline cores display higher $\delta^{11}\text{B}$ values between +11.0‰ and +14.6‰, whereas rims record lower values ranging from +3.4 to +9.8‰ (Fig. 8I, J).

Discussions

Sources of boron and evolution of associated hydrothermal fluids

Tourmaline can preserve its boron isotopic signature during deformation and recrystallization from diagenetic and low-grade metamorphism to (ultra)-high pressure metamorphism (Marschall et al., 2009; Henry et al., 2012), but not during high-fluid-flux events (Marschall and Jiang, 2011). Thus, the interpretation of boron isotope signatures in tourmaline from the IOCG deposits of Carajás must be cautious, since they experienced a long history of successive hydrothermal and deformational events.

Most of the analyzed tourmaline crystals were sampled from mylonitic rocks related to ductile deformation due to shear zone development or reactivation (i.e. Cinzento and Carajás Shear Zones). In the GT-46 deposit, however, tourmaline (II) grains are spatially associated with pegmatite intrusions and bear no relationship with ductile deformation.

The high $\delta^{11}\text{B}$ values recorded in hydrothermal tourmaline from Salobo, Furnas, Grota Funda, and Igarapé Bahia deposits are close to those of the fields of marine evaporites, marine carbonates, and submarine hydrothermal fluids (Fig. 9). Modern seawater and evaporated seawater usually show even higher $\delta^{11}\text{B}$ values, close to 40‰

(Barth 1993, Marschall and Jiang, 2011). Although the Precambrian boron isotopic evolution of seawater remains unconstrained up to the late Neoproterozoic (Marschall, 2018), seawater likely represented the main reservoir of isotopically heavy boron even in the Archean (Chaussidon and Appel, 1997; Grew et al. 2015).

Bittern fluids and evaporated seawater brines could represent a source for both boron and hypersalinity of the ore-forming fluids. However, to form these hypersaline fluids it is necessary to have seawater trapped in a semi-closed coastal plain (evaporite platform; Nichols, 1999) with continuous evaporation and likely precipitation of evaporites. Evaporite rocks and shallow-water sedimentary rocks were not found within the sedimentary record related to the main metavolcanosedimentary sequences at Carajás (i.e. Rio Novo Group, Itacaiúnas Supergroup, and Águas Claras Formation). This may suggest that the geological scenario of the Carajás Province did not allow the generation of evaporative fluids. However, we cannot rule out this possibility, once the extension and geology of the basin are still poorly characterized. In this case, however, more investigation must be done to confirm the presence of shallow water sedimentary facies, which could have allowed the circulation of these fluids.

High $\delta^{11}\text{B}$ values in tourmaline were previously reported by Xavier et al. (2008) in the Salobo (+14.5 to +24‰) and Acampamento Sul (+14 to +26‰) orebody of the Igarapé Bahia deposit. These results were assigned to the participation of initial hydrothermal fluids that interact with marine evaporites. Thus, this was interpreted as an evidence of participation of evaporites in the evolution of the IOCG system. Cl/Br and Na/Cl ratios in fluid inclusions of several IOCG deposits at Carajás, in contrast, have demonstrated the importance of residual evaporated seawater as one of the sources for the ore-forming fluids, but excluded the possibility of fluids originated from halite dissolution (Xavier et al., 2009).

Nevertheless, the high $\delta^{11}\text{B}$ values characterized in those deposits clearly demonstrate the participation of externally-derived sources for boron. This likely points to contribution of submarine hydrothermal fluids in the mineral system.

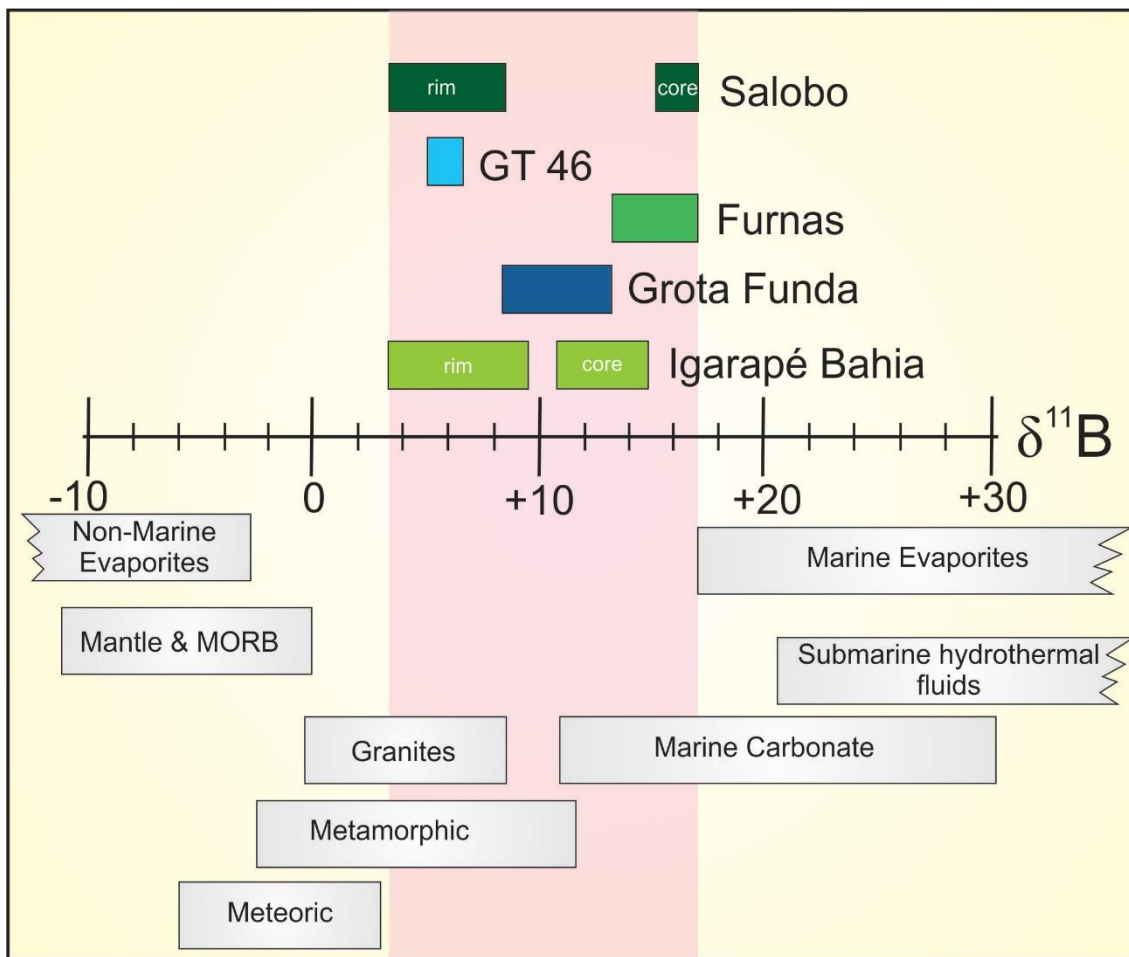


Fig. 9. Distribution of the $\delta^{11}\text{B}$ values of tourmaline from the IOCG deposits of the northern sector and main boron reservoirs. Data extracted from Barth (1993), Marschall and Jiang (2011), Hinsberg et al. (2011).

The presence of an extensive submarine hydrothermal system generating fluids can explain the high $\delta^{11}\text{B}$ values of these tourmaline grains. In this case, these exhalative fluids might have been originated from seawater circulation and fluid-rock interaction in sub seafloor. During this interaction, the incoming seawater (with $\delta^{11}\text{B}$ as high as +40‰) leaches the isotopically light boron from the mafic crust (Marshall 2018). In this process, the convective fluids ascend and are expelled from hydrothermal vents. Those modified seawater-derived fluids may have boron isotopic composition near +17.8‰ (Marshall, 2018). On the other hand, low-temperature alteration by seawater leads to an ^{11}B -enriched isotopic signature in the volcanic rocks compared to unaltered MORB, resulting in $\delta^{11}\text{B}$ values of up to +25‰ (Marshall, 2018).

The evidence of participation of an important ^{11}B -enriched fluid become clearer when considering the boron isotopic signature of the hydrothermal fluids in equilibrium

with tourmaline of each deposit. ^{11}B preferentially fractionates into the fluids and isotope boron fractionation between mineral and fluid increases with temperature decrease (Palmer et al., 1992; Meyer et al., 1992). Due to this fractionation process, there are significant differences in the $\delta^{11}\text{B}$ values of high-temperature fluids and tourmaline (Meyer et al., 2008). It can reach $-2\text{\textperthousand}$ to $-3\text{\textperthousand}$ at $750\text{ }^{\circ}\text{C}$ or even higher fractionation ($-6\text{\textperthousand}$) under lower temperature conditions ($350\text{ }^{\circ}\text{C}$) at 200 MPa (Palmer et al., 1992). Meyer et al. (2008), in contrast, proposed that typical boron isotope fractionation between mineral–fluid is $-4.2\text{\textperthousand}$.

In contrast, low $\delta^{11}\text{B}$ values are also recognized within these deposits, especially at GT-46 (+5.1 to +6.4‰), Salobo (+3.4 to +8.2‰) and Igarapé Bahia (+3.4 to +9.8‰). In the GT-46 deposit, there is a spatial connection between tourmaline (II) grains and pegmatite intrusions. Tourmaline from the GT-46 deposit, therefore, records a strong evidence of boron derived from magmatic fluids, due to both textural-spatial evidences and its boron isotopic signature.

Boron isotope composition in I-type (mean $\delta^{11}\text{B} = -2\text{\textperthousand}$), A-type ($\delta^{11}\text{B} = -7\text{\textperthousand}$), and S-type ($\delta^{11}\text{B} = -11\text{\textperthousand}$) magma and granites reflects typically ^{11}B -depleted signatures (Trumbull and Slack, 2018). However, an aqueous fluid exsolved from silicate magma, and any hydrothermal tourmaline formed from it, will be enriched in ^{11}B relative to the starting melt (Trumbull and Slack, 2018).

In addition, a remarkable feature of Salobo and Igarapé Bahia is the presence of zoned tourmaline crystals with core-to-rim decrease in $\delta^{11}\text{B}$ values. Whereas cores are enriched in ^{11}B (+11.0‰ to +17‰), the rims display lower $\delta^{11}\text{B}$ values (+3.4‰ to +9.8‰), which overlap those of pegmatite-related tourmaline.

Hydrothermal and metamorphic tourmaline may record boron isotopic zonation. Similar patterns of decrease of $\delta^{11}\text{B}$ values towards tourmaline rims are attributed to loss of ^{11}B to the fluid phase during prograde metamorphism. However, isotopic zoning might also result of introduction of isotopically light boron from later fluids (Trumbull and Slack, 2018). This process may be also important during the evolution of a hydrothermal system.

During hydrothermal process, the heavy boron isotope, ^{11}B , tends to fractionate to the fluid during fluid–tourmaline reaction. The continuous crystallization of tourmaline results in fluids increasingly heavier concerning boron. Thus, large tourmaline crystals, likely zoned, tend to be more heterogeneous, with lower $\delta^{11}\text{B}$

values in the cores and higher ones in the rims (Meyer et al., 2008). This is the opposite observed in tourmaline grains at Salobo and Igarapé Bahia.

Therefore, the low $\delta^{11}\text{B}$ values recorded at GT-46 and in the tourmaline rims of Salobo and Igarapé Bahia can reflect its formation from a distinct boron source. This excludes the possibility of an evolution from a single fluid. The participation of ^{11}B -depleted magmatic brines could explain the low $\delta^{11}\text{B}$ values recorded in these deposits, and also the intermediate $\delta^{11}\text{B}$ values of the Grotá Funda deposit.

At the Acampamento Norte orebody, similar $\delta^{11}\text{B}$ values (+5.8‰ to +8.8‰) have been already reported (Xavier et al., 2008), indicating that magmatic brines are also present in the others orebodies of the Igarapé Bahia deposit. Similarly, relatively low $\delta^{11}\text{B}$ values were also recorded in tourmaline from the Pista orebody of the Sossego deposit ranging from -8.1 to +11.2‰. These data were interpreted as mixed sources including isotopically light boron leached from felsic intrusive and volcanic rocks and heavy boron inherited from marine evaporites (Xavier et al., 2008). However, these data could also point to contribution of magmatic brines as the source of boron.

Implications for the IOCG metallogenesis in the Carajás Province

Boron isotopic data point to the presence of hydrothermal fluids associated with submarine hydrothermal fluids. These fluids formed and circulated within a sedimentary basin for a long period during the establishment of exhalative systems in deep-water. This geological setting is in accordance to previous studies that showed the involvement of deep-seated sedimentary rocks and development of exhalative hydrothermal systems at the seafloor (Dreher et al., 2008; Schwarz & Frantz, 2013; Melo et al., in prep.). Precipitation of banded iron formation in this scenario also evidences an exhalative hydrothermal system (Isley, 1995; Bekker et al., 2010). Nonetheless, exhalative processes were intrinsically related to the metavolcanosedimentary Itacaiúnas Supergroup formed at ca. 2.76 to 2.73 Ga. There are no supracrustal rocks recognized at Carajás in ca. 2.5 Ga, which rules out the possibility of heavy boron sources at this time. The isotopic signature of tourmaline with high $\delta^{11}\text{B}$ values recorded in the IOCG deposits, therefore, might be acquired from the Neoarchean Itacaiúnas metavolcanosedimentary sequences.

Thus, the ^{11}B -enriched composition of tourmaline may reflect a complex history of fluid-rock interaction. Its boron isotope composition could have been inherited at ca.

2.5 Ga from hydrothermal fluids that leached ^{11}B from volcanic rocks altered by seawater at ca. 2.76 – 2.73 Ga.

The Salobo, Grotá Funda and Igarapé Bahia deposits record their main IOCG mineralization event at ca. 2.5 Ga. However, we cannot rule out the possibility that these deposits have an older metallogenetic history with overlapping of hydrothermal events. Nevertheless, some clues are still preserved within them. This older history may be recorded by the geochronological data from GT-46 (Re–Os in molybdenite, $2,718 \pm 56$ Ma), Salobo (Pb–Pb in chalcocite, $2,705 \pm 42$ Ma, Tassinari et al., 2003) and Igarapé Bahia (Pb–Pb in gold, $2,744 \pm 12$ Ma; Pb–Pb in chalcopyrite, $2,772 \pm 46$ Ma; $2,754 \pm 36$ Ma, $2,756 \pm 24$ Ma, $2,777 \pm 22$ Ma; Galarza et al., 2008). Although of unknown age, the Furnas deposit also display the similar source for the B^{11} -enriched fluids.

The IOCG deposits at Carajás experienced a protracted metallogenetic evolution with successive episodes of hydrothermalism (Moreto et al., 2015a, 2015b). Thus, it is possible that hydrothermal minerals (e.g. tourmaline cores) in the IOCG deposits were formed during the Neoarchean (2.76 – 2.73 Ga) and preserved even in high-temperature hydrothermal systems at ca. 2.5 Ga. Evidences of transposed metamorphic foliations, which are pre-kinematic in relation to shear zone development, were reported in the GT-46 and Furnas deposits (Jesus, 2016; Toledo 2017). Thus, metamorphic assemblages, including a boron-retentive mineral, such as tourmaline, were likely formed prior to the ca. 2.5 Ga metallogenetic event. This also reinforces that those deposits are part of a long lasting mineral system.

Magmatic brines were claimed to explain the relatively low $\delta^{11}\text{B}$ values in tourmaline at GT-46, Salobo and Igarapé Bahia deposits and intermediate values at Grotá Funda deposit. Tourmaline at GT-46 seems to be genetically linked with pegmatite and granite intrusions crystallized at $2,562 \pm 39$ Ma (Toledo, 2017). This connection and the boron isotopic signature might comprise the strongest evidence of tourmaline crystallizing from magmatic fluids. These ages may not be connected with the main mineralization stage at GT-46 (i.e. Re–Os in molybdenite, $2,718 \pm 56$ Ma, Toledo, 2017), but they represent recurrences of hydrothermal pulses, likely associated with magmatic brines.

Granitic magmatism might be associated with an important, regional-scale, tectono-thermal event (Machado et al., 1991; Barbosa, 2004; Melo et al., 2016). Some authors suggested that granitic magmatism at this period played an important role in the IOCG formation (Réquia et al., 2003; Tallarico et al., 2005).

Recent studies demonstrated that ore-forming fluids at Salobo and Igarapé Bahia show a strong magmatic component (Melo et al., in prep). The ca. 2.5 Ga granites may have exsolved a fluid phase under higher pressure conditions in deeper portions of the crust (Pollard, 2006) and ascended by regional-scale shear zones. Magmatic fluids have already been recognized in the IOCG deposits of the Southern Copper Belt (i.e. Sossego, Bacaba, Bacuri and Visconde deposits; Monteiro et al., 2008, Pestilho, 2011; Silva et al., 2015), but in this case developed at ca. 2.7 Ga.

Therefore, tourmaline in these IOCG deposits had boron sources from i) 2.76 – 2.73 Ga submarine hydrothermal fluids, and at ii) 2.57 Ga magmatic brines responsible for tourmaline crystallization.

Boron sources and IOCG deposits in the world

Tracing the origin of the ore-forming fluids for the IOCG deposits in the world have been a challenge task in the last years. Several studies point to the contribution of different sources for the ore-forming fluids, including externally-derived and magmatic brines (Chiaradia et al., 2006; Hunt et al., 2007; Xavier et al., 2008, 2009; Chen et al., 2011; Tornos et al., 2016).

The boron isotopic data obtained in this study for the IOCG deposits from Carajás show the highest $\delta^{11}\text{B}$ values amongst the IOCG deposits in the world. The exception is the Pista orebody at Sossego deposit, which show $\delta^{11}\text{B}$ values between -8.1 and +11.2‰ (Xavier et al., 2008). In the Andean IOCG deposits, including Carola, Candelaria, Silvia and Tropezon deposits, $\delta^{11}\text{B}$ values ranging from -10.4 to +6‰ were recorded (Tornos et al., 2012). These results were assigned to the development of large magmatic–hydrothermal system that provided the boron for the deposits (Tornos et al., 2012). The Andean IOCG deposits share a common boron source with coeval porphyry copper deposits (Tornos et al., 2012). In the IOCG deposits from Kangdian region, SW China, different stages of tourmaline formation and $\delta^{11}\text{B}$ values were characterized (stage I = -14.7 to -5.7‰, stage II = -11.6 to -6.0‰, stage III = -4.4 to -0.6‰, stage IV = +2.9 to +5.9‰,), showing that ore-forming fluids were initially derived from magmatic sources, but later influx of non-magmatic fluids was essential for sulfide mineralization (Zhi-Kun et al., 2016).

Externally-derived brines associated with evaporitic sequences are also reported for other IOCG deposits. The Wernecke IOCG deposit, at Yukon Territory, Canada, represents a typical non-magmatic IOCG deposit and is hosted by evaporitic sequences

(Hunt et al., 2007). Brines derived from evaporitic sequences are considered the main ore-forming fluids (Hunt et al., 2007).

Boron isotopic data reinforces the complexity of the IOCG systems and suggest that a single fluid source is not applicable for their origin (Tornos et al., 2012; Zhi-Kun et al., 2016). Fluid mixing with participation of externally-derived and magmatic brines may be one of the key processes for the IOCG formation, especially for the world-class deposits. This hypothesis could also explain the discrepancies of boron isotopic signature of the IOCG deposits worldwide (Zhi-Kun et al., 2016), although these data are still scarce within these deposits.

In the Carajás Province, however, the history of tourmaline formation in the IOCG deposits was probably more complex. Boron isotopic data obtained in this study reveal different episodes of tourmaline crystallization and overgrowing separated in time. In this context, hydrothermal events developed at ca. 2.76–2.73 Ga and ca. 2.57 Ga evidence different boron sources, related to modified seawater and magmatic fluids, respectively.

Conclusions

The boron isotopic data obtained in tourmaline from different IOCG deposits of the northern sector of Carajás Domain reveal the predominance of ^{11}B -rich tourmaline at Salobo (core, +14.9 to +17.0‰), Furnas (+13.1 to +17.2‰), Grota Funda (+8.2 to +13.6‰) and Igarapé Bahia (core, +11.0‰ to +14.6‰). These data suggest that submarine hydrothermal fluids or evaporated seawater brines circulated in regional-scale. This isotopic signature in the ca. 2.5 Ga IOCG deposits (i.e. Salobo, Igarapé Bahia, GT-46 and Grota Funda) may have been inherited from preexisting tourmaline formed in the Neoarchean, likely synchronous with deposition of the metavolcanosedimentary Itacaiúnas Supergroup (i.e. 2.76 – 2.74 Ga) or during its metamorphism. In contrast, relatively low $\delta^{11}\text{B}$ values in tourmaline are also recognized at Salobo (rim, +3.4 to +8.2‰), Igarapé Bahia (rim, +3.4 to +9.8‰) and GT-46 (+5.1 to +6.4‰) deposits. In this case, magmatic brines could be the responsible for the tourmaline crystallization at GT-46 and tourmaline overgrowing at Salobo and Igarapé Bahia. Exsolution of magmatic brines from granitic intrusions in ca. 2.5 Ga associated with a tectonic event comprise an important metallogenetic event at this period. The discrepancies found for boron isotopes in the IOCG deposits worldwide suggest that a

singular source of boron, metals and ore-forming fluids is not applicable to explain the IOCG ore genesis.

References

- Araújo, O.J.B., Maia, R.G.N., 1991. Serra dos Carajás: folha SB.22-Z-A, Estado do Pará, Escala 1:250.000. Texto explicativo. DNPM/CPRM. 164 p.
- Barros, C.E.M., Sardinha A.S., Barbosa J.P.O., Macambira M.J.B., 2009. Structure, Petrology, Geochemistry and zircon U/Pb and Pb/Pb geochronology of the synkinematic Archean (2.7 Ga) A-type granites from the Carajás Metallogenic Province, northern Brazil: Canadian Mineralogist 47, 1423-1440.
- Barth, S., 1993. Boron variations in nature: A synthesis: Geologische Rundschau 82, 640–651.
- Barton, M.D., Johnson, D.A., 2000. Alternative brine sources for Fe-oxide (-Cu-Au) systems: implications for hydrothermal alteration and metals. In: Porter, T.M. (Ed.), Hydrothermal Iron Oxide Copper-Gold & Related Deposits: A Global Perspective. Adelaide, pp. 43–60.
- Barton, M.D., Johnson, D.A., 1996. Evaporitic-source model for igneous-related Fe oxide-(REE–Cu–Au–U) mineralization: Geology 24, 259–262.
- Bekker, A., Slack, F.F., Planavsky, N., Krapez, B., Hofmann, A., Konhauser, K.O., Rouxel, O.J., 2010. Iron Formation: The sedimentary product of a complex interplay among mantle, tectonic, oceanic, and biospheric processes. Economic Geology 105, 467 – 508.
- Chaussidon, M., Appel, P.W.U., 1997. Boron isotopic composition of tourmalines from the 3.8-Ga-old Isua supracrustals, West Greenland: implications on the $\delta^{11}\text{B}$ value of early Archean seawater. Chemical Geology 27, 171-180.
- Chen, H., Kyser, T.K., Clark, A.H., 2011. Contrasting fluids and reservoirs in the contiguous Marcona and Mina Justa iron oxide–Cu (–Ag–Au) deposits, south-central Perú: Mineralium Deposita, v. 46, p. 677-706.
- Delinardo da Silva, M.A., 2014. Metatexitos e diatexitos do Complexo Xingu na região de Canaã dos Carajás: Implicações para a evolução mesoarqueana do Domínio Carajás, PA. Unpublished MSc. Thesis, Campinas, University of Campinas.
- Chiadria M, Banks D, Cliff R, 2006. Origin of fluids in iron oxide-copper-gold deposits: Constraints from $\delta^{37}\text{Cl}$, $87\text{Sr}/86\text{Sr}$ and Cl/Br. Mineralium Deposita 41, 565–573.
- DOCEGEO, 1988, Revisão litoestratigráfica da Província Mineral de Carajás - Litoestratigrafia e principais depósitos minerais: 35th Congresso Brasileiro de Geologia, Belém. (Proceedings).

- Dreher, A.M., Xavier, R.P., Taylor, B.E., Martini, S., 2008. New geologic, fluid inclusion and stable isotope studies on the controversial Igarapé Bahia Cu-Au deposit, Carajás province, Brazil: *Mineralium Deposita* 43, 161–184.
- Dreher, A.M., Xavier, R.P., Taylor, B.E., Martini, S., 2005, Fragmental rocks of the Igarapé Bahia Cu-Au deposit, Carajás Mineral Province, Brazil: *Revista Brasileira de Geociências* 35(3), 359–368.
- Dutrow, B.L., Henry, D.J., 2011. Tourmaline: a geologic DVD. *Elements* 7, 301–306.
- Feio, G.R.L., Dall’Agnol, R., Dantas, E.L., Macambira, M.J.B., Gomes, A.S., Sardinha, D.C., Oliveira, D.c., Santos, R.D., Santos, P.A., 2012, Geochemistry, geochronology, and origin of the Neoarchean Planalto Granite suite, Carajás, Amazonian craton: A-type or hydrated charnockitic granites? *Lithos* 151, 57 – 73.
- Feio, GRL, Dall’Agnol R., Dantas, E.L., Macambira, M.J.B., Santos, J.O.S., Althoff, F.J., Soares, J.E.B., 2013. Archean granitoid magmatism in the Canaã dos Carajás area: implications for crustal evolution of the Carajás province, Amazonian craton, Brazil: *Precambrian Research* 227, 157-185.
- Gibbs, A.K., Wirth K.R., Hirata W.K., Olszewski Jr., W.J., 1986. Age and composition of the Grão Pará Group volcanics, Serra dos Carajás: *Revista Brasileira de Geociências* 16, 201–211.
- Grew E.S., Dymek, R.F., DeHoog, J.C.M., Harley, S.L., Boak, J., Hazen, R.M., Yates, M.G., 2015. Boron isotopes in tourmaline from the ca. 3.7–3.8 Ga Isua supracrustal belt, Greenland: sources for boron in Eoarchean continental crust and seawater. *Geochim Cosmochim Acta* 163:156–177
- Hawthorne, F.C., Henry, D.J., 1999. Classification of the minerals of the tourmaline group. *Eur J Mineral* 11, 201–215
- Henry, D.J., Dutrow, B.L., 2012. Tourmaline at diagenetic to low-grade metamorphic conditions: Its petrologic applicability: *Lithos* 154, 16-32.
- Hirata, W.K., Rigon, J.C., Kadekaru, K., Cordeiro, A.A.C., Meireles, E.A., 1982. *Geologia Regional da Província Mineral de Carajás: 1st Simpósio de Geologia da Amazônia, Belém. (Proceedings)*
- Hou, K., Li., Y., Xiao, Y., Liu, F., Tian, Y., 2010. In Situ boron isotope measurements of natural geological materials by LA-MC-ICP-MS. *Chinese Science Bulletin*, 55, 3305–3311.

- Huhn, S.R.B., Macambira, M.J.B., and Dall'Agnol, R., 1999b. Geologia e geocronologia Pb-Pb do Granito Alcalino Planalto, Região da Serra do Rabo, Carajás-PA. Simpósio de Geologia da Amazônia, 6th, Sociedade Brasileira de Geologia-Núcleo Norte (SBG/NO), p. 463–466.7
- Hunger, R.B., 2016. O depósito de óxido de ferro-cobre-ouro (IOCG) Grotá Funda, Domínio Carajás (PA): alteração hidrotermal, regime de fluidos e idade da mineralização. Unpublished Master Dissertation, Campinas, University of Campinas, p. 91.
- Hunt, J., Baker, T., Thorkelson, D., 2007. A review of iron oxide copper-gold deposits, with focus on the Wernecke Breccias, Yukon, Canada, as an example of a non-magmatic end member and implications for IOCG genesis and classification: Exploration and Mining Geology, v. 16, p. 209–232
- Holdsworth, R., and Pinheiro, R., 2000. The anatomy of shallow-crustal transpressional structures: Insights from the Archean Carajás fault zone, Amazon, Brazil: Journal of Structural Geology, v. 22, p. 1105–1123.
- Isley, A.E., 1995. Hydrothermal plumes and the delivery of iron to banded iron formation. Journal of Geology. 103, 169–185.
- Jesus, S.S.G.P., 2016. Múltiplos estágios de alteração hidrotermal do depósito de óxido de ferro-cobre-ouro furnas, província carajás: evolução paragenética e química mineral. Unpublished Master Dissertation, São Paulo, University of São Paulo, p. 164.
- Lindenmayer, Z.G., Ronchi, L.H., and Laux, J.H., 1998. Geologia e geoquímica da mineralização de Cu-Au primária da mina de Au do Igarapé Bahia, Serra dos Carajás: Revista Brasileira de Geociências 28, 257–268.
- Lindenmayer, Z.G., Teixeira, J.B.G., 1999. Ore genesis at the Salobo copper deposit, Serra dos Carajás, *in* Silva, M.G., and Misi, A., eds., Base metal deposits of Brazil: MME/CPRM/DNPM, p. 33–43.
- Lindenmayer, Z. G., Fleck, A., Gomes, C.H., Santos, A.B.S., Caron, R., Paula, F.C., Laux, J.H., Pimentel, M.M., e Sardinha, A.S., 2005. Caracterização geológica do alvo estrela (Cu-Au), Serra dos Carajás, Pará In: Caracterização de Depósitos Minerais em Distritos Mineiros da Amazônia. DNPM, CT-Mineral / FINEP, ADIMB, CD-ROM, 2005, cap. IV, 1, 137-205.

- Lobato, L.M., Rosière, C.A., Silva, R.C.F., Zucchetti, M., Baars, F.J., Seoane, J.C.S., Rios, F.J., Pimentel, M., Mendes, G.E., and Monteiro, A.M., 2005. A mineralização hidrotermal de ferro da Província Mineral de Carajás, controle estrutural e contexto na evolução metalogenética da Província, *in* Marini, J.O., Queiróz, E.T., and Ramos, W.B., eds., Caracterização de Distritos Mineiros da Amazônia” DNPM-CT-Mineral-ADIMB, p. 25–92.
- Marschall, H.R., 2018. Boron isotopes in the ocean floor realm and the mantle, *In* Marschall H.R., Foster, G., Boron isotopes. Advances in Isotope Geochemistry, Springer, p. 189-215.
- Marschall, H.R., Meyer, C., Wunder, B., Ludwig, T., Heinrich, W., 2009. Experimental boron isotope fractionation between tourmaline and fluid: confirmation from in situ analyses by secondary ion mass spectrometry and from Rayleigh fractionation modelling. *Contrib. Mineral. Petrol.* 158 (5), 675–681.
- Machado, N., Lindenmayer, D.H., Kroughe TE, Lindenmayer, Z.G., 1991, U-Pb geochronology of Archean magmatism and basement reactivation in the Carajás Area, Amazon Shield, Brazil: *Precambrian Research*, 49, 1–26.
- Meyer, C., Wunder, B., Meixner, A., Romer, R.L., Heinrich, W., 2008. Boron-isotope fractionation between tourmaline and fluid: an experimental re-investigation. *Contrib. Mineral. Petrol.* 156 (2), 259–267.
- Melo, G.H.C., Monteiro, L.V.S., Xavier, R.P., Moreto, C.P.N., In prep, The geology of the Igarapé Bahia deposit: host rocks, hydrothermal alteration and U-Pb geochronology of the Alemão, Acampamento Norte, Acampamento Sul and Furo 30 orebodies, Carajás Province (Brazil). To be submitted to *Ore Geology Reviews*
- Melo, G.H.C., Monteiro, L.V.S., Xavier, R.P., Moreto, C.P.N., Santiago, E.B.S., Dufrane, S.A., Aires, B., Santos, A.F.F., 2016, Temporal evolution of the giant Salobo IOCG deposit, Carajás Province (Brazil): constraints from paragenesis of hydrothermal alteration and U-Pb geochronology. *Mineralium Deposita* 52, 709-732.
- Mougeot, R., Respaut J.P., Briquel L., Ledru P., Milesi J.P., Macambira M.J.B., Huhn S.B., 1996, Geochronological constrains for the age of the Águas Claras Formation (Carajás Province, Pará, Brazil). *In: Cong. Bras. Geol.* 39, Anais., Salvador, SBG. 6:579-581.
- Moreto, C.P.N., Monteiro, L.V.S., Xavier RP, Creaser, R.A., Dufrane, S.A., Tassinari, C.C.G., Sato, K., Kemp, A.I.S., Amaral,W.S., 2015b. Neoarchean and Paleoproterozoic Iron Oxide-Copper-Gold events at the Sossego deposit, Carajás Province, Brazil, Re-Os and U-Pb geochronological evidence: *Economic Geology* 110, 809–835.
- Nichols, G., 1999, *Sedimentology and Stratigraphy*: Wiley-Blackwell Publishing, 456 p.

- Nogueira, A.C.R., Truckenbrodt W., Pinheiro R.V.L., 1995, Formação Águas Claras, Pré-Cambriano da Serra dos Carajás: redescrição e redefinição litoestratigráfica. Bol. Mus. Par. Em. Goeldi, 7: 177-277.
- Pestilho, A.L.S., 2011. Sistemática de isótopos estáveis aplicada à caracterização da evolução dos paleo-sistemas hidrotermais associados aos depósitos cupríferos Alvo Bacaba e Alvo Castanha, Província Mineral de Carajás, PA: Unpublished MSc. Dissertation, Campinas, Universty of Campinas
- Pidgeon, R.T., Macambira, M.J.B., Lafon, J.M., 2000, Th–U–Pb isotopic systems and internal structures of complex zircons from an enderbite from the Pium Complex, Carajás Province, Brazil: evidence for the ages of granulite facies metamorphism and the protolith of the enderbite: *Chemical Geology* 166, 159–171.
- Pinheiro, R.V.L., 2013, Carajás, Brazil – A short tectonic review: 13th Simpósio de Geologia da Amazônia, Belém (Proceedings).
- Pinheiro, R.V.L., Holdsworth, R.E., 1997. Reactivation of Archean strike-slip fault systems, Amazon region, Brazil. *Journal of the Geological Society* 154, 99–103.
- Pollard, J.P., 2006. An intrusion-related origin for Cu-Au mineralization in iron oxide-copper-gold (IOCG) provinces: *Mineralium Deposita* 41, 179.
- Réquia, K, Stein, H., Fontboté, L., Chiaradia, M., 2003. Re–Os and Pb–Pb geochronology of the Archean Salobo iron oxide copper–gold deposit, Carajás Mineral Province, northern Brazil: *Mineralium Deposita* 38, 727–738.
- Santos, J.O.S., 2003. Geotectônica do Escudo das Guianas e Brasil-Central. In: Bizzi LA,(ed) Geologia, tectônica e recursos minerais do Brasil: texto, mapas e SIG. Brasília, CPRM, pp 169-226.
- Sardinha, A.S., Barros, C.E.M., and Krymsky, R., 2006. Geology, geochemistry, and U-Pb geochronology of the Archean (2.74 Ga) Serra do Rabo granite stocks, Carajás province, northern Brazil: *Journal of South American Earth Sciences* 20, 327–339.
- Slack, J.F., Trumbull, R.B., 2011. Tourmaline as a recorder of ore-forming processes. *Elements* 7 (5), 321–326.
- Silva, A.R.C., Villas, R.N.N., Lafon, J.M., Craveiro, G.S., Ferreira, V.P., 2015. Stable isotope systematics and fluid inclusion studies in the Cu–Au Visconde deposit, Carajás Mineral Province, Brazil: implications for fluid source generation: *Mineralium Deposita* 50, 547-569

- Tallarico, F.H.B., Figueiredo, B.R., Groves, D.I., Kositcin N., McNaughton, N.J., Fletcher, I.R., Rego, J.L., 2005. Geology and SHRIMP U-Pb geochronology of the Igarapé Bahia deposit, Carajás copper-gold belt, Brazil: an Archean (2.57 Ga) example of iron-oxide Cu-Au-(U-REE) mineralization: *Economic Geology* 100, 7-28.
- Tavares, F., 2015. Evolução Geotectônica do nordeste da Província Carajás. Unpublished PhD Thesis, Rio de Janeiro, University of Rio de Janeiro. pp. 130.
- Toledo, P.I.F., 2017. Geologia do depósito IOCG Igarapé Cinzento/GT-46, Província Carajás. Unpublished Master Dissertation, Campinas, University of Campinas, p. 115.
- Tonarini, S., Pnnise, M., Adorni-Braccesi, A., Dini, A., Feerara, G., Gonfiantini, R., Wiedenbeck, M., Gröning, M., 2003. Intercomparison of Boron Isotope and Concentration Measurements. Part I: Selection, Preparation and Homogeneity Tests of the Intercomparison Materials. *Geostandards Newsletter* 27, 21–39.
- Tornos F., Velasco F., Barra F., Morata D., 2010. The Tropezón Cu-Mo-(Au) deposit, Northern Chile: the missing link between IOCG and porphyry copper systems? *Mineralium Deposita* 45, 313–321.
- Tornos, F., Wiedenbeck, M., Velasco, F., 2012. The boron isotope geochemistry of tourmaline-rich alteration in the IOCG systems of northern Chile: implications for a magmatic-hydrothermal origin. *Mineral. Deposita* 47 (5), 483–499.
- Torresi, I., Xavier, R.P., Bortholoto, D.F.A., and Monteiro, L.V.S., 2011. Hydrothermal alteration, fluid inclusions and stable isotope systematics of the Alvo 118 iron oxide-copper-gold deposit, Carajás mineral province (Brazil): Implications for ore genesis: *Mineralium Deposita* 47, 299–323.
- Vasquez, L.V., Rosa-Costa, L.R., Silva, C.G., Ricci, P.F., Barbosa, J.O., Klein, E.L., Lopes, E.S., Macambira, E.B., Chaves, C.L., Carvalho, J.M., Oliveira, J.G., Anjos, G.C., and Silva, H.R., 2008^a. *Geologia e Recursos Minerais do Estado do Pará: Sistema de Informações Geográficas—SIG: Texto explicativo dos Mapas Geológico e Tectônico e de Recursos Minerais do Estado do Pará, 1:1.000.000*, Belém, Companhia de Pesquisa de Recursos Minerais.
- Wirth, K.R., Gibbs, A.K., Olszewski, W.J., 1986. U-Pb ages of zircons from the Grão Pará Group and Serra dos Carajás Granite, Pará, Brazil: *Revista Brasileira de Geociências* 16, 195–200.

- Xavier, R.P., Wiedenbeck, M., Trumbull, R.B., Dreher, A.M., Monteiro, L.V.S., Rhede, D., Araújo, C.E.G., Torresi, I., 2008. Tourmaline B-isotopes fingerprint marine evaporites as the source of high-salinity ore fluids in iron oxide-copper-gold deposits, Carajás Mineral Province (Brazil): *Geology* 36, 743-746.
- Xavier, R.P., Rusk, B., Emsbo, P., and Monteiro, L.V.S., 2009. Composition and source of salinity of ore-bearing fluids in Cu-Au systems of the Carajás mineral province, Brazil: Society for Geology Applied to Mineral Deposit (SGA) 2009, Biennial Meeting 10_{th}, Townsville, Australia, Proceedings, p. 272–274.
- Yang, S.Y., Jiang, S.Y., Palmer, M.R., 2015. Chemical and boron isotopic compositions of tourmaline from the nyalam leucogranites, south Tibetan Himalaya: Implication for their formation from B-rich melt to hydrothermal fluids. *Chemical Geology* 419